Nucleic Acid Delivery –

Biocompatible Yet Efficient Platforms

A dissertation submitted in partial fulfilment

of the requirements for the degree of

Doctor of Philosophy

at the

School of Pharmacy,

University College London

Margarida Isabel Simão Carlos

October 2014

Declaration

This thesis describes research conducted at the UCL School of Pharmacy between 2nd November 2010 and 15th January 2014 under the supervision of Professor Ijeoma Uchegbu. I certify that the research described is original and that any parts of the work that have been conducted by collaboration are clearly indicated. I also certify that I have written all the text herein and have clearly indicated by suitable citation any part of this dissertation that has already appeared in publication.

…….. ……..……

Margarida Isabel Simão Carlos Date

Abstract

Gene therapy aims to act on the genetic cause of a pathology by gene inhibition or substitution. Gene delivery systems are necessary to deliver intact nucleic acids to the cells in order to achieve a therapeutic effect. Chitosan is a linear polysaccharide that displays properties such as biocompatibility and biodegradability. Despite the efforts to develop chitosan-based vectors, the therapeutic effectiveness of chitosan-base gene therapy still needs to be improved in order to achieve clinical significance.

This work introduces a new chitosan-based polymer: N-(2-ethylamino)-6-O-glycol chitosan (EAGC). The new polymer aims to overcome the disadvantages of chitosan for gene delivery, such as poor solubility at physiological pH and low buffer capacity, in order to enhance its transfection efficiency while retaining its main benefits of low toxicity and biocompatibility.

Three batches of EAGC were synthesized with different degrees of ethylamino substitution: EAGC17, EAGC21 and EAGC30. The EAGC synthesis and the degree of substitution of monomers with the new ethylamino group were confirmed by Nuclear Magnetic Resonance. The agarose gel retardation assay revealed that all polymers had the ability to condense with DNA/siRNA at different polymer, DNA/siRNA mass ratios. EAGC30 was able to condense both nucleic acids at smaller polymer, DNA/siRNA mass ratios due to its higher charge density. The nanoparticles formed between the different polymers and DNA/siRNA presented sizes between 100 and 450nm with a positive charge of +40mV and spherical shape. The stability of the DNA/siRNA nanoparticles was tested in the presence of different biological challenges.

All EAGC polymers were able to deliver the β-galactosidase plasmid to A431 cells *in vitro*. EAGC30 showed the best transfection capacity at lower polymer, DNA mass ratios. Differences in charge density of the polymers resulted in different gene activity. Nevertheless, all EAGC polymers were superior transfection agents to lipofectamine, particularly at high polymer, DNA mass ratios. *In vitro* down regulation of proteins was obtained for EAGC30, siRNA mass ratios 30 and 60.

Delivery to the brain of a complex formed between siRNA and a chitosan derivative, with a nose to brain delivery method, will be presented for the first time. Fluorescent EAGC30, siRNA nanoparticles were visualized on the olfactory bulb tissue after nasal administration. The results of this study confirmed Ethylamino Glycol Chitosan as a good candidate for *in vitro* and *in vivo* gene delivery.

Acknowledgements

I would like to express my gratitude to my principal supervisor Prof. Ijeoma Uchegbu for giving me the opportunity to do this PhD, and for her guidance and support through all this work. I also would like to give my special thanks to my co-supervisor Prof. Andreas Schätzlein for his contribution with valuable ideas that allowed the progress of the project.

This thesis would have not be possible without many different people that through the years helped me in different situations. I am grateful to all my colleagues from my laboratory with whom I discussed my experiments and results. A special thank you to Dr. Antonio Iannitelli for all the guidance during the synthesis experiments and to Dr. Lisa Godfrey for her help with the animal experiments. I am especially grateful for their encouragement and friendship. I am grateful to Dr. Natalie Garrett from the University of Exeter for advising on and performing the *in vivo* analysis.

I would also like to recognize the friendship of different people outside my group that were always available to allow me to use their laboratory equipment or were there to offer some guidance, particularly Dr. Helena Rosado. Also a big thank you to all my friends back in Portugal and the ones I met during the last four years as well as my family.

I am deeply grateful to Chris. We did start this journey together and you kept always by me. Thank you for being always there in the good and especially in the bad moments where your love and support kept me going. Thank you for listening to my endless monologues about my experiments that allowed me to solve what looked like another problem. Without your infinite love and patience this thesis would not have been possible.

Finally, to my parents and sister that despite being far away were always present. O meu muito obrigada por todo o vosso amor, estímulo e apoio durante os últimos quatros anos. Este tese é mais um exemplo dos valores que me ensinaram. Lutar sempre pelos nossos sonhos. This thesis is dedicated to them.

Table of Contents

List of Figures

List of Tables

List of Abbreviations

BBB	Blood Brain Barrier
BCA	Bicinchoninic Acid
Boc	*tert*-butoxycarbonyl
CARS	Coherent anti-stokes Raman scattering
COSY	Correlated Spectroscopy
D_2O	Deuterium Oxide
DAPI	4',6-diamidino-2-phenylindole
DEPT	Distortionless Enhancement by Polarization Transfer
DMEM	Dulbecco's Modified Eagle Medium
DMF	N,N-Dimethylformamide
DMSO	Dimethyl Sulfoxide
DNase	Deoxyribonuclease
DOPE	Dioleoylphosphatidylethanolamine
DOTMA	N-[1-(2,3-dioleyloxy) propyl]-N,N,N-trimethylammonium chloride
DPBS	Dulbecco’s phosphate-buffered saline
EAGC	N-(2-ethylamino)-6-O-glycol chitosan
EDTA	Ethylenediaminetetraacetic Acid
EGFP	Enhanced Green Fluorescent Protein
EPR	Enhanced Permeability and Retention
FBS	Foetal Bovine Serum
FITC	Fluorescein Isothiocyanate
GC	Glycol Chitosan
GPC	Gel Permeation Chromatography
HMGB1	high-mobility group box 1
HMQC	Heteronuclear Multiple Quantum Correlation
HRP	Horseradish Peroxidase
IC50	concentration required for 50% inhibition *in vitro*
IV	Intravenous
LLS	Laser Light Scattering
MALLS	Multi-angle Laser Light Scattering
MEM	Minimum Essential Medium
Mn	Number average molecular weight

MPEG	Methoxy Poly(ethylene glycol)
mRNA	messenger RNA
MTT	3-(4,5-Dimethylthiazol-2-yl)-2,5-diphenyltetrazolium bromide
Mw	Weight averaged molecular weight
NMP	N-methyl-2-pyrrolidone
NMR	Nuclear Magnetic Resonance
ONPG	O-nitrophenyl-β-D-galactopyraniside
PAMAM	Polyamidoamine
PCL	Polycaprolactone
PCR	Polymerase chain reaction
pDNA	Plasmid DNA
PEG	Polyethylene glycol
PEI	Polyethylenimine
PES	Polyethersulfone
PLL	Poly(lysine)
RI	Refractive Index
RIPA	Radio-Immunoprecipitation Assay
RISC	RNA-induced Silencing Complex
RNAi	RNA interference
RNase	Ribonuclease
SCID-X1	X-linked severe combined immunodeficiency
siRNA	small interfering RNA
S_N2	2^{nd} order nucleophilic substitution
TAE	Tris Acetate EDTA
TEA	Triethylamine
TEM	Transmission Electron Microscopy
TMS	Tetramethylsilane
TPF	Two Photon Fluorescence microscopy

1. Introduction

Gene therapy can be defined as the introduction of exogenous, therapeutic nucleic acids in target cells, enabling the treatment of diseases at a genetic level [1]. The concept was first shown by Mulligan *et al*. in 1979, when they introduced recombinant plasmid DNA using calcium phosphate transfection technology [2]. Transfection of cells was done later by liposomes (in 1980) [3], polylysine [4] and polyethyleneimine (in 1990) [5]. Various diseases have been targeted for the treatment with gene therapy, such as haemophilia [6], muscular dystrophy [7], cystic fibrosis [8] and age-related macular degeneration [9]. Gene therapies have also been developed for cardiovascular [10], and neurological [11] diseases as well as cancer [12].

Gene therapy aims to act on the genetic cause of a pathology by gene inhibition or gene substitution. Gene substitution relies on the introduction, into the cell, of transcriptionally fully competent genes, to augment the production of a specific protein in order to restore its functional expression. Gene inhibition silences overexpressed genes, normally at the messenger RNA (mRNA) level, stopping the expression of proteins at the post-transcriptional level [13, 14]. Nucleic acid therapy can be based on DNA (including plasmids, oligonucleotides (antisense and antigene applications), DNA aptamers and DNAzymes) or RNA (including antisense RNA, ribozymes, RNA decoys, RNA aptamers, small interfering RNA (siRNA) and microRNA) [1].

Plasmid DNA (pDNA) is a high molecular weight, double-stranded DNA construct that encodes a specific gene sequence. Inside the cell it expresses a functional protein through transcription and translation in order to produce a therapeutic effect [1, 15]. pDNA requires access into the nucleus to be expressed by the host-cell transcription machinery [16]. It might be integrated into the host genome, causing long-term gene expression, or stay outside the chromosome with a transient effect [17].

Gene inhibition can be achieved by the RNA interference (RNAi) mechanism for down-regulation of protein expression. RNA interference was discovered in 1998 by Mello *et al.* in the nematode *Caenorhabditis elegans* [18]. The RNAi pathway is fundamental in eukaryotic cells for post-transcriptional protein expression regulation [19, 20]. A double stranded RNA is introduced in the cell and cleaved by the enzyme Dicer (cytoplasmic ribonuclease III) into small fragments (21-23 nucleotides long) called short interference RNA. siRNA is a small macromolecule (approximately 13 kDa) comprising two strands: the sense and antisense [20]. siRNA operates in the cytosol where the siRNA antisense

strand is integrated into the RNA-induced silencing complex (RISC). RISC binds and cleaves complementary mRNA, thereby preventing its translation into a protein [16]. siRNA can be synthetically produced and directly introduced in the cell at the level of RISC, circumventing the Dicer mechanism [19-21]. The effect of siRNA is normally transient due to the dilution of the siRNA in the cytosol for dividing cells, although it is possible to observe a longer effect for slowly or non-proliferating cells [17].

The first clinical trial of gene therapy took place in 1990 for the treatment of severe combined immunodeficiency [22]. However, it was not until 2000 that the first successful, clinical gene therapy treatment was reported by Cavazzana-Calvo *et al*. [23]. The condition, X-linked severe combined immunodeficiency (SCID-X1), commonly diagnosed in early infancy, is characterized by recurrent infection as a result of an absence of cell-mediated and humoral immunity [24]. However, the success of this trial was questioned when two of the ten children treated developed a leukaemia-like condition [25]. One treatment based in adenoviral vectors (Gendicine) has been approved in China and an adenoassociated viral vector (Glybera®) was approved by the European Commission for treatment of lipoprotein lipase deficiency, proving that reaching the goal of gene therapy is not an impossible task [25, 26].

1.1 Gene Delivery Barriers

An important prerequisite for plasmid DNA and siRNA to be used as therapeutic molecules for different human diseases is the successful delivery to the cells and subsequent release in the intracellular space [15]. After administration in the body, the nucleic acids need to remain stable and avoid enzymatic degradation, as well as target specific cellular sites. Once inside the cell, the nucleic acids need to be released from the endosome to be active in the cytoplasm (in the case of siRNA) or migrate to the nucleus (for plasmid DNA) [17].

Extracellular barriers

Therapeutic genes can be administered in different ways into the body such as via the intramuscular or intravenous (IV) routes, as well as by inhalation (intranasal) or ingestion (oral). Depending on the route of administration, nucleic acids will encounter several barriers such as blood components, the blood brain barrier, immune defence mechanisms and enzymatic degradation [27]. Blood is one of the major barriers after IV administration. Exogenous materials in the blood led to the activation of the

complement system, as well as clearance by the reticuloendothelial system, non-specific interactions with serum proteins (e.g. albumin) and enzymatic degradation [17, 27]. The half-life of unprotected nucleic acids in mouse blood is approximately 10 minutes [15].

Cellular uptake

The targets of plasmid DNA and siRNA are located inside the cells, in the nucleus and cytoplasm respectively. These large, charged molecules need to cross the lipophilic and negatively charged plasma membrane in order to reach their therapeutic targets [28]. Endocytosis is the main process of uptake of macromolecules and solutes by internalization of membrane vesicles. There are various endocytic pathways such as clathrin-mediated endocytosis (via coated pits), caveolae, macropinocytosis and clathrin/caveolae-independent endocytosis [28, 29]. After internalization by the cell the molecules tend to be entrapped in intracellular vesicles known as endosomes.

Endosomal release

Endosomes have an internal pH around 6 and, during maturation, they are either recycled back to the membrane internalized content or develop into late endosomes which fuse with intracellular organelles called lysosomes. These present a lower pH of around 4.5 and contain digestive enzymes which facilitate substrate degradation [15, 30]. Therefore, the successful release of nucleic acids from the endosomes/lysosomes is one of the key steps for nucleic acid delivery.

Nuclear internalization

The therapeutic target of plasmid DNA is within the cell nucleus, making the nuclear envelope the ultimate obstacle. The entrance of the necessary macromolecules in the nucleus is controlled by the nuclear pore complex, which forms a channel through the nuclear envelope. Molecules smaller than 50 kDa are able to passively diffuse through the pore complex, while bigger compounds either have a specific target ligand or associate with polypeptides [28, 29]. Due to the elevated size of the plasmid DNA, it is unlikely that it can reach the nucleus of the cell by passive diffusion. According to the literature, dividing cells present higher transfection ability than non-dividing cells, suggesting that the plasmid DNA enters the nucleus during cell division. During mitosis the integrity of the nuclear membrane is lost with the disassembly of the nuclear envelope, enabling foreign DNA to enter the nucleus [28, 31].

1.2 Gene Delivery Systems

In order to overcome the challenges associated with the nucleic acids reaching their therapeutic target, an effective nucleic acid delivery system is needed. This delivery system should be able to (i) bind and condense the nucleic acids into nanoparticles, (ii) protect the nucleic acids from enzymatic degradation, (iii) promote cellular uptake, (iv) release the nucleic acids into the cytoplasm, and (v) promote nuclear entry (for DNA). Furthermore, a gene delivery vector should not trigger a strong immune response, but should allow sustained and regular expression of the genes [15, 32].

Regarding their mode of action there are two main gene delivery methods: physical and non-physical.

1.2.1 Physical methods

Physical gene delivery methods mediate the direct penetration of genes inside the cell by forming transient membrane holes. These methods circumvent limitations, such as cell penetration and endosomal release, of non-physical methods. Various methods are available with different advantages and limitations (Table 1).

Table 1 - Summary table of physical gene delivery methods.

Method	Mode of Action	Advantages	Limitations
Needle injection[33, 34]	Direct local injection of naked nucleic acids in tissues such as muscles, liver, and skin.	Simple method, lack of safety concerns.	Localized pain, oedema, and bleeding at the injection site
Jet injection [33, 34]	High-speed, ultrafine stream of DNA solution driven by a pressurized gas, usually CO_2. The injection generates pores on membranes of target cells.	Needle free, well tolerated by the target tissues.	Localized pain, oedema, and bleeding at the injection site.
Hydrodynamic gene transfer [35]	Increased liquid pressure injection of a large volume of gene solution to create pores in the cell membranes by reversible permeability changes in the endothelium.	The simplicity and safety of hydrodynamic gene delivery allows the use of this technique for the *in vivo* transfection of hepatocytes and the transfection of other organs.	Large doses required and non-specific targeting. Not possible to translate to *in vivo* human gene delivery.

Method	Mode of Action	Advantages	Limitations
Electroporation [36]	An electric field alters the cell permeability. Electric pulses generate transient pores in the cell membrane, followed by intracellular electrophoretic DNA movement.	Safe, efficient, with good reproducibility.	Gene delivery to *in vivo* solid tissues with this method is limited as electrodes need to be placed near the internal, target organs.
Gene Gun [37]	Impact of heavy metal particles on target tissues and delivery of coated DNA particles. The efficiency of the gene gun method depends on particle size, gas pressure, and dosing frequency.	Has been extensively applied to the intramuscular, intratumoral, and intradermal route.	Triggers immune responses at lower doses.
Sonoporation [34]	Use of ultrasound waves to create membrane defects by acoustic cavitation.	Safety, non-invasiveness, and being able to reach internal organs without surgical procedure.	Loss of cell viability and enhanced apoptosis

1.2.2 Non-Physical methods

1.2.2.1 Viral vectors

Viral vectors are one of the major gene delivery systems due to the capacity of viruses to insert a functional gene into the host cell genome. The viral vectors are derived from viruses with either RNA (e.g. Retrovirus) or DNA (e.g. Adenovirus) genomes [32]. The preparation of a viral vector includes the removal of the pathogenic part of the virus and replacement by a therapeutic gene, while the virus retains its non-pathogenic structures that allow it to infect the cell [31, 38]. Viruses mediate efficient gene transfer through favourable cell uptake and intracellular trafficking machineries [34]. To date, viral vectors are the most often used gene delivery vectors since they display good transfection properties both *in vitro* and *in vivo* [39]. One treatment based in adenoviral vectors (Gendicine) has been approved in China and an adenoassociated viral vector (Glybera®) was approved by the European Commission for treatment of lipoprotein lipase deficiency [25, 26]. Despite the advantages of viruses as gene delivery systems, there are still major drawbacks including the risk of immunogenicity, random integration of vector DNA into the host chromosome, specific tissue tropism, limited DNA carrying capacity and recombination with wild-type viruses and related toxicity [13, 34, 40].

1.2.2.2 Non-Viral vectors

Liposomes

Cationic lipids are amphiphilic molecules that contain a hydrophilic positively charge polar head group connected by a linker to a hydrophobic domain [41]. The positive charge of the head group is due to the presence of amines, which will interact with the anionic nucleic acids. The linker that connects the hydrophobic domain and the cationic head group may contain a glycerol-type moiety, a phosphate or a phosphonate linker, amino acids, peptides or aromatic rings [34, 40]. The hydrophobic domain is constituted of a cholesterol derivative or an aliphatic chain with different lengths and compositions [34, 41]. The most common chain lengths are C8 or C18 with mono-unsaturated fatty acids. Amphiphilic lipids are poorly soluble in water, and when suspended in water can adopt different structures including micellar, lamellar, cubic and inverted hexagonal phase with the hydrophobic tails facing each other and the hydrophilic heads facing water [41, 42].

Cationic lipids can be mixed with neutral lipids to form cationic liposomes for nucleic acid delivery. Dioleoylphosphatidylethanolamine (DOPE) and cholesterol are often used as neutral lipids. DOPE reduces the charge ratio of liposomes leading to reduced toxicity and increased transfection ability [34, 41]. Liposomes containing cholesterol are normally more stable in physiological medium enabling the nucleic acids to reach their target cells [34, 41].

Liposomes are defined as unilamellar or multilamellar microvehicles consisting of a phospholipid bilayer [34]. Cationic liposomes are complexed with nucleic acids by self-assembly, forming a lipoplex. Lipoplexes can also present different structures, including multilamellar, with DNA/siRNA monolayers between cationic membranes, or inverted hexagonal structure, with DNA/siRNA encapsulated within cationic lipid monolayer tubes. The hexagonal structure has shown advantages in transfection of nucleic acids [40].

After electrostatic interactions between the positively charged lipoplexes and the anionic structures (glycoproteins and proteoglycans) of the cellular membrane, the lipoplexes may enter the cell by fusion with the plasma membrane or by endocytosis [15, 40]. Once inside the cell, the lipoplexes are incorporated into the endosomes. Inside the endosomes there is a “flip-flop” mechanism by which anionic lipids diffuse from the endosomal membrane into the complex, forming neutral ion pairs with cationic

lipids. This leads to destabilization of the endosomal membrane, displacement of the nucleic acid from the delivery system, and release to the cytosol [15].

The main advantages of liposomes are their biodegradability and low toxicity, both a result of their composition from naturally occurring substances. Liposomes are able to protect the nucleic acids against enzymatic degradation as well as facilitate cellular uptake and endosomal escape, leading to effective gene transfer. They present low immunogenicity, and are easy to prepare and handle.

DNA delivery by liposomes was first reported in 1987 by Felgner *et al.* using N-[1-(2,3-dioleyloxy) propyl]-N,N,N-trimethylammonium chloride (DOTMA) [43]. Since then, liposomes have been reported for plasmid DNA and siRNA delivery [44-46]. Cationic liposomes showed higher transfection efficiency due to their ability to promote cellular internalization and the release of nucleic acids.

However, due to their positive charge, they may lead to non-specific interactions with serum proteins and cause haemolysis, they present low circulation half-life with systemic elimination, and low transfection efficiency [38]. Additionally, the presence of diethyl ether and chloroform (organic reagents involved in their preparation) may lead to cytotoxicity [42].

Cationic polymers

Cationic polymers are a safer alternative to viral delivery, since the risk of immunogenicity is lower [38]. They are easy to prepare, with flexibility regarding the size of the nucleic acids to be transfected. Their main drawback falls on the transient nature of transfection as well as the lower transfection efficiency when compared with the viral vectors [47]. When compared with liposomes, cationic polymers are more stable and show good biodegradability, low toxicity, structural diversity and relatively higher transfection efficiency [48].

Cationic polymers present different molecular weights and structure including linear, branched and dendritic structures. These polymers bind to the anionic phosphate groups along the backbone of the nucleic acids through electrostatic interactions, prompted by cationic primary, secondary, tertiary and quaternary amines present in the polymers [49]. These interactions enable the packing of the nucleic acids, reducing the DNA/siRNA to nanosized particles called polyplexes [31]. The presence of serum

proteins and other blood components may lead to destabilization of the complexes. Characteristics of the polymers provide increased stability to the nanoparticles, preventing disaggregation in the presence of these biological challenges. Furthermore, cationic polymers offer protection from enzymatic degradation [50] (Figure 1).

The delivery of nucleic acids to specific cells with cationic gene delivery systems can be done by passive or active targeting. Passive targeting relies on the tumour morphology via the enhanced permeability and retention (EPR) effect. A prolonged circulation of small nanoparticles (10-100nm) combined with the leaky blood vasculature in these tissues leads to an accumulation in the tumour site. This is a non-selective targeting approach [17] that presents major drawbacks including heterogeneous carrier extravasion comprising delivery efficiency as well as off-target delivery to healthy cells, leading to toxicity and adverse side effects [51, 52]. Active targeting relies on the presence of specific receptors on target tissues. This allows the functionalization of nanoparticles with specific ligands such as transferrin and folic acid. This kind of delivery prevents the non-specific, off-target effects described for passive targeting [53].

The polyplexes interact with the negatively charged cell membrane and enter the cell mainly by endocytosis. Size, surface potential and the ratio between the number of amines in the polymer and phosphates in the nucleic acids (N:P ratio) strongly influence the gene delivery capacity of each polymer, as well as endosomal escape and unpacking of DNA/siRNA from the complexes [54].

The release of nucleic acids from the carrier upon entry into the cell is an important feature that highly affects the gene delivery outcome. Plasmid DNA needs to migrate to the nucleus, while the siRNA mechanism happens at the cytoplasm [17]. Chain length and polymer molecular weight are the most important features for nucleic acid unpacking. Generally, longer chains and higher molecular weight polymers provide improved stability which may impair nucleic acid release. A balance between the stability of the polyplexes in serum and salt solutions and release of nucleic acids should be obtained [55].

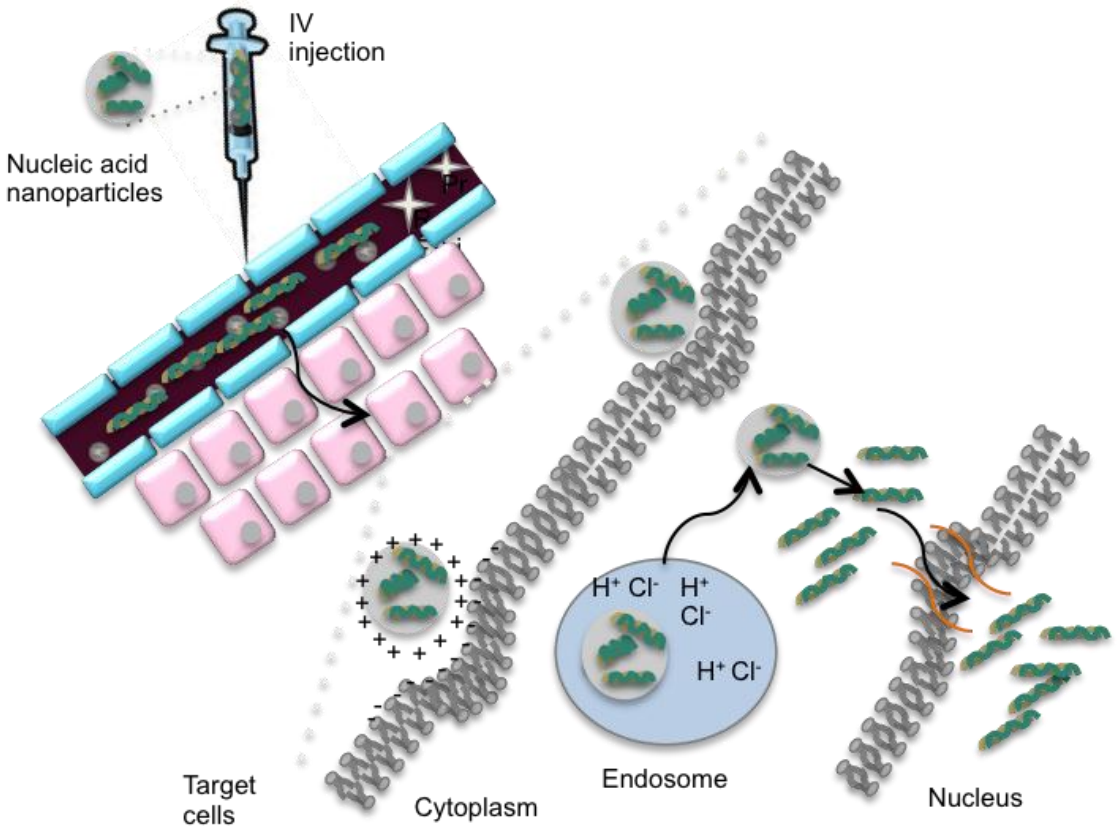

Figure 1 - Schematic representation of gene delivery. Adapted from Raemdonck *et al.* [14].

Different kinds of cationic polymers have been studied. Here, I will discuss polylysine (PLL), Polyethylenimine (PEI), dendrimers and chitosan. PLL was the first cationic polymer to be used in gene delivery. However, it presented low transfection efficiency [4]. PEI and dendrimers present good transfection capacity, but nevertheless their use is still limited by their low biocompatibility [56]. Chitosan presents lower transfection efficiency than the previous but it is a biocompatible polymer [57]. These polymers set the main characteristics for a successful gene delivery system, and therefore this review constitutes an important background to the development of a new gene delivery system.

Poly (L-Lysine)

Poly(L-lysine) was first used for *in vitro* gene delivery by Wu *et al.* in 1987 [4]. PLL is a cationic linear polypeptide with the amino acid lysine as the repeating unit (Figure 2). It is regarded as biocompatible and biodegradable [13]. Nucleic acid condensation and transfection efficiency increases with the molecular weight; however, so does toxicity.

PLL with molecular weight lower than 3 kDa showed a limited capacity to transfect cells, while high molecular weight PLL has shown high toxicity [58]. The structure of PLL presents primary amino groups that are all protonated at endosomal pH, resulting in poor buffer capacity for the polymer and consequently poor endosomal escape leading to low gene expression [59, 60]. In order to increase transfection efficiency, several conjugates such as endosomolytic agents, histidine and imidazole have been used [59-61]. Substitution of PLL with histidine increased the transfection of the polymer 4-fold due to the presence of the imidazole ring that has a pKa around 6 increasing the buffer capacity of the polymer [15].

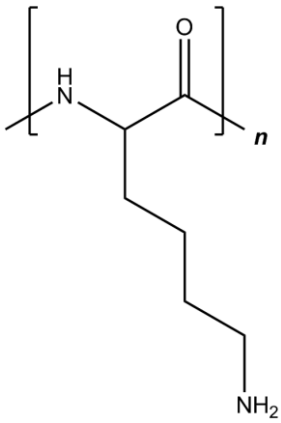

Figure 2 - Representative chemical structure of PLL.

Polyethylenimine

Polyethylenimine has been one of the most studied gene delivery systems since the polymer successfully enabled transfection of DNA in 1995 [5]. It is commercially marketed as a transfection reagent in preparations such as ExGen500R, jetPEIR and PEIproTM.

PEI is a cationic polymer with one third of its atoms being nitrogens, presented as primary, secondary and tertiary amino groups in a 1:2:1 ratio (Figure 3). This high number of amines gives the polymer a high charge density, conferring unique features such as strong DNA condensation with protection from enzymatic degradation, intrinsic endosomal activity, and a unique buffer capacity called the proton sponge effect [60].

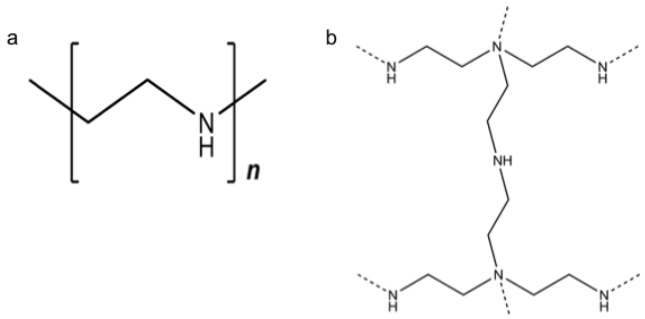

Figure 3 - Representative chemical structure of a) linear PEI and b) branched PEI.

The primary amines (pKa ≈ 9, higher than the endosomal pH) are generally regarded as responsible for nucleic acid condensation, while secondary and tertiary amines (pKa ≈ 5-7, around the endosomal pH) contribute to the buffer capacity of the polymer [62, 63]. The degree of protonation of PEI increases from 20 to 45% when the pH decreases from 7 to 5 in the endosomes [64]. The pH-buffering property presented by PEI is an important feature that allows endosome disruption (proton sponge effect - Figure 4) and prevents lysosomal degradation of the nucleic acids. Once the PEI-DNA/siRNA complexes enter the cell, they are trapped into the endosomes. These present membrane ATPase ion channels that pump protons to the inside, leading to the acidification of the endosomal compartments and activation of hydrolytic enzymes. PEI becomes protonated preventing the acidification of the endosomes and resulting in a continuous influx of protons (to attempt to lower the pH), as well as passive entry of chloride ions. Consequently there is an increase of ionic concentration, with an influx of water leading to endosomal swelling and rupture of the endosomal membrane. In this way PEI nanoparticles are able to be released from the endosomes with intact nucleic acids [15, 65].

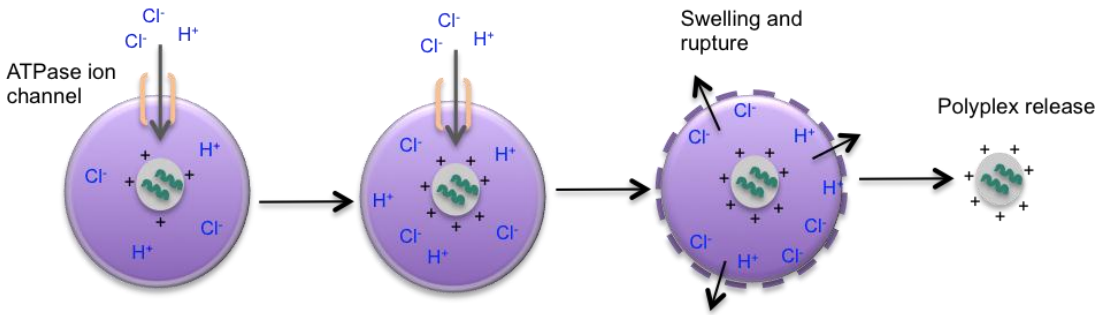

Figure 4 - Schematic representation of proton sponge effect. Adapted from Aied *et al.* [31].

PEI presents as two forms: linear and branched (Figure 3). The degree of branching affects complexation with the nucleic acids and transfection efficiency [66]. Linear PEI is less effective at condensing DNA compared with the branched form for similar molecular weights. Branched PEI presents a higher number of primary amines, allowing for the formation of more stable complexes [67, 68]. Nevertheless, linear PEI has shown better transfection of plasmid DNA than the branched form [69]. The same results were not obtained for the delivery of siRNA, where branched PEI was able to achieve gene silencing while the linear polymer did not show any knock-down effect. These different results are explained by the stability of the complexes between PEI and DNA/siRNA. Linear PEI leads to less stable complexes, which is advantageous for the release of plasmid DNA. However, since electrostatic interactions of siRNA with the polymer are weaker, due to the small structure and low charge density of the nucleic acid, the extra charge density presented by the branched form of PEI is necessary for the delivery of siRNA [70].

The transfection efficiency of PEI also depends on its molecular weight, with polymers with molecular weight lower than 25 kDa showing poor transfection ability. Transfection efficiency increases with the increase of the molecular weight for molecular weights of between 6 and 70 kDa [71]. High molecular weight (800 kDa) PEI is significantly cytotoxic due to its high charge density and lack of degradable linkages inducing cell membrane disruption followed by apoptosis. An optimum molecular weight seems to range between 12 and 70 kDa [71, 72]. However, one study showed that a low molecular weight (10 kDa), moderately branched polymer resulted in efficient delivery with low toxicity when compared to commercial, high molecular weight PEI [56]. This shows that the right balance between molecular weight and branched/linear forms can lead to successful gene delivery.

Despite showing good transfection efficiency *in vitro* and *in vivo*, PEI toxicity, related to the lack of degradable linkages and high charge density, still presents a major hurdle to the translation of the polymer to the clinic [73, 74]. Godbey *et al.* reported that the charge density of free PEI leads to precipitation and aggregation of the polymer when administered *in vivo* due to the interactions with anionic charged proteins (e.g. albumin). Also, the interactions of PEI with cellular components inhibit normal cellular processes and cause several changes to cells, including cell shrinkage, reduced number of mitoses and vacuolization of the cytoplasm [56].

In order to overcome the cytotoxicity of high molecular weight PEI, degradable linkers such as disulfide bonds have been used [75]. This acid-labile PEI may be rapidly

degraded into low molecular weight PEI in acidic endosomes. In toxicity assays, the modified PEI was much less toxic than PEI with a molecular weight of 25 kDa, due to the degradation of the acid-labile linkages [76]. Also, cholesterol and polyethylene glycol (PEG) have been introduced to reduce the cytotoxicity of the polymer, by masking the positive surface charge of PEI [77, 78]. A PEI-PEG polyelectrolyte complex has been used for delivery of siRNA into tissue cells in tumour-bearing mice [79].

Dendrimers

Dendrimers are monodispersed, hyperbranched macromolecules, with a well-defined size and shape and high density of functional groups, that are regarded as good candidates for gene delivery [80]. The structure of dendrimers may be divided into three parts: (1) a central core, (2) repeating branches called generations and (3) terminal functional groups which play a role in gene complexation [81, 82].

Dendrimers complex with the nucleic acids through electrostatic interactions between the positively charged terminal groups of the dendrimers and the anionic phosphates of the nucleic acids backbone [80]. The resulting “dendriplex” presents a positive charge, enabling interaction with the cell membranes. Dendrimers with a higher number of generations are regarded as more toxic due to their high charge density [81].

Polyamidoamine (PAMAM) dendrimers are the most well characterized and commercialized dendrimers (Figure 5). They are water soluble and non-immunogenic, with terminal amino groups that can be modified to allow specific targeting [80]. PAMAM dendrimers produce high transfection efficiency and are the most commonly used dendrimers for gene delivery [82].

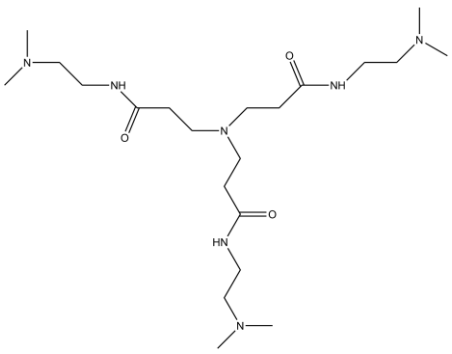

Figure 5 - Representative chemical structure of PAMAM dendrimers.

1.2.3 Chitosan

Chitosan is obtained by partial deacetylation of chitin, which is the natural structural component of the crustacean exoskeleton [83]. It is a linear polysaccharide composed of D-glucosamine and N-acetyl-D-glucosamine subunits linked by β(1,4)-glycosidic bonds (Figure 6). The relative proportion of the different sub-units determines the degree of deacetylation, which in turn influences different characteristics of the polymer such as solubility [84]. The polymer displays properties such as biocompatibility and biodegradability, and its degradation products are non-toxic, non-immunogenic and non-carcinogenic [85]. Chitosan is a biodegradable polymer that can be degraded by enzymes which hydrolyse glucosamine–glucosamine, glucosamine–N-acetyl-glucosamine and N-acetyl-glucosamine-N-acetyl-glucosamine linkages, leading to small fragments that are suitable for renal clearance [31, 86]. Chitosan also presents mucoadhesive properties, being known for its ability to transiently open the tight junctions of the intestinal barrier [87]. Due to these unique features, chitosan and its derivatives have found fruitful applications in various fields such as water treatment [88], the food industry [89],cosmetics [90] and agriculture [91].

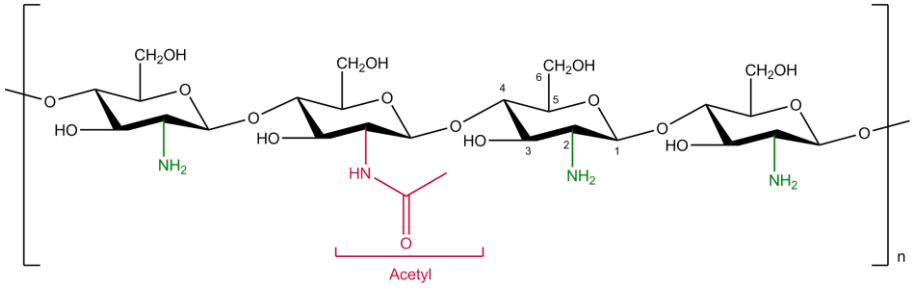

Figure 6 - Representative chemical structure of chitosan.

Biocompatibility

Chitosan biocompatibility is influenced by different polymer characteristics such as molecular weight, polymer structure (including branched derivatives), charge density, cationic functionality of derivatives, degree of biodegradability and conformational flexibility [71, 92].

An increase of cytotoxicity as a function of the molecular weight was previously reported for different cationic polymers including PEI [72], PLL [93, 94] and

chitosan [95]. Branched molecules were found to be slightly more toxic than linear polymers [93, 96]. The toxicity of different cationic groups has also been studied; more specifically, the difference between primary, secondary and tertiary amines. Primary amines led to red blood cell agglutination, while tertiary amino groups showed lower toxicity [97]. However, Fisher *et al.* concluded that it is not only the kind of amine that has an impact on toxicity, but also the overall charge density. It was demonstrated that the cytotoxicity of different types of polycationic polymers depend on the number and arrangement of the cationic charges [71]. A comparative study between polycationic, neutral and polyanionic polymers revealed that the polycationic polymers have the highest toxicity, followed by neutral and anionic ones [98].

It is hypothesized that the strong ionic interaction between the positive charges of the polymers with the anionic structures of the cell membrane affects membrane integrity, altering cell function and ultimately leading to cell death [99, 100]. The mechanism of cytotoxicity caused by cationic polymers is due to the electrostatic interactions between the positively charged polymers and the anionic membranes which can lead to destabilization and ultimately rupture of the cell membrane. When exposed to cationic polymers, the cell suffers membrane leakage followed by a decrease in metabolic activity [71]. Polyethylenimine cytotoxicity was characterized as a two-phase process where the polycation-cell interaction induces loss of cell membrane integrity and the induction of programmed cell death, leading to cell shrinking and reduced mitoses [56, 73].

Chitosan presents low toxicity when compared with other cationic polymers such as PEI. For chitosan, IC50 (concentration of polymer at which 50% of cells are viable) values have been reported between 0.2-20 mg mL^{-1} [86] in different cell lines. Conversely, PEI presents an IC50 of <20 µg mL^{-1} [101, 102]. Chitosans with different molecular weights and degrees of deacetylation (<5 kDa, 65.4%; 5–10 kDa, 55.3%; and >10 kDa, 55.3%) showed an IC50 >1 mg mL^{-1} in CCRF-CEM (human lymphoblastic leukaemia cells) and L132 (human embryonic lung cells). Haemolysis was not observed (<10%) over 1 h and 5 h with chitosans of <5 kDa, 5–10 kDa and >10 kDa at concentrations of up to 5 mg mL^{-1} [103].

The molecular weight and charge density (degree of deacetylation) are the main factors that contribute to chitosan's cell biocompatibility [86, 104]. High molecular weight polymers (>100 kDa) with a high degree of deacetylation were less biocompatible [95] than lower molecular weight chitosans (10 kDa) [105].

Huang *et al.* found higher attenuated cytotoxicity of chitosan when the degree of deacetylation decreased, and less attenuation when the molecular weight was reduced, suggesting that the degree of deacetylation has a greater effect than the molecular weight on chitosan's biocompatibility [95]. Chitosans with a degree of deacetylation of 88% and molecular weight between 10 and 213 kDa showed comparable biocompatibility in A549 cells. Decreasing the polymer charge density (61% and 46% of deacetylation) resulted in increased viability of the cells (60% of cells alive when compared with less than 10% for chitosan 88% deacetylated). Reducing the chitosan molecular weight from 213 kDa to 10 kDa did not change the IC50 value (IC50 1.1 to 1.2 mg mL^{-1}). However when the degree of deacetylation decreased from 88% to 61%, the IC50 increased from 1.2 to 2.0 mg mL^{-1} and to 2.2 mg mL^{-1} with a further decrease of the degree of deacetylation to 46% [95].

After evaluation of the biocompatibility of chitosan in CaCo-2 and HT29-H cells and *in situ* rat jejunum, Schipper *et al.* also concluded that toxicity is dependent on the degree of deacetylation and molecular weight. At a high degree of deacetylation, the biocompatibility of chitosan is related to the molecular weight and the concentration; at a lower degree of deacetylation toxicity is less pronounced and less related to the molecular weight. However, most of the chitosans tested did not increase dehydrogenase activity in CaCo-2 cells significantly in the concentration range tested (1–500 μg mL^{-1}) [106, 107].

The biocompatibility of chitosan with a high degree of deacetylation (92%) and low molecular weight (10 kDa) was studied by Nimesh *et al.* [105]. After 48h of incubation, more than 85% of cells were viable at pH 6.5 and 96% at pH 7.1. These results corroborate the theory that the charge density may contribute to the biocompatibility of chitosan, since the cell viability was lower at lower pH when the protonation of chitosan is higher [105]. In the same study, lower biocompatibility for chitosan alone was reported when compared with chitosan-DNA complexes, since the charge of the polymer is partially neutralized by the binding of DNA.

The modifications made to chitosan can make it more or less toxic. Carreno-Gomez showed that glycol chitosan (GC) is one of the chitosan derivatives with lower toxicity [108]. Trimethyl chitosan is more toxic than chitosan, and its toxicity was found to be directly related with the degree of trimethylation (charge density) [102].

Transfection efficiency

The transfection efficiency of chitosan is also dependent on polymer characteristics such as molecular weight, charge density and buffer capacity [40, 105]. Because of its cationic nature, chitosan is a very popular candidate for nucleic acid delivery. Features including the pH of transfection medium, degree of deacetylation (charge density), molecular weight, and nitrogen to phosphate ratio (N:P ratio) determine the transfection efficiency of DNA and siRNA [55, 59, 109].

At physiological pH, the gene transfection efficiency of chitosan is lower compared with other cationic gene delivery systems such as PEI [57, 110, 111] or cationic lipids [112, 113]. The transfection efficiency of chitosan is dependent on the pH of the transfection medium, due to the protonation of its primary amine groups. The pKa of these amines has been calculated as 6.5, meaning that at a higher (more basic) pH, the amines will not be protonated and the overall positive charge of the polymer will be low [114]. Therefore, at pH 7.4 chitosan presents minimal solubility, low intracellular delivery resulting in low transfection ability [104, 105].

The transfection efficiency of a 10 kDa chitosan with a 92% of degree of deacetylation, was studied in HEK 293 cells and compared against lipofectamine. The gene expression was assessed at different pH values: 6.5, 7.1 and 7.4, in the presence of 10% serum. Enhanced Green Fluorescent Protein (EGFP) was expressed in 26.3% of cells at pH 6.5, with only 9.2% at pH 7.1 and 0.2% at pH 7.4. The cell uptake was also studied at different pHs: 100% of the cells internalized the complexes at pH 6.5, while only 50 % cellular uptake was observed at pH 7.1. Further studies revealed that changing from pH 6.5 to 7.4 at 8, 12 or 24 h after initiating transfection led to higher gene expression than the positive control lipofectamine [105].

Sato *et al.* evaluated the transfection efficiency of chitosan, DNA complexes (52% and 92% degree of deacetylation) in A549 cells and found it higher at pH 6.9 than at pH 7.6 [115]. Additionally, Zhao *et al.* investigated the effect of transfection medium pH on the transfection efficiency of chondrocytes using chitosan-DNA complexes with 800 kDa chitosan with an 82% degree of deacetylation. Four pH values were studied: 6.8, 7.0, 7.2 and 7.6; higher expression levels were obtained at pH 6.8 and 7.0 with more than 50% of cells transfected [116].

Finally, Lavertu *et al.* studied the transfection efficiency of two chitosans with a molecular weight of 40 kDa and an 80% degree of deacetylation and a molecular

weight of 80 kDa and a 72% degree of deacetylation at pH values 6.5, 6.8, 7.1 and 7.4. The percentage of transfected cells was comparable for pH 6.5 and 7.1, with the lowest transfection happening at pH 7.4 [104].

Further to the pH of the transfection media, the degree of deacetylation of chitosan plays a role in the polymer's capacity to condense with nucleic acids and perform gene transfection.

The importance of the degree of deacetylation was showed by Kiang *et al.*. Three different cell lines were used to test the transfection efficiency of chitosan-DNA nanoparticles with a chitosan with a molecular weight of 390 kDa. Three different degrees of deacetylation were studied (62%, 70% and 90%). For all cell types tested, the chitosan formulations with the lower degrees of deacetylation resulted in lower gene expression levels. Furthermore, for the chitosans with the lower degrees of deacetylation (62% and 72%) the level of gene expression was not significantly greater than the background [117].

The effect of the degree of deacetylation was also studied by Huang *et al.* with three chitosan polymers of high molecular weight (213 kDa). The polymer with a degree of deacetylation of 88% showed a transfection efficiency of 12.1% while chitosans with lower degrees of deacetylation, 61% and 46%, showed residual transfection efficiencies of 0.2 and 0.05%, respectively [95, 118].

Five chitosans with a molecular weight range between 31 and 190 kDa, and with different degrees of deacetylation (31 kDa, 99%; 170 kDa, 99%; 190 kDa, 85%; 170 kDa, 65%; 98 kDa, 51%) were studied by Koping-Hoggart *et al.* in the 293 kidney cell line. The lowest gene expression was obtained using chitosans 170 kDa, 65% and 98 kDa, 51% at an N:P ratio of 3.0 and 3.6 respectively. Chitosan 190 kDa, 85% showed the highest transfection efficiency at N:P ratio of 3.0 (70 times higher than 98 kDa, 51%), followed by 31 kDa, 99%, and 170 kDa, 99% both at N:P ratio of 3.6. The results showed that the transfection ability of the polyplexes did not depend on the molecular weight in the range from 31 to 170 kDa but on the percentage of deacetylation; chitosan with a percentage of positive charge lower than 65% did not show transfection ability. Following these results, a chitosan (degree of deacetylation of 83%) with a molecular weight of 162 kDa (N:P ratio 2.4) was studied in comparison with PEI, 800 kDa (N:P ratio 9). The percentage of transfected cells was of 35% for PEI and 25% for chitosan polyplexes with similar results for gene expression [110].

The previous results demonstrate that the charge density of chitosan is intimately related with its transfection efficiency and dependent on two main factors: degree of deacetylation of the polymer and pH of the transfection solution. Polymers with higher degree of deacetylation at lower pH showed a higher charge density along the chain [119]. Furthermore, it has been demonstrated that cellular uptake of chitosan-DNA complexes depends strongly on the stability of the nanoparticles in medium as well as on their surface charge [118]. It is already recognized in the literature that complexes that are not sufficiently stable will dissociate too early and will show little or no transgene expression. On the other hand, highly stable complexes might not release DNA once inside the cells or may only release it slowly, resulting in low or delayed expression. Thus, an intermediate stability is desired [110, 112]. In addition, the internalization of chitosan in the cells is non-specific and highly dependent on electrostatic interactions between the positive polymer and the negative membrane. Therefore, the high positive charge presented by chitosan at lower pH enhances cellular uptake [105]. In summary, in order to achieve high transfection efficiency, chitosan should present a high degree of deacetylation and the complexes with DNA and siRNA should be prepared in a slightly acidic solution (pH lower than 7.1) in order to raise the polymer's positive charge, enhancing in this way the binding efficiency to the cell membrane and cellular uptake [95, 110, 117, 118].

The molecular weight of chitosan is one of the major characteristics of the polymer that also influences the gene expression results. Some studies with chitosan as a gene delivery system showed that a high molecular weight polymer (100-400 kDa) associated with a high degree of deacetylation were essential requirements for nucleic acid transfection [112, 120-122].

Other authors confirmed that the transfection efficiency was low for chitosan with low molecular weights (<100 kDa) [112, 120] and decreased with a decrease of the molecular weight. MacLaughin *et al.* described that the highest transfection efficiency was achieved with a chitosan of 102 kDa (89.4% degree of deacetylation, N:P 2) when compared with chitosans between 7 and 92 kDa. Nevertheless, the gene expression of the polymer with 102 kDa was still 250-fold less than that observed with the plasmid-lipofectamine positive control complex [112].

Leong *et al.* evaluated the transfection efficiency of Chitosan (390 kDa) in a 293 cell line. Chitosan nanoparticles showed lower luciferase expression than lipofectamine (positive control) with no improvement of transfection when in presence of chloroquine or transferrin conjugated to the surface [113].

Huang *et al.* observed that the transfection efficiency, in A549 cells at an N:P ratio of 6, was significantly reduced for a chitosan with molecular weight of 10 kDa (0.6% of positive cells), when compared with chitosan with 213 kDa (12.1% of positive cells), both polymers with 88% deacetylation [118]. Furthermore, the transfection efficiency decreased with the decrease of the molecular weight (213 kDa, 88% = 12.1%; 98 kDa, 88% = 8.3%; 48 kDa, 88% = 6.4%; 17 kDa, 88% = 2.9%; 10 kDa, 88% = 0.6% of positive cells) [95, 118]. Delgado *et al.* also studied the transfection efficiency of three chitosans with molecular weight of 40, 100 and 125 kDa with a degree of deacetylation of 85%. The DNA-chitosan aqueous solutions were prepared at different chitosan, DNA mass ratios (w/w) 1:1, 2.5:1, 5:1, 7.5:1, 10:1, 12.5:1 and 15:1. The highest transfection levels were obtained with the chitosan with 125 kDa of molecular weight at a polymer, DNA mass ratio of ratio 2.5:1; however, the results were still considered low (less than 10% of EGFP positive cells) [121].

Chitosan of high molecular weight was also used for the delivery of siRNA in different studies. Howard *et al.* showed siRNA delivery with chitosan (114 kDa, 84% degree of deacetylation) *in vitro*. Significant knockdown (77.9%) of EGFP was achieved in human lung carcinoma cells 48h post-transfection. The transfection levels were comparable to the positive control (78%, TransIT-TKO). Transfection with siRNA was also tested in the K562 cell line (N:P 57). Western blotting results demonstrated approximately 90% knockdown of BCR/ABL-1 protein [20].

The work of Katas *et al.* focused only on high molecular weight chitosans, and showed no correlation between chitosan molecular weight and *in vitro* siRNA delivery for chitosans with 110, 160, 270 and 470 kDa [123]. Ji *et al.* showed knockdown of 70% of FHL2 gene expression in human colorectal cancer Lovo cells when using of chitosan with a molecular weight of between 190 and 310 kDa and a degree of deacetylation between 75 and 85% [124].

Liu *et al.* demonstrated EGFP silencing of 45%-65%, with high molecular weight chitosans (65, 114 and 170 kDa) and a high degree of deacetylation (78% and 84%) whereas only 5% of EGFP down regulation was achieved with low molecular weight chitosans (9 and 12 kDa) and with a low degree of deacetylation (54%). It was also reported that low N:P ratio (N:P 2 and 10) nanoparticles resulted in lower knockdown when compared with higher N:P ratio (50 and 150) nanoparticles formed with 170 kDa chitosan. Nanoparticles formed at an N:P ratio of 150 showed the greatest level (80%) of EGFP knockdown [125].

Although the previous studies showed good results for high molecular weight chitosans (100-400 kDa) in comparison with low molecular weight (<100 kDa), there are also examples in the literature of chitosans with low molecular weight which outperformed the high molecular weight polymers [55, 126].

Strand *et al.* studied the influence of the molecular weight of chitosan in a range between 5 and 146 kDa. Four N:P ratios (3, 5, 10 and 20) were transfected at pH 7. The polyplexes formed with chitosans of 8 and 12 kDa of molecular weight showed the highest luciferase expression in HEK293 cells. Luciferase expression was 10-fold higher than the transfection efficiency of chitosan with 25 and 33 kDa [55]. Gene expression was also dependent on the N:P ratio increasing, with the increase of the N:P ratios achieving a plateau after which transfection efficiency decreased [55].

Chitosan with 70 kDa transfected HeLa cells in the presence of 10% serum [57]. The highest transfection efficiency was obtained at an N:P ratio of 3, 72h after transfection. Over the same timeline, PEI gene expression was lower than the gene expression seen with chitosan polyplexes [57].

The transfection efficiency of an even lower molecular weight chitosan, 22 kDa, with a degree of deacetylation of 72.5% was determined by a transfection assay into 293T cells with β-galactosidase. Different mass ratios (chitosan, DNA) were studied, with a mass ratio of 3 showing 37% higher transfection efficiency than PLL (20 kDa) at a mass ratio of 2 [94].

Furthermore, a chitosan oligomer was used to transfect a 293 kidney cell line. Chitosan (<4.7 kDa) polyplexes were prepared at pH 6 in water. Transfection efficiency was studied with three N:P ratios: 10, 30 and 60. N:P 60 showed the highest transfection ability, 100-fold higher than transfection results obtained with N:P 10 [126]. The efficiency of low molecular weight chitosan was then compared with a high molecular weight (162 kDa, 83% deacetylated) polymer for three cell lines: kidney epithelial 293 cells, airway epithelial Calu-3 cells and cervix epithelial HeLa cells with an N:P ratio of 60. The low molecular weight chitosan showed a gene expression 4 to 24 fold higher than the high molecular weight chitosan. This low molecular weight chitosan was then compared with PEI (25 kDa at N:P ratio of 5) for transfection efficiency in the 293 cell line. The transfection results were dependent on the pH of the transfection medium. PEI showed a higher level of transfection at pH 7.4 while at pH 5 the polyplexes with low molecular weight were more efficient (four-fold higher than luciferase gene expression) [126].

Down-regulation of specific genes through siRNA delivered by low molecular weight chitosan was also studied. Three different chitosans (44, 63 and 93 kDa) showed an 80% down regulation of luciferase expression at chitosan, siRNA mass ratios 2.5 and 5. The fourth chitosan, with a molecular weight of 143 kDa, was less effective with a reduction of only 60%, while lipofectamine (positive control) showed 90% down regulation [127].

Two linear chitosans with molecular weights of 75.7 kDa and 150 kDa, and one self-branched chitosan polymer of molecular weight 40 kDa, were evaluated as siRNA-carriers by Jogersen *et al.* A silencing effect of 60% was obtained with 75.5 kDa chitosan, the better of the two polymers in RMS melanoma cell line and SKBR3 breast cancer cell line. A higher knockdown effect was obtained in OHS cell line (95%) [128].

Techaarpornkul *et al.* concluded that the molecular weight of chitosan and the chitosan, siRNA mass ratios of the nanoparticles influence the final gene knockdown results more than the nature of salt forms. Silencing (around 50%) was achieved with low molecular weight chitosan of 20 kDa at a chitosan, siRNA mass ratio of 32, while gene knockdown of chitosans with molecular weights of 200 and 460 kDa was rather poor (below 20%). Gene silencing results, for 20 kDa chitosan, were lower for chitosan, siRNA mass ratios of 4 and 8 (chitosan, siRNA mass ratio 4 had a gene silencing of 20%) when compared with higher chitosan, siRNA mass ratios 16 and 32 [129].

The previous literature review, on the effect of molecular weight of chitosan, in its ability for gene delivery, showed contradictory results. Initial reports demonstrated that high molecular weight polymers (100-400 kDa) [20, 112, 113, 118, 123, 125] performed better than low molecular weight chitosan for gene delivery of DNA and siRNA. However, other authors reported that chitosans with a molecular weight lower than 100 kDa are also suitable gene delivery candidates [55, 57, 94, 110, 127-129].

To try to understand how the different factors that influence transfection efficiency of chitosan (molecular weight, degree of deacetylation, pH and N:P) correlate between each other and what the ideal characteristics to enhance the gene delivery ability of chitosan are, Lavertu *et al.* studied the transfection efficiency of chitosan with four different molecular weights (10, 40, 80 and 150 kDa) and four different degrees of deacetylation (72, 80, 92 and 98%). The luciferase expression was evaluated at different pH values of the transfected solution (6.5 and 7.1) and different polyplex N:P ratios (5 and 10). Two formulations of chitosan (10 kDa, 92% degree of deacetylation,

N:P ratio 5 and 10 kDa, 80 % degree of deacetylation, N:P ratio of 10) showed the highest luciferase expression and similar results to the positive control (FuGene) [104].

The comparison of the four different chitosans in different conditions allowed Lavertu *et al.* to understand the importance of the different variables that influence chitosan transfection. The results did not show an influence of the degree of deacetylation *per se* in the gene expression. However, in some formulations it was observed that a decrease in charge density led to a decrease in transfection efficiency. Regarding the molecular weight, Lavertu *et al.* concluded that a change in the molecular weight either had no effect on the gene expression, or this was increased for chitosan with lower molecular weight depending on the degree of deacetylation. For some formulations, increasing the N:P ratio from 5 to 10 led to an increase in gene expression. Also, a decrease in the pH, creating a more acidic environment, resulted in an increase of luciferase expression. Overall, for the chitosans with the lowest molecular weight (10 and 40), the gene expression was lower for low degrees of deacetylation, low N:P ratios and high pH due to weaker association of the chitosan with DNA, leading to DNA release [104].

In conclusion, high molecular weight polymers offered enhanced nucleic acid complexation and stability, but also led to aggregation and low solubility at physiological pH [130]. The high stability of the nanoparticles may result in difficulty releasing the nucleic acids inside the cell, leading to low or delayed transfection [38]. Complexes with low molecular weight and low degree of deacetylation are not stable enough for transfection due to low complexation. Nevertheless, efficient intracellular release would be easy to achieve [104, 130]. Transfection efficiency with this kind of chitosan is, however, improved when the complexes are formulated at high polymer, nucleic acid mass ratios [104, 126]. A balance between these two extreme situations needs to be achieved in order to an enhanced *in vitro* gene delivery by chitosan.

Chitosan derivatives

Different derivatives of chitosan have been synthesized to address some of the issues that impair the transfection efficiency of chitosan (Table 2). Chitosan was modified to enhance solubility at physiological pH [131] and to increase colloidal stability of the nanoparticles between chitosan and nucleic acids, in order to increase the circulation

time [132], to allow specific targeting by grafting of ligands [133] and to the increase proton sponge capacity [134].

Table 2 - Summary table of chitosan derivatives.

Chitosan derivative	Chemical Structure	Aim of Substitution
Trimethylated chitosan or N-trimethyl chitosan [135]	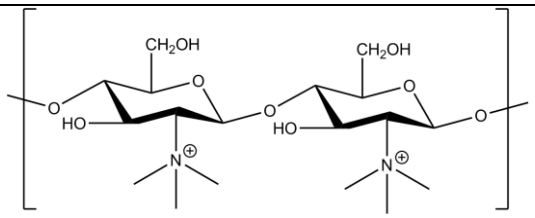	To increase water solubility as well as give a permanent positive charge independent of the pH of the medium
Urocanic acid-modified chitosan [136]	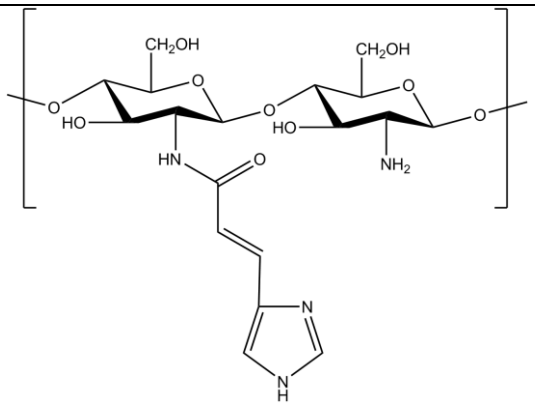	To increase buffer capacity of chitosan.
Imidazole modified chitosan [111]	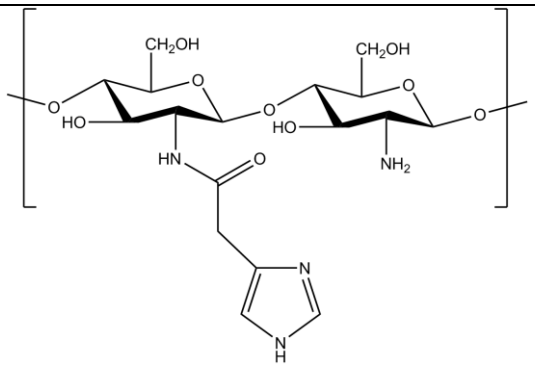	To increase buffer capacity of chitosan.
Polyethylenimine-graft-chitosan [137-139]	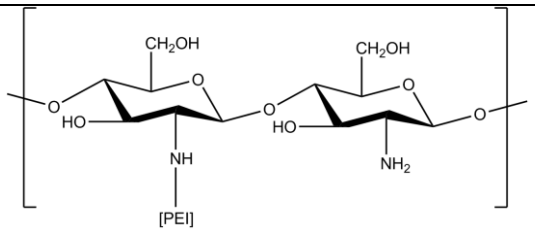	To increase buffer capacity of chitosan.

The first of these strategies involves the N-quaternization of chitosan amines to increase water solubility as well as give a permanent positive charge independent of the pH of the medium. Thanou *et al.* was the first to test, in COS-1 and Caco-2 cells, two substituted low molecular weight chitosans with two different degrees of quaternization 40% and 50%. Both polymers showed improved transfection efficiency when compared with chitosan (1-fold higher) and naked DNA in both cell lines (52-fold

higher than naked DNA for chitosan 50% quaternized and 131-fold higher for chitosan 40% quaternized in COS-1 cells). Both polymers showed lower gene expression results than the positive control lipoplex DOTAP for both cell lines in the absence of serum. The viability of the cells was studied by 3-(4,5-Dimethylthiazol-2-yl)-2,5-diphenyltetrazolium bromide (MTT) assay after 6h of incubation. Neither chitosan nor trimethylated chitosan had an effect on the viability of the two cell lines [135].

The impact of molecular weight and degree of trimethylation on cell viability and transfection efficiency was further evaluated by Kean *et al.*. The N-trimethyl chitosan polymers (100 kDa) and oligomers (3-6 kDa) showed improved transfection efficiency when compared with PEI (16- to 50-fold increase). The transfection efficiency was dependent on the percentage of quaternization with a maximum obtained for the polymer 44% quaternized in COS-7 cells. Toxicity of the different derivatives of chitosan was also studied. High molecular weight polymers (100 kDa, 55% degree of trimethylation, IC50 > 10000 µg mL^{-1}) had a higher effect on cell viability than oligomers (6 kDa, 57% degree of trimethylation, IC50 = 676±329 µg mL^{-1} in COS-7) at the same degree of trimethylation. For both sets of polymers, biocompatibility decreased with an increase of the degree of trimethylation. This was observed to a greater extent for chitosans with high molecular weights. Nevertheless, all the derivatives presented lower toxicity than PEI (25 kDa linear IC50 < 30 µg mL^{-1}) [102]. To overcome toxicity and further improve transfection rates, a number of secondary derivatives have been made. These include PEG-graft-trimethyl chitosans [131, 140] and thiolated trimethyl chitosans [141].

The increase of the buffer capacity of chitosan was attempted by the synthesis of chitosan derivatives with an imidazole ring through the addition of different functional groups such as histidine [111] or urocanic acid to the chitosan backbone [136]. Kim *et al.* conjugated chitosan with various ratios of urocanic acid, showing reduced cytotoxicity (over 90% cell viability) and enhanced transfection efficiency [136]. The transfection efficiency for all derivatives was higher than chitosan (1- to 3-fold) and increased with an increase in the substitution. However, the gene expression of all the polymers was still lower when compared with the positive control lipofectamine (100-fold) in the absence of medium.

Also, with the objective of increasing the transfection efficiency of chitosan through the increase of the buffer capacity of the polymer, several authors reported on the modification of chitosan or chitosan derivatives with PEI [137-139]. The objective was the combination of a biocompatible and biodegradable backbone (chitosan) with

increased charge density (PEI) to enable an increased proton sponge effect. The obtained PEI-chitosan polymers revealed transfection efficiencies in HepG2, HeLa, and primary hepatocytes, 5.2-, 4.3-, and 1.5-fold higher than PEI (25 kDa). The new derivatives also showed higher biocompatibility, with an IC50 of 97.3 μg mL^{-1} when compared with 13.5 μg mL^{-1} for PEI [137]. Delivery of siRNA was also achieved with PEI-chitosan. Down-regulation of EGFP was approximately 2.5-fold higher when compared with PEI (25 kDa) in A549 cells. The chitosan derivative showed good biocompatibility, with 90% of the cells viable [139].

Nose to brain delivery of chitosan

Despite the good results with chitosan and siRNA *in vitro,* the use of chitosan *in vivo* is impaired by chitosan's low solubility at physiological pH and its poor buffer capacity. *In vivo* delivery of siRNA by chitosan is characterized by instability due to the presence blood components, such as serum proteins and nucleases, and insufficient intracellular siRNA release [142].

The first human clinical trial using siRNA started in 2004 for the treatment of blinding choroidal neovascularization by direct intraocular siRNA injections [143]. Other human trials have been reported with intranasal administration of siRNA against the N-protein of respiratory syncytial virus [144] and intradermal direct injection of siRNA against a skin disorder called pachyonychia congenital [145].

In vivo administration of nucleic acids to the central nervous system is restrained by the blood brain barrier (BBB). The BBB is a physical barrier with endothelial tight junctions that present very low permeability, with the transport across mainly possible due to the presence of selective receptors. Only small (molecular weight < 500 Da), lipophilic molecules are able to cross the BBB via transcellular passive diffusion. The majority of high molecular weight molecules (> 500 Da) are not able to cross the barrier [146, 147].

siRNA is a hydrophilic molecule with a molecular weight of 13 kDa that does not cross the BBB passively. Different methods have been used for its delivery to the central nervous system. Intraparenchymal, intracerebroventricular, and intrathecal injections/infusions were used for siRNA delivery; however, these procedures are invasive and not practical for long treatments [147].

Intranasal administration is a non-invasive method of bypassing the BBB. This route is an appropriate method for the delivery of therapeutic molecules with a specific targeting to the brain in a practical, rapid and simple way, avoiding the adverse effects of systemic delivery. Nose to brain delivery is mainly mediated by the olfactory and trigeminal nerve pathways that connect the brain with the nasal cavity. These routes present the most direct, non-invasive entry into the brain [146, 148]. Intranasal delivery is a comfortable method of administration that affords an opportunity for repeated self-dosing. However, this kind of delivery presents some limitations such as a restricted compound molecular weight, variability in the concentration achieved in different regions of the brain and rapid elimination of the substances from the nasal cavity due to mucocilliary clearance. Mucosal damage and irritation can also arise due to frequent use of this route [149, 150].

The delivery of siRNA to the brain through the nasal cavity has been tried by different groups. Some investigators attempted nose to brain delivery of naked siRNA [151, 152]. Others tested the use of a range of delivery systems to protect the siRNA from enzymatic degradation and to enhance its delivery, cellular uptake and release in the cell cytoplasm in order to be incorporated in the RNAi machinery [153-155].

Kim *et al.* examined the efficiency of intranasal delivery of naked siRNA to normal rat brains. The group also studied specific gene silencing using fluorescence labelled non-specific siRNA and gene-specific siRNA for the protein αB-crystallin. *In vivo* target gene knockdown by the intranasal delivery of αB-crystallin siRNA was examined in the olfactory bulb, amygdala and hypothalamus. After 3 hours of delivery there was no change in αB-crystallin immunoreactivity in any of the brain areas studied. However, after 12 hours of siRNA delivery, αB-crystallin levels were significantly reduced in all three regions. For non-specific siRNA transfection there was no change in the αB-crystallin immunoreactivity at any time point. These results indicated that the intranasal siRNA delivery enhanced the access to the central nervous system by the olfactory nerve pathway, allowing gene silencing in specific regions of the brain [151].

The work of Renner *et al.* confirmed the role of the olfactory nerve pathway in the delivery of siRNA to the central nervous system. The route followed by fluorescently-labelled siRNA after intranasal administration was visualized by confocal laser microscopy. Again, the siRNA was administered without any gene delivery system. Thirty minutes after administration it was possible to observe siRNA in the olfactory epithelia, olfactory bulbs and along the length of the olfactory nerve pathway. Furthermore, intact siRNA was extracted from the olfactory bulbs of the mice [152].

Intranasal delivery of fluorescently-labelled siRNA with a biodegradable PAMAM dendrimer was reported [153]. The efficiency of intranasal siRNA delivery was studied in normal rat brains by triple fluorescent labelling with fluorescein isothiocyanate (FITC)-labelled control siRNA, cell-type specific immunostaining, and 4',6-diamidino-2-phenylindole (DAPI) staining. One hour after intranasal delivery, fluorescently-labelled cells were observed in the frontal cortex. The same was observed after 3 and 12 hours. Fluorescently-labelled cells were also found in other parts of the brain such as the olfactory bulb, amygdala and hypothalamus. Expression levels of HMGB1 (high-mobility group box 1, a gene implicated in stroke pathology) were studied by immunohistochemical analysis using anti-HMGB1 antibody in the olfactory bulb, amygdala and hypothalamus after delivery of HMGB1 siRNA or nonspecific siRNA with a PAMAM dendrimer. The immunoreactivity of HMGB1 decreased in the three brain areas, in the study, after 3 hours of siRNA intranasal delivery. The decrease was prolonged for 12 hours. In contrast, no decrease of HMGB1 expression was found for nonspecific siRNA. These results indicated that access to the central nervous system through the olfactory pathway was possible after intranasal administration. Gene silencing in other parts of the brain was also analysed, showing HMGB1 knockdown in the prefrontal cortex as well as in the pons and hippocampus. The previous results were confirmed by immunoblot and real-time polymerase chain reaction (PCR) analysis. Target gene expression suppression was reported in many brain regions [153].

Intranasal delivery of siRNA with cell-penetrating, peptide-modified, nanosized micelles was studied [154]. The micelles were prepared from methoxy poly(ethylene glycol) (MPEG) / polycaprolactone (PCL) copolymers conjugated with a cell-penetrating peptide, Tat (MPEG-PCL-Tat). The brain distribution of fluorescently-labelled siRNA was significantly higher after intranasal administration when compared with intravenous administration. Levels in brain tissue after intranasal delivery of siRNA with MPEG-PCL-Tat were also higher when compared with naked siRNA. The delivery system enhanced the distribution in the olfactory bulb when compared with naked siRNA, suggesting the delivery of siRNA to the brain is through the olfactory bulb pathway. Similar results were obtained in the trigeminal nerve, suggesting that it is also a possible way to reach the brain. In addition, fluorescence was also visible in the brainstem, rostral brain tissue and caudal brain tissue following intranasal delivery of siRNA with the micellar system, suggesting that after migration through the olfactory and trigeminal nerve to the olfactory bulb, siRNA was also delivered to other brain tissues [154].

The intranasal delivery of siRNA with the previous micellar system was studied in a Intracranial C6 Glioma Model [155]. Intracellular delivery and antitumour effects of siRNA for Raf-1 (involved in cell proliferation and apoptosis) were investigated in rats with malignant glioma. The association of siRNA and an anti-cancer drug (CPT) was also evaluated. Untreated rats had a mean survival period of 16.6 days and 18.4 days for rats treated with naked siRNA solution. Significant differences were observed when the previous results were compared with the mean survival period of rats treated with MPEG-PCL-Tat/siRaf-1 (20.4 days), CPT-loaded MPEG-PCL-Tat/siRNA Control (20.6 days), and CPT-loaded MPEG-PCL-Tat/siRaf-1 (28.4 days) [155].

To date, chitosan has only been used for siRNA delivery from nose to the brain as an adjuvant in a dendrimer-siRNA formulation. [^{32}P]-siRNA, complexed with Poly(amidoamine) G7 dendrimers, was administered intranasally within an *in situ*-forming mucoadhesive gel prepared with thermosensitive poloxamer and mucoadhesive chitosan. Brain radioactivity was higher after intranasal delivery of dendriplexes both in the gel and in the buffer when compared with the intravenous route. After two doses of siRNA gel delivery the brain radioactivity increased by two-fold when compared with siRNA buffer delivery, and by eight-fold when compared with naked siRNA. Radioactivity was higher in the olfactory bulb and hypothalamus after siRNA intranasal gel administration than after intravenous or intranasal in buffer administration [156].

Chitosan presents mucoadhesive properties that make it a good candidate for nasal delivery of high molecular weight compounds [157]. Chitosan has been successfully used as adjuvant for nose to brain delivery due to its mucoadhesive permeation properties [156]. These properties are probably linked to its cationic structure, which can interact with the anionic structures present in the mucus layer. The mucoadhesive characteristics of the chitosans may help to overcome the rapid turnover rate of the secretions allowing prolonged contact between the formulation and the olfactory region [149, 158].

1.3 Aims

Despite the efforts to develop chitosan-based vectors, the therapeutic effectiveness of chitosan-based gene therapy still needs to be improved in order to achieve clinical significance. To date there have been no reports of clinical trials for the delivery of DNA or siRNA using chitosan as the delivery system [54]. Chitosans need to overcome the different extracellular and intracellular barriers in order to be used successfully as nanocarriers for gene therapy [159]. The success of gene therapy is dependent on the ability of the delivery system to protect nucleic acids in physiological conditions, to reach the target cells, to be internalized and to deliver sufficient DNA/siRNA molecules into the cytoplasm or nucleus to obtain gene silencing [160].

The research performed with chitosan has helped researchers understand its limitations, including poor water solubility at physiological pH, and low buffer capacity, which affects its gene delivery efficiency [14, 115]. In order to increase translation from bench to bedside, efforts are focusing on the chemical and biological modification of chitosan in order to increase its solubility, specificity and endosomal escape [142].

This work introduces a new chitosan based polymer: Ethylamino Glycol Chitosan. The new polymer aims to overcome the previously described disadvantages of chitosan for gene delivery, particularly relating to chitosan's solubility and protonation at physiological pH and its low buffer capacity. The aim is to enhance chitosan's transfection efficiency while retaining its main benefits of low toxicity and biocompatibility. Nose to brain delivery of a complex formed between siRNA and a chitosan derivative will be presented for the first time.

General Objectives

1. Synthesis and physicochemical characterization of a new chitosan-based polymer for gene delivery: Ethylamino Glycol Chitosan - Chapter 2
2. Characterization of the nanoparticles formed between Ethylamino Glycol Chitosan and DNA/siRNA with regard to size, zeta potential, morphology, and behaviour when in the presence of biological challenges - Chapter 3
3. Study of the biocompatibility of Ethylamino Glycol Chitosan and its *in vitro* transfection efficiency as a delivery system for DNA - Chapter 4
4. *In vitro* and *in vivo* biological studies with Ethylamino Glycol Chitosan as a delivery system for siRNA – Chapter 5

2. Synthesis and Characterization of Ethylamino Glycol Chitosan

2.1 Introduction

Chitosan is obtained by partial deacetylation of chitin, which is the natural structural component of the crustacean exoskeleton [83]. It is a linear polysaccharide composed of D-glucosamine and N-acetyl-D-glucosamine subunits linked by β(1,4) glycosidic bonds. Because of its cationic nature, chitosan is a very popular candidate among natural polysaccharides for nucleic acid delivery. Furthermore, it displays properties such as biocompatibility and biodegradability, and its degradation products are non-toxic, non-immunogenic and non-carcinogenic [85]. Despite these advantages, the low water-solubility of chitosan at physiological pH is an important limitation for its clinical use. Deacetylated chitosan presents primary amines with a pKa ≈ 6.5, explaining why chitosan is only soluble in an acidic aqueous environment [160]. Features including the degree of deacetylation, molecular weight, and charge of chitosan determine its transfection efficiency when complexed with DNA and siRNA [109]. Chitosan polymer chains should have a sufficient charge density to avoid dissociation of the polymer and nucleic acids in the extracellular environment. Optimal transfection efficiency of chitosan polyplexes was achieved only at acidic pH. Intracellular nucleic acid delivery is further restricted by limited endosomal escape, due to the weak buffer capacity of the polymer [14, 115].

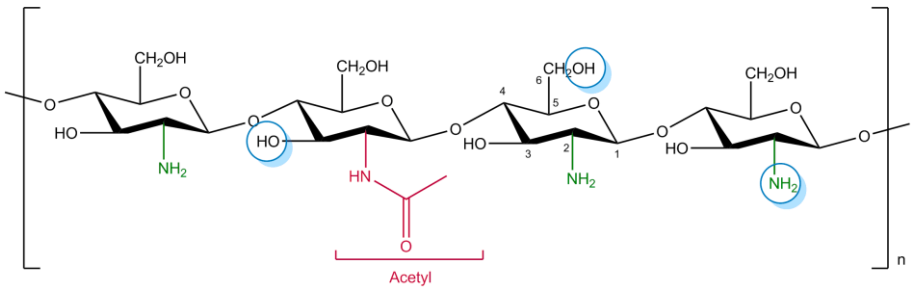

Figure 7 - Representative chemical structure of chitosan.

To improve the nucleic acid delivery capacity of chitosan, modifications to the polymer structure have been made. The chitosan monomer contains two hydroxyl groups and

one primary amine that are regarded as potential reactive sites for chemical modifications (highlighted in Figure 7). The main objectives of the synthesis of chitosan derivatives were to enhance solubility, pharmacokinetics, cationic charge density, endosomal escape, transfection efficiency and specific cell targeting [109, 161, 162].

One potential derivatisation involves the N-quaternization of the terminal amine groups on chitosan, increasing its water solubility and resulting in a permanent positive charge on the molecule [135]. These N-trimethyl chitosan polymers (100 kDa) and oligomers (3-6 kDa) showed a 16- to 50-fold increase in transfection efficiency when compared with PEI. The transfection efficiency was dependent on the percentage of quaternization, with a maximum obtained for the polymer 44% quaternized in COS-7 cells. However, increasing the degree of trimethylation increased the toxicity of the polymer [102, 135]. To overcome the toxicity issues and further improve transfection rates a number of secondary derivatives have been made, including PEG-graft-trimethyl chitosans [131, 140] and thiolated trimethyl chitosans [141].

To increase the cationic charge density and endosomal escape of chitosan, an imidazole ring was grafted to the chitosan backbone through the addition of different functional groups such as histidine [111] or urocanic acid [136]. Kim *et al.* conjugated chitosan with various ratios of urocanic acid, and showed reduced cytotoxicity (over 90% cell viability) and enhanced transfection efficiency. All the derivatives tested showed a higher transfection efficiency than unmodified chitosan (1- to 3- fold), and increased with an increase in the level of substitution. However, the gene expression of all the polymers was still lower when compared with the positive control lipofectamine (100-fold) in the absence of medium [136].

Several authors reported on the addition of PEI to chitosan or chitosan derivatives. The objective of these studies was the combination of a biocompatible and biodegradable backbone (chitosan) with increased charge density (PEI) to enable an increased proton sponge effect. The obtained PEI-chitosan polymers showed lower cytotoxicity (IC50 of 97.3 µg mL^{-1} when compared with 13.5 µg mL^{-1} for PEI) and higher transfection efficiency for DNA and siRNA when compared with PEI both *in vitro* and *in vivo* [137-139]. In HepG2, HeLa, and primary hepatocytes, the obtained PEI-chitosan polymers revealed transfection efficiencies 5.2-, 4.3-, and 1.5-fold higher than PEI alone (25 kDa). Delivery of siRNA was also achieved with PEI-Chitosan. Down-regulation of EGFP was approximately 2.5-fold higher when compared with PEI (25 kDa) in A549 cells [139].

This chapter presents the results of the synthesis and characterization of a new chitosan-based polymer for gene delivery: Ethylamino Glycol Chitosan. The different steps of the synthesis of the new polymer will be discussed as well as the reaction conditions that might affect the final product. The molecular weight and buffer capacity of three batches of EAGC were determined.

2.2 Methods

2.2.1 Synthesis of Ethyl Amino Glycol Chitosan

The acid degradation of glycol chitosan was carried out as previously described [163]. Glycol Chitosan (1g) (Sigma Aldrich, Dorset, UK) was dissolved in hydrochloric acid (4M, 76 mL) and placed for 4 or 8 hours in a preheated water bath at 50ºC. The product resulting from the acid degradation was purified by dialysis (Visking seamless cellulose tubing, molecular weight cut off 7000 Da) against deionised water (5L) with six changes over 24 hours. The dialysed solution was freeze-dried and the product recovered looked like cotton with a cream colouration.

The degraded GC (100 mg) was dissolved in a solution of N-methyl-2-pyrrolidone (NMP) (20 mL) (Sigma Aldrich, Dorset, UK) and triethylamine (TEA) (Sigma Aldrich, Dorset, UK) in excess (500μL). The solution was allowed to stir for 1h at 40ºC in an oil bath until the GC was completely dissolved. The primary amino end group of the introduced ethylamine was protected with *tert*-butoxycarbonyl (Boc) to avoid cross-reaction during synthesis 2-(Boc-amino) ethyl bromide ($BrCH_2CH_2NHCO_2C(CH_3)_3$) (200 mg) (Sigma Aldrich, Dorset, UK), with a molar ratio between the GC and $BrCH_2CH_2NHBoc$ of 1:2, 1:5 or 1:10 was added. This reaction was left to stir for 24h, at 40ºC. Finally the solution was mixed with water (40 mL) and washed with diethyl ether (3x50 mL) to extract the unreacted 2-(Boc-amino) ethyl bromide. The aqueous phase was collected and dialyzed, as previously, against deionised water (5L) with six changes over 24 hours. The final polymer solution was freeze-dried. The polymer recovered was dissolved in a hydrochloric acid solution (50 ml, 4M) and stirred for 3 hours at room temperature, allowing the cleavage of the Boc group. This solution was dialyzed as previously described and freeze dried to give N-(2-ethylamino)-6-O-glycol chitosan.

2.2.2 Characterization of Ethylamino Glycol Chitosan

2.2.2.1 Laser Light Scattering (LLS) and Gel Permeation Chromatography (GPC)

Gel permeation chromatography, also known as size exclusion chromatography, is a chromatographic approach used to separate macromolecules according to their hydrodynamic volume, which is dependent on both molecular weight and molecular

conformation of a compound in solution [164]. Molecules with large hydrodynamic radii cannot diffuse into the pores of the gel filtration medium and elute first from the column, while smaller molecules that diffuse inside the pores, elute later from the column based on their size. The eluting compound is characterized for molecular weight by an interferometric refractometer, which measures changes in the refractive index (RI) of the sample, with changes in concentration (dn/dc), and a multi-angle laser light scattering (MALLS) detector which measures the intensity of light scattered by the polymers.

The molecular weight of GC and EAGC were determined by GPC-MALLS equipped with DAWN® EOS® MALLS, Optilab rEX Interferometric Refractometer (λ = 690 nm) and QELS detectors (Wyatt Technology Corporation, USA), using as mobile phase sodium acetate buffer (0.5 M CH_3COONa (anhydrous) / 0.2 M CH_3COOH, pH 4.5). Filtered samples were injected using an Agilent 1200 Series into a POLYSEP-GFC-P guard column (35 x 7.8 mm, Phenomenex, UK) attached to a POLYSEP-GFC-P 4000 column at a loading concentration of 5 mg mL^{-1}. The measurements were performed at room temperature with a mobile phase flow rate of 0.7 mL min^{-1}. The data were processed using ASTRA for Windows version 5 software (Wyatt Technology Corporation, USA).

dn/dc Measurement

The specific refractive index increment (*dn/dc*) of GC and EAGC were measured in sodium acetate buffer, as previously, with an Optilab rEX Interferometric Refractometer. Filtered samples (0.2 µm, 33 mm Millex MP syringe driven filter unit, polyethersulfone (PES) membrane for sterilization of aqueous solutions) of 6 different concentrations ranging from 0.1-0.6 mg mL^{-1} were manually injected using an injection system (Wyatt Technology Corporation, USA) at a pump flow rate of 0.3 mL min^{-1}. The data were processed using Wyatt ASTRA for Windows version 5 software.

2.2.2.2 Nuclear Magnetic Resonance (NMR) Spectroscopy

Nuclear magnetic resonance spectroscopy is a very important technique in polymer characterization, since NMR signals can be assigned to specific atoms along the polymer backbone and side chains. The identification of certain atoms or groups in a polymer molecule as well as their positions relative to each other can be obtained by one- and two-dimensional NMR spectra [164].

The principles of nuclear magnetic resonance (NMR) spectroscopy are based on the excitation of protons (^{1}H) or carbon-13 (^{13}C) atoms by radiation in the radiofrequency region. When a compound containing protons or carbon nuclei is placed in a very strong magnetic field and simultaneously irradiated with electromagnetic energy of the appropriate frequency, nuclei of the compound absorb energy through a process called magnetic resonance [165]. The range of frequencies required for excitation and the signal patterns produced when the excited atoms relax are characteristic of the chemical structure of the molecule. The frequency of the signal is known as the chemical shift (δ) and is determined in relation to the protons of a standard, usually tetramethylsilane (TMS), which are arbitrarily assigned a shift of δ=0ppm. The area under each peak in the ^{1}H NMR spectrum is proportional to the number of contributing protons [166]. In the presence of an electronegative group, which withdraws electron density from neighbouring protons, the deshielded proton will require less applied magnetic field to change the direction of its spin. This results in a downfield shift (i.e. to the left of a spectrum) compared to the more shielded protons, which are surrounded by circulating electrons. ^{1}H-^{1}H Correlated Spectroscopy (COSY) shows the NMR spectra in two dimensions and the interactions between neighbouring protons, while Heteronuclear Multiple Quantum Correlation (HMQC) shows correlation between carbon atoms and the protons attached to them [165, 166].

^{1}H NMR, ^{1}H-^{1}H COSY, ^{13}C Distortionless Enhancement by Polarization Transfer (DEPT) NMR and HMQC were performed on GC and EAGC in Deuterium Oxide (D_2O, Sigma Aldrich, Dorset, UK) (25 mg mL^{-1}) (Bruker AMX 500 MHz spectrometer, Bruker Instruments, UK). Number of scans: 128 for ^{1}H, 16 for COSY, 6000 for ^{13}C and 104 for HMQC. Full parameters are attached to each spectrum.

2.2.3 Titration

In a potentiometric titration the potential of a suitable indicator electrode is measured as a function of titrant volume [167]. The electrode that is usually used to make the measurements is a pH-sensitive glass indicator electrode.

GC and EAGC were dissolved in water (2 mg mL^{-1}) and titrated with NaOH (0.05M). The pH of the initial solutions was adjusted to 2 with HCl (0.1M). Under continuous stirring, titrant was added dropwise. The volume of NaOH added and pH values of

polymer solutions were recorded thoroughly using a MPT-2 Autotitrator, (Malvern Instruments, Malvern, UK).

The buffer capacity was defined as the percentage of amino groups that become protonated in the pH range 5.1 to 7.4, and can be calculated from the following equation:

$$\textit{Buffer capacity (\%)} = [(\Delta V_{NaOH} \times 0.05M)/Nmol]*100$$

where ΔV_{NaOH} , is the volume of NaOH solution (0.05 M) required to bring the pH value of the polymer solution from 5.1 to 7.4, and Nmol is the total moles of protonatable amine groups in the known amount of EAGC and GC (20 mg) [168].

2.3 Results

EAGC was prepared in a two-step reaction (Figure 8). Firstly, 2-(Boc-amino) ethyl bromide ($BrCH_2CH_2NHCO_2C(CH_3)_3$) was reacted in a basic environment with the primary amines of GC. TEA was added to maintain a basic environment that avoids protonation of the GC primary amines. The primary amino end group of the introduced ethylamine was protected with Boc to avoid cross-reaction during synthesis. A water/ether extraction was performed to solubilize the substituted polymer in water and extraction with ether of the unreacted products. Finally, the Boc-protection was removed from the amino groups by acidic cleavage. EAGC was isolated as its HCl-salt by dialyses and freeze-drying, with a final yield range between 31 and 88% (Table 3). The number of ethylamino groups per mole of GC was controlled regarding the initial molar ratio between GC and $BrCH_2CH_2NHBoc$.

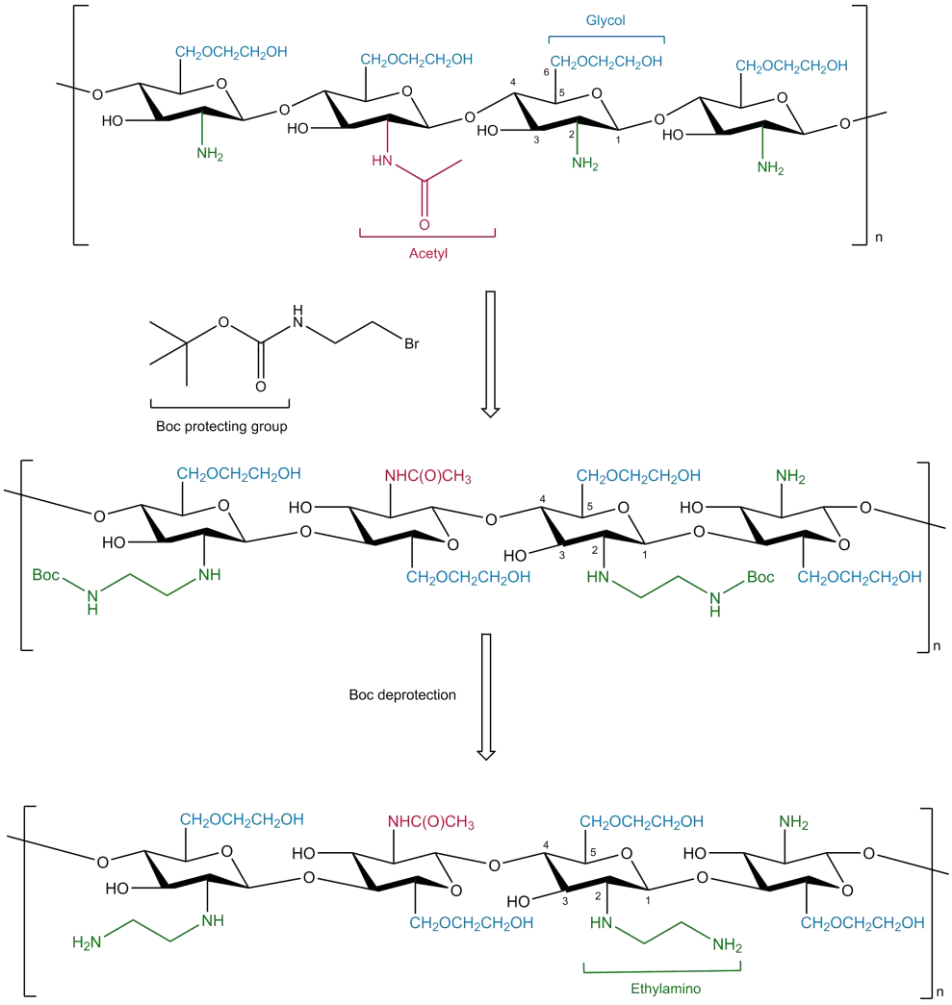

Figure 8 - Expected chemical reaction between GC and 2-(Boc-amino) ethyl bromide with N-(2-ethylamino)-6-O-glycol chitosan as final product.

Table 3 - Yield of the different polymers synthesized.

Polymer	Yield (%)
EAGC14 (Figure 23)	31%
EAGC11 (Figure 27)	76%
EAGC13 (Figure 33)	88%
EAGC17 (Figure 38)	65%
EAGC21 (Figure 42)	60%
EAGC30 (Figure 46)	60%

2.3.1 Laser Light Scattering and Gel Permeation Chromatography

Figure 9 shows the chromatogram of degraded Glycol Chitosan (8h) and Figure 10 dn/dc curve. Figure 11 shows the chromatogram of Ethylamino Glycol Chitosan (EAGC21) and Figure 12 the *dn/dc* curve (the chromatograms and dn/dc curves of GC (4h), EAGC17 and EAGC30 can be found in appendix). Table 4 summarizes the molecular weights obtained by GPC-MALLS for two batches of GC and three batches of EAGC. The molecular weight results were expressed as Mn, the number averaged molecular weight, and Mw, the weight averaged molecular weight. The polydispersity was calculated as a ratio Mw/Mn.

The Mn of Glycol Chitosan was 28480 Da for GC28 (4h) and 17430 Da for GC17 (8h) and Mw/Mn 1.026 and 1.006 respectively. Increasing the acid degradation time decreased the molecular weight of the resulting polymer. Two different polymers with different molecular weight were used to synthesize EAGC different batches. EAGC17 and 21 were synthesized from GC17 and EAGC30 was synthesized from GC28. Mn, Mw and Mw/Mn of the three batches of EAGC are presented in Table 4. It is of note that EAGC17 presents a slightly smaller molecular weight than the starting material, GC17. Nevertheless, the difference is so small that it is probably related with the sensitivity of the technique used. In the following text, GC17 will refer to glycol chitosan with 17 kDa and GC28 to glycol chitosan with 28 kDa. EAGC, however, will be referred to regarding the degree of substitution. Therefore EAGC17 has a degree of substitution of 17%, EAGC21 of 21% and EAGC30 of 30%.

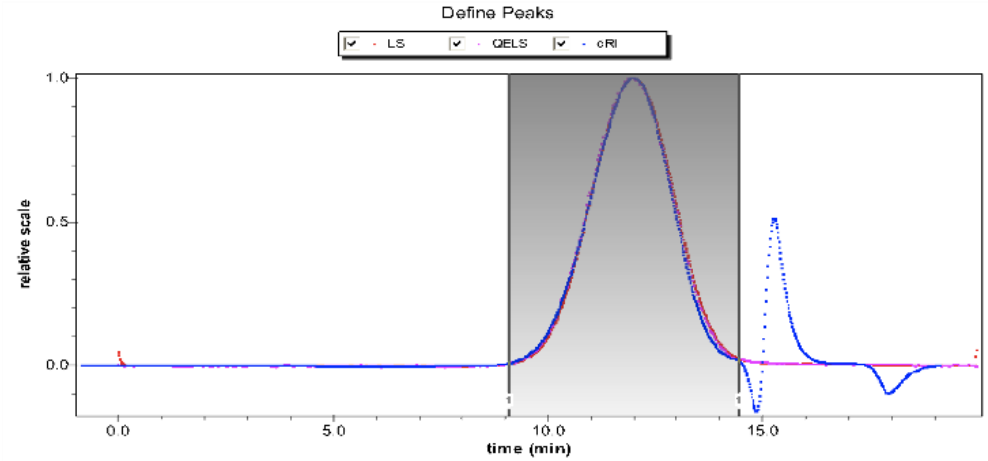

Figure 9 - GPC-MALLS Chromatogram of degraded Glycol Chitosan (8h) (5 mg mL^{-1}).

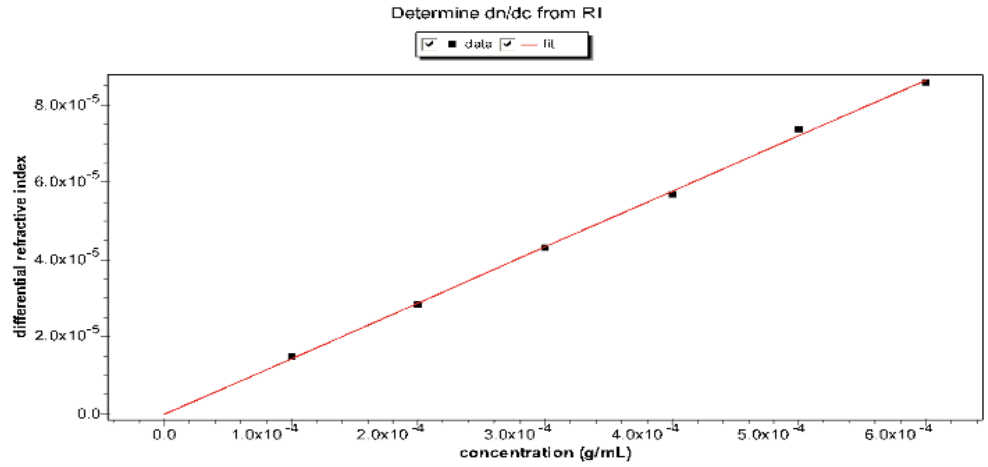

Figure 10 - dn/dc curve of Glycol Chitosan (8h).

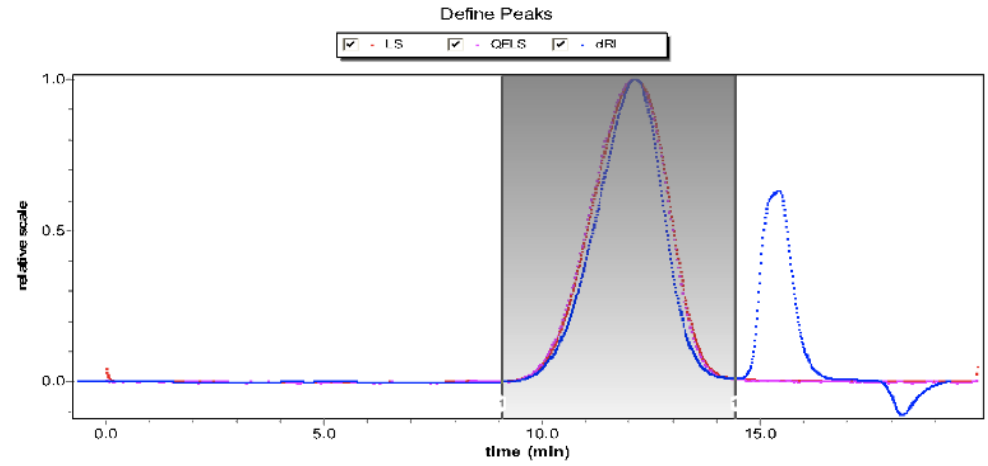

Figure 11 - GPC-MALLS Chromatogram of Ethylamino Glycol Chitosan (EAGC21) (5 mg mL^{-1}).

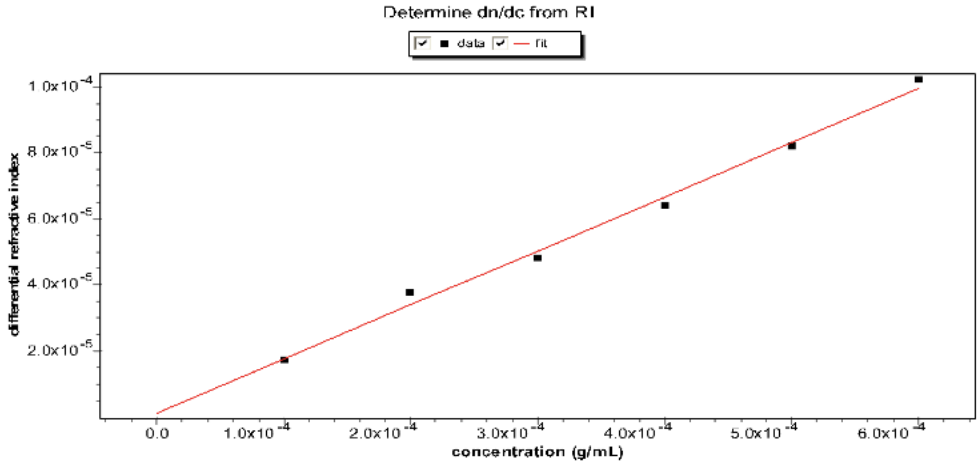

Figure 12 - dn/dc curve of Ethylamino Glycol Chitosan (EAGC21).

Table 4 - GPC-MALLS results for GC and EAGC.

Polymer	dn/dc (mL g^{-1})	Mw (Da)	Mn (Da)	Mw/Mn
GC17	0.1443±0.0026	17430	17330	1.006
GC28	0.0149±0.0002	28480	27750	1.026
EAGC17	0.1565±0.0005	16910	16730	1.011
EAGC21	0.1642±0.0072	17620	17340	1.016
EAGC30	0.1544±0.0036	29850	28290	1.055

2.3.2 NMR Spectroscopy

The structure and degree of substitution of the new polymer, EAGC, was confirmed by comparing its NMR spectra with those of the initial material, GC (Figure 13). The protons assignments for degraded GC (Figure 14) are given in Table 5.

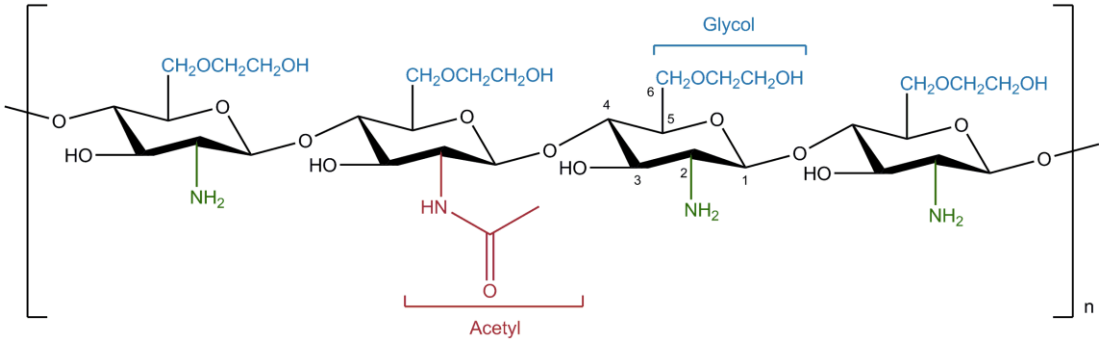

Figure 13 - Chemical Structure of Glycol Chitosan.

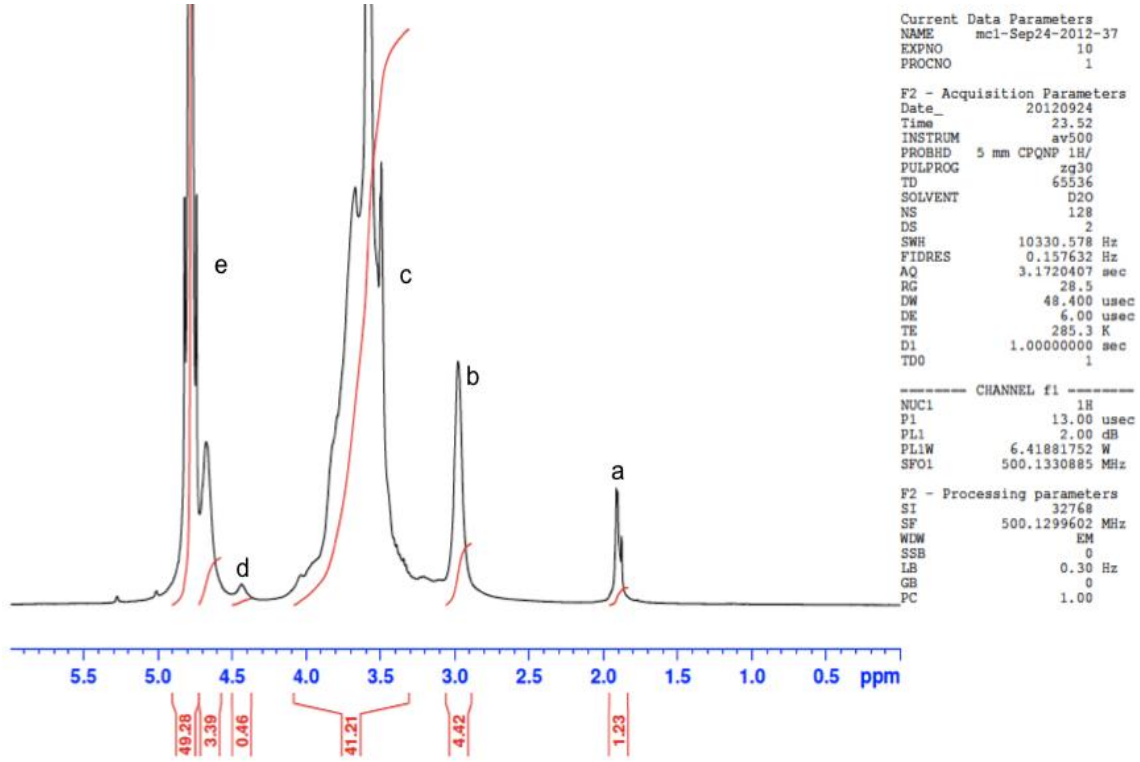

Figure 14 - ^{1}H-NMR for degraded Glycol Chitosan 17 (8h).

Table 5 - Protons assignments and chemical shifts for GC17.

Position on the H-NMR spectra	**NMR Chemical Shift**	**Corresponding proton on the structure**
a	1.9 ppm	CH_3 (acetyl group)
b	3 ppm	CH (C2)
c	3.4-4.1ppm	CH (C3, C4, C5 and Glycol)
d	4.5ppm	CH (C1)
e	4.5-5ppm	D_2O (water protons)

In the ^{1}H-^{1}H COSY NMR it is possible to observe a cross peak between the protons on C1 and C2 (d,b) and between the protons on C2 and C3 (c,b) (Figure 15).

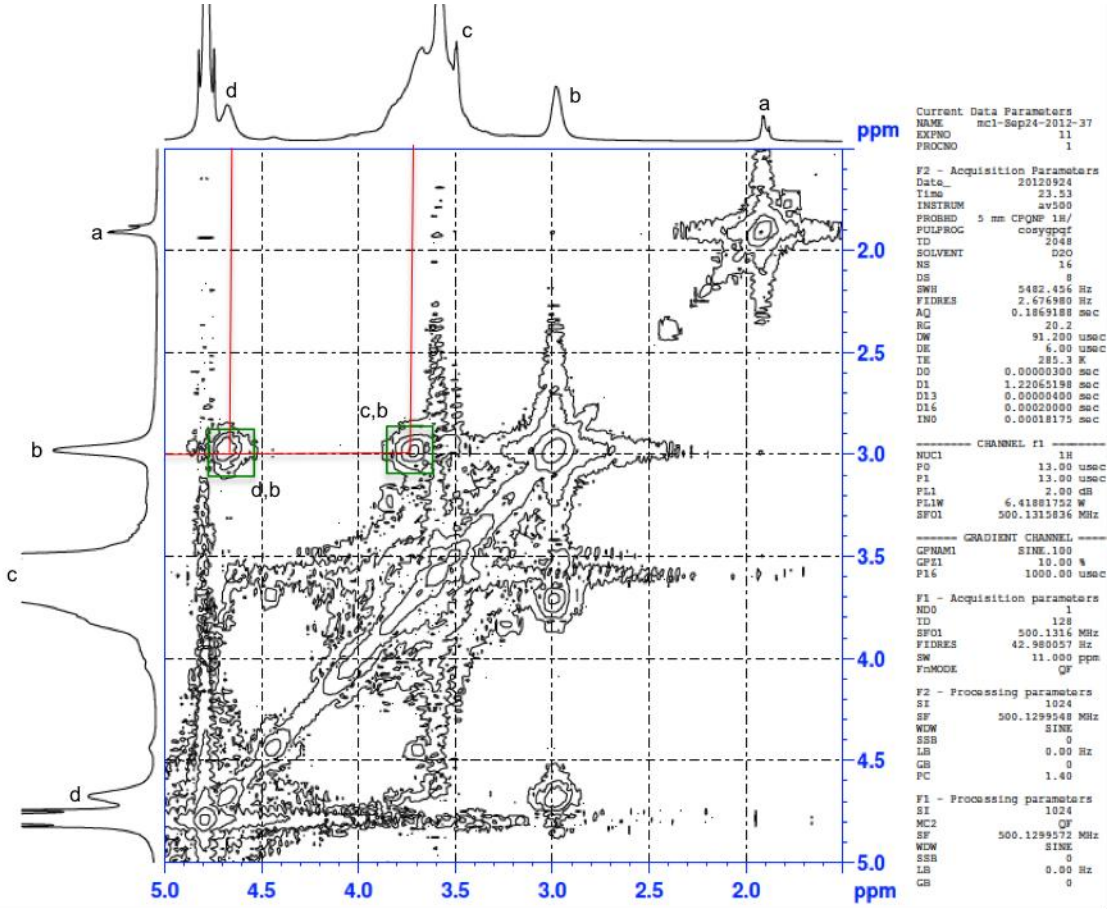

Figure 15 - ^{1}H-^{1}H COSY NMR for degraded Glycol Chitosan 17 (8h).

In the ^{13}C-DEPT NMR spectrum the positive peaks represent CH and CH_3 carbons and the negative peaks CH_2 carbons. The carbon assignments for degraded GC are presented in Table 6 and Figure 16.

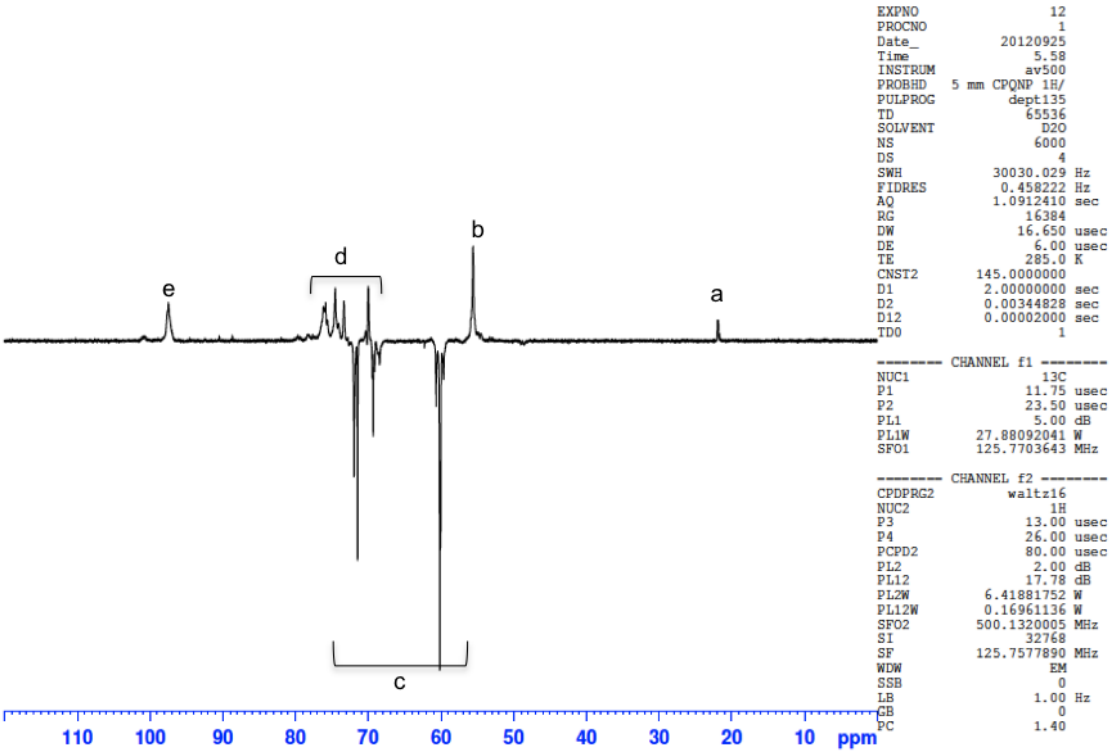

Figure 16 - ^{13}C-DEPT NMR for degraded Glycol Chitosan 17 (8h).

Table 6 - Carbons assignments and chemical shifts for GC.

Position on the C-NMR spectra	**NMR Chemical Shift**	**Corresponding carbon on the structure**
a	20 ppm	CH_3 (acetyl group)
b	56 ppm	CH (C2)
c	60, 69, 72ppm	CH_2 (Glycol)
d	73, 75, 78ppm	CH (C3, C4, C5)
e	100ppm	CH (C1)

In ^{1}H-^{13}C HMQC NMR spectrum (Figure 17) it is possible to observe the bond connection between carbons and hydrogens. The acetyl group protons 1.9ppm=CH_3 correlated with the carbon at 20ppm=CH_3 (acetyl carbon). The proton on the C2 at δ=3 ppm is aligned with carbon at δ=56 ppm. The glycol protons δ=3.4-4.1ppm correlated with CH_2 at δ=60, 69, 72 ppm. The protons C3, C4 and C5 at δ=3.5-4.1ppm are aligned with the carbons at δ=73, 75 and 78 ppm. The proton on C1 at 4.7ppm correlated with the carbon at δ=100 ppm.

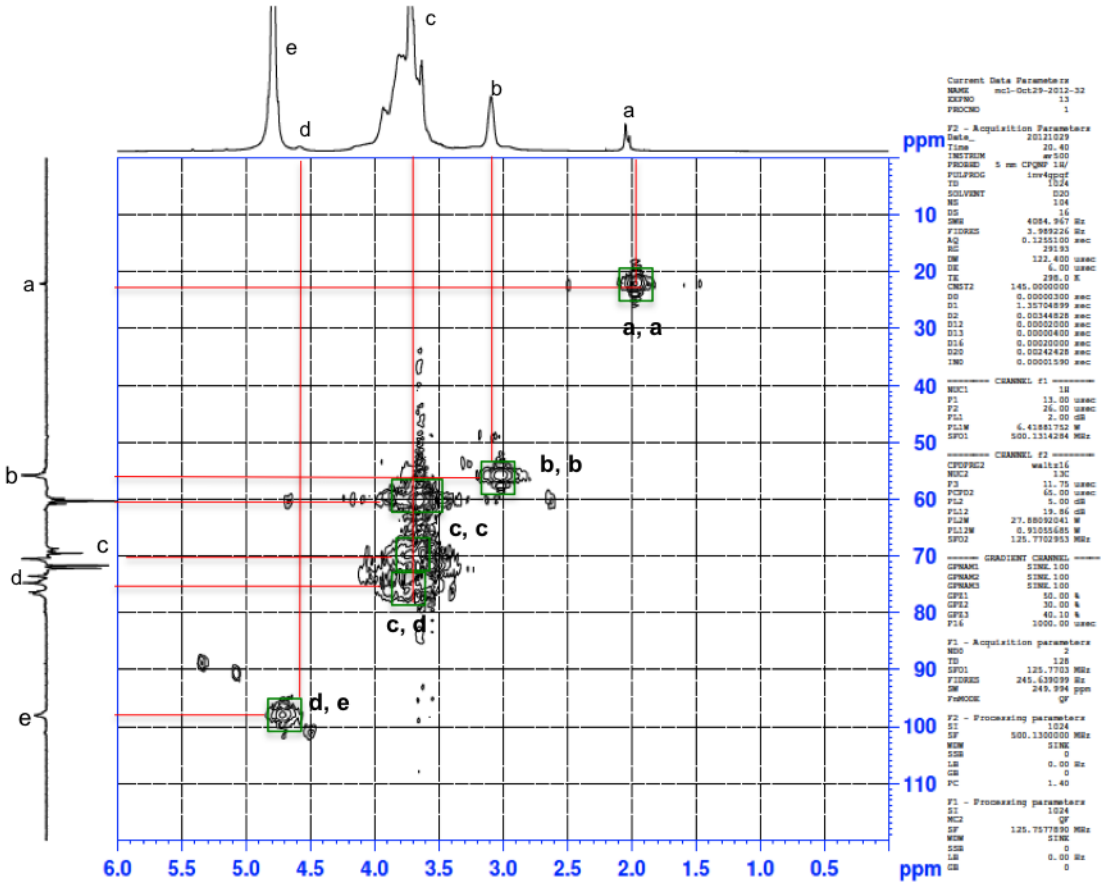

Figure 17 - ^{1}H-^{13}C HMQC NMR for degraded Glycol Chitosan 17 (8h).

The potential mechanism of the reaction between GC and $BrCH_2CH_2NHBoc$ was considered. Among the factors evaluated were the structure of the substrate, the reactivity of the nucleophile, the effect of the solvent, the nature of the leaving group, and temperature. In the reaction, the primary amines of GC behaved like a nucleophile while $BrCH_2CH_2NHBoc$ was the substrate, with the bromide anion as the leaving group. Each of these limiting steps were studied, and decisions were made, using NMR results, to achieve the best protocol conditions. As it will be discussed below, the reaction was concluded to be a 2nd order nucleophilic substitution (S_N2) (Figure 8). This type of reaction proceeds in one step (without any intermediates) through an arrangement of atoms called a transition state [169].

Structure of the substrate

The $BrCH_2CH_2NHBoc$ was chosen as the substrate considering 2 main characteristics of its structure: the stability of the carbocation (formed during the reaction) and favourable leaving group.

The stability of the carbocation is related to the number of alkyl groups attached to the positively charged trivalent carbon. Tertiary carbocations are the most stable, and the methyl carbocation is the least stable. The reactivity proceeds as follows: methyl > primary > secondary > tertiary (unreactive) [165]. Tertiary cations are not present in a S_N2 reaction since the nucleophile would have to thread its way into the carbon atom through the alkyl groups. It is better for an S_N2 reaction if there are only small hydrogen atoms on the carbon - methyl groups and primary carbocations react fastest by the S_N2 mechanism [169].

Leaving group

Two main factors should be considered when evaluating the leaving group: the strength of the C–X bond and the stability of the resultant ion. The best leaving groups are those that become either a relatively stable anion or a neutral molecule. Among the halogens, an iodide ion is the best leaving group and a fluoride ion is the poorest. (I^- > Br^- > Cl^- > F^-). The order is the opposite of the basicity. The best leaving groups are weak bases since these stabilize a negative charge effectively. The negative charge on the leaving group stabilizes the transition state of S_N2 reactions and therefore the free energy of activation is lower increasing the rate of the reaction [165, 169].

Also important was the presence of the Boc group as protection for the amines of [GC]-$CH_2CH_2NH_2$. Without protection these primary amines would behave as nucleophiles and attack the primary carbocation of the ethyl group, resulting in more than one product with different substitutions (Figure 18). These introduced amines would be at least as nucleophilic as the primary amines on the GC backbone. These cross-reactions are well known in the nucleophilic substitution of amines, and the protection with Boc group is widely used in organic chemistry because of its ease of removal.

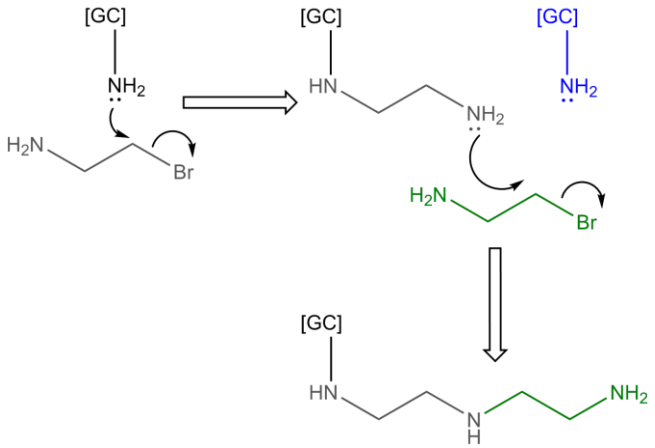

Figure 18 - Cross reaction between primary amines on GC and unprotected amines in $BrCH_2CH_2NH_2$.

Reactivity of the nucleophile

GC presents three possible nucleophiles, the primary amine (C2 amine) and the hydroxyl groups on the sugar ring and glycol chain, all of which can be modified. The majority of the chemical grafting of molecules or polymers happens on the C2 amine. The higher basicity of the amine group (compared to the hydroxyls) makes it the more reactive nucleophile [165, 170]. In order to modify the hydroxyl groups the amine group needs to be protected [171].

Effect of the solvent

Two sets of solvents were tested for the solubility of GC: ethanol/water and NMP. The objective was to find a solvent able to solubilize GC without interfering with the synthesis. NMR results obtained after the first step of the reaction (Figure 8) were used as an indicator of its success. The Boc group presents 3 methyl groups that, regarding their chemical structure, would be more shielded when compared with the other protons, resulting in a strong signal in the right side of the spectra (lower chemical shift).

Choice of Solvent

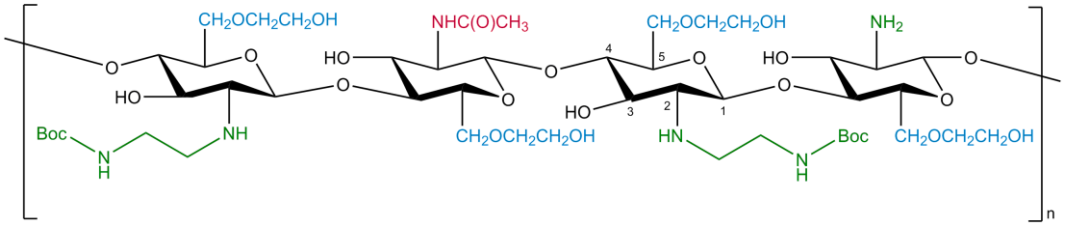

Figure 19 - Proposed chemical structure of [GC]-CH_2CH_2NHBoc.

GC, being a water-soluble derivative of chitosan, was easily soluble in the mixture water/ethanol. In the ^{1}H-NMR spectra (Figure 20) of the product between GC and $BrCH_2CH_2NHBoc$, the Boc protons signal at 1.5 ppm is very low (integration=0.05). A protic solvent (such as water/ethanol) has a hydrogen atom attached to a strongly electronegative element (oxygen or nitrogen). Therefore molecules of these solvents can form hydrogen bonds with nucleophiles [165]. It is possible that hydrogen bonding hampered the nucleophile and obstructed its reactivity in the substitution reaction resulting in a very poor degree of substitution revealed by the NMR results (Figure 20).

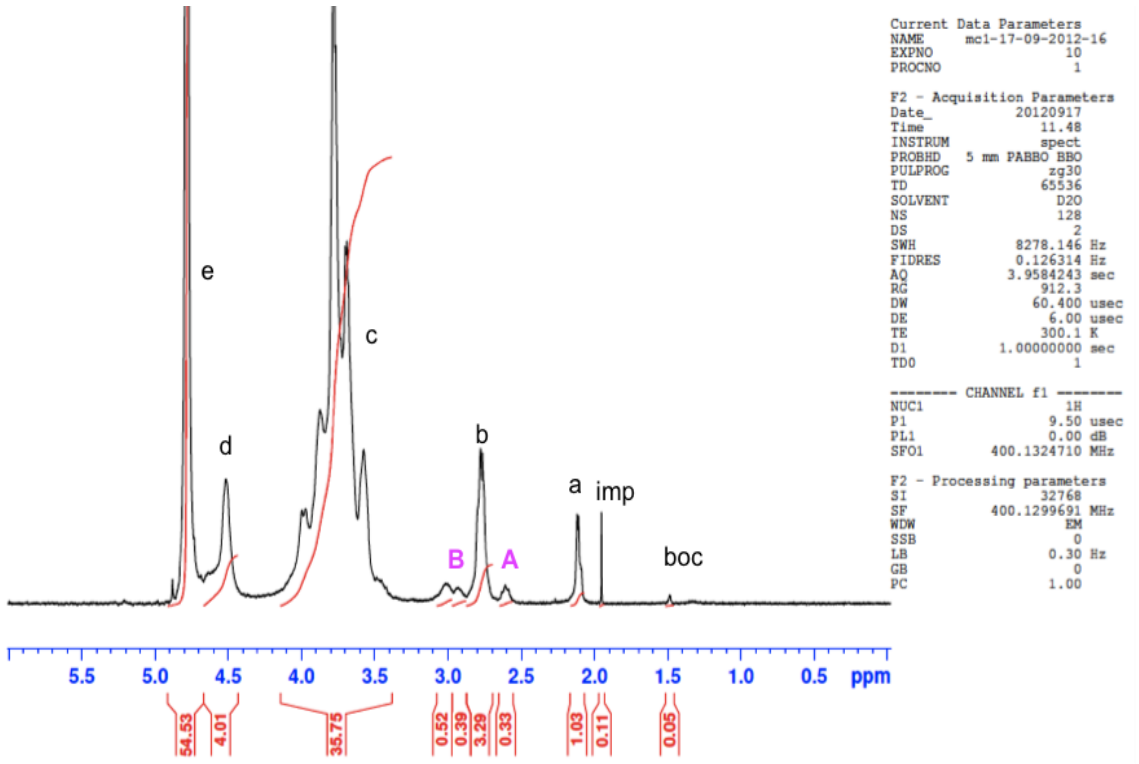

Figure 20 - ^{1}H-NMR of [GC]-CH_2CH_2NHBoc (ratio 1:2). GC solubilized in water/ethanol.

Table 7 - Protons assignments and chemical shifts for [GC]-CH_2CH_2NHBoc. GC solubilized in water/ethanol.

Position on the H-NMR spectra	**NMR Chemical Shift**	**Corresponding proton on the structure**
Boc	1.5 ppm	$(CH3)_3$ (Boc Group)
imp	1.9ppm	Solvent Impurity
a	2.1ppm	CH_3 (acetyl group)
A	2.6 ppm	CH (C2 substituted)
b	2.7ppm	CH (C2 unsubstituted)
B	2.9 and 3ppm	CH_2 (ethyl amino group)
c	3.5-4.1ppm	CH and CH_2 (C3, C4, C5 and Glycol
d	4.5ppm	CH (C1)
e	4.7-4.9ppm	D_2O (Water protons)

GC was not as soluble in NMP as in water/ethanol, though the NMR results were more promising with an integration of the Boc methyl groups twenty times higher, (integration=1.03) (Figure 21). Polar aprotic solvents (e.g. N,N-dimethylformamide (DMF), dimethyl sulfoxide (DMSO), NMP) do not have a hydrogen atom bonded to an electronegative atom, and therefore do not hinder nucleophiles through hydrogen bonding. In these solvents anions are unencumbered by a layer of solvent molecules and they are consequently poorly stabilized by solvation. This makes them highly reactive as nucleophiles [165]. Furthermore, the rates of S_N2 reactions generally are vastly increased when they are carried out in aprotic solvents [165, 172]. NMR results showed that NMP was a more suitable reagent, and was used for the following experimental reactions.

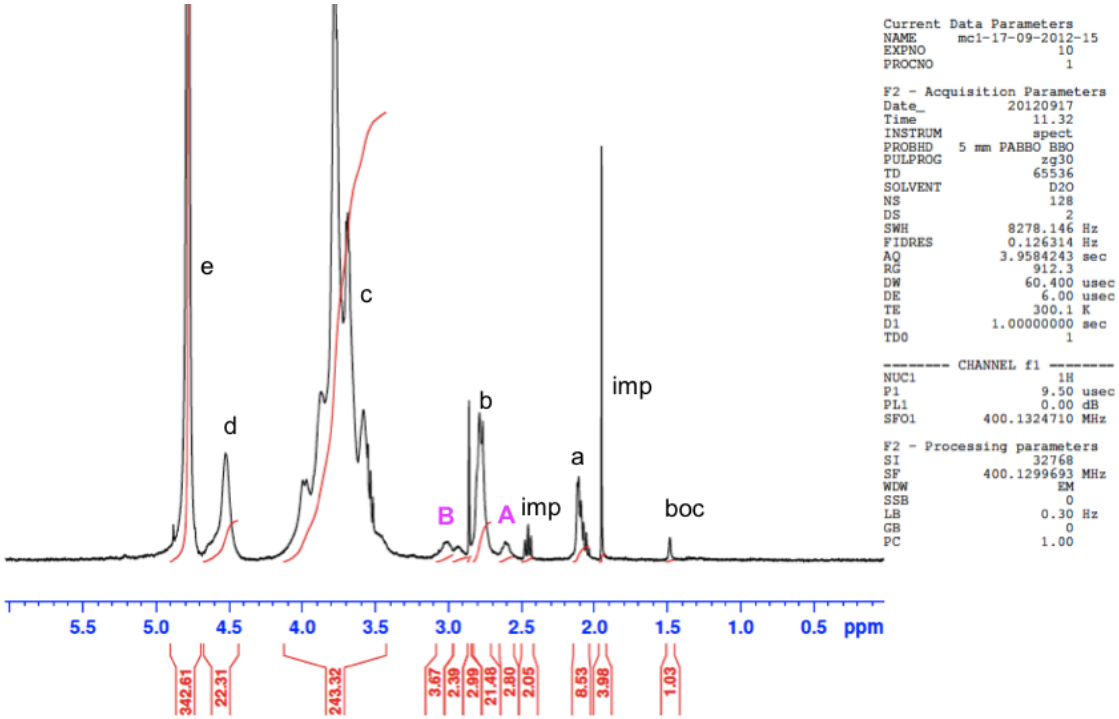

Figure 21 - ^{1}H-NMR of [GC]-CH_2CH_2NHBoc (ratio 1:2). GC solubilized in NMP.

Table 8 - Protons assignments and chemical shifts for [GC]-CH_2CH_2NHBoc. GC solubilized in NMP

Position on the H-NMR spectra	**NMR Chemical Shift**	**Corresponding proton on the structure**
Boc	1.5 ppm	$(CH3)_3$ (Boc Group)
imp	1.9ppm	Solvent Impurity
a	2.1ppm	CH_3 (acetyl group)
imp	2.4ppm	Solvent Impurity
A	2.6 ppm	CH (C2 substituted)
b	2.7ppm	CH (C2 unsubstituted)
B	2.9 and 3.1ppm	CH_2 (ethyl amino group)
c	3.5-4.1ppm	CH and CH_2 (C3, C4, C5 and Glycol
d	4.5	CH (C1)
e	4.7-4.9	D_2O (Water protons)

Choice of Molar Ratio

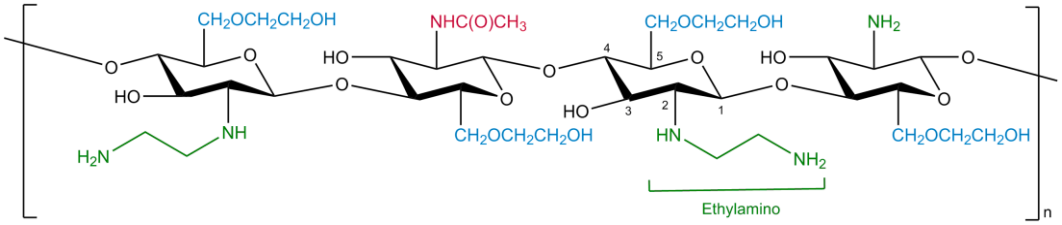

Figure 22 - Proposed chemical structure of EAGC.

The number of amines substituted with the new ethylamino group were characterized by NMR after deprotection of the Boc group with HCl. Different molar ratios of GC:$BrCH_2CH_2NHBoc$ were tested. The protons assignments for EAGC (Figure 23) are:

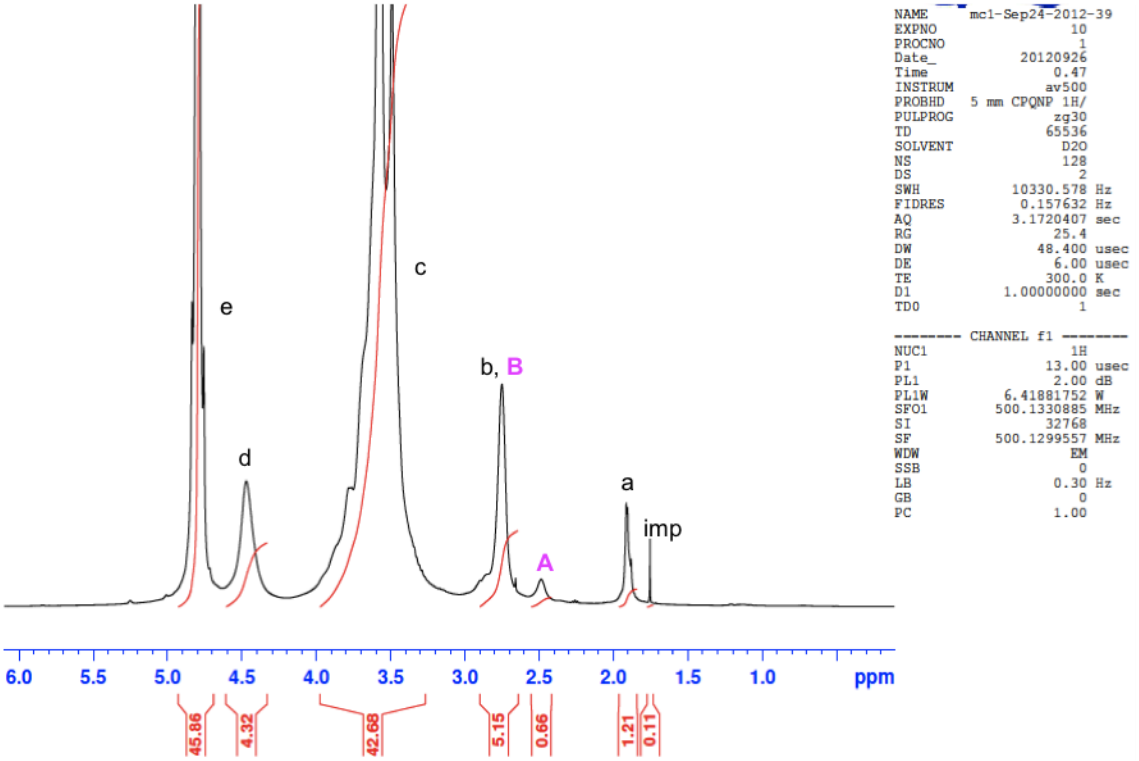

Figure 23 - ^{1}H-NMR EAGC with a level of substitution of 14% (ratio 1:2).

Table 9 - Protons assignments and chemical shifts for EAGC (ratio 1:2, room temperature).

Position on the H-NMR spectra	**NMR Chemical Shift**	**Corresponding proton on the structure**
imp	1.7 ppm	Solvent Impurity
a	1.9ppm	CH_3 (acetyl group)
A	2.5ppm	CH (C2 substituted)
b	2.6-2.9ppm	CH (C2 unsubstituted)
B	2.6-2.9ppm	CH_2 (ethyl amino group)
c	3.3-4ppm	CH and CH_2 (C3, C4, C5 and Glycol
d	4.5ppm	CH (C1)
e	4.7-4.9ppm	D_2O (Water protons)

Comparing the EAGC ^{1}H-NMR spectra (Figure 23) to the GC ^{1}H-NMR spectra (Figure 14) it is possible to observe a new peak at 2.5ppm. This new peak (**A**) corresponds to the proton of the substituted C2. It is in a more shielded position due to the new group introduced ($-CH_2CH_2NH_2$). This group behaves like an electron donor dispersing the negative charge of the amine and moving the C2 proton upfield to a more shielded position. The new CH_2CH_2 of the ethylamino group (peak **B**) appeared in the spectra at 3ppm in the same position as the unsubstituted C2. In the original spectra of $BrCH_2CH_2NHBoc$ (Appendix – Figure A.8) the CH_2CH_2 peaks appeared at 3.5ppm. However, when reacted with GC the CH_2CH_2 peaks moved upfield due to the lower electronegativity of the amines when compared with Br^-. COSY spectra (Figure 24) showed cross peaks between the substituted C2 and C1 (d,**A**) and substituted C2 and C3 (c,**A**) that also confirmed that the new peak (**A**) represents the proton of the substituted C2.

The degree of substitution was calculated with the following formula:

$$\text{Degree of substitution} = \frac{\text{(Area under the peak of the C2 proton substituted / 1 proton)}}{\text{(Area under the C3,C4,C5 and Glycol protons peak / 9 protons)}}$$

In this first reaction the degree of substitution was:

$$\text{Degree of substitution (\%)} = \frac{(0.66/1)}{(42.68/9)} \text{ X } 100 = 13.9\%$$

The new CH_2 protons (**B**) from the substituted group -$CH_2CH_2NH_2$ were also visible in the Carbon DEPT spectra (Figure 25) and HMQC (Figure 26) as well as the C2 substituted (**A**).

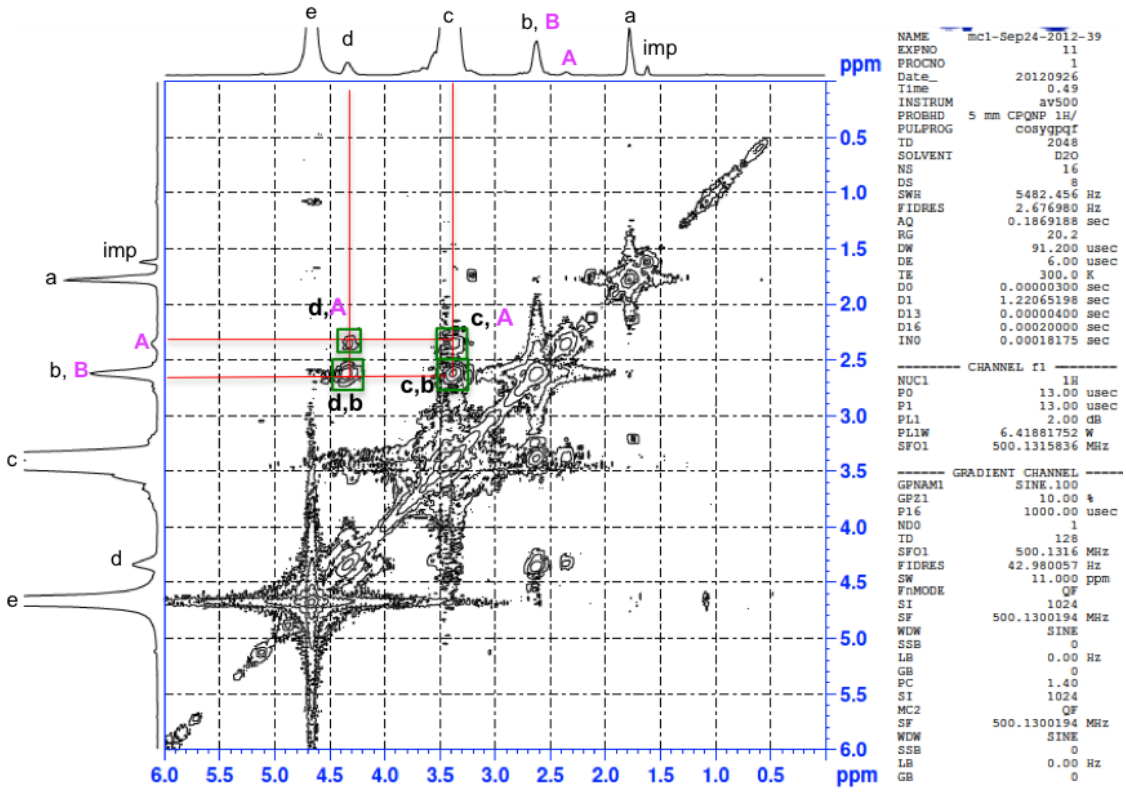

Figure 24 - COSY NMR of EAGC with a level of substitution of 14% (ratio 1:2).

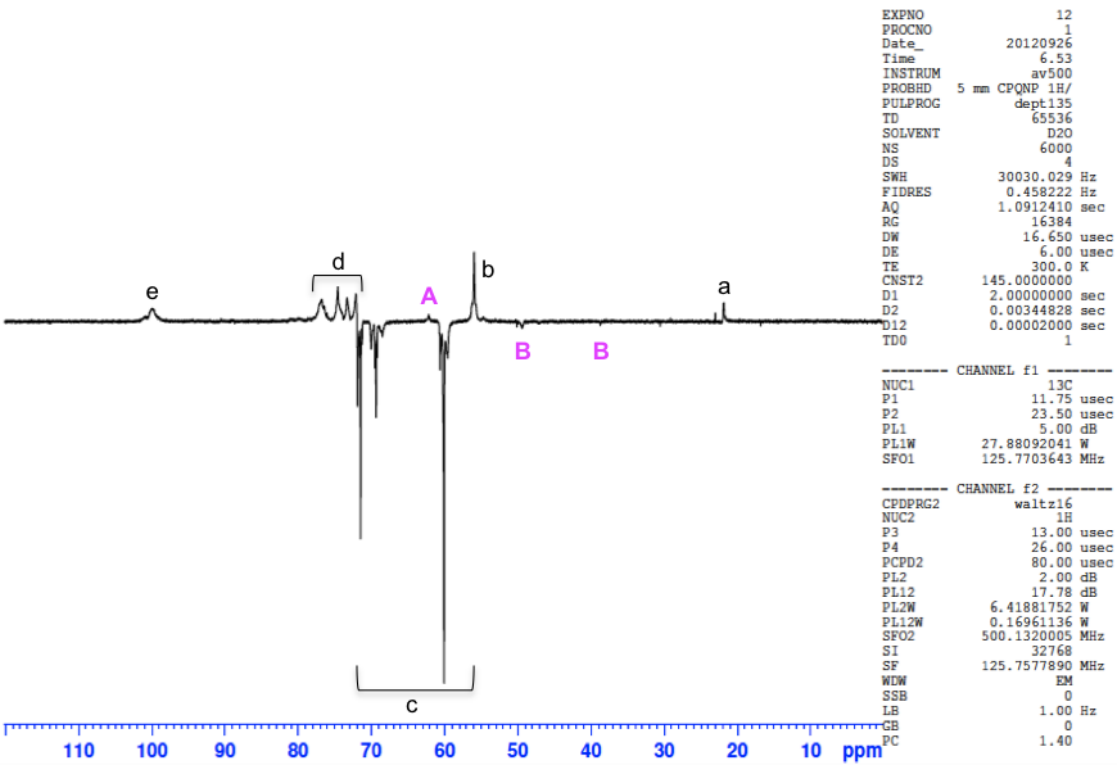

Figure 25 - ^{13}C–DEPT NMR of EAGC with a degree of substitution of 14% (ratio 1:2).

Table 10 - Carbons assignments and chemical shifts for EAGC (ratio 1:2, room temperature).

Position on the C-NMR spectra	**NMR Chemical Shift**	**Corresponding carbon on the structure**
a	20 ppm	CH_3 (acetyl group)
B	39 ppm and 50ppm	CH_2 (-**C**H_2**C**H_2NH_2)
b	56 ppm	CH (C2)
A	63ppm	CH (C2 substituted)
c	60, 69, 72ppm	CH_2 (Glycol)
d	73-78ppm	CH (C3, C4, C5)
e	100ppm	CH (C1)

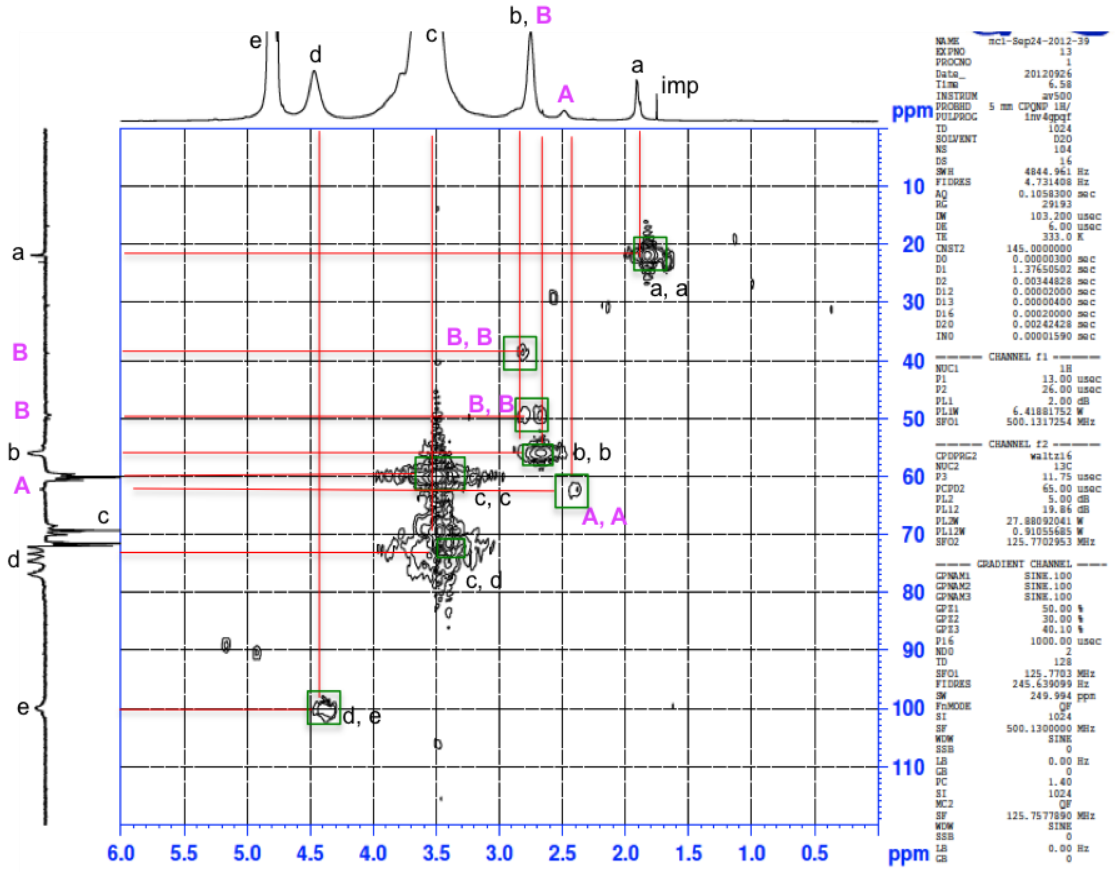

Figure 26 - ^{1}H-^{13}C HMQC NMR of EAGC substituted 14% (ratio 1:2).

The molar ratio of GC:$BrCH_2CH_2NHBoc$ was further increased to increase the degree of substitution, with the ultimate objective of increasing the charge ratio of the polymer. Results for molar ratios of 1:10 are present in Figure 27 and Table 11. It is possible to observe that when the ratio was increased there are two new peaks (**A1** and **A2**) between 2.5 and 3ppm on the ^{1}H-NMR of EAGC (Figure 27) compared with ^{1}H-NMR of GC (Figure 14). The COSY (Figure 28) revealed that these peaks interact with C1 (interaction d,**A1** and d,**A2**) and C3 (interaction c,**A1** and c,**A2**) exactly like the proton of unsubstituted C2 (interaction c,b and d,b). This means that these two new peaks also represent protons of C2 but substituted with the new ethylamino group. Since they (**A1** and **A2**) appeared at different chemical shifts the kind of substitution in each of them needs to be different. Regarding the previous results a new chemical structure of EAGC was proposed with a double substitution in some of the primary amines of GC (Figure 29).

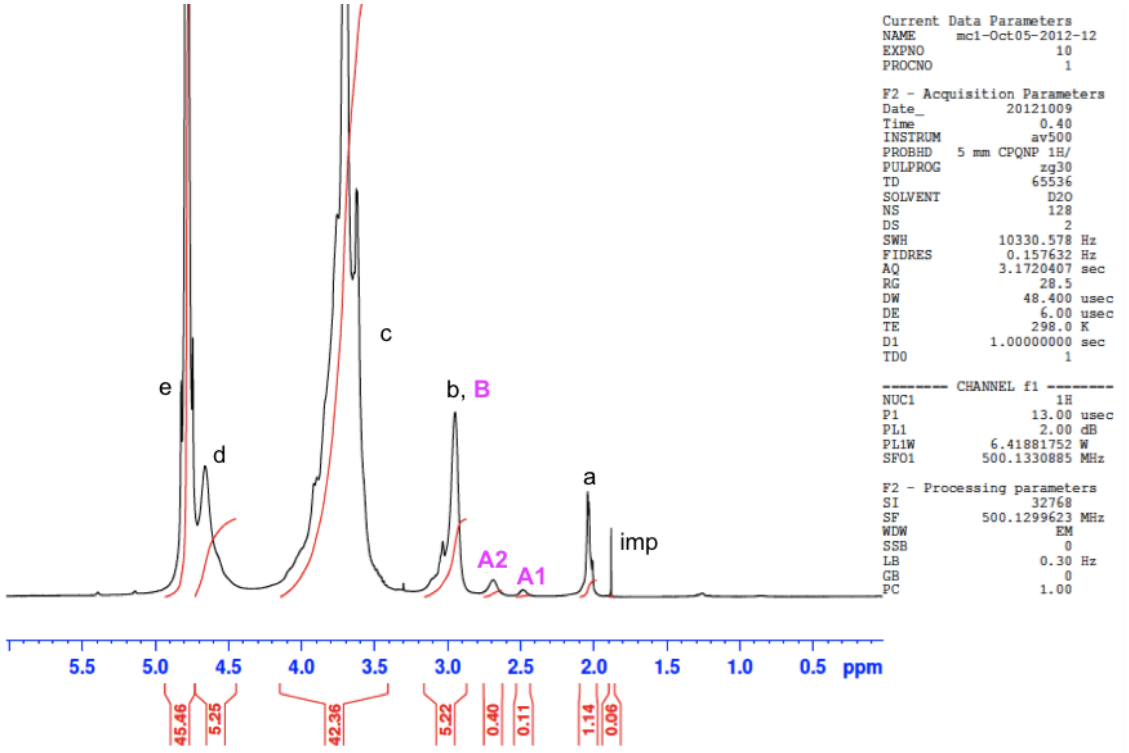

Figure 27 - ^{1}H-NMR EAGC with a level of substitution of 11% (ratio 1:10).

Table 11 - Protons assignments and chemical shifts for EAGC (ratio 1:10, room temperature).

Position on the H-NMR spectra	**NMR Chemical Shift**	**Corresponding proton on the structure**
imp	1.9ppm	Solvent Impurity
a	2.0ppm	CH_3 (acetyl group)
A1	2.5ppm	CH (C2 double substituted)
A2	2.7ppm	CH (C2 single substituted)
b	2.9-3.2ppm	CH (C2 unsubstituted)
B	2.9-3.2ppm	CH_2 (ethyl amino group)
c	3.5-4.2ppm	CH and CH_2 (C3, C4, C5 and Glycol
d	4.7ppm	CH (C1)
e	4.7-4.9ppm	D_2O (Water protons)

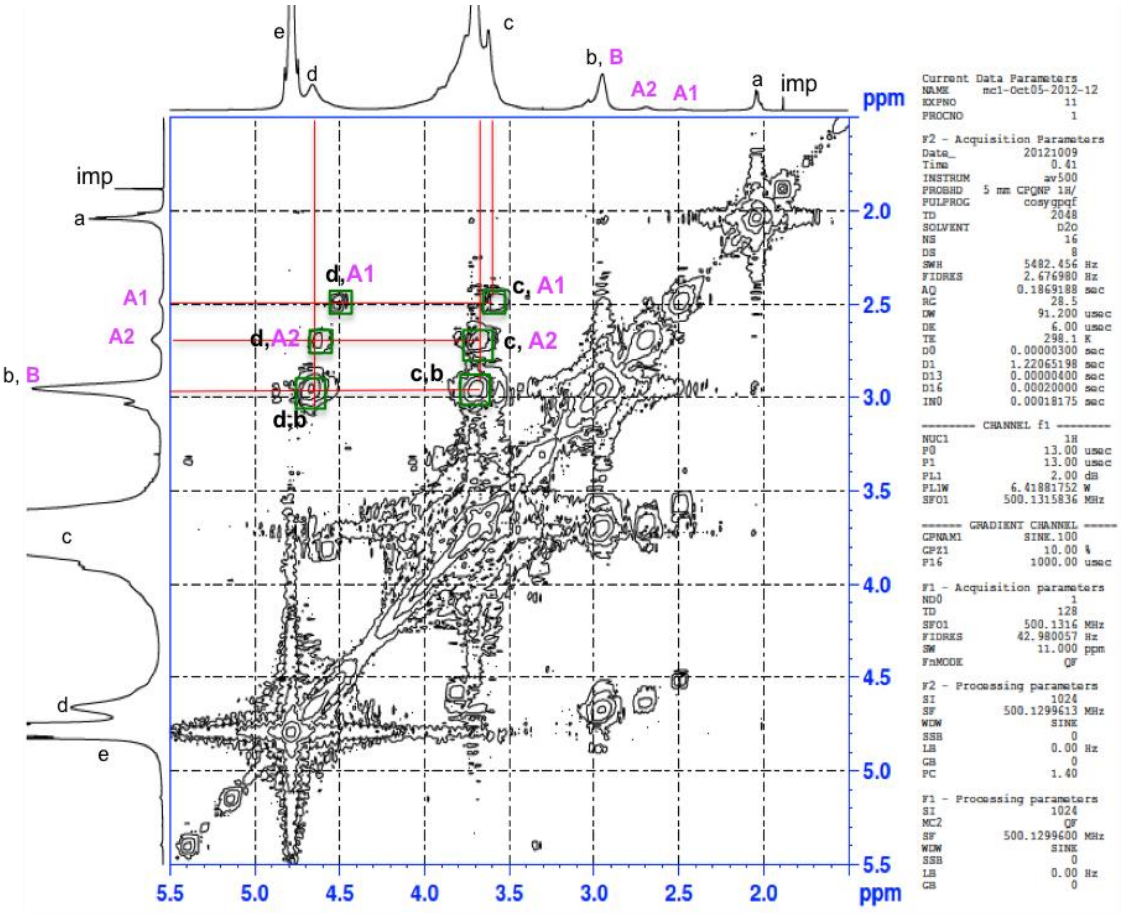

Figure 28 - COSY NMR EAGC with a level of substitution of 11% (ratio 1:10).

The double substitution was possible due to the reactivity of the secondary amines. When a hydrogen in an amine is substituted by an electron-releasing alkyl group, the basicity of the amine group increases. All secondary amines have slightly higher pKa than primary, meaning they behave as stronger nucleophiles [165, 169]. The charge density was increased with this double substitution, allowing the introduction of a higher total number of amines and the presence of tertiary amines. The degree of substitution should now be calculated considering the new peak.

$$\text{Degree of substitution} = \frac{\begin{array}{c}\text{(Area under the peak of the C2 proton single substituted / 1 proton) +} \\ \text{(Area under the peak of the C2 proton double substituted / 1 proton)}\end{array}}{\text{(Area under the C3,C4,C5 and Glycol protons peak / 9 protons)}}$$

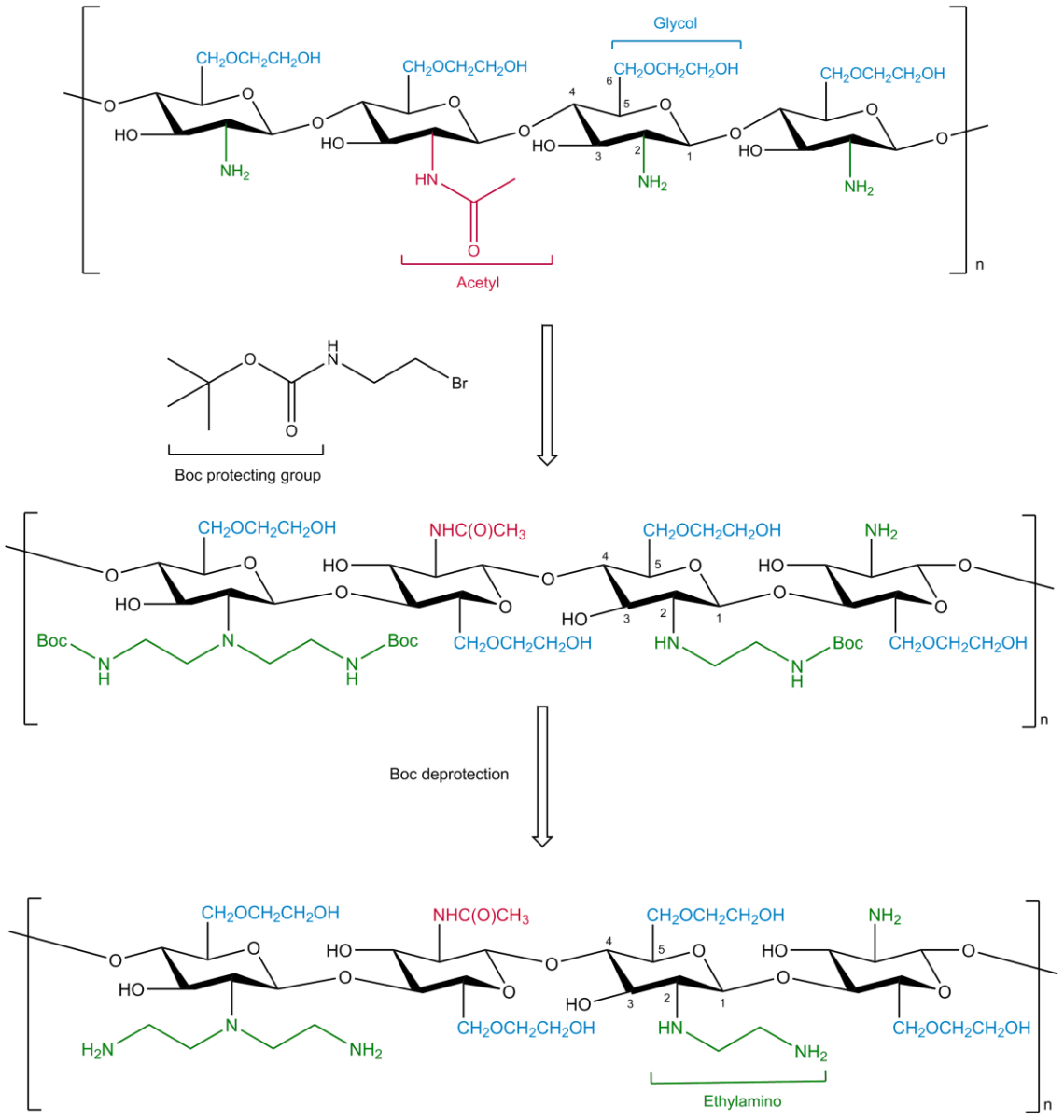

Figure 29 - Reaction between GC and $BrCH_2CH_2NHBoc$ with EAGC double substituted as final product.

It is not possible to distinguish the two new peaks **(A1** and **A2**) in the ^{13}C-DEPT NMR spectrum (Figure 30). Only a new peak appears at 63ppm. Furthermore, in the ^{1}H -^{13}C HMQC NMR spectrum (Figure 31) is not possible to observe the one bond connection between the proton and carbons of **A1** and **A2**. This was probably due to the poor resolution of the spectrum since even the interaction between C1 proton and C1 carbon is missing.

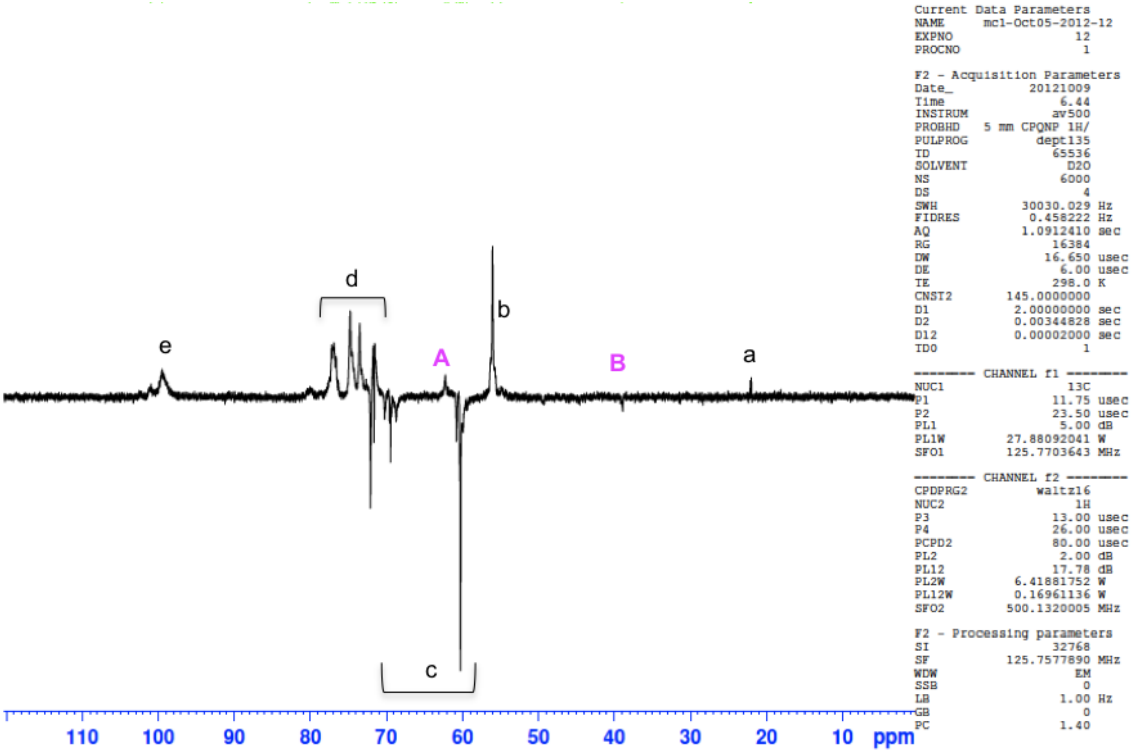

Figure 30 - ^{13}C-DEPT NMR of EAGC with a degree of substitution of 11% (ratio 1:10).

Table 12 - Carbons assignments and chemical shifts for EAGC (ratio 1:10, room temperature).

Position on the C-NMR spectra	**NMR Chemical Shift**	**Corresponding carbon on the structure**
a	20 ppm	CH_3 (acetyl group)
B	39 ppm	CH_2 (-**C**H_2**C**H_2NH_2)
b	56 ppm	CH (C2 unsubstituted)
A	63ppm	CH (C2 double substituted) and (C2 single substituted)
c	60, 69, 72ppm	CH_2 (Glycol)
d	73-78ppm	CH (C3, C4, C5)
e	100ppm	CH (C1)

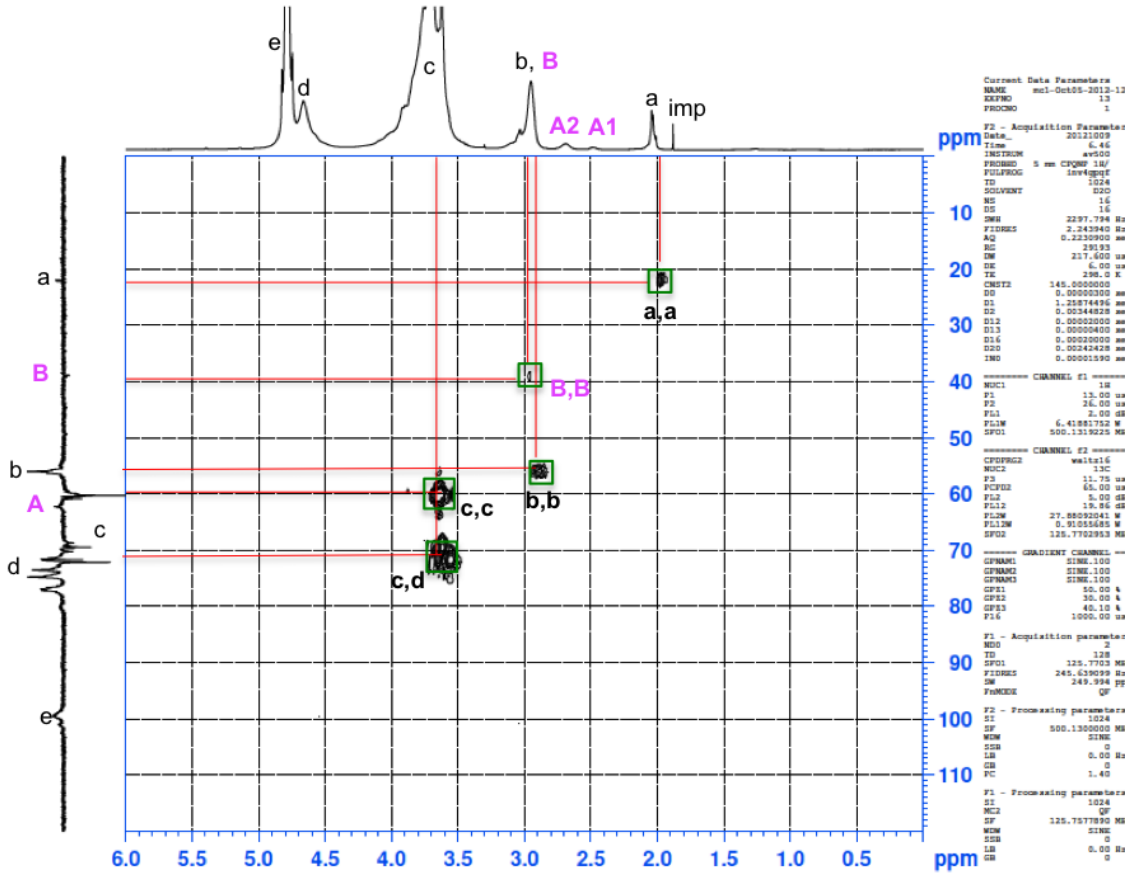

Figure 31 - ^{1}H -^{13}C HMQC NMR of EAGC substituted 11% (ratio 1:10).

The molar ratio of GC:$BrCH_2CH_2NHBoc$ was further increased and the following spectra (Figures 33 to 36) present the results for the reaction between GC and $BrCH_2CH_2NHBoc$ with a molar ratio of 1:20. It is possible to observe in the ^{13}C DEPT NMR three new CH_2 signals at 39, 45 and 50ppm (Figure 35). These peaks confirm the proposed double substitution. When in presence of a double and single substitution three different CH_2 are present (peak **B1, B2** and **B3**) (Figures 32 and 35). On the HMQC spectrum (Figure 36) it is possible to see the interaction between carbons **B1** and protons **B** confirming that the protons of the CH_2 of the ethylamino group are present in the ^{1}H-NMR spectra at 3ppm, as previously described.

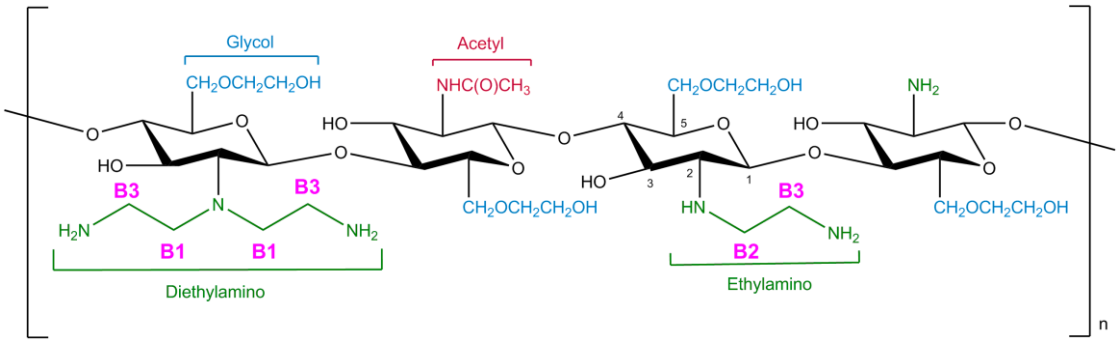

Figure 32 - Chemical Structure of EAGC.

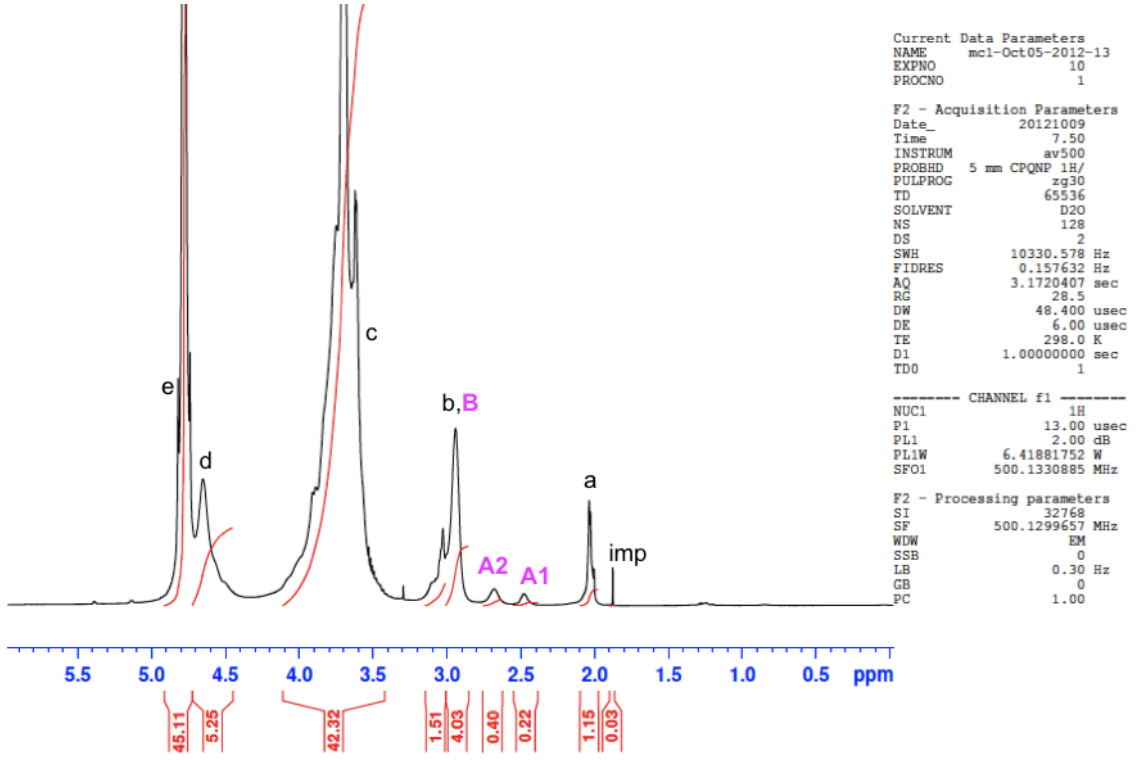

Figure 33 - ^{1}H-NMR EAGC with a level of substitution of 13%. (ratio 1:20).

Table 13 - Protons assignments and chemical shifts for EAGC (ratio 1:20, room temperature).

Position on the H-NMR spectra	NMR Chemical Shift	Corresponding proton on the structure
Imp	1.9ppm	Solvent Impurity
a	2.0ppm	CH_3 (acetyl group)
A1	2.5ppm	CH (C2 double substituted)
A2	2.7ppm	CH (C2 single substituted)
b	2.9-3.1ppm	CH (C2 unsubstituted)
B	2.9-3.1ppm	CH_2 (ethyl amino group)
c	3.5-4.1ppm	CH and CH_2 (C3, C4, C5 and Glycol
d	4.7ppm	CH (C1)
e	4.7-4.9ppm	D_2O (Water protons)

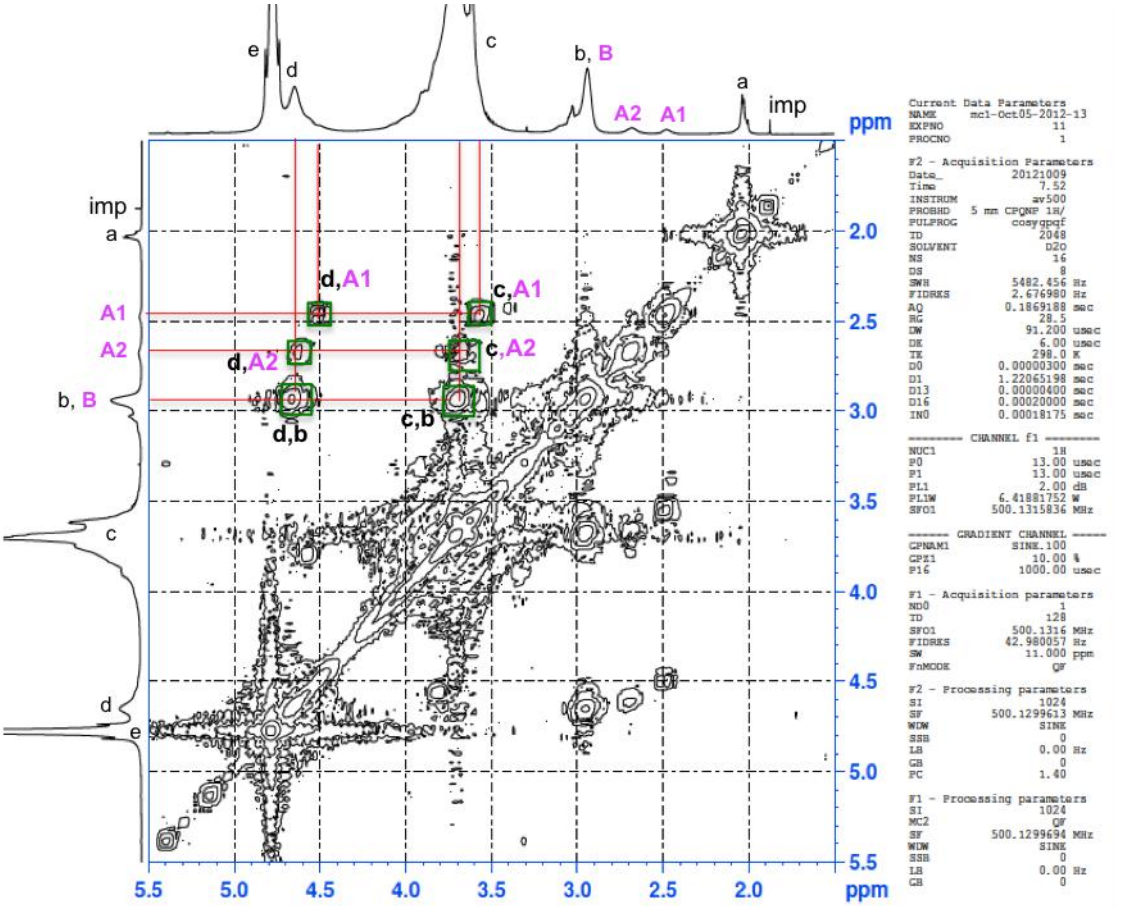

Figure 34 - COSY-NMR EAGC with a level of substitution of 13% (ratio 1:20).

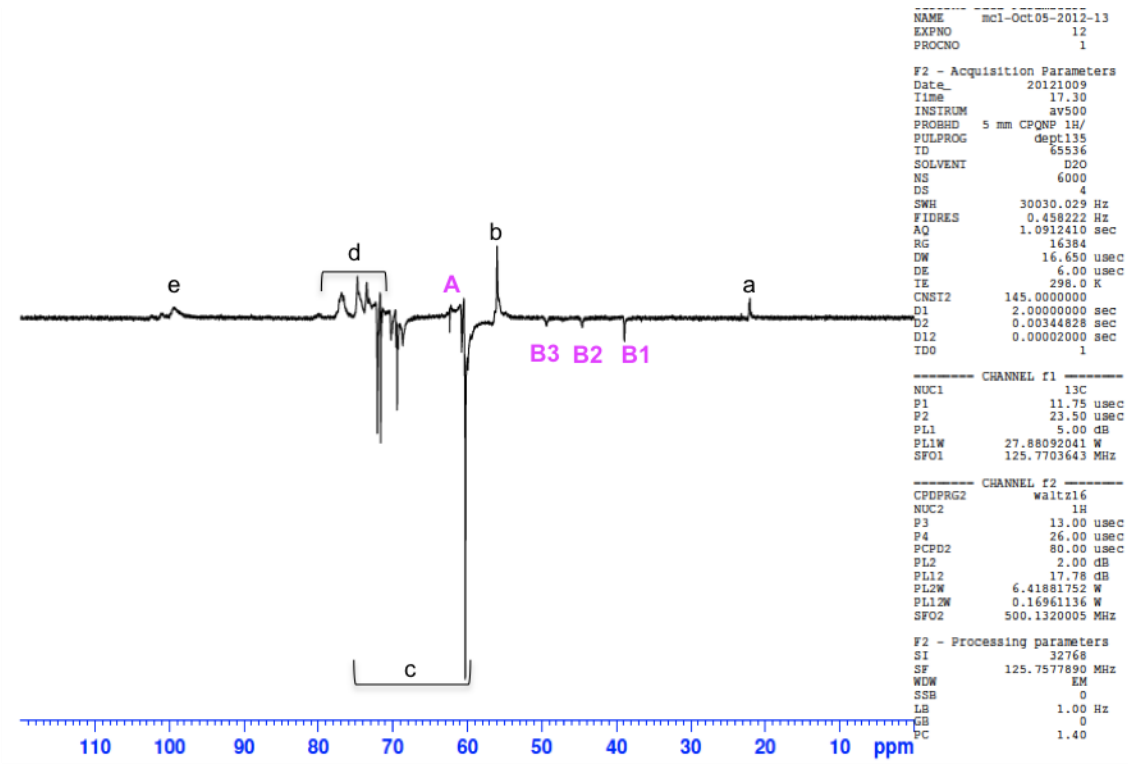

Figure 35 - ^{13}C – DEPT NMR of EAGC with a degree of substitution of 13% (ratio 1:20).

Table 14 - Carbons assignments and chemical shifts for EAGC (ratio 1:20, room temperature).

Position on the C-NMR spectra	**NMR Chemical Shift**	**Corresponding carbon on the structure**
a	20 ppm	CH_3 (acetyl group)
B1	39ppm	CH_2 (-**CH_2**CH_2NH_2) double substitution
B2	45ppm	CH_2 (-**CH_2**CH_2NH_2) single substitution
B3	50ppm	CH_2 (-CH_2**CH_2**NH_2) double and single substituted
b	56 ppm	CH (C2 unsubstituted)
A	63ppm	CH (C2 double substituted) and (C2 single substituted)
c	60, 69, 72ppm	CH_2 (Glycol)
d	73-78ppm	CH (C3, C4, C5)
e	100ppm	CH (C1)

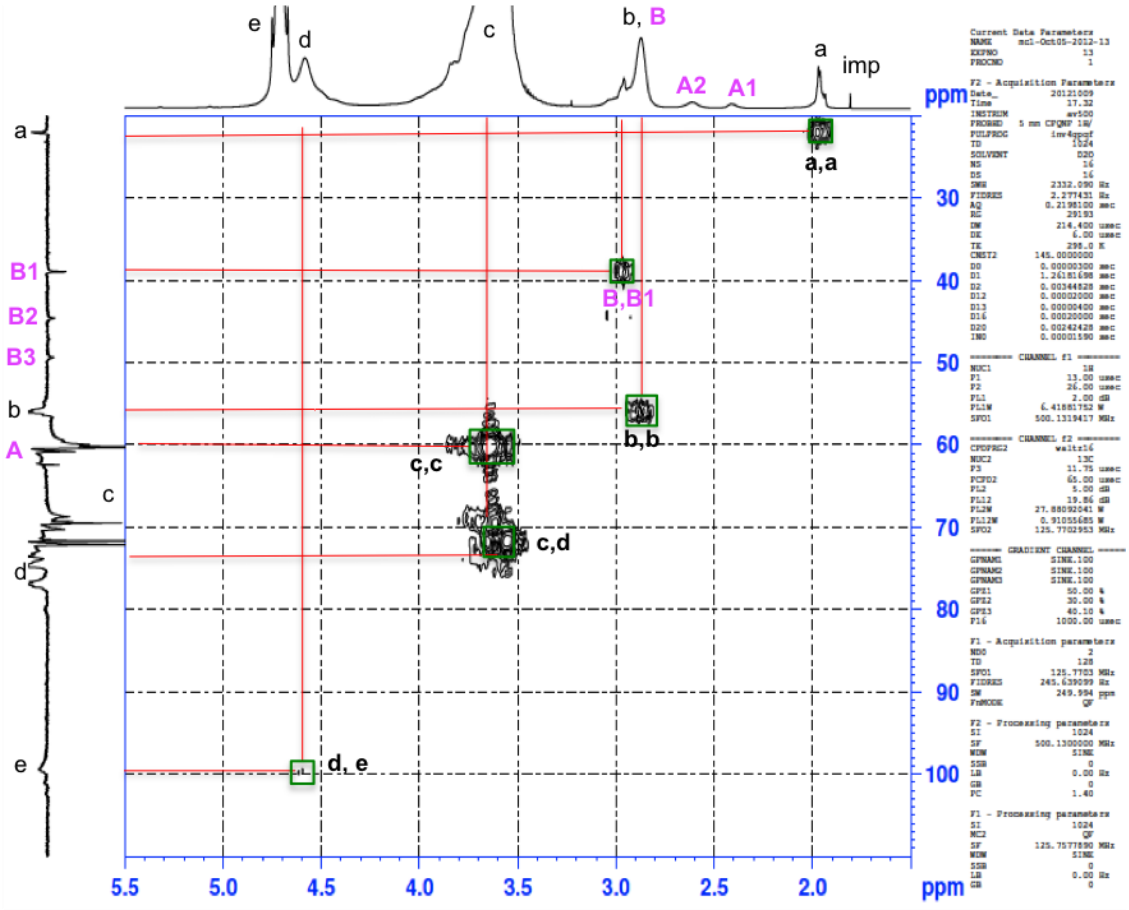

Figure 36 - ^{1}H -^{13}C HMQC NMR of EAGC substituted 13% (ratio 1:20).

Table 15 - Total number of amines calculated regarding degree of substitution (GC soluble in NMP at room temperature).

Molar ratio GC:$BrCH_2CH_2NHBoc$	Total polymer substitution (%)	Total number of amines	Primary amines (%)	Secondary amines (%)	Tertiary amines (%)
1:2	13.9	87	89	11	0
1:10	9.5	86	93	6	1
1:20	13.2	89	90	7	3

The total number of amines in this reaction (Molar ratio 1:20) is not much higher than in the previous one (Molar ratio 1:10) despite the number of moles of $BrCH_2CH_2NHBoc$ being double (Table 15). The importance of the solvent for GC solubility has been discussed before. It was found that even though GC was not completely soluble in NMP, the level of substitution with $-CH_2CH_2NHBoc$ was higher with NMP when compared with water/ethanol (integration of the Boc methyl groups was twenty times higher with GC dissolved in NMP than dissolved in water/ethanol). Still, the solubility of GC was probably a limiting step regarding the maximum number of amines that it is possible to introduce in the polymer backbone. As seen previously, even increasing the amount of substrate did not increase considerably the number of new amines, (Table 15) perhaps due to the amount of GC available. To increase the solubility of GC the temperature of the reaction was raised to 40ºC. This increase not only benefited the solubility of GC but also amplified the reaction rate since, for S_N2 reactions, higher temperatures amplifies the number of collisions between reactants [165]. Three new batches of EAGC (EAGC17, EAGC21 and EAGC30) were synthesized at this higher temperature. Below are presented the final spectra for the three batches.

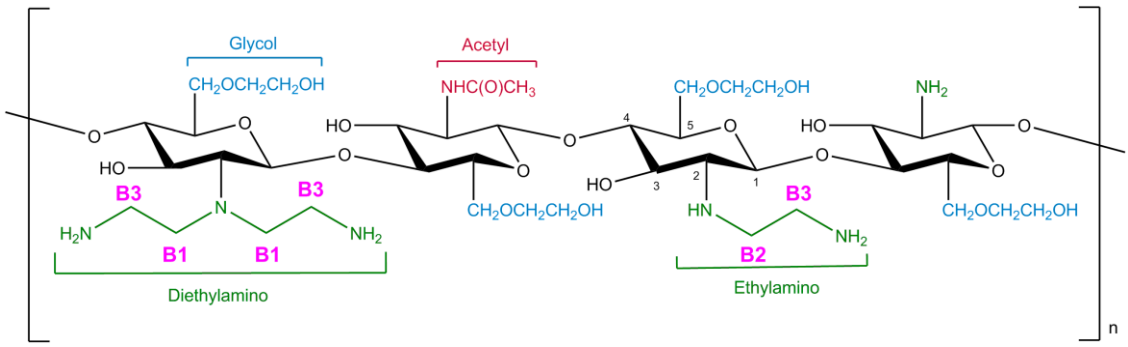

Figure 37 - Chemical Structure of EAGC.

EAGC17

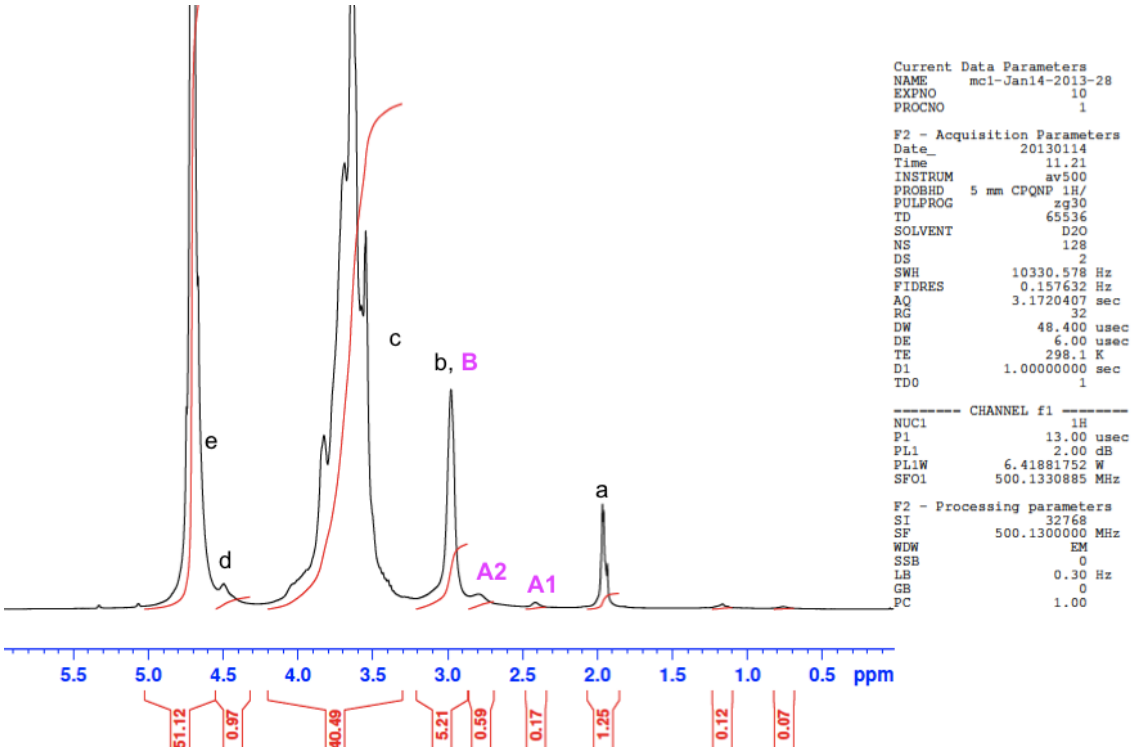

Figure 38 - ^{1}H NMR EAGC with a level of substitution of 17% (ratio 1:2).

Table 16 - Protons assignments and chemical shifts for EAGC (ratio 1:2, 40°C).

Position on the H-NMR spectra	NMR Chemical Shift	Corresponding proton on the structure
a	2.0ppm	CH_3 (acetyl group)
A1	2.5ppm	CH (C2 double substituted)
A2	2.7ppm	CH (C2 single substituted)
b	2.9-3.1ppm	CH (C2 unsubstituted)
B	2.9-3.1ppm	CH_2 (ethyl amino group)
c	3.5-4.1ppm	CH and CH_2 (C3, C4, C5 and Glycol
d	4.7ppm	CH (C1)
e	4.7-4.9ppm	Water protons

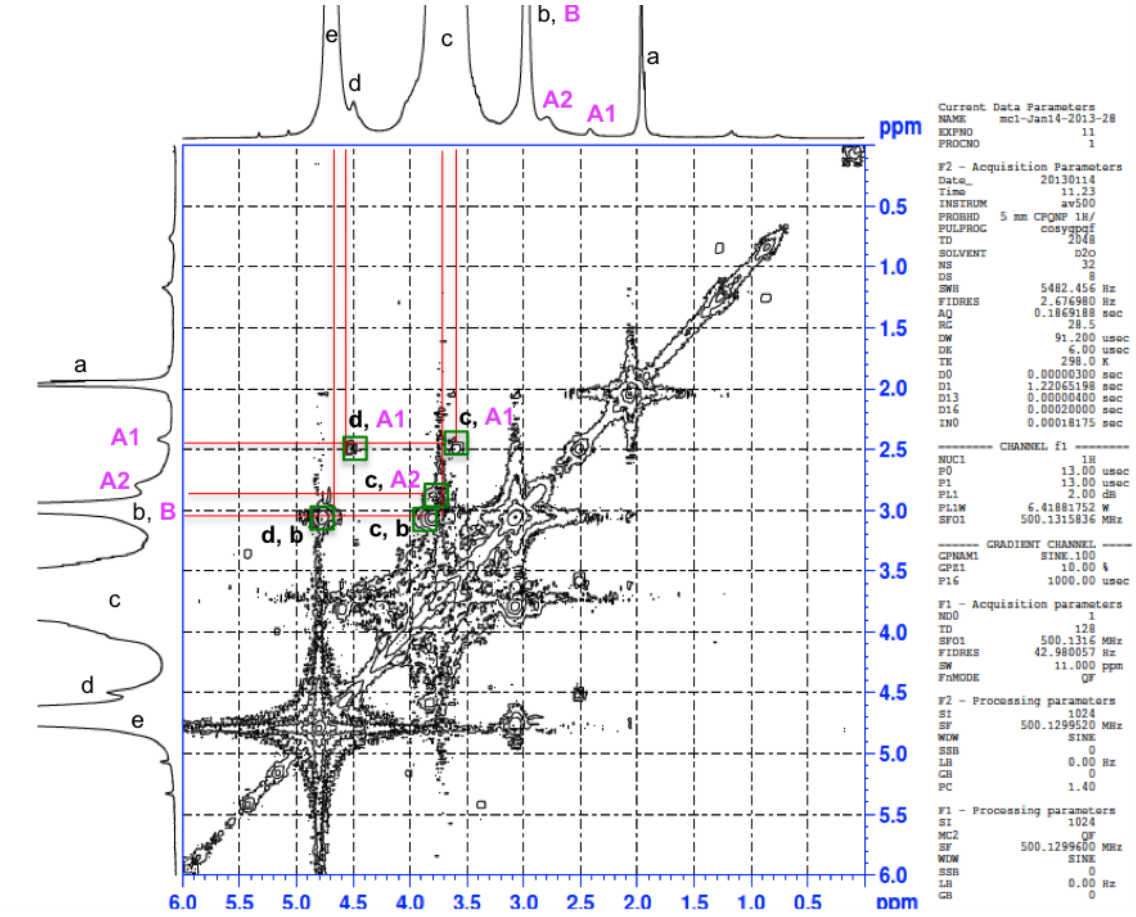

Figure 39 - COSY NMR EAGC with a level of substitution of 17% (ratio 1:2).

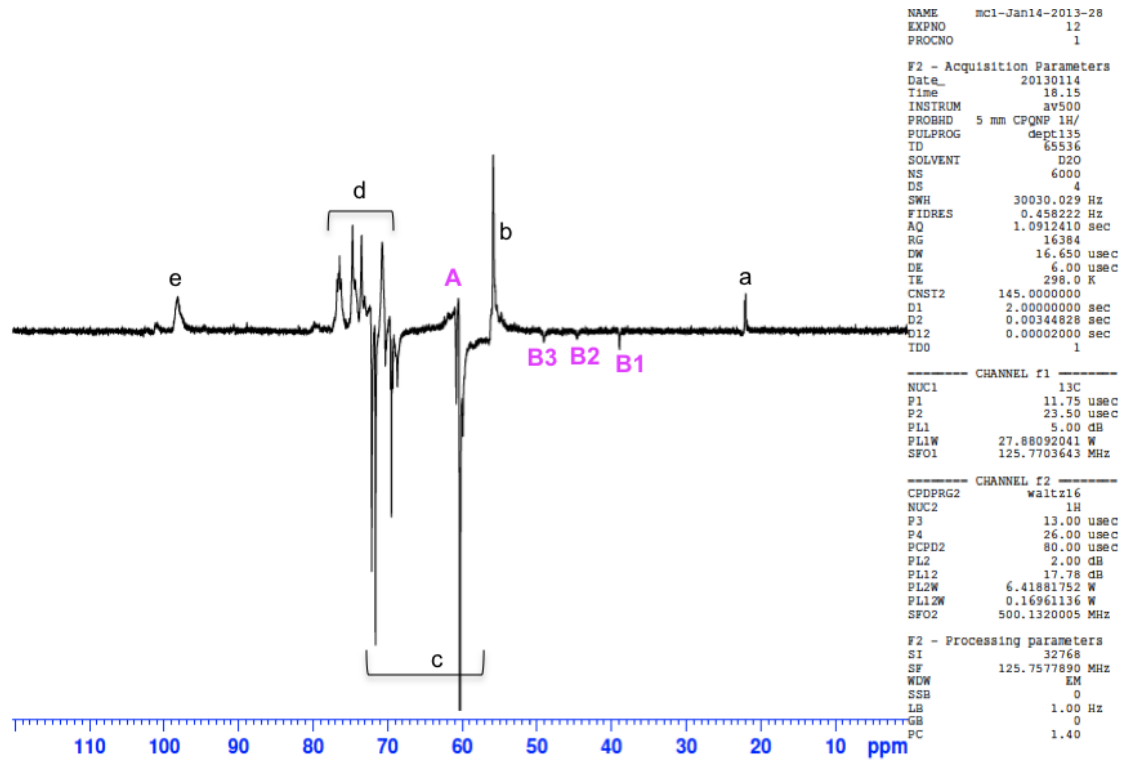

Figure 40 - ^{13}C – DEPT NMR of EAGC with a degree of substitution of 17% (ratio 1:2).

Table 17 - Carbons assignments and chemical shifts for EAGC (ratio 1:2, 40°C).

Position on the C-NMR spectra	NMR Chemical Shift	Corresponding carbon on the structure
a	20 ppm	CH_3 (acetyl group)
B1	39ppm	CH_2 (-**CH_2**CH_2NH_2) double substitution
B2	45ppm	CH_2 (-**CH_2**CH_2NH_2) single substitution
B3	50ppm	CH_2 (-CH_2**CH_2**NH_2) double and single substituted
b	56 ppm	CH (C2 unsubstituted)
A	63ppm	CH (C2 double substituted) and (C2 single substituted)
c	60, 69, 72ppm	CH_2 (Glycol)
d	73-78ppm	CH (C3, C4, C5)
e	100ppm	CH (C1)

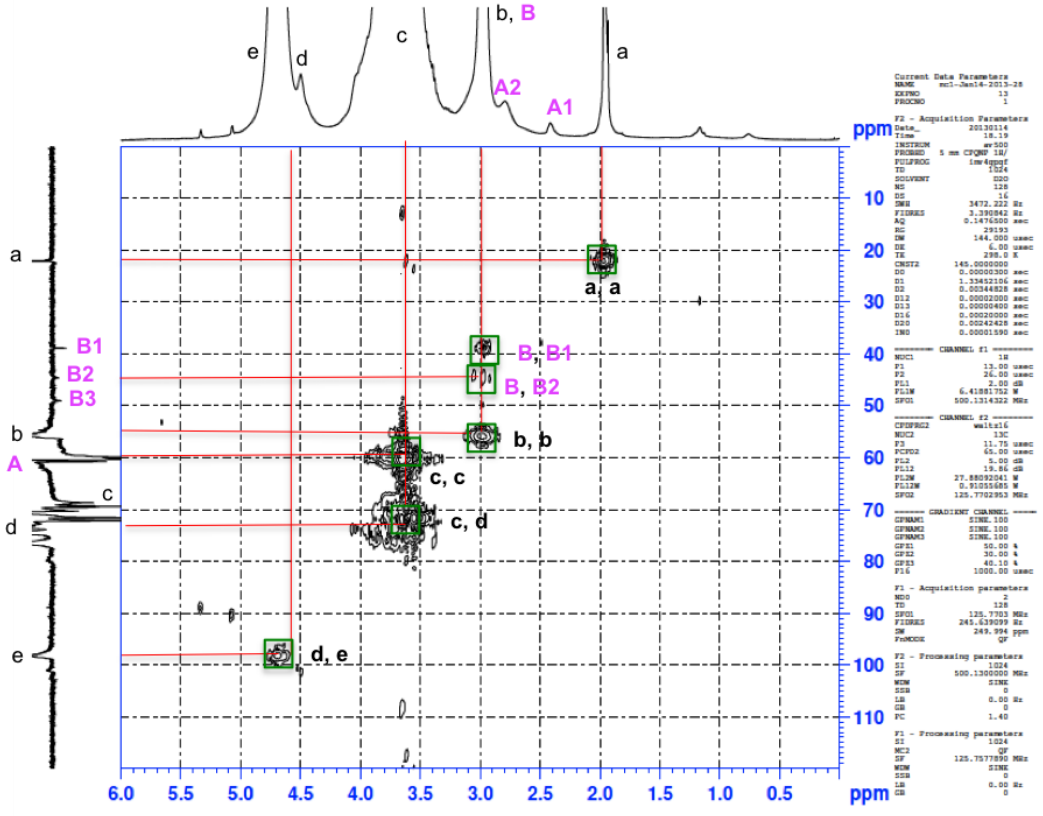

Figure 41 - ^{1}H -^{13}C HMQC NMR of EAGC substituted 17% (ratio 1:2).

EAGC21

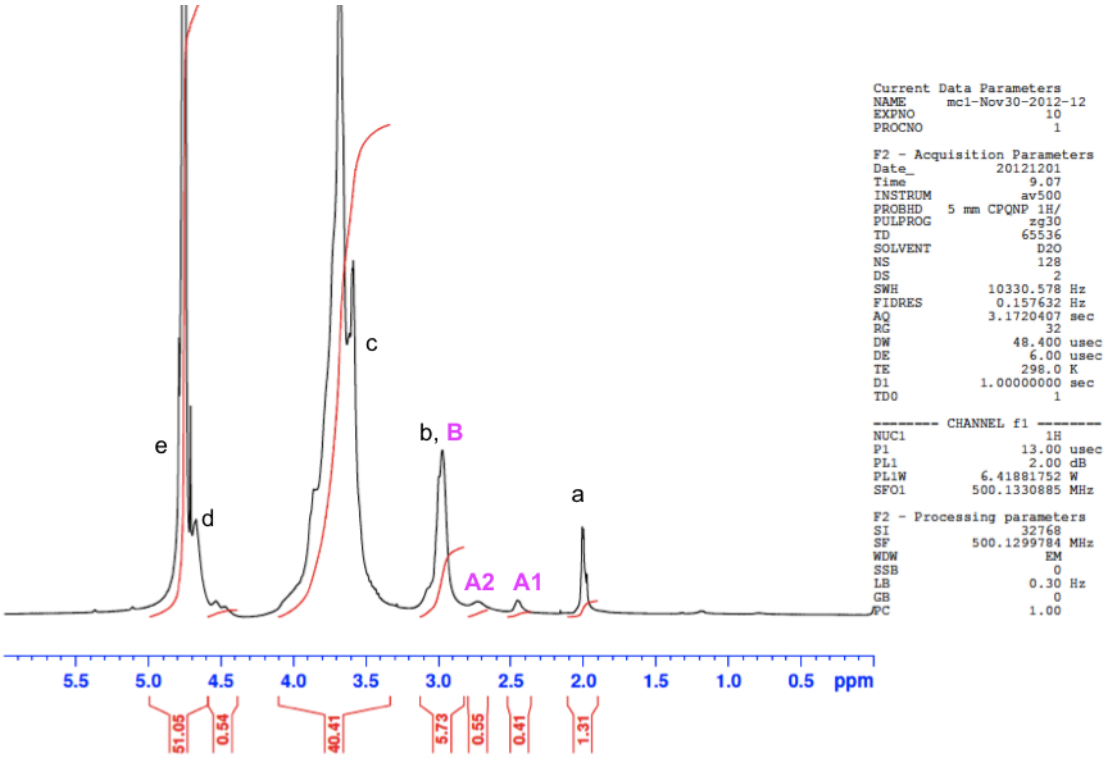

Figure 42 - ^{1}H-NMR EAGC with a level of substitution of 21% (ratio 1:5).

Table 18 - Protons assignments and chemical shifts for EAGC (ratio 1:5, 40°C).

Position on the H-NMR spectra	**NMR Chemical Shift**	**Corresponding proton on the structure**
a	2.0ppm	CH_3 (acetyl group)
A1	2.5ppm	CH (C2 double substituted)
A2	2.7ppm	CH (C2 single substituted)
b	2.9-3.1ppm	CH (C2 unsubstituted)
B	2.9-3.1ppm	CH_2 (ethyl amino group)
c	3.5-4.1ppm	CH and CH_2 (C3, C4, C5 and Glycol
d	4.7ppm	CH (C1)
e	4.7-4.9ppm	Water protons

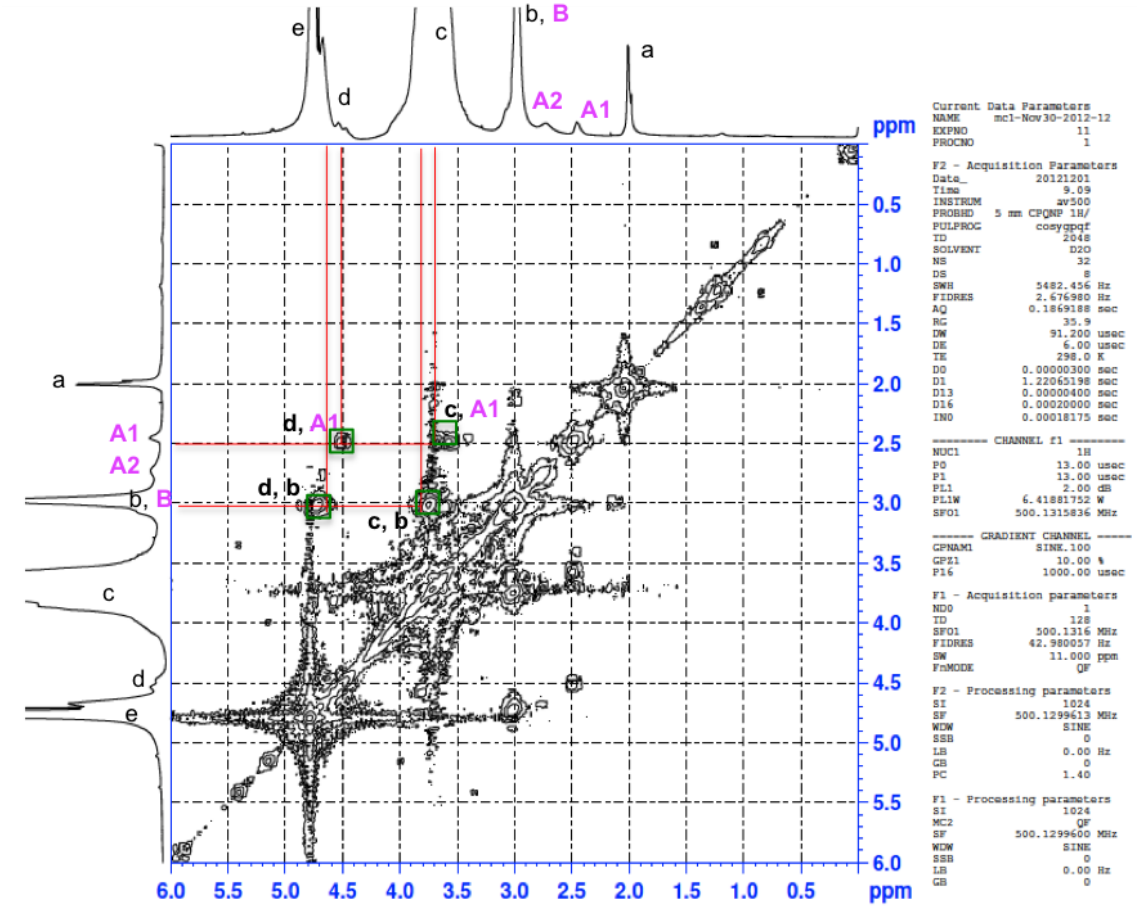

Figure 43 - COSY NMR EAGC with a level of substitution of 21% (ratio 1:5).

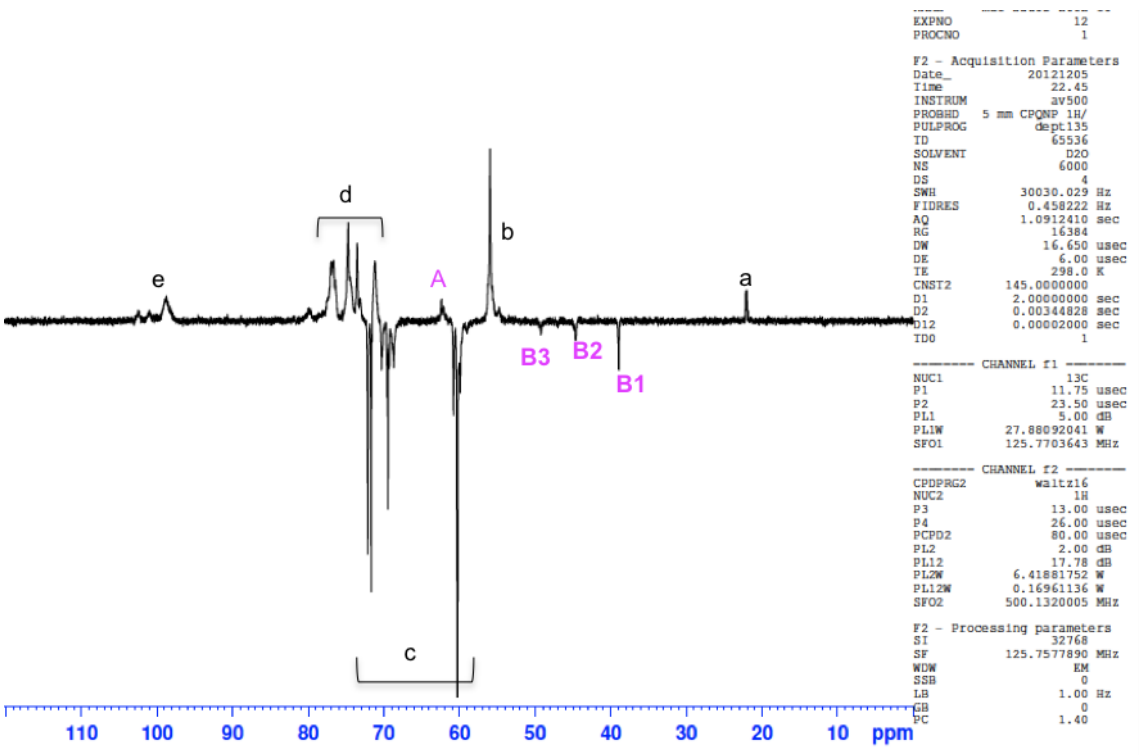

Figure 44 - ^{13}C – DEPT NMR of EAGC with a degree of substitution of 21% (ratio 1:5).

Table 19 - Carbons assignments and chemical shifts for EAGC (ratio 1:5, 40°C).

Position on the C-NMR spectra	NMR Chemical Shift	Corresponding carbon on the structure
a	20 ppm	CH_3 (acetyl group)
B1	39ppm	CH_2 (-**CH_2**CH_2NH_2) double substitution
B2	45ppm	CH_2 (-**CH_2**CH_2NH_2) single substitution
B3	50ppm	CH_2 (-CH_2**CH_2**NH_2) double and single substituted
b	56 ppm	CH (C2 unsubstituted)
A	63ppm	CH (C2 double substituted) and (C2 single substituted)
c	60, 69, 72ppm	CH_2 (Glycol)
d	73-78ppm	CH (C3, C4, C5)
e	100ppm	CH (C1)

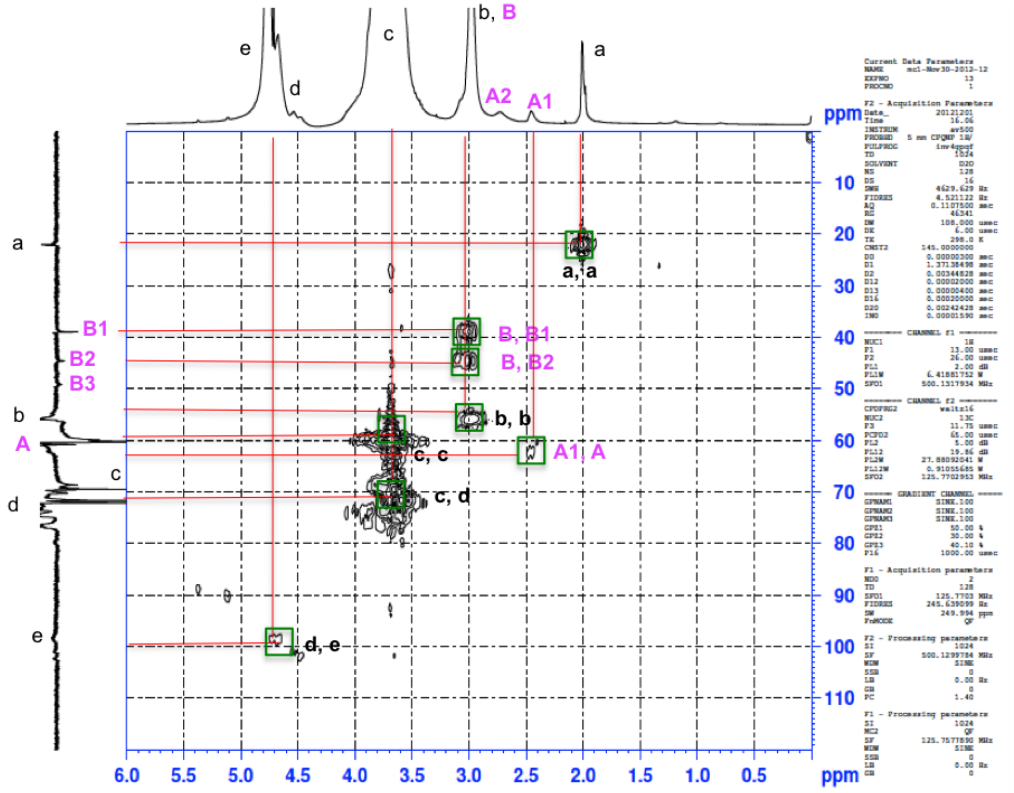

Figure 45 - ^{1}H -^{13}C HMQC NMR of EAGC substituted 21% (ratio 1:5).

EAGC30

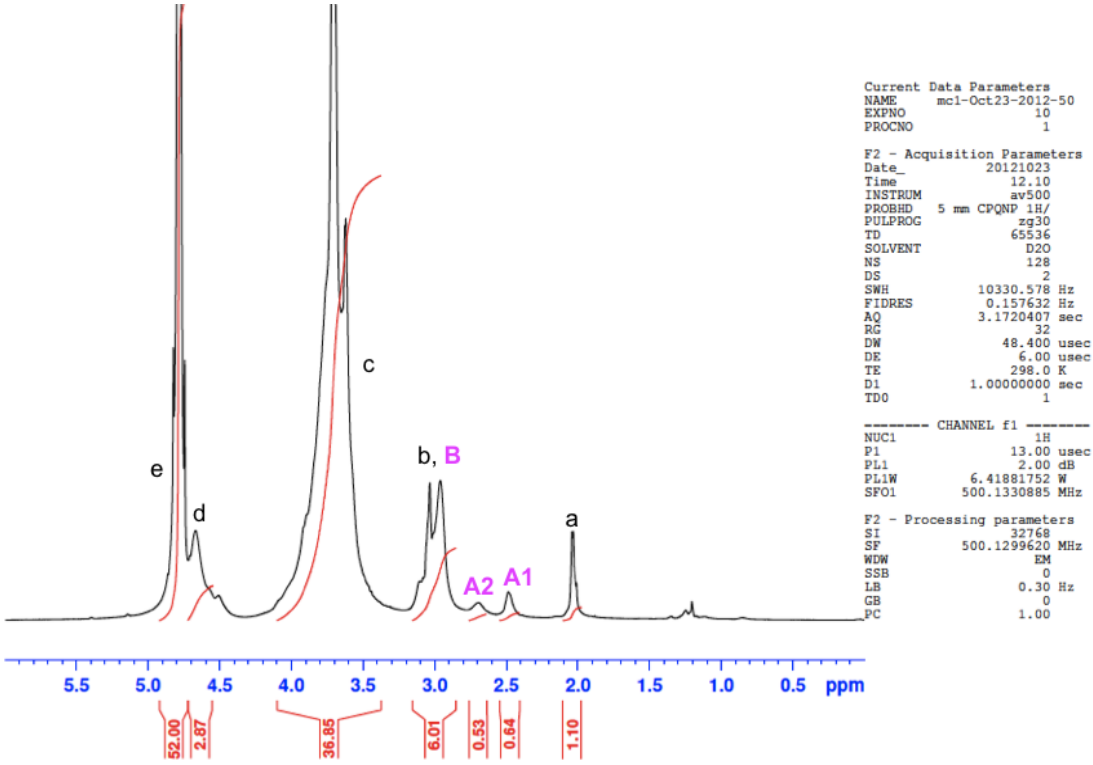

Figure 46 - ^{1}H-NMR EAGC with a level of substitution of 30% (ratio 1:10).

Table 20 - Protons assignments and chemical shifts for EAGC (ratio 1:10, 40°C).

Position on the H-NMR spectra	NMR Chemical Shift	Corresponding proton on the structure
a	2.0ppm	CH_3 (acetyl group)
A1	2.5ppm	CH (C2 double substituted)
A2	2.7ppm	CH (C2 single substituted)
b	2.9-3.1ppm	CH (C2 unsubstituted)
B	2.9-3.1ppm	CH_2 (ethyl amino group)
c	3.5-4.1ppm	CH and CH_2 (C3, C4, C5 and Glycol
d	4.7ppm	CH (C1)
e	4.7-4.9ppm	Water protons

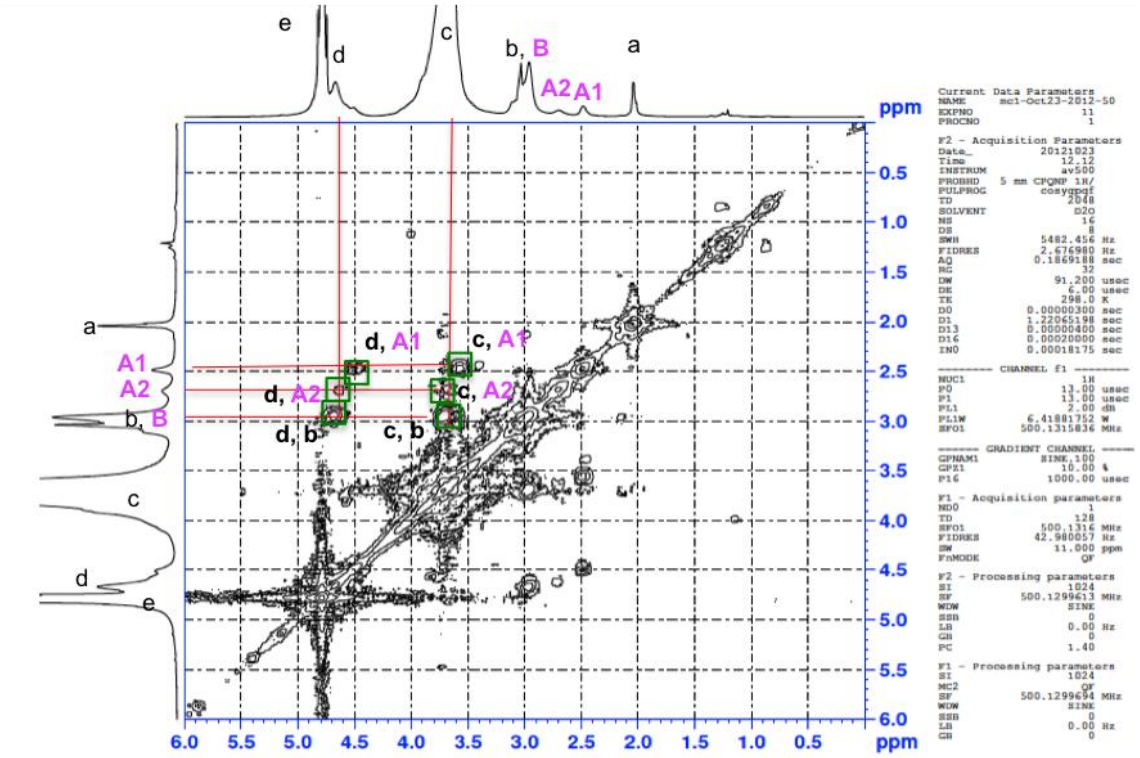

Figure 47 - COSY-NMR EAGC with a level of substitution of 30% (ratio 1:10).

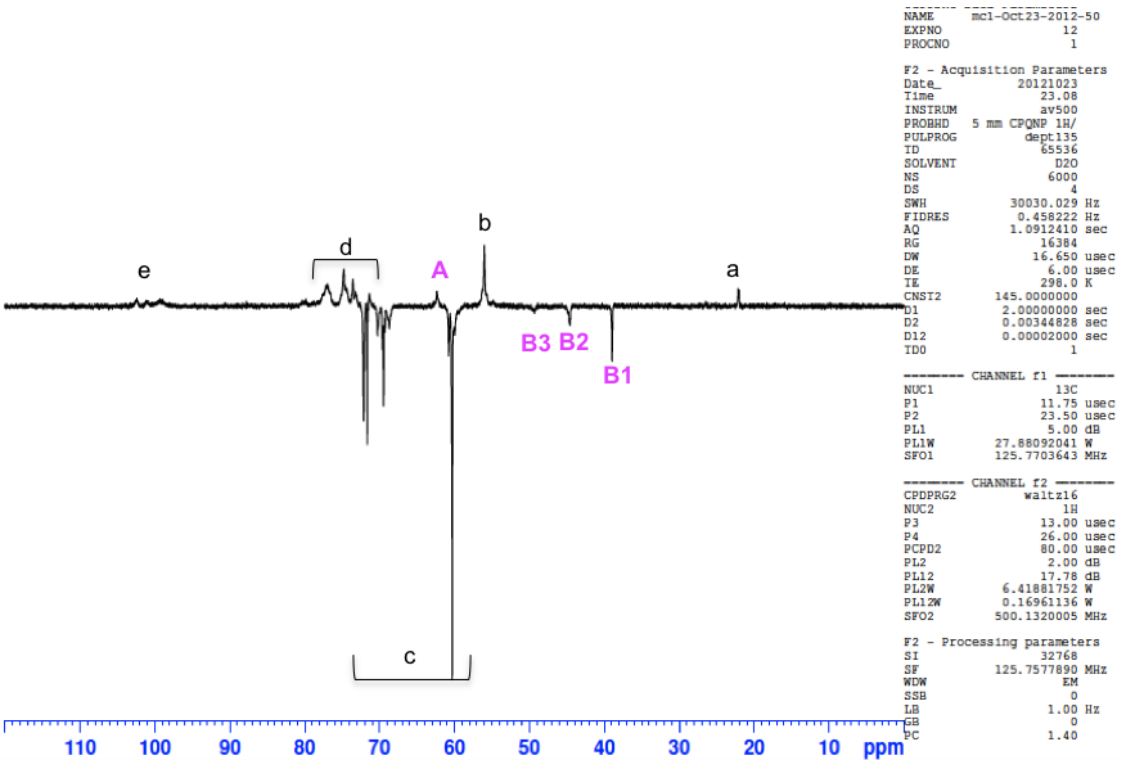

Figure 48 - ^{13}C – DEPT NMR of EAGC with a degree of substitution of 30% (ratio 1:10).

Table 21 - Carbons assignments and chemical shifts for EAGC (ratio 1:10, 40°C).

Position on the C-NMR spectra	NMR Chemical Shift	Corresponding carbon on the structure
a	20 ppm	CH_3 (acetyl group)
B1	39ppm	CH_2 (-**CH_2**CH_2NH_2) double substitution
B2	45ppm	CH_2 (-**CH_2**CH_2NH_2) single substitution
B3	50ppm	CH_2 (-CH_2**CH_2**NH_2) double and single substituted
b	56 ppm	CH (C2 unsubstituted)
A	63ppm	CH (C2 double substituted) and (C2 single substituted)
c	60, 69, 72ppm	CH_2 (Glycol)
d	73-78ppm	CH (C3, C4, C5)
e	100ppm	CH (C1)

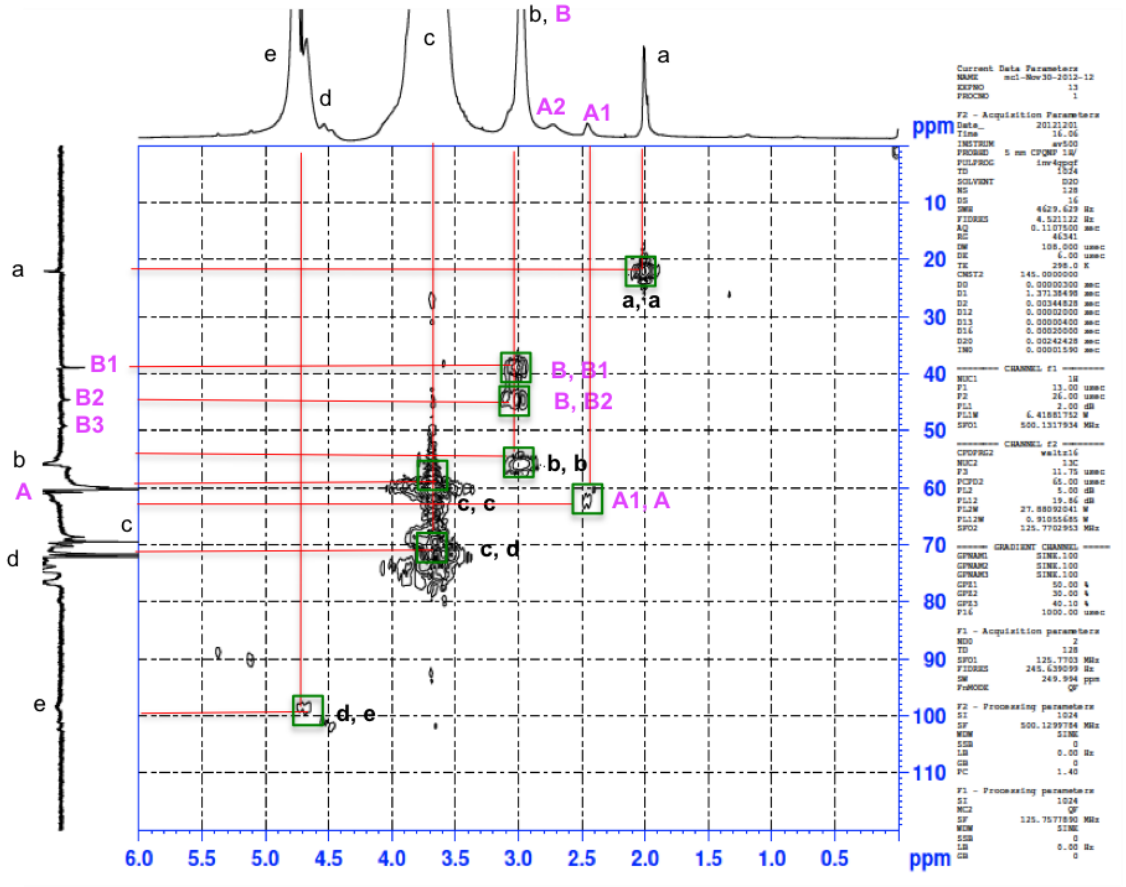

Figure 49 - ^{1}H -^{13}C HMQC NMR of EAGC substituted 30% (ratio 1:10).

The ^{1}H-NMR spectra revealed an increase of substitution with an increase in molar ratio at 40 degrees. It is possible to observe that the overall increase of substitution is due mainly to an increase in the number of double substituted primary amines (peak **A1** Figure 38, Figure 42 and Figure 46). With this substitution the percentage of tertiary amines increased (Table 22). With the increase of the double substitution (peak **A1**) it is possible to see in the ^{1}H -^{13}C HMQC NMR the one bond connection between the proton and carbon of **A1** (Figure 45 and Figure 49).

Table 22 - Total number of amines calculated regarding degree of substitution (GC soluble in NMP at 40ºC).

Molar ratio GC:$BrCH_2CH_2NHBoc$	Total polymer substitution (%)	Total number of amines	Primary amines (%)	Secondary amines (%)	Tertiary amines (%)
1:2	16.4	89	87	10	3
1:5	21.3	97	85	9	6
1:10	28.5	163	82	9	9

2.3.3 Titration

The potentiometric titration curves of GC and EAGC (Figure 50) were based on the following chemical reactions:

$$HCl + GC\text{-}NH_3^+ + NaOH \leftrightarrow NaCl + GC\text{-}NH_2 + H_2O$$

$$HCl + GC\text{-}^+NR_2H + NaOH \leftrightarrow NaCl + GC\text{-}NR_2 + H_2O$$

where R is hydrogen or ethylamino. Figure 50 shows two inflection points. The first point corresponds to the neutralization of excess hydrochloric acid and the second to the neutralization of available amine groups. It was not possible to separate out the neutralization of primary, secondary and tertiary amine groups, and calculate the correspondent pKa values, due to the effects of local groups, which led to different ionization constants for every amino group [78, 173]. However, a lower pKa would be expected for the tertiary amines (pKa 5-7), and higher for the primary amines (pKa 9-10) [174].

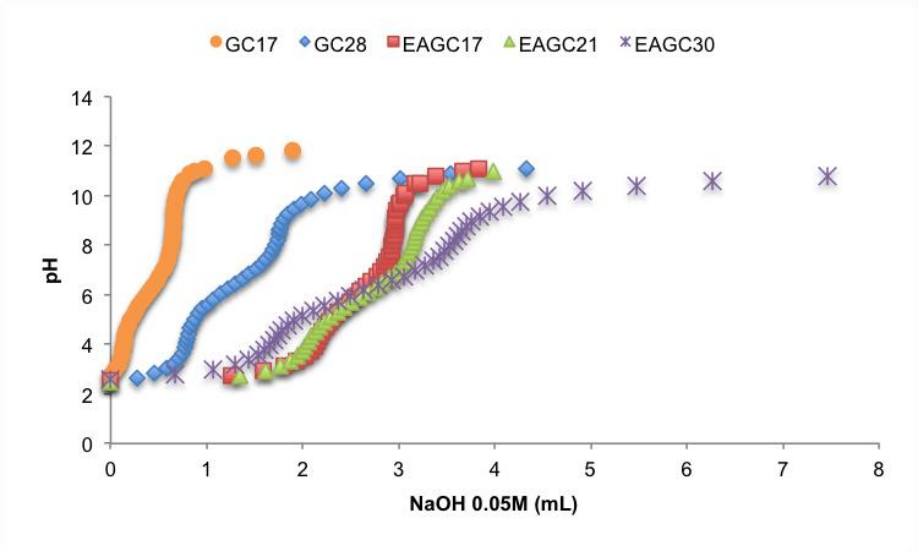

Figure 50 - Titration curves of GC28, GC17, EAGC17, EAGC21 and EAGC30. A polymer solution (2 mg mL^{-1} adjusted to pH 2 with 0.1M HCl) was titrated with NaOH (0.05M).

In the graph (Figure 50) it is possible to observe that the volume of NaOH required to bring the pH from 5.1 to 7.5 in the case of EAGC17, EAGC21 and EAGC30 was higher than the volume required for GC. This indicated a higher buffer capacity for the new synthesized polymers compared with GC. EAGC17, EAGC21 and EAGC30 were the polymers with the highest degree of substitution from all the polymers synthesized and therefore were chosen for the determination of their buffer capacity.

The buffer capacity of the different batches of EAGC and GC (Table 23), was defined as the percentage of amino groups that become protonated in the pH range 5.1 to 7.4, and can be calculated from the following equation:

$$\textit{Buffer capacity (\%)} = [(\Delta V_{NaOH} \times 0.05M)/Nmol]*100$$

where ΔV_{NaOH} , is the volume of NaOH solution required to bring the pH value of the polymer solution from 5.1 to 7.4, and Nmol is the total moles of protonatable amine groups in the known amount of EAGC and GC [168].

Table 23 - Buffer Capacity of the different polymers in a pH range of 5.1 to 7.4.

Polymer	Buffer capacity (%)
GC17	20
GC28	36
EAGC17	24
EAGC21	36
EAGC30	59

EAGC17 and 21 were synthesized from GC17 and EAGC30 from GC28. EAGC30 almost doubles its buffer capacity regarding the initial GC28. EAGC17 and EAGC21 also present higher buffer capacity than GC17. Increasing the degree of substitution increased the buffer capacity of EAGC (Table 23). The introduction of the new ethylamino groups provided the polymer with secondary and tertiary amines. These amines present pKa values in the range of 5-7 and consequently protonation/deprotonation of these determined the buffering capacity of the polymers [78, 174-176].

2.4 Discussion

This chapter introduced a new chitosan based polymer, Ethylamino Glycol Chitosan that was synthesized with four important considerations in mind: (i) the resulting polymer should be soluble at physiological pH, (ii) it should efficiently complex the nucleic acids to provide stable polyplexes (iii) it should have improved buffering capacity to be able to release the nucleic acids inside the cell and (iv) it should retain the biocompatibility and low cell toxicity of the parent polymer chitosan.

Glycol chitosan was chosen as the starting material for the synthesis of EAGC due to its higher solubility in water when compared with chitosan and low cytotoxicity regarding other chitosan salts [108, 159].

The molecular weight and charge density of EAGC is an important factor to be considered, since it influences the polymer biocompatibility, the size and stability of polymer-nucleic acid complexes as well as its transfection efficiency. Different studies with chitosan as a gene delivery system showed that a high molecular weight polymers (100-400 KDa) associated with a high degree of deacetylation were essential requirements for nucleic acid transfection and performed better than low molecular weight chitosan for gene delivery of DNA and siRNA [112, 118, 120-122]. Transfection efficiency in A549 cells increased with the molecular weight of chitosan polyplexes (213 kDa > 98 kDa > 48 kDa > 17 kDa) [118]. Decreasing either the polymer molecular weight or degree of deacetylation led to decreased protection of the condensed nucleic acids and less efficient cellular uptake, causing low transfection efficiency [117, 118]. Plasmid-chitosan complexes made with higher molecular weight chitosan were more stable to salt and serum challenge [112]. Nevertheless, high molecular weight polymers (>100 kDa) with a high degree of deacetylation were associated with high toxicity [103, 112] and were less biocompatible [95] than lower molecular weight chitosans (10 kDa) [105].

Recent work has shown that low molecular weight chitosans (<100 kDa) are also suitable gene delivery candidates, and in some studies had out-performed the high molecular weight polymers [55, 57, 94, 110, 127-129]. Down-regulation of specific genes through siRNA delivered by low molecular weight chitosan was studied. Three different chitosans (44, 63 and 93 kDa) showed an 80% down regulation of luciferase expression at chitosan, siRNA mass ratios 2.5 and 5. The fourth chitosan, with a molecular weight of 143 kDa, was less effective with a reduction of only 60%, while lipofectamine (positive control) showed 90% downregulation [127].

Furthermore, chitosans with 24 monomer units (4.7 kDa) formed stable complexes with high transfection efficiency *in vitro*. The efficiency of low molecular weight chitosan was compared with a high molecular weight (162 kDa, 83% deacetylated) polymer for three cell lines at an N:P ratio of 60. The low molecular weight chitosan showed a gene expression 4- to 24-fold higher than the high molecular weight chitosan [119].

In summary, high molecular weight polymers with high degree of deacetylation offered enhanced nucleic acid complexation and stability, but also led to aggregation, low solubility at physiological pH and low biocompatibility [130]. The high stability of the nanoparticles may result in difficulty releasing the nucleic acids inside the cell, leading to low or delayed transfection [38]. Complexes with low molecular weight and low degree of deacetylation are not stable enough for transfection due to low complexation. Nevertheless, efficient intracellular release would be easy to achieve [104, 130]. Transfection efficiency with this kind of chitosan is improved when the complexes are formulated at high polymer, nucleic acid mass ratios and with a high degree of deacetylation [104, 126].

Considering the previous findings for chitosan, it was believed that an appropriate polymer molecular weight was needed to confer enough stability to the EAGC complexes for nucleic acid protection, but also allowing efficient intracellular DNA/siRNA release to obtain high levels of transfection [159]. The molecular weight of the three different EAGC polymers was confirmed by GPC (Table 4). Two molecular weights (17 and 27 kDa) were chosen for EAGC. The larger polymer was required because the maximum charge density of the smaller molecule was not enough to provide complete condensation with DNA and siRNA. Low molecular weight polymers were preferred to avoid the drawbacks of high molecular weight such as toxicity and low intracellular release of nucleic acids.

However, low molecular weight polymers may lead to instability of the nanoparticles in physiological media and result in early dissociation of the complexes. To address this instability it was decided to substitute the initial glycol chitosan with ethylamino groups in order to increase the charge density of the polymer. The influence of the charge density of chitosan in transfection efficiency of the polymers was previously addressed. Five chitosans with a molecular weight range between 31 and 190 kDa, and with different degrees of deacetylation (51%-99%), were studied by Koping-Hoggart *et al.* in the 293 kidney cell line. The results showed that the transfection ability of the polyplexes depended on the percentage of deacetylation, since chitosan with a percentage of positive charge lower than 65% did not show transfection ability.

Furthermore, chitosan with 50 kDa grafted with PEI (1.8 kDa) showed the same buffer capacity as PEI. The transfection efficiency of these copolymers was significantly enhanced when compared with chitosan and PEI, and similar to the positive control lipofectamine towards chondrocytes and synoviocytes. The copolymers showed increased cell biocompatibility when compared with PEI [177].

The pKa of chitosan primary amines has been calculated as 6.5, meaning that at higher pH (more basic), the amines will not be protonated and the overall positive charge of the polymer will be low [114]. Therefore, at pH 7.4 chitosan presents minimal solubility, and low intracellular delivery resulting in low transfection ability [104, 105]. The ethylamino group introduced in glycol chitosan had the objective of increasing EAGC condensation with nucleic acids at physiological pH and the polymer buffer capacity.

The chemical structure and degree of substitution of EAGC were confirmed by NMR. The ^{1}H-NMR spectra of EAGC17, 20 and 30 revealed that increasing the molar ratio of GC:$BrCH_2CH_2NH_2$ increased the overall substitution of the polymers. The substitution of the primary amines of chitosan with one or two ethylamino groups provided the new polymers with primary, secondary and tertiary amines that are required for good buffering, proper binding and release of nucleic acids [138, 178].

The buffer capacity of the polymers is a relevant parameter for the endosomal escape capability of the polyplexes. The remarkable nucleic acid delivery ability of cationic polymers is attributed to a “proton sponge effect” that induces endosomal disruption and prevents degradation of nucleic acids in the lysosome. This buffering effect causes an increase in osmotic pressure in the endosome, leading to the disruption of the endosomal membrane to facilitate polyplex transport into the cytoplasm [15, 168].

The buffer capacity of EAGC polymers, expressed as the percentage of amino nitrogens that become protonated in the pH range 7.4–5.1, was determined from the acid–base titration curves (Fig. 2). All the EAGC polymers showed an increased buffer capacity compared with unmodified GC. Also, it was possible to observe that the buffer capacity of EAGC increased with the increasing degree of substitution.

It has been previously described that tertiary amines, with a pKa similar to the pH of the endosome, contribute to the increase of the buffer capacity of cationic polymers [138, 178]. The calculation of the percentage of the different amino groups in each synthesized EAGC polymer revealed that the more substituted polymer presented the

highest percentage of tertiary amines. This is likely to have been responsible for the trend in increasing buffer capacity across the EAGC polymers with increasing degrees of substitution.

The final degree of substitution of the different batches of EAGC was controlled by the molar ratio of GC:$BrCH_2CH_2NHBoc$. However, it was not possible to control the number of double or single substitutions during synthesis. This was due to the reactivity of the secondary amines (with a slightly higher pKa than primary) behaving as stronger nucleophiles [165, 169]. It is believed that increasing the amount of substrate ($BrCH_2CH_2NHBoc$), increased the number of secondary amines available to react, leading to a higher percentage of tertiary amines in the final polymer. Different batches of polymer synthesized with the same molar ratio presented equivalent percentages of primary, secondary and tertiary amines, confirming a reproducible reaction.

In conclusion, three new batches of EAGC – EAGC17, EAGC21 and EAGC30 – with different degrees of substitution were synthesized and characterized. These polymers presented a higher buffer capacity when compared with the initial GC that may favour the uptake process and the nucleic acid delivery in the cell, increasing the transfection efficiency.

3. Characterization of Ethylamino Glycol Chitosan-nucleic acid nanoparticles

3.1 Introduction

Cationic polymers have been widely used for nucleic acid delivery. The positive charge on the polymer backbone facilitates the electrostatic interaction with the negative phosphates along the nucleic acid chains. Polymers such PLL, PEI, and Chitosan possess amino groups that, once protonated, enable spontaneous polyplex formation upon mixing with DNA or siRNA [176]. The condensation of nucleic acids allows the neutralization of the negative charge of the phosphates, which normally prevents intracellular uptake of naked DNA and siRNA due to charge repulsion between the DNA/siRNA and the anionic cell surface [176, 179].

The result of the interaction between nucleic acids and cationic polymers are small particles with size, normally, in the nanometre range (nanoparticles). Of the different characteristics presented by these nanoparticles, size is one of the most important since it determines tissue distribution as well as cellular uptake [110, 180]. It has been described that the size of the complexes formed between polymers and nucleic acids should be between 50 to several hundred nanometres for efficient cell uptake by endocytosis. Each polyplex particle may comprise of several DNA/siRNA molecules along with many polymer chains [70, 181, 182].

Surface charge is also an important feature of the nanoparticles. Proteoglycans, highly anionic molecules, at the surface of the cell membrane are responsible for the cell's overall negative charge [183, 184]. Unless a specific ligand is attached to the polyplex structure, the binding of polyplexes to the cell surface is due to nonspecific electrostatic interactions between the positive charge of the complexes and the negative charge of the cell surface [183, 185]. The adsorption of the nanoparticles at the cell surface is the first step for internalization of nanoparticles by endocytosis [29, 186].

After systemic administration, nanoparticles face biological challenges related to the extra- and intracellular environments. Examples of these challenges are negatively charged molecules, like serum albumin, and other extracellular proteins as well as nucleases [187]. Negatively charged proteins interact with the complexes and can result in aggregation followed by immune system clearance, or complex disassembly and release of DNA or siRNA [176, 185]. Unprotected plasmid DNA and siRNA are

rapidly degraded by nucleases *in vivo*. When protected by polymers, nucleic acids can remain stable for hours [185, 187].

In summary, for successful nucleic acid delivery it is necessary to employ a vector that is able to condense the DNA and siRNA into small particles, to provide the right charge surface for cell interaction and cell internalization, and to protect the nucleic acids from the different biological challenges.

This chapter will present the results for the characterization of the nanoparticles formed between EAGC, DNA and siRNA. These particles were studied with respect to the size, zeta potential, morphology, and behaviour when in the presence of biological challenges. Different techniques including nanoparticle tracking analysis, zeta potential measurements, gel retardation (in presence and absence of displacing polyanions such as heparin) and nuclease resistance assays were performed.

3.2 Methods

3.2.1 Plasmid DNA preparation

E. coli DH5α strain was used to produce plasmid DNA. Briefly, a medium of LB broth base (25 g L^{-1}, 2L, Sigma Aldrich, Dorset, UK) in MilliQ water was autoclaved. Using aseptic techniques, ampicillin (50 µg mL^{-1}, Sigma Aldrich, Dorset, UK) was supplemented in the medium at room temperature and an aliquot of the solution was transferred to a 25 mL centrifuge tube. The seed culture of *E. coli* DH5α strain was transferred to the centrifuge tube and incubated at 37ºC for 4 hr. Subsequently, the whole bacterial solution from the centrifuge tube was expressed in the autoclaved medium culture and fermented at 37ºC for 16 h with shaking at 120 rpm. The bacterial cells were harvested by centrifugation at 6000 rpm and 4ºC for 15 min (Hermle Z323K, Baltimore, USA). The supernatant was removed and the pellet was processed by a plasmid extraction kit according to the manufacturer's instruction (Qiagen: EndoFree Plasmid Giga Kit, Manchester, UK). The DNA solution in MilliQ water was desalted through the illustra NAP™ Columns (GE Healthcare life Sciences, London, UK). The final solution was measured for the DNA concentration (260 nm) and purity (260/280 nm) by UV-VIS spectroscopy. The obtained concentration range was 600 - 1200 ng mL^{-1} and the total yield of the extracted plasmid DNA was in the range of 6-12 µg for each batch.

3.2.2 Nanoparticles Preparation

a. EAGC-DNA nanoparticles

The complexes were prepared to a final DNA concentration of 0.1 mg mL^{-1}. Each polymer stock solution (EAGC17, EAGC21 and EAGC30) was prepared in sterile dextrose (5% (w/v) filtered with a 0.22 µm Millex filter) to which was added equal volumes of the DNA stock solution (in MiliQ water) to give polymer, DNA mass ratios of 1-60. The complexes were allowed to incubate at room temperature before use.

b. EAGC-siRNA nanoparticles

The complexes were prepared to a final siRNA concentration of 0.1 mg mL^{-1}. The polymer stock solution (EAGC30) was prepared in sterile dextrose (5% (w/v) filtered with a 0.22 µm Millex filter) to which was added an equal volume of the siRNA stock

solution (in insiMAX universal buffer) to give polymer, siRNA mass ratios of 1-60. The complexes were allowed to incubate at room temperature before use.

3.2.3 Agarose gel retardation assay

Gel electrophoresis is the standard procedure to analyse the binding affinity between a polymer and DNA/siRNA. Electrophoresis uses an electrical field to move the negatively charged DNA toward a positive electrode through an agarose gel matrix. The nucleic acids are visualized in the gel by addition of ethidium bromide. This binds strongly to DNA/siRNA by intercalating between the bases, and when exposed to a UV light transmits energy as visible orange light.

An agarose gel solution (1% w/w) in (1X) Tris Acetate EDTA (TAE) buffer was heated in a microwave oven and stained with ethidium bromide (0.3 µg mL^{-1}, Sigma Aldrich, Dorset, UK). After cooling, the solution was set to solidify at room temperature in the casting tray containing a sample comb. The comb was then removed and the solidified gel-tray was inserted into the electrophoresis chamber covered with (1X) TAE buffer. Complex samples (prepared as previously described in section 3.2.2, and incubated for 30min or 1h) and naked DNA/siRNA (control) mixed with loading buffer (2 µL consisted of bromophenol blue and xylene cyanol dyes) were pipetted (12 µL) into the sample wells with the end of the lane towards the cathode. The power supply (PowerPac™, Bio Rad, Hemel, UK) was connected with the chamber and applied for 1 h at 60 V. The results were imaged on a UV Transilluminator (ChemiDoc™ MP System, Bio Rad, Hemel, UK) to illustrate the ethidium bromide-stained DNA/siRNA in gels.

.

3.2.4 Transmission Electron Microscopy (TEM)

TEM produces high-resolution, black and white images from the interaction that takes place between prepared samples and energetic electrons in a vacuum chamber. A "light source" at the top of the microscope emits the electrons that travel through vacuum in the column of the microscope. The electrons then pass through multiple electromagnetic lenses to focus the electrons into a very thin beam. The electron beam then travels through the sample in study. At the bottom of the microscope the beam makes contact with a screen where the electrons are converted to light and form an image with varied darkness according to sample density. The lighter areas of the image

represent the places where a greater number of electrons were able to pass through the sample and the darker areas reflect the dense areas of the object. The image is finally photographed with a camera [188].

One drop of polymer-DNA/siRNA complexes (prepared as previously described, section 3.2.2, 1h incubation, polymer, DNA/siRNA mass ratios 5, 10, 30 and 60) was placed onto a carbon/Formvar coated 200 mesh copper grid (Agar Scientific, Stansted, UK) and negatively stained with 1% aqueous uranyl acetate solution. Polymer and naked nucleic acid solutions were used as negative controls. Imaging was carried out under Philips CM120 Biotwin Transmission Electron Microscope (Philips, Eindhoven, The Netherlands). Digital images were captured using a 5MP AMT camera (Deben Uk Ltd, Suffolk, UK).

3.2.5 Size and Zeta Potential

Nanoparticle Tracking Analysis is a new approach to the measurement of size compared to more traditional techniques such as Dynamic Light Scattering. A microscope, incorporating a camera, captures an image of the particles scattering of the laser light. Each individual particle seen is 'tracked' by the nanoparticle tracking analysis software. The particle size may be calculated from the Brownian motion with the Stokes–Einstein equation [189].

The size of the complexes was determined by nanoparticle tracking analysis (NanoSight LM20, NanoSight Limited, Malvern, UK). The samples were prepared as previously described (section 3.2.2) and allowed to incubate at room temperature for 1h. A volume of the sample (0.2 mL) was injected into the sample chamber. Videos of 30s in length were made and repeated 3 times with 0.2 mL of sample being injected each time. The camera settings for the instrument were set using the 'Autosettings' option on the software. The focus used was judged by eye, and was adjusted so that the majority of particles seen were in focus at any one time. The minimum expected particle size was set at 30 nm for all samples and the minimum track length set to automatic. The mean obtained from the NanoSight instrument is a number weighted average. The size is presented as an average of three measurements. In the nanoparticle tracking analysis the standard deviation measures the spread of the sizes in the particle size distribution. The higher the value of the standard deviation, the more polydisperse is the sample.

Surface charge was measured by determination of zeta potential using a Zetasizer Nano ZS (Malvern Instruments, Malvern, UK). The samples were prepared as previously described (section 3.2.2) and incubated for 1h at room temperature. A disposable folded capillary cell (0.5 mL) was used for zeta potential measurements. Zeta potential is presented as the average of three measurements ± standard deviation.

3.2.6 Biological challenges

a. Heparin

Nanoparticles were prepared as previously described (section 3.2.2) at polymer, DNA/siRNA mass ratios 5, 10, 30 and 60, and incubated for 1h at room temperature. Each heparin concentration (0.1 and 1 mg mL^{-1}, 1 µL, Sigma Aldrich, Dorset, UK) was added to the complex dispersion and incubated for 15 min. Samples were subjected to gel electrophoresis (1X TAE buffer) for 1 h at 60 V to investigate the stability of the binding complex in the presence of heparin. The results were imaged on a UV Transilluminator (ChemiDoc™ MP System, Bio Rad, Hemel, UK).

b. Salt

Nanoparticles were prepared as previously described (section 3.2.2) at polymer, DNA/siRNA mass ratios 5, 10, 30 and 60 and incubated for 1h at room temperature. NaCl (0.5 M, 3 µL, Sigma Aldrich, Dorset, UK) was added to the complex dispersion and incubated for 15 min. Samples were subjected to gel electrophoresis (1X TAE buffer) for 1 h at 60 V to investigate the stability of the binding complex. The results were imaged on a UV Transilluminator (ChemiDoc™ MP System, Bio Rad, Hemel, UK).

c. Nuclease

Resistance to nuclease digestion was determined using a deoxyribonuclease **(**DNase) and ribonuclease (RNase) protection assay. Nanoparticles were prepared as previously described (section 3.2.2) at polymer, DNA/siRNA mass ratios 5, 10, 30 and 60, and incubated for 1h at room temperature. DNase/RNase (1 unit μL^{-1}, 1 µL, Sigma Aldrich, Dorset, UK) was added to the complex or to naked DNA/siRNA. The samples were incubated at 37 °C for 15 min. Immediately following incubation, all samples were treated with ethylenediaminetetraacetic acid (EDTA, 50 mM, 10 µL, Sigma Aldrich,

Dorset, UK) for 10 min to deactivate the DNase/RNase. Finally, heparin solution (20 mg mL^{-1}, 1 µL, Sigma Aldrich, Dorset, UK) was added and the mixture was incubated for 30 min at room temperature to allow complete dissociation of the complexes. Samples were subjected to gel electrophoresis (1X TAE buffer) for 1 h at 60 V to investigate the stability of the complex against enzymatic degradation. The results were imaged on a UV Transilluminator (ChemiDoc™ MP System, Bio Rad, Hemel, UK).

3.3 Results

3.3.1 Agarose gel retardation essay

Agarose gel electrophoresis was performed to investigate the binding capability of GC and EAGC polymers with plasmid DNA (Figure 51). The complexes were allowed to interact for 30min or 1h before electrophoresis. Naked DNA (red, Figure 51) was used as the control. It is possible to observe (Figure 51) that both GC17 and GC28 were unable to condense with DNA, even at high polymer, DNA mass ratios. This was due to the non-protonation of the primary amines in the glycol chitosan backbone at physiological pH, preventing the polymer from interacting with the negatively charged plasmid DNA. Figure 51 also shows that the less substituted polymers, EAGC14, EAGC11 and EAGC13, were unable to condense the plasmid DNA after 30min of incubation for all polymer, DNA mass ratios. Increasing the degree of substitution (EAGC17 and EAGC21) increased the capacity of the polymers to retain the plasmid DNA for smaller polymer, DNA mass ratios. EAGC30 had the strongest DNA binding capacity, with full condensation of the plasmid at EAGC30, DNA mass ratios as low as 5.

When the incubation time was increased to 1 hour, the series of less-substituted polymers enhanced their capacity to condense the DNA at low polymer, DNA mass ratios (Figure 51). The exception was EAGC14 which released some plasmid, even for the high polymer, DNA mass ratios (50 and 60). The influence of the increase of the incubation time is mainly visible for EAGC13 and EAGC17 (Figure 51). These polymers were able to fully retard the plasmid mobility for polymer, DNA mass ratios as low as 10. EAGC21 after 1h completely retained the plasmid DNA for all polymer, DNA mass ratios to the same extent as EAGC30 (Figure 51).

The agarose gel experiments were used to screen the binding capacity of all the polymers synthesized in Chapter 2. Regarding the previous results it was decided that the polymers EAGC17, EAGC21 and EAGC30 were the best candidates for gene delivery, and therefore the following experiments (TEM, size, zeta and biological challenges) were only performed with these three polymers.

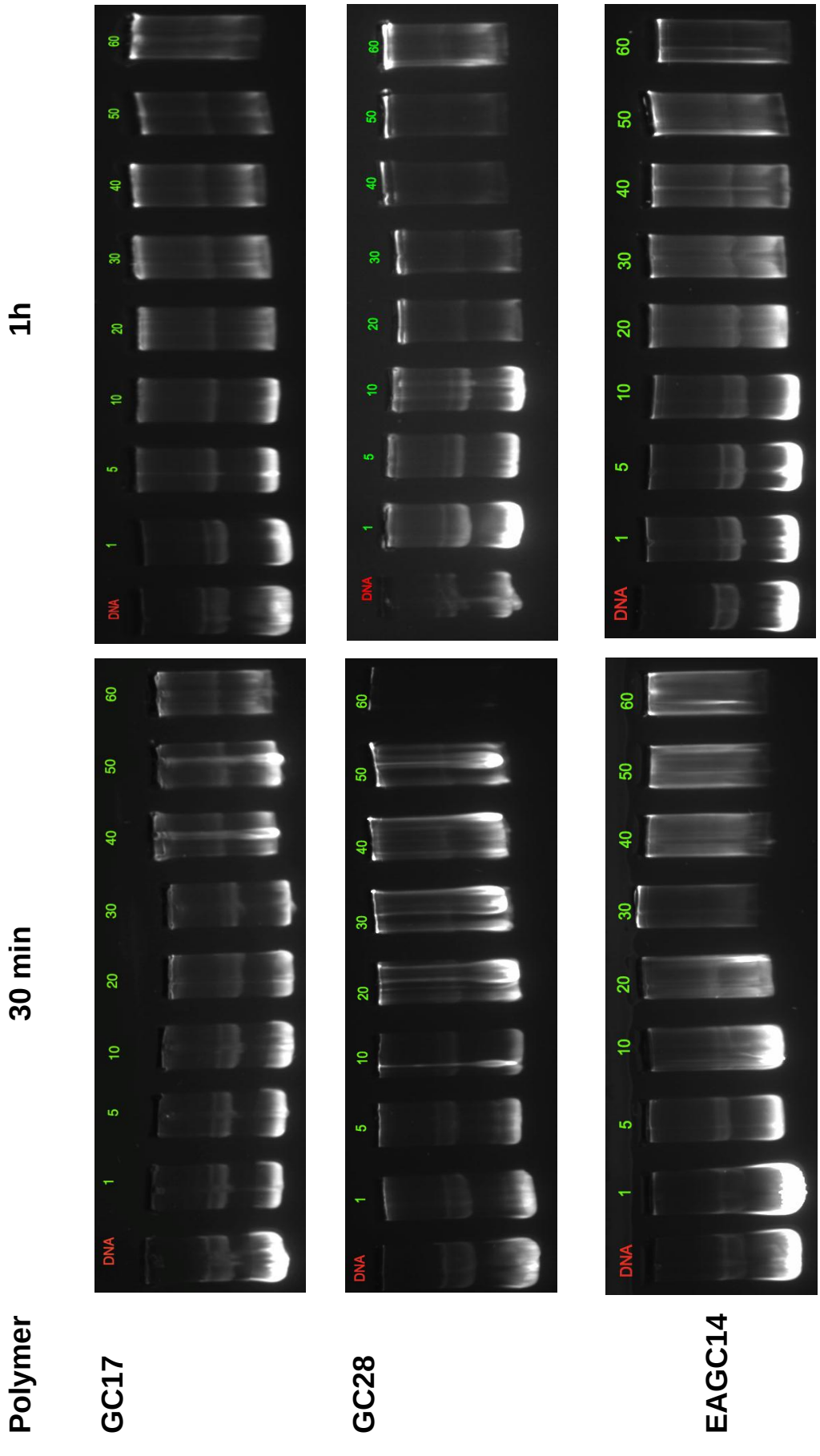
Polymer
30 min
1h
GC17
GC28
EAGC14
DNA
1
5
10
20
30
40
50
60

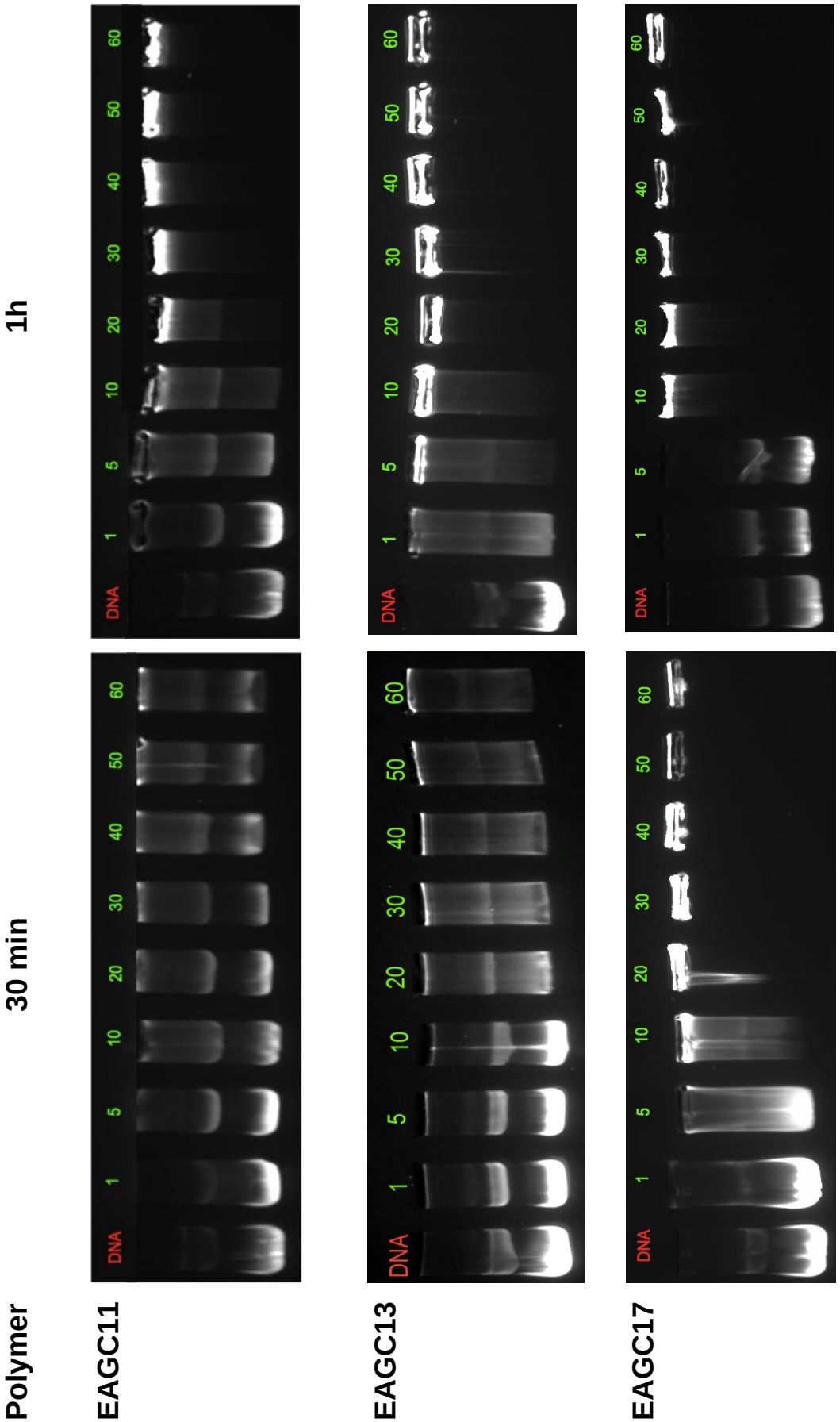
Polymer
30 min
1h
EAGC11
EAGC13
EAGC17
DNA
1
5
10
20
30
40
50
60

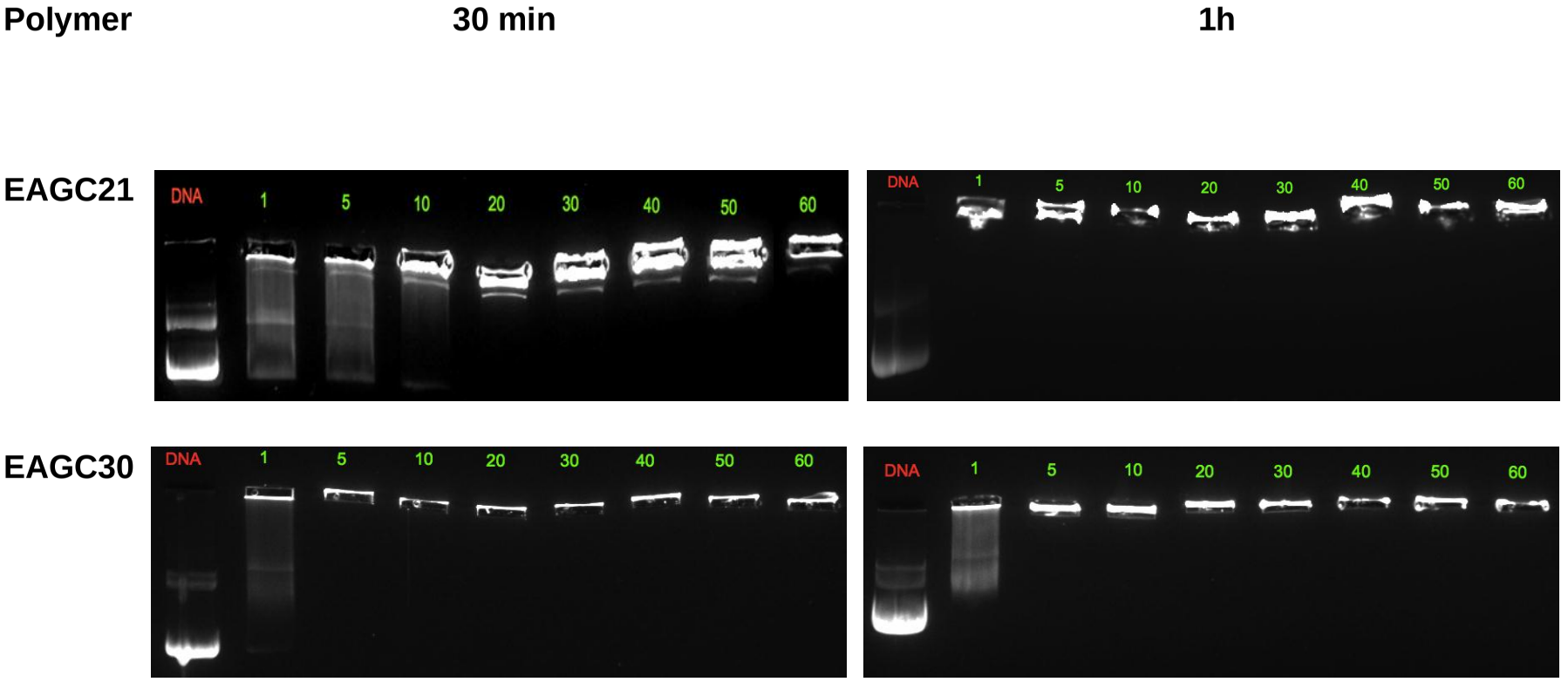

Figure 51 - Agarose gel electrophoresis of GC28, GC17, EAGC14, EAGC11, EAGC13, EAGC17, EAGC21 and EAGC30 complexed with plasmid DNA in dextrose 5%. DNA concentration 0.1 mg mL^{-1}. Incubation time 30min and 1h. Naked DNA (red) and increasing GC/EAGC, DNA mass ratios (green).

It has been described that siRNA polyplexes with chitosan are more unstable when compared with DNA complexes. Liu *et al.* studied the capacity of chitosan to complex with siRNA. Agarose gel results showed that chitosans with low molecular weight (9 and 12 kDa) were not able to retain siRNA at N:P ratio of 50 [125]. On the other hand, a low molecular weight chitosan (4.7 kDa) was able to fully condense plasmid DNA at a N:P ratio of 60 [126]. The difference of chitosan condensation with DNA and siRNA for low molecular weight polymers may be due to the longer DNA strands, that are able to compensate the shorter chitosan chains in the assembly process. The smaller strands of siRNA need longer chitosan chains to achieve stable complexes [125].

Furthermore, chitosan with a low degree of deacetylation (54%, 173 kDa) led to unstable polyplexes when compared with chitosans with higher charge density (78%), that were able to better retard the migration of siRNA in the agarose gel [125]. The difference of negative charge in the backbone of the two nucleic acids, with plasmid DNA providing a much higher amount of anionic charge (and consequently a higher charge interaction between polymer and DNA), contributes to the difference of stability of complexes formed with DNA or siRNA [190].

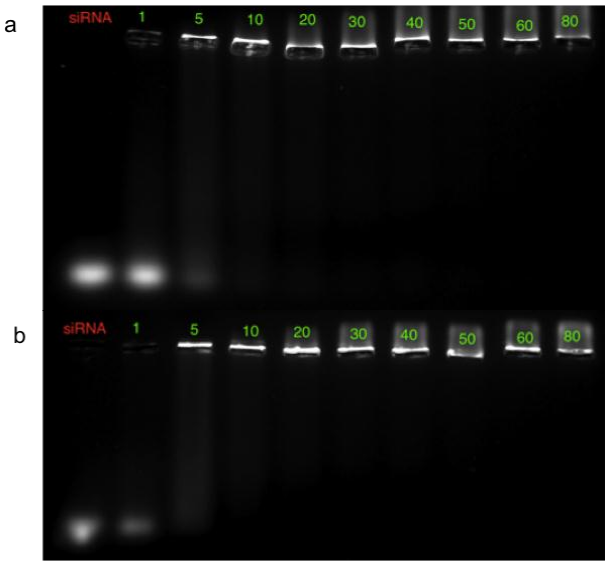

Figure 52 - Agarose gel electrophoresis of EAGC30 with siRNA at different EAGC30, siRNA mass ratios after a) 30min and b) 1h incubation. Polyplexes in 5% dextrose. siRNA concentration 0.1 mg mL^{-1}. Naked siRNA (red) and increasing EAGC30, siRNA mass ratios (green).

EAGC30 was able to fully retain the DNA for all polymer, DNA mass ratios, after just 30 min incubation, due to its higher charge density and molecular weight compared with the other EAGC polymers. Considering the molecular differences between DNA and siRNA described above, EAGC30 was concluded to be the best candidate for siRNA condensation and cell transfection.

Agarose gel electrophoresis was performed to investigate the binding capability of EAGC30 with siRNA. The complexes were allowed to interact for 30min or 1h before electrophoresis. Naked siRNA was used as control. Figure 52 shows that EAGC30 was able to completely condense siRNA for EAGC30, siRNA mass ratios as small as 5 after 30min of incubation. The same results were observed for 1h incubation.

3.3.2 Transmission Electron Microscopy

Morphological characterization of the nanoparticles formed between EAGC17, EAGC21 and EAGC30 and DNA was performed by TEM. Areas of greater electron density (such as particles) are visible as dark patches. Four polymer, DNA mass ratios were studied 5, 10, 30 and 60.

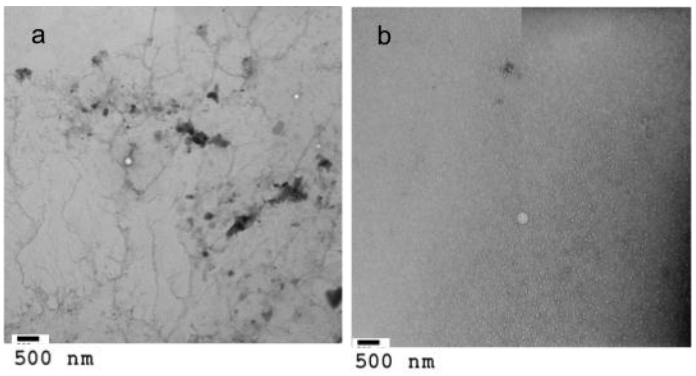

Figure 53 - TEM pictures of a) naked plasmid DNA at a concentration of 0.5 mg mL^{-1} in dextrose 5% and b) EAGC21 alone at a concentration of 1 mg mL^{-1} in dextrose 5%. No particles were observed.

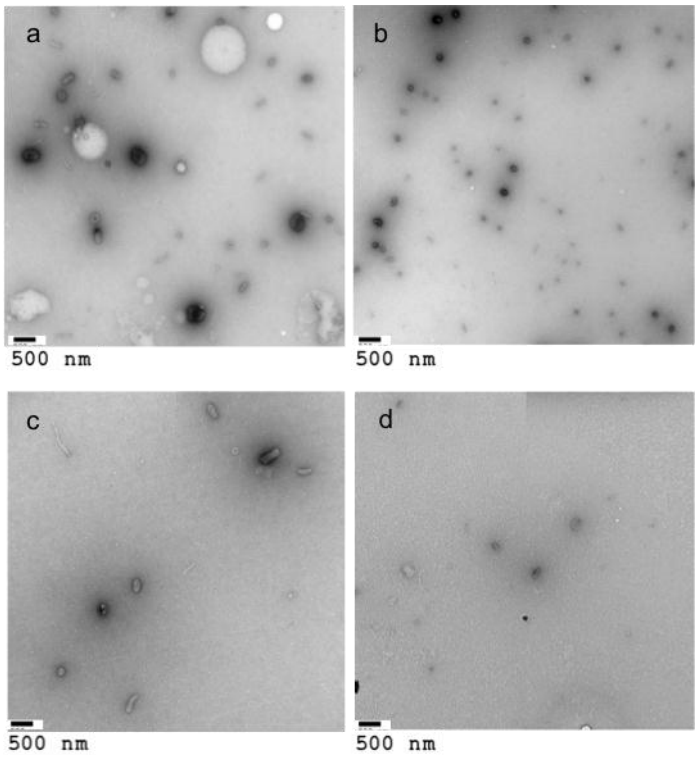

Figure 54 - Morphological characterization of EAGC17, DNA nanoparticles using TEM. EAGC17 was incubated with DNA in dextrose 5% for 1h. DNA concentration 0.1 mg mL^{-1}. EAGC17, DNA mass ratio of a) 5 b) 10 c) 30 d) 60. Nanoparticles are seen as the darker patches.

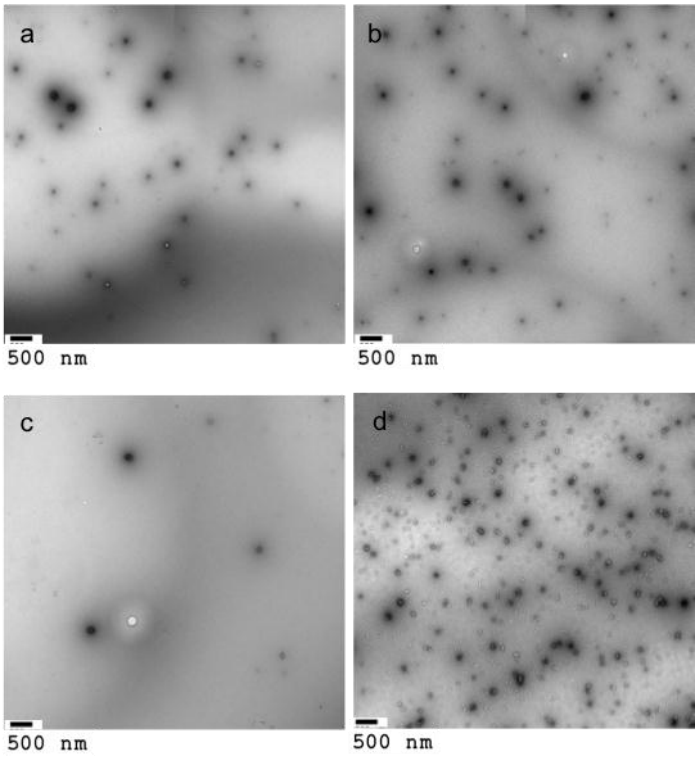

Figure 55 - Morphological characterization of EAGC21, DNA nanoparticles using TEM. EAGC21 was incubated with DNA in dextrose 5% for 1h. DNA concentration 0.1 mg mL^{-1}. EAGC21, DNA mass ratio of a) 5 b) 10 c) 30 d) 60. Nanoparticles are seen as the darker patches.

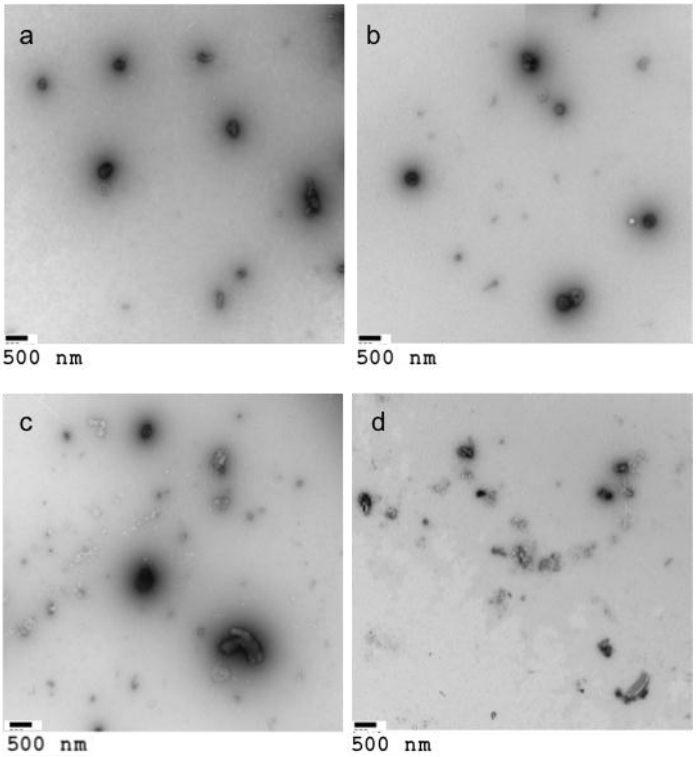

Figure 56 - Morphological characterization of EAGC30, DNA nanoparticles using TEM. EAGC30 was incubated with DNA in dextrose 5% for 1h. DNA concentration 0.1 mg mL-1. EAGC30, DNA mass ratio of a)5 b)10 c)30 d)60. Nanoparticles are seen as the darker patches.

TEM pictures showed that DNA alone presents a network structure as previously described [191]. EAGC21 alone presented quite homogenously through the entire grid, with no aggregation or particle formation observed (note the lack of dark patches in Figure 53). In the presence of the different polymers, the long interconnecting fibres of the anionic charged molecules of DNA were compacted into nanoparticles. The particles presented a spherical or toroid shape, with a relatively homogenous size between 50 and 200 nm. This was seen with all three polymers, at each polymer, DNA mass ratio (visible as dark patches in Figure 54, Figure 55 and Figure 56). For EAGC30 at the polymer, DNA mass ratio 60 (Figure 56d) it is possible to observe some polymer aggregation.

TEM pictures showed that siRNA alone has a network structure similar to plasmid DNA (Figure 57). When in presence of EAGC30 the siRNA was compacted into nanoparticles (Figure 58). These particles were spherical or in toroid shape with a size again between 50 and 200 nm for each of the four EAGC30, siRNA mass ratios.

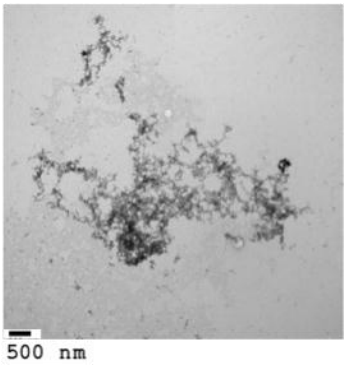

Figure 57 - TEM pictures of naked siRNA at a concentration of 0.5 mg mL^{-1} in dextrose 5%. No particles were observed.

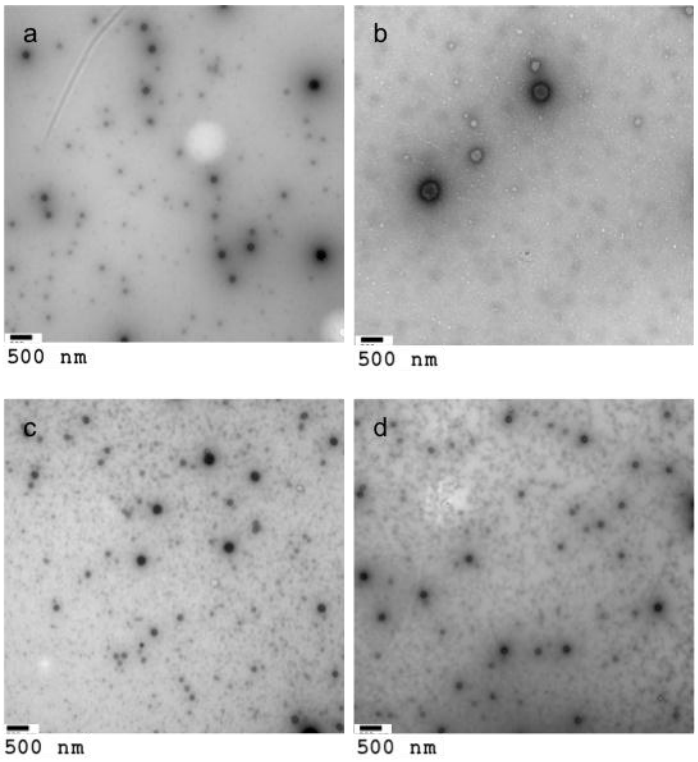

Figure 58 - Morphological characterization of EAGC30, siRNA nanoparticles using TEM. EAGC30 was incubated with siRNA in dextrose 5% for 1h. siRNA concentration 0.1 mg mL^{-1}. EAGC30, siRNA mass ratio of a)5 b)10 c)30 d)60. Nanoparticles are seen as the darker patches.

3.3.3 Size and Zeta Potential

Particle size was determined by nanoparticle tracking analysis for the three polymers EAGC17, EAGC21 and EAGC30 with plasmid DNA. The higher the value of the standard deviation, the more polydisperse is the sample. The particles presented sizes of between 100 and 450 nm (Figure 59 and Table 24). The nanoparticle tracking analysis data is in agreement with the TEM results.

EAGC17 nanoparticles presented smaller sizes and lower polydispersity with an increase of the polymer, DNA mass ratios (Table 24 and Figure 59). The smallest size was obtained for EAGC17, DNA mass ratio 60 (167nm). The size of EAGC17 nanoparticles was statistically (***$p \leq 0.001$) higher than the size of the nanoparticles formed with EAGC21 and EAGC30 for lower polymer, DNA mass ratios (Figure 59). These results are probably a consequence of the incapacity of EAGC17 to fully compact the DNA molecules at low polymer, DNA mass ratios, as revealed by the agarose gel assay (Figure 51). Since EAGC17 was the polymer with the lowest charge density (compared with EAGC21 and EAGC30) it was necessary to use more polymer (i.e. to have a higher polymer, DNA mass ratios) to compact the DNA in smaller nanoparticles.

EAGC21 showed uniform sizes through all the polymer, DNA mass ratios (Table 24 and Figure 59), while the size of the nanoparticles formed with EAGC30 increased with an increase of the polymer, DNA mass ratios (Table 24 and Figure 59). EAGC30 presented the highest charge density, and therefore at small polymer, DNA mass ratios the polymer was able to fully condense the DNA into particles with small size. With an increase of the polymer, DNA mass ratios the size of the particles grew, probably due to an aggregation of the polymer as observed in the TEM pictures (Figure 56d). The size of the nanoparticles formed between EAGC30 and DNA was statistically ($^{###}p \leq 0.001$) higher when compared with nanoparticles formed with EAGC17 and EGCC21 for high polymer, DNA mass ratios (Figure 59).

For each polymer, the particle size distribution was measured three times. The software calculated the mean (the average particle size measured), mode (the most frequent particle size found) and standard deviation (the breadth of the log-normal distribution fitted to the data). In addition, each value is reported with its standard error. In this work the size is presented as mean values ± standard error and standard deviation ± standard error.

Table 24 - Mean size and standard deviation (± standard error (SE)) of EAGC17, EAGC21 and EAGC30 complexes at various polymer, DNA mass ratios from nanoparticle tracking analysis measurements. EAGC17, EAGC21 and EAGC30 were incubated with DNA in dextrose 5% for 1h. DNA concentration 0.1 mg mL^{-1}. The data was expressed as mean values of three experiments. See Appendix for example graphical output.

Polymer, DNA mass ratio	EAGC17		EAGC21		EAGC30	
	Mean Size ± SE (nm)	Standard Deviation ± SE (nm)	Mean Size ± SE (nm)	Standard Deviation ± SE (nm)	Mean Size ± SE (nm)	Standard Deviation ± SE (nm)
1	356±21.6	140±18	157±3.2	82±4.5	169±6.2	47±0.9
5	401±11.8	178±19.1	222±2.5	96±3	221±3.1	183±5.2
10	338±11.7	130±10.9	228±3.0	102±4.2	143±6.1	66±1.6
20	187±3.8	87±3.3	184±2.5	93±6.7	206±4.4	101±4.5
30	299±3.6	99±2.9	174±1.2	86±1.9	225±4.2	130±5.0
40	183±1.5	79±1.4	212±3.4	91±0.7	243±4.8	118±5.7
50	281±3	100±4.2	296±5.5	106±6.7	441±17.8	181±23.2
60	167±3	79±0.5	242±10.2	129±12.6	347±5.4	153±3.9

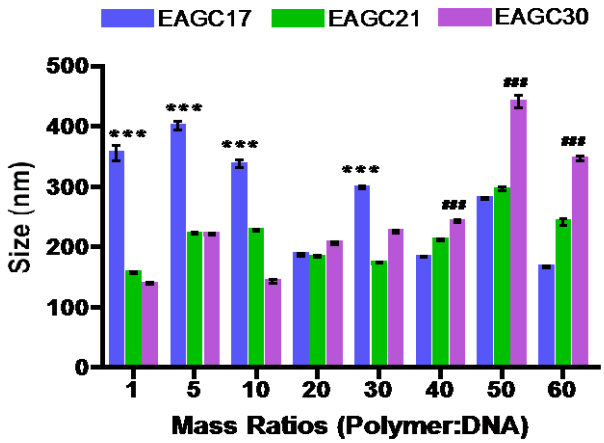

Figure 59 - Average particle size of EAGC17/21/30-DNA complexes at various polymer, DNA mass ratios. EAGC17, EAGC21 and EAGC30 were incubated with DNA in dextrose 5% for 1h. DNA concentration 0.1 mg mL^{-1}. The data was expressed as mean values (standard error) of three experiments. Two way ANOVA, Bonferonni post hoc test, EAGC17 vs EAGC21 and EAGC30 *p≤0.05, **p≤ 0.01, ***p≤0.001 and EAGC30 vs EAGC17 and EAGC21 #p≤0.05, ##p≤ 0.01, ###p≤0.001.

The zeta potential provides an indirect measurement of particle surface charge density. The values of zeta potential may depend on the pH and ionic strength of the measurement solution, the N:P ratio of the nanoparticles and the polymer characteristics [115]. Nanoparticles with high surface charge density present colloidal stability and high cellular uptake and transfection efficiency *in vitro* [105].

Regarding the surface charge of the nanoparticles formed between the three polymers and plasmid DNA, it was possible to observe a positive charge (+30mV to +40mV) for

all polymer, DNA mass ratios higher than 5 (Figure 60). At a polymer, DNA mass ratio of 1 all the nanoparticles showed a negative charge, since the excess of polymer that provided the positive charge at higher polymer, DNA mass ratios was absent. Nanoparticles formed with EAGC30 at a polymer, DNA mass ratio of 60 showed the highest zeta potential for all the polymers and polymer, DNA mass ratios measured (***p≤0.001). This high value of zeta is probably due to the presence of a higher number of protonated amines on the EAGC30 backbone when compared with EAGC17 and EAGC20. It should also be noted that the polymer by itself showed positive zeta values around +40mV.

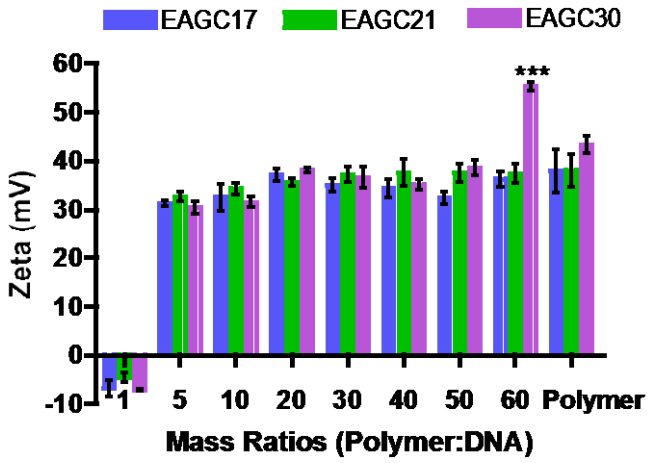

Figure 60 - Average zeta potential of EAGC17/21/30-DNA complexes at various polymer, DNA mass ratios. EAGC17, EAGC21 and EAGC30 was incubated with DNA in dextrose 5% for 1h. DNA concentration 0.1 mg mL^{-1}. The data was expressed as mean values (standard error) of three experiments. Two way ANOVA, Bonferonni post hoc test, EAGC30 vs EAGC17 and EAGC21 *p≤0.05, **p≤ 0.01, ***p≤0.001.

The particles formed between EAGC30 and siRNA presented a size between 150 and 500nm. The highest size was reported for EAGC30, siRNA mass ratio 1 (***p≤0.001, Table 25 and Figure 61). The high level of standard deviation for EAGC30, siRNA mass ratio 1 indicates a polydisperse solution where siRNA molecules, polymer aggregates and nanoparticles may be present. These results are in accordance with the agarose gel results where there was no retardation of siRNA for EAGC30, siRNA mass ratio 1 (Figure 52). To allow a full condensation of the siRNA in small nanoparticles it was necessary to increase the EAGC30, siRNA mass ratios. The size of the nanoparticles decreased for higher EAGC30, siRNA mass ratios.

Table 25 - Mean size and standard deviation (± standard error (SE)) of EAGC30 complexes at various polymer, siRNA mass ratios from nanoparticle tracking analysis measurements. EAGC30 was incubated with siRNA in dextrose 5% for 1h. siRNA concentration 0.1 mg mL^{-1}. The data was expressed as mean values of three experiments.

EAGC30, siRNA mass ratio	Mean Size ± SE (nm)	Standard Deviation ± SE (nm)
1	484±53.5	217±35
5	225±10.7	101±9.5
10	167±3.1	85±0.8
20	218±19.2	99±6.2
30	205±13.1	106±7.1
40	254±9.2	120±6.9
50	278±10.1	139±2
60	255±4.5	135±1.3

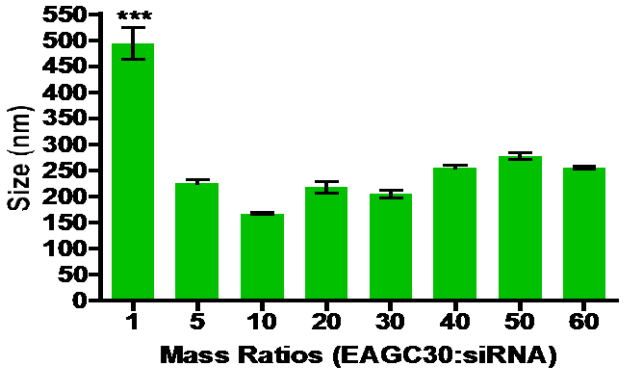

Figure 61 - Average particle size of EAGC30-siRNA complexes at various polymer, siRNA mass ratios. EAGC30 was incubated with siRNA in dextrose 5% for 1h. siRNA concentration 0.1 mg mL^{-1}. The data was expressed as mean values (standard deviation) of three experiments. Mean ± SEM (n=3), One way ANOVA, Bonferonni post hoc test, EAGC30, siRNA mass ratios >5 vs EAGC30, siRNA mass ratio 1 *p≤0.05, **p≤ 0.01, ***p≤0.001.

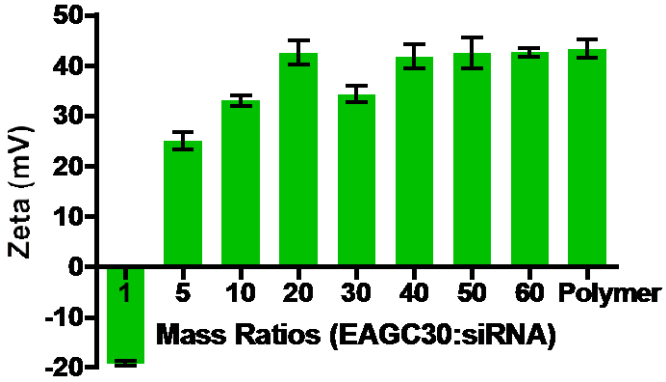

Figure 62 - Average zeta potential of EAGC30-siRNA complexes at various polymer, siRNA mass ratios. EAGC30 was incubated with siRNA in dextrose 5% for 1h. siRNA concentration 0.1 mg mL^{-1}. The data was expressed as mean values (standard deviation) of three experiments.

Regarding the surface charge of the nanoparticles formed between EAGC30 and siRNA (Figure 62) it was possible to observe a positive charge for all EAGC30, siRNA mass ratios higher than 5. At an EAGC30, siRNA mass ratio of 1, the nanoparticles presented a negative charge. At this EAGC30, siRNA mass ratio there was not an excess of amines when compared with the negative charge in the siRNA backbone, resulting in negative values for the overall charge.

3.3.4 Biological Challenges

a. Heparin

In the extracellular compartments, the presence of negatively charged molecules such as serum albumin and other extracellular proteins that interact with the positively charged nanoparticles may introduce instability in the gene delivery systems [185]. These anionic molecules may lead to aggregation of the nanoparticles and displacement of the nucleic acids from the delivery system due to competition [185].

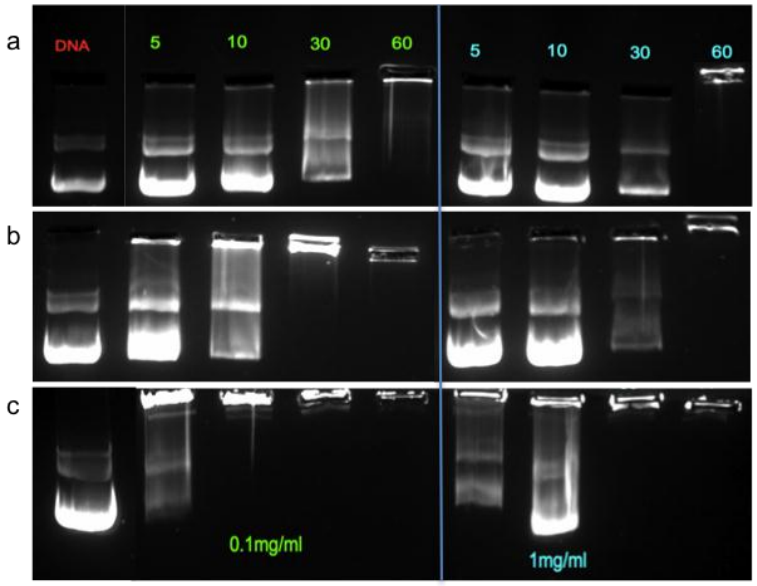

Figure 63 - Agarose gels of EAGC-DNA complexes (polymer, DNA mass ratios 5, 10, 30 and 60) after incubation with heparin (0.1 and 1 mg.mL^{-1}) for 15min. Polymers were incubated with DNA in dextrose 5% for 1h. DNA concentration 0.1 mg mL^{-1}. a) EAGC17-DNA b) EAGC21-DNA c) EAGC30-DNA.

The stability of the complexes in biological fluids was investigated through incubation of the former with increasing concentrations of heparin (0.1 and 1 mg mL^{-1}). Heparin is an anionic protein that competes with the nucleic acids to bind to cationic polymers. This competition can lead to the dissociation of the polyplexes.

It is possible to observe in Figure 63a that EAGC17 is just able to retain the plasmid DNA for high EAGC17, DNA mass ratios (EAGC17, DNA mass ratio 60) for both heparin concentrations. With the increase of the number of amines in the polymer backbone (and consequently the charge ratio), EAGC21 was able to keep stable nanoparticles for EAGC21, DNA mass ratio 30 in the presence of the smallest concentration of heparin (0.1 mg mL^{-1}, Figure 63b). Finally, EAGC30 showed total condensation of DNA for EAGC30, DNA mass ratios 10, 30 and 60 in the presence of 0.1 mg mL^{-1} of heparin and for EAGC30, DNA mass ratios 30 and 60 with the highest concentration (Figure 63c). EAGC30 nanoparticles were the most stable in the presence of both concentrations of heparin, due probably to the molecular weight and charge density of EACG30 when compared with the other EACG polymers synthesized.

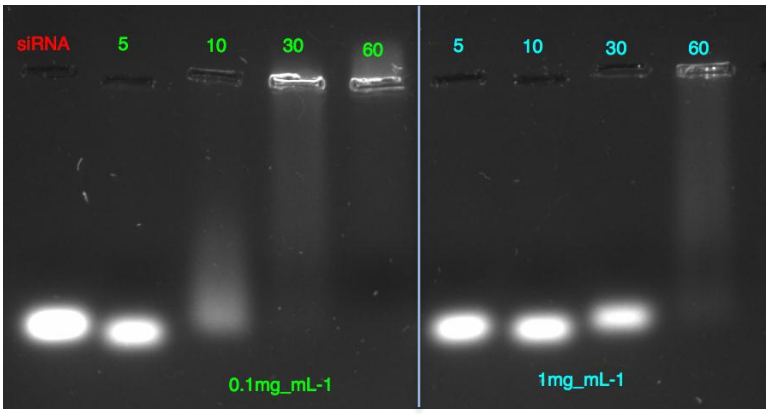

Figure 64 - Agarose gels of EAGC30-siRNA complexes (EAGC30, siRNA mass ratios 5, 10, 30 and 60) after incubation with heparin (0.1 and 1 mg mL^{-1}) for 15min. Polymers were incubated with siRNA in dextrose 5% for 1h. siRNA concentration 0.1 mg mL^{-1}.

It is possible to observe in Figure 64 that EAGC30 was able to retain the siRNA for high EAGC30, siRNA mass ratios, 30 and 60, in the presence of 0.1 mg mL^{-1} of heparin. When the concentration of heparin was increased the complexes appeared to be quite unstable and the release of some siRNA occurred even for the highest EAGC30, siRNA mass ratio (EAGC30, siRNA mass ratio of 60). These results are in

line with the previously described instability of siRNA nanoparticles [125]. Chitosans with high molecular weight and/or high degree of deacetylation were required to obtain chitosan siRNA, complexes as stable as chitosan, DNA complexes [125]. This instability in the presence of negatively charged molecules, such as heparin, resulted in the release of the siRNA for smaller EAGC30, siRNA mass ratios (Figure 64) when compared with EAGC30, DNA results (Figure 63 c).

b. Salt

The high ionic strength of the *in vivo* environment may disturb the colloid stability of the complexes, and release of the nucleic acids may occur due to charge screening. The complexes were incubated with 150mM of NaCl for 15 minutes and compared by gel electrophoresis to complexes in 5% dextrose.

As described before (agarose gel experiments, Section 3.3.1) an increase of the polymer substitution, associated with an increase in charge density, delivered more stable complexes. The same was observed in the presence of salt. Furthermore, the presence or absence of salt did not influence the DNA release for any EAGC polymer (Figure 65).

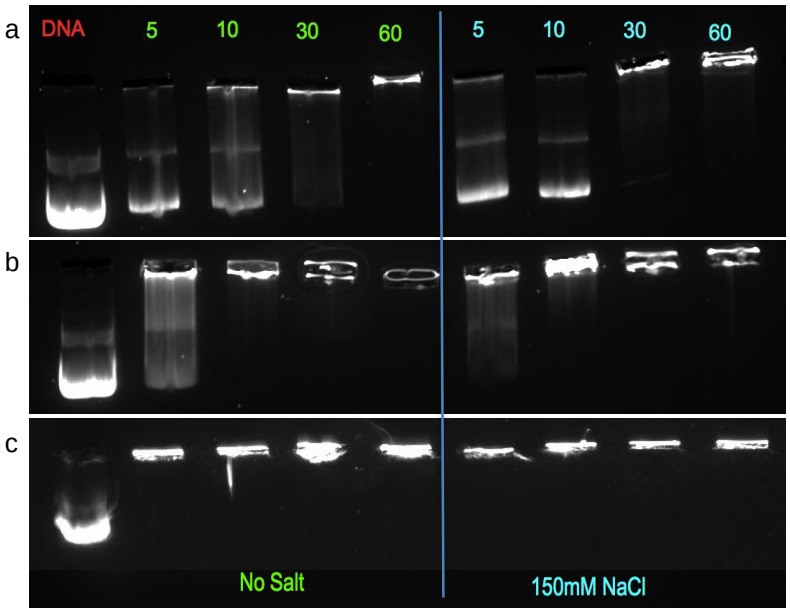

Figure 65 - Agarose gels of EAGC-DNA complexes (polymer, DNA mass ratios 5, 10, 30 and 60) after incubation with NaCl (150mM) for 15min. Polymers were incubated with DNA in dextrose 5% for 1h. DNA concentration 0.1 mg mL^{-1}. a) EAGC17-DNA b) EAGC21-DNA c) EAGC30-DNA.

The presence of 150 mM NaCl in the nanoparticle solution formed between EAGC30 and siRNA led to disassembly of the complexes and release of siRNA. siRNA was released for EAGC30, siRNA mass ratios 5 and 10 in the presence of salt. There was no release of siRNA for EAGC30, siRNA mass ratios 30 and 60 in the absence or presence of 150mM NaCl (Figure 66).

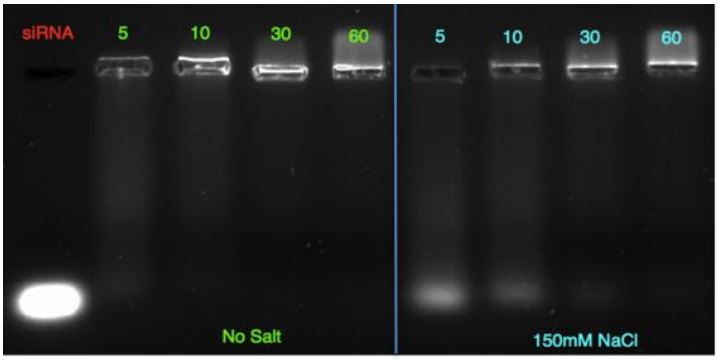

Figure 66 - Agarose gels of EAGC30-siRNA complexes (MR 5, 10, 30 and 60) after incubation with NaCl (150mM) for 15min. Polymers were incubated with siRNA in dextrose 5% for 1h. siRNA concentration 0.1 mg mL^{-1}.

c. Nuclease

One of the challenges upon administration of nucleic acids *in vivo* are the endogenous nucleases. Gene delivery systems need to protect the nucleic acids from enzymatic degradation in order to enhance bioavailability and improve the pharmacokinetic profile [192]. DNase is an endonuclease that hydrolyses the double-stranded DNA. DNase is present *in vivo* on the extra- and intracellular spaces, and is one of the major barriers for gene delivery. Unprotected DNA is easily degraded by DNase in a matter of minutes [187].

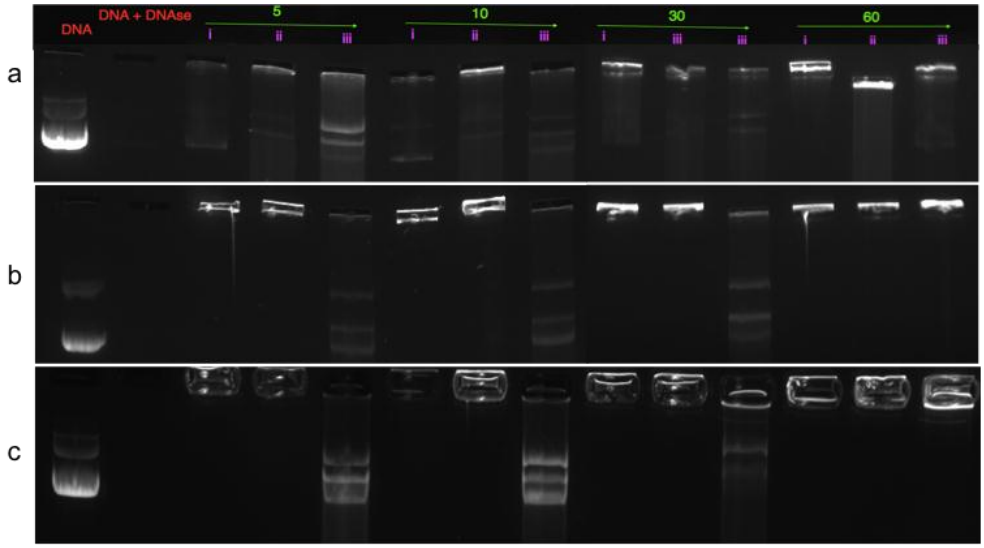

Figure 67 - Agarose gels of EAGC – DNA complexes (MR 5, 10, 30 and 60) after incubation with DNAse (1 unit) for 15min. Polymers were incubated with DNA in dextrose 5% for 1h. DNA concentration 0.1 mg mL^{-1}. a) EAGC17-DNA b) EAGC21-DNA c) EAGC30-DNA. i) EAGC-DNA complexes ii) EAGC-DNA complexes + DNase iii) EAGC-DNA complexes + DNase + Heparin.

It is possible to observe that DNA alone in the presence of DNase was completely degraded (red: DNA+DNase, Figure 67) when compared with DNA without DNase (red: DNA, Figure 67). For all the polymer, DNA mass ratios, the complexes were incubated with DNase and heparin (that would release the DNA) to confirm if there was nucleic acid degradation or not. All polymers were able to offer some protection to DNA from nuclease degradation for all polymer, DNA mass ratios. EAGC17 (Figure 67a) and EAGC21 (Figure 67b) agarose gels show some degradation of DNA for all polymer, DNA mass ratios when compared with EAGC30. EAGC30 was able to completely protect DNA from degradation. At polymer, DNA mass ratio 60 for EAGC21 and EACG30, the amount of heparin was not enough to release the DNA. However it was possible to visualize the DNA fluorescence in the application point, which indicates that there was no degradation of the DNA by the DNase.

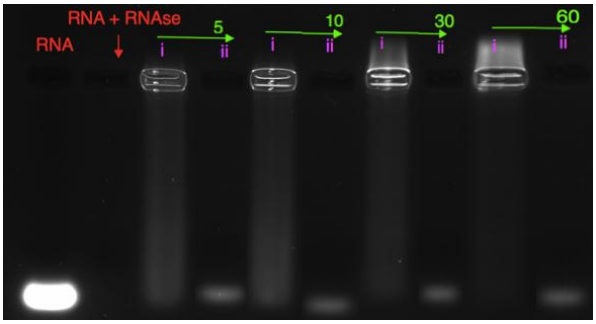

Figure 68 - Agarose gel of EAGC30-siRNA complexes (EAGC30, siRNA mass ratios 5, 10, 30 and 60) after incubation with RNase (1 unit) for 15min. Polymers were incubated with siRNA in dextrose 5% for 1h. siRNA concentration 0.1 mg mL^{-1}. A) EAGC-siRNA complexes B) EAGC-siRNA complexes + RNase + Heparin.

RNase is an endonuclease that hydrolyses the molecules of siRNA. Like DNase, RNase is present *in vivo* in the extra- and intracellular spaces, and is one of the major barriers for gene delivery [187]. EAGC30 protected the siRNA against degradation, for all EAGC30, siRNA mass ratios as it is possible to observe in Figure 68. RNA alone in the presence of RNase was completely degraded (red: RNA+RNase, Figure 68) when compared with siRNA without RNase (red: RNA, Figure 68). For all the EAGC30, siRNA mass ratios the complexes were incubated with RNase and then heparin, to release the siRNA in order to verify if there has been degradation or not.

3.4 Discussion

A gene delivery vector should be able to interact with the nucleic acid molecules, in order to condense their structure to appropriate sizes that will allow DNA and siRNA delivery to the cells. The capacity of cationic polymers, like EAGC, to compact the structure of nucleic acids relies on electrostatic interactions between the positively charged polymer and negatively charged DNA/siRNA. These interactions are highly dependent on different factors, for example EAGC charge density and polymer, nucleic acid mass ratio.

The results of the agarose gel retardation assay revealed that GC28 and GC17 were not able to completely condense with DNA at any polymer, DNA mass ratios. Since the primary amines of the glycol chitosan backbone are not protonated at physiological pH (pKa=6.5), an electrostatic interaction with the negatively charged DNA was not possible and therefore the entire DNA was released.

EAGC14, with the smallest amount of amines introduced on the GC backbone, revealed condensation results as poor as GC17. However, when the number of amines was increased, through the introduction of the ethylamino double substitution, EAGC11, EAGC13 and EAGC17 showed improved retention capacity of the DNA after 1h of incubation. EAGC30 presented the strongest DNA binding ability, as the DNA mobility was fully retarded at polymer, DNA mass ratios as low as 5 after 30min of incubation.

The results indicated that the binding ability of EAGC with DNA increased with the increasing charge density of the polymer, which is in agreement with the literature [193, 194]. Howard *et al.* studied several chitosans with different molecular weights and degrees of deacetylation. Only chitosans with a high degree of deacetylation (85% and 99%) were able to retain the plasmid DNA for low N:P ratios, (N:P ratio 1.8:1) [110]. Chitosans with a degree of deacetylation of 51% and 65% were not able to completely retain the plasmid DNA [110].

EAGC30 presented the highest total number of amines of the polymers synthesized, including primary amines that are an important factor when considering the condensation of DNA. It has been described that a high density of positive charges, i.e. primary amino groups, is required to obtain stable polyplexes [110, 180, 195]. The high pKa of the primary amines of the ethylamino groups of all EAGC polymers, between 9 and 10, makes them fully protonated at physiological pH, and the positive charge

readily enables condensation with the negatively charged nucleic acids. This is in particular contrast to chitosan, where the pKa of the amine groups, as previously discussed, does not allow them to be protonated at physiological pH [114].

As previously explained, EAGC30 was the polymer chosen to condense siRNA due to the characteristics of the nucleic acid. Previously authors had demonstrated that to achieve stable nanoparticles, siRNA requires polymers with high molecular weight and high charge density [125, 190]. The difference of chitosan condensation with DNA and siRNA for low molecular weight polymers may be due to the longer DNA strands that are able to compensate for the shorter chitosan chains in the assembly process. The smaller strands of siRNA need longer chitosan chains to achieve similarly stable complexes [125]. Also, the difference of the negative charge in the backbone of the two nucleic acids, with plasmid DNA providing a much higher amount of anionic charge (and therefore higher charge interaction between polymer and DNA) contributes to the difference of stability of complexes formed with DNA or siRNA [190].

Agarose gel results for EAGC30 with siRNA showed that the polymer was able to retain the nucleic acid for EAGC30, siRNA mass ratios above 5. These are similar results to the ones obtained for EAGC30 with DNA, but are nevertheless in contrast with the literature. Techarporknoly *et al.* showed that chitosans with low molecular weight (20 and 45 kDa, 85% degree of deacetylation) required higher polymer, siRNA mass ratios, above 16, when compared with high molecular weight polymers (200 and 460 kDa, 85% degree of deacetylation) that were able to completely retain the siRNA for polymer, siRNA mass ratios above 8 [129].

Alaemah *et al.* demonstrated that different factors may influence the stability of the nanoparticles and therefore influence the final results in the agarose gel assay. Nanoparticle stability regarding incubation time (0.5, 4 and 20h), pH of the buffer (pH 6.5 and 8) and N:P ratio (0, 0.5, 2 and 10) was studied. Low molecular weight chitosan (12 kDa) was able to completely retain siRNA at low N:P ratios (above 2) after condensation between the polymer and the nucleic acid for 20h. The electrophoresis was performed at a pH of 6.5, leading to a higher degree of protonation of the chitosan amines and therefore increased electrostatic interactions with the nucleic acids. After 0.5 and 4 hours of complexation, release of siRNA was observed for all N:P ratios at pH 8. No release was observed at pH 6.5. Therefore, an increase in the condensation time and decrease in the pH of the electrophoresis buffer results in more stable particles for lower N:P ratios [192]. Due to the characteristics of EAGC30 (higher charge density and primary amines with pKa ≈ 9-10) the nanoparticles formed with this

polymer and siRNA were stable after only 30min of incubation and at a pH 8 of the electrophoresis buffer.

Particle size and shape are important characteristics for intracellular delivery of genes as well as tissue distribution [123, 192]. Morphological characterization of the polyplexes formed between EAGC and DNA/siRNA was made by TEM. The complexes were spherical or toroid for all EAGC-DNA and EAGC30-siRNA nanoparticles. Spherical nanoparticles have been described as result of the complexation between low molecular weight chitosans and DNA. High molecular weight polymers when in the presence of DNA resulted in elongated and irregular nanoparticles with a polydisperse morphology [127].

It has been reported that particles in the nanometre range (20-500nm) are more successful for intracellular uptake when compared with microparticles [193, 196]. Particle size was determined by nanoparticle tracking analysis for the three polymers EAGC17, EAGC21 and EAGC30 with plasmid DNA. EAGC17 nanoparticles presented smaller sizes and polydispersity with the increase of the polymer, DNA mass ratios. Due to the polymer lower charge density (compared with EAGC21 and EAGC30) it was necessary to use more polymer (higher polymer, DNA mass ratios) to compact the DNA in small nanoparticles. A decrease of chitosan nanoparticle size with an increase of the N:P ratio was previously described by Romeren *et al.* A decrease in size was observed when the N:P ratio was increased from 0.5 to 5 [130]. Conversely, the size of the nanoparticles formed with EAGC30 increased with an increase of the polymer, DNA mass ratios, probably due to aggregation of the polymer. Similar findings were described for chitosan with 32 kDa where an excess of polymer relative to plasmid DNA resulted in an increase of the nanoparticle size [112]. EAGC21 showed uniform sizes and standard deviation through all the polymer, DNA mass ratios. Regarding the previous results it is possible to conclude that the right balance between polymer molecular weight and charge density is necessary to obtain a monodisperse formulation with nanoparticles in the nanometre range (20-500nm).

The particles formed between EAGC30 and siRNA presented a size between 150 and 500nm. The biggest size was reported for EAGC30, siRNA mass ratio 1. These results are in accordance with the agarose gel results, where there was no retardation of siRNA for EAGC30, siRNA mass ratio 1. To allow a full condensation of the siRNA in small nanoparticles it was necessary to increase the EAGC30, siRNA mass ratios.

The surface charge of the complexes is very important for the interaction with the cell surface. The cellular membrane is negatively charged, making it a good target for the positively charged nanoparticles [196, 197]. Zeta potential values for chitosan nanoparticles depend mainly on the pH of the media [104] as well as on the chitosan, DNA/siRNA ratios [129] and characteristics of chitosan such as degree of deacetylation [104]. The high surface charge density of the polyplexes formed with cationic polymers such as chitosan determines the complexes colloidal stability which correlates with the transfection efficiency of the nanoparticles [105]. The polyplexes formed between EAGC17, EAGC21, EAGC30 and DNA presented a positive charge of around +40mV for all polymer, DNA mass ratios above 5. These results confirm the high protonation of EAGC polymers at physiological pH. Similar results were obtained for siRNA nanoparticles with EAGC30. Previous studies had reported that in the presence of an excess of chitosan, nanoparticles formed between chitosan and DNA/siRNA presented positive zeta potential [125]. However, N:P ratios higher than 32 were necessary to obtain chitosan, siRNA polyplexes with a positive zeta potential [129].

The extra and intracellular environment has a strong impact on the stability of the nanoparticles formed with cationic polymers. Anionic proteins, salt and nucleases are among the major hurdles that polyplexes need to overcome even before reaching the cell surface [179]. The biological stability tests studied the EAGC particles' stability in challenging environments. After preparation of the polyplexes they were incubated with heparin, NaCl and DNase or RNase.

Non-specific interactions of serum proteins with the polyplexes may lead to aggregation of the nanoparticles and displacement of the nucleic acids from the delivery system due to competition [185]. Heparin is a strongly negatively charged protein that was incubated with the nanoparticles at two different concentrations (0.1 mg mL^{-1} and 1 mg mL^{-1}). EAGC17 nanoparticles with DNA showed poor stability in the presence of heparin even at the lowest concentration. Increasing the substitution of the polymer, leading to higher charge density, improved the capacity of the polymers to retain the DNA at lower polymer, DNA mass ratios. EAGC30 completely condensed the DNA for a polymer, DNA mass ratio of 10. When compared with chitosan nanoparticles it is possible to conclude that the introduction of the ethylamino group provided higher stability to the nanoparticles formed with EAGC30. Strand *et al.* reported that the DNA release from chitosan polyplexes decreased with an increase in the N:P ratio and the molecular weight of chitosan in the presence of 0.1 mg mL^{-1} of heparin. Nanoparticles

prepared with chitosans with molecular weight of 17 and 33 kDa were only able to retain the DNA for N:P ratios higher than 20 after 4 and 14h of incubation [55].

siRNA nanoparticles did not show the same stability with EAGC30 in the presence of heparin as DNA nanoparticles formulated with the same polymer. The polymer was only able to completely retain the siRNA for EAGC30, siRNA mass ratio of 60 in the presence of the higher concentration of heparin. These results confirm the higher instability of nanoparticles formed with siRNA previously described for other polymers [125].

The increased ionic strength present in *in vivo* environments can lead to aggregation or disassembly of the complexes due to screening of the electrostatic interactions [185]. EAGC complexes showed good stability when in presence of NaCl. There was no difference in the release of DNA from the complexes in the presence of NaCl. EAGC30-siRNA particles were unstable in the presence of NaCl for small EAGC30, siRNA mass ratios with release of siRNA at EAGC30, siRNA mass ratios of 5 and 10. It was not possible to conclude from the agarose gel results if there was aggregation of the complexes. The measurement of the nanoparticles size over the time in the presence of NaCl would be one of the possible experiments to detect aggregation.

Finally, the complexes were tested against the presence of nucleases. When naked nucleic acids are introduced in the blood stream they are easily degraded. One of the major functions of polymers is to protect the nucleic acid so they are able to reach the cell surface intact [29, 185]. The EAGC complexes were incubated with nucleases (DNase and RNase) and subsequently with heparin, which caused the release of the nucleic acid from the complexes in order to confirm their intact structure. All polymers were able to offer some protection to DNA from nuclease degradation for all polymer, DNA mass ratios. EAGC17 and EAGC21 agarose gels show some degradation of DNA for all polymer, DNA mass ratios when compared with EAGC30. These results are probably a consequence of the degree of substitution of the polymers and stability of the nanoparticles. The more substituted polymer (EAGC30) previously showed more stable nanoparticles, that probably led to a higher degree of protection when in the presence of DNase. EAGC30 was also able to protect siRNA for all EAGC30, siRNA mass ratios. Similar results were obtained by Lee *et al.* for polyplexes formed with low molecular weight chitosan, 22 kDa for a mass ratio (DNA, chitosan) of 1:1 and 1:2 [94]. Low molecular weight chitosan (10 kDa at pH 6.5) has been previously described as able to effectively protect siRNA from degradation in the presence of RNase [192].

In summary, three polymers (EAGC17, EAGC21 and EAGC30) were condensed with DNA and the resultant complexes were characterized. All the polymers formed small nanoparticles with positive surface charge. EAGC30 nanoparticles showed the best stability when in presence of biological challenges, meaning that the increase of the charge density on the polymer backbone delivered more stable particles. EAGC30-siRNA polyplexes showed small size and a positive surface charge. The stability of the siRNA nanoparticles in biological conditions (in the presence of heparin and salt) was reduced when compared with DNA particles, for low EAGC30, siRNA mass ratios.

4. Biological Studies with plasmid DNA

4.1 Introduction

In the previous chapters was presented the synthesis and characterization of N-(2-ethylamino)-6-O-glycol chitosan (EAGC) with three levels of ethylamino substitution (EAGC17, EAGC21 and EAGC30). The three polymers showed the ability to complex with plasmid DNA. The resultant nanoparticles were of an acceptable size and zeta potential, and displayed stable behaviour in biological fluids. All of these are important characteristics that may contribute to the transfection efficiency of the polymers *in vitro.* Also, the biocompatibility of EAGC in cells is an aspect that can impair the gene delivery capacity of the polymers.

The toxicity of cationic polymers is mostly related with the charge density that these vectors present [99, 100]. The strong ionic interaction between the positive charges of the polymers and the negatively charged cell membrane components is purported to affect membrane integrity, causing changes to the overall function of the cell and ultimately leading to its death [99, 100].

Chitosan presents low toxicity when compared with other cationic polymers such as PEI. For chitosan, IC50 (the concentration of polymer at which 50% of cells are viable) values have been reported between 0.2-20 mg mL^{-1} in different cell lines [86]. Conversely, PEI presented an IC50 <20 µg mL^{-1} [101, 102]. Chitosans with different molecular weights and degrees of deacetylation (<5 kDa, 65.4%; 5–10 kDa, 55.3%; and >10 kDa, 55.3%) showed an IC50 >1 mg mL^{-1} in CCRF-CEM (human lymphoblastic leukaemia cells) and L132 (human embryonic lung cells). Haemolysis was not observed (<10%) over 1 h and 5 h with chitosans of <5 kDa, 5–10 kDa and >10 kDa at concentrations of up to 5 mg mL^{-1} [103].

As well as the charge density (determined by degree of deacetylation), the molecular weight contributes to chitosan's cell biocompatibility [86, 104]. High molecular weight polymers (>100 kDa) with a high degree of deacetylation were less biocompatible [95] than lower molecular weight chitosans (10 kDa) [105].

Huang *et al.* suggested that the degree of deacetylation has a greater effect than the molecular weight on chitosan's biocompatibility [95]. IC50 values for chitosans with degrees of deacetylation of 88%, 61% and 46% showed an increasing trend with values of 1.2, 2.0 and 2.2 mg mL^{-1}, respectively [95].

The results of Nimesh *et al.* corroborate the theory that the charge density may contribute to the biocompatibility of chitosan, since the cell viability was lower at lower pH when the protonation of chitosan is higher. After 48h of incubation with chitosan (10 kDa, 92% degree of deacetylation), more than 85% of cells were viable at pH 6.5 and 96% at pH 7.1 [105]. In their studies, Schipper *et al.* also concluded that toxicity of chitosan is dependent on the degree of deacetylation and molecular weight. At a high degree of deacetylation, the biocompatibility of chitosan is related to the molecular weight and the concentration; at a lower degree of deacetylation toxicity is less pronounced and less related to the molecular weight. [106, 107].

The modifications made to chitosan can make it more or less biocompatible. Carreno-Gomez showed that glycol chitosan (IC50 = 2.47 mg mL^{-1}) is more biocompatible when compared with other chitosan salts such as chitosan hydroglutamate (IC50 = 1.73 mg mL^{-1}) [108]. Trimethyl chitosan is more toxic than chitosan, and its toxicity was found to be directly related with the degree of trimethylation (charge density) [102]. Trimethyl chitosan (100 kDa) with a percentage of trimethylation of 93% presented an IC50 of 0.293 mg mL^{-1} after 6h in contact with human breast epithelial cells (MCF-7 cells).

The gene transfection efficiency of chitosan is lower when compared with other cationic gene delivery systems like PEI [57, 110, 111] or cationic lipids [112, 113]. This lower transfection ability is attributed mainly to chitosan's minimal solubility and low buffering capacity at endosomal pH [31]. The transfection efficiency of chitosan is dependent on polymer characteristics such as molecular weight, degree of deacetylation (charge density) and polymer buffer capacity [40, 105]. Furthermore, solution pH and nitrogen to phosphate ratio (N:P ratio) determine the transfection efficiency of DNA [55, 59, 109].

The transfection efficiency of chitosan is dependent on the pH of the transfection medium due to the protonation of its primary amine groups. The pKa of these amines has been calculated as 6.5, meaning that at a higher (more basic) pH, the amines will not be protonated and the overall positive charge of the polymer will be low [114]. Therefore, at pH 7.4 chitosan presents minimal solubility, low intracellular delivery and low buffering capacity, resulting in low transfection ability [104, 105].

The transfection efficiency of a 10 kDa chitosan with a 92% of degree of deacetylation, was studied in HEK 293 cells and compared against lipofectamine. The gene expression was assessed at different pH values: 6.5, 7.1 and 7.4, in the presence of

10% serum. There was a marked decrease in expression of Enhanced Green Fluorescent Protein (EGFP) with an increase of pH. EGFP was expressed in 26.3% of cells at pH 6.5, but in only 9.2% at pH 7.1 and 0.2% at pH 7.4 [105].

Sato *et al.* evaluated the transfection efficiency of chitosan-DNA complexes (52 and 92% degree of deacetylation) in A549 cells. Higher transfection was obtained at pH 6.9 than at pH 7.6 [115]. Additionally, Lavertu *et al.* studied the transfection efficiency of two chitosans (40 kDa, 80% degree of deacetylation and 80 kDa, 72% degree of deacetylation) at pH values 6.5, 6.8, 7.1 and 7.4. The percentages of transfected cells were comparable for pH 6.5 and 7.1, with the lowest transfection results obtained at the highest pH [104].

Further to the pH of the transfection media, the degree of deacetylation of chitosan plays a role in the polymer's capacity to condense with nucleic acids and perform gene transfection. The importance of the degree of deacetylation was demonstrated by Kiang *et al..* Chitosan-DNA nanoparticles with a chitosan with molecular weight of 390 kDa and degrees of deacetylation of 62%, 70% and 90% were tested. The formulations with the lower two degrees of deacetylation resulted in lower gene expression levels, not significantly greater than the background [117]. The effect of the degree of deacetylation was also studied by Huang *et al.* with a chitosan of molecular weight 213 kDa. The polymer with a degree of deacetylation of 88% showed a transfection efficiency of 12.1% while chitosans with lower degrees of deacetylation, 61% and 46%, showed only residual transfection efficiency 0.2 and 0.05%, respectively [95, 118].

Five chitosans (molecular weights 31-190 kDa, degrees of deacetylation 51-99%) were studied by Koping-Hoggart *et al.* in the 293 kidney cell line. The lowest gene expression was obtained using the chitosans with the lowest degrees of deacetylation (170 kDa, 65% and 98 kDa, 51%). Chitosan 190 kDa, 85% showed the highest transfection efficiency, 70-times higher than 98 kDa, 51%. The results showed that the transfection ability of the polyplexes did not depend on the molecular weight in the range from 31 to 170 kDa but on the percentage of deacetylation, since chitosan with a percentage of positive charge lower than 65% did not show transfection ability [110].

In summary, in order to achieve high transfection efficiency chitosan should present a high degree of deacetylation, and the complexes with DNA should be prepared in a slightly acidic solution (pH lower than 7.1) in order to raise the polymer's positive

charge. This enhances the binding efficiency to the cell membrane and subsequent cellular uptake [95, 110, 117, 118].

Several studies have reported that chitosan with a molecular weight lower than 100 kDa is a suitable gene delivery candidate [55, 57, 94, 110, 127-129]. Strand *et al.* studied a range of chitosans (5-146 kDa) at N:P ratios 3, 5, 10 and 20. Gene expression was found to be dependent on the N:P ratio, increasing with the increase of the N:P ratios and achieving a plateau after which transfection efficiency decreased [55].

The transfection efficiency of a low molecular weight chitosan (22 kDa), with a degree of deacetylation of 72.5% was determined by a transfection assay into 293T cells with β-galactosidase. Different chitosan, DNA mass ratios were studied, with a mass ratio of 3 showing 37% higher transfection efficiency than PLL (20 kDa) at a polymer, DNA mass ratio of 2 [94]. Furthermore, a chitosan oligomer was used to transfect a 293 kidney cell line. Chitosan (<4.7 kDa) polyplexes were prepared at pH 6 in water. Transfection efficiency was studied with three N:P ratios: 10, 30 and 60. N:P 60 showed the highest transfection ability, 100-fold higher than transfection results obtained with N:P 10 [126].

To try to understand how the different factors that influence transfection efficiency of chitosan (molecular weight, degree of deacetylation, pH and N:P) correlate between each other, Lavertu *et al.* studied the transfection efficiency of chitosan with four different molecular weights (10, 40, 80 and 150 kDa) and four different degrees of deacetylation (72, 80, 92 and 98%). The luciferase expression was evaluated at different pH values (6.5 and 7.1) and different N:P ratios (5 and 10). Two formulations of chitosan (10 kDa, 92% degree of deacetylation, N:P ratio 5 and 10 kDa, 80 % degree of deacetylation, N:P ratio of 10) showed the highest luciferase expression, and similar results to the positive control (FuGene) [104].

The comparison of the four different chitosans in different conditions allowed Lavertu *et al.* to understand the importance of the different variables that influence transfection with chitosan. In some formulations it was observed that a decrease in charge density led to a decrease in transfection efficiency. Regarding the molecular weight, Lavertu *et al.* concluded that a change in the molecular weight either had no effect on the gene expression, or this was increased for chitosan with lower molecular weight depending on the degree of deacetylation. For some formulations, increasing the N:P ratio from 5 to 10 led to an increase in gene expression. Also, a decrease in the pH, creating a

more acidic environment, resulted in an increase of luciferase expression. Overall, for the chitosans with the lowest molecular weight (10 and 40 kDa), the gene expression was lower for low degrees of deacetylation, low N:P ratios and high pH due to weaker association of the chitosan with DNA, leading to premature DNA release [104].

This chapter will present the cytotoxicity results for EAGC17, EAGC21 and EAGC30. Furthermore, different factors, such as transfection time, presence of proteins, presence of chloroquine, dose of DNA and cell type, that may affect the transfection efficiency of the polymers, will be analyzed. Finally, the transfection ability of the three polymers will be studied and a comparison between EAGC17, EAGC21 and EAGC30 will be made to evaluate how the characteristics of the polymers can affect the transfection results.

4.2 Methods

4.2.1 MTT Assay

The MTT (3-(4,5-dimethylthiazol-2-yl)-2,5-diphenyltetrazolium bromide) assay is a colorimetric cytotoxicity assay. MTT is a yellow, water-soluble tetrazole salt that is reduced to purple, water-insoluble formazan crystals by metabolically active cells [198]. The cleavage of MTT has several desirable properties for assaying cell survival and proliferation since the cleavage is effected by all living, metabolically-active cells, but not by dead cells. The amount of formazan generated is directly proportional to the number of live cells. The absorbance of the formazan produced by the cells can be measured with a spectrophotometer at 500–600 nm after dissolving the formazan crystals in DMSO [198].

The MTT reagent (Thiazolyl Blue tetrazolium bromide) was purchased from Alfa Aesar (Ward Hill, USA). Cells were seeded at 500 cells per well in 96-well plates. They were allowed to grow for three days and then treated with EAGC17, EAGC21, EAGC30 or Lipofectamine 2000 (Invitrogen, Paisley, UK) at increasing concentrations (1×10^{-9} to 10 mg mL^{-1}, 50 µL per well) for 6h. Subsequently, cells were washed with Dulbecco's phosphate-buffered saline (DPBS, Invitrogen, Paisley, UK) and incubated for another 48h with normal medium. Medium was discarded, cells washed with DPBS and MTT solution (50 µg, 0.5 mg mL^{-1}, 100µl) was added. Cells were incubated with the MTT solution for 2 h at 37°C, after which medium was removed, and DMSO (100 µL, Sigma Aldrich, Dorset, UK) was added to each well to ensure complete solubilization of the formed formazan crystals. After incubation for 10min at 37°C, the absorbance at 570 nm was measured using an ELx808 microplate reader (Bio-tek instruments, Potton, UK). For analysis, background values were subtracted. The cytotoxicity was determined as the ratio between the measured absorbance value of treated and untreated cells. Lysed cells (with Triton X-100 from Sigma Aldrich, Dorset, UK) were used as a control - 100% effect.

The IC50 values (concentration of polymer at which 50% of cells are viable) were determined by analysis of the data using Prism4. The sigmoidal dose response was analysed with Rmax fixed at 100 and Rmin at 0. Cytotoxicity results are presented as the average of three measurements ± standard deviation.

4.2.2 Cell Transfection efficiency

β-Galactosidase, the product of the lacZ gene of *Escherichia coli*, is one of the most widely used reporters of gene expression. In the standard assay for quantifying the amount of β-galactosidase activity in cells, the O-nitrophenyl-β-D-galactopyraniside (ONPG) is used as the β-galactosidase substrate. The hydrolytic product is a yellow chromophore, o-nitrophenol, which is measured by spectrophotometry.

Briefly, 96-well plates were seeded with 10000 cells (A431, U87MG or MiaPaCa-2) per well and incubated overnight. The complexes were prepared to a final DNA concentration of 0.1 mg mL^{-1}. Each polymer stock solution (EAGC17, EAGC21 and EAGC30) was prepared in sterile dextrose (5% (w/v) filtered with a 0.22 μm Millex filter) to which was added equal volumes of the DNA stock solution (in MiliQ water) to give polymer, DNA mass ratios of 1 to 60. The complexes were allowed to incubate at room temperature, for 1 hour, after which the polymer-DNA complexes were added to the cells (50 μL, 1 μg plasmid DNA per well) and incubated for 6h in Dulbecco's Modified Eagle Medium (DMEM, Life Technologies, Paisley, UK) for U87MG or MiaPaCa-2 cells or Minimum Essential Medium (MEM, Life Technologies, Paisley, UK) for A431 cells serum free. The complexes were replenished with fresh DMEM or MEM daily and incubated for a further 48 hr. The transfection efficiency was determined by measuring the enzyme activity of β-galactosidase using the ONPG assay. The cells were lysed with Triton X-100 (2% w/v, 50 μL) and stored at -80ºC for at least 15 min. After defrosting, deactivated Foetal Bovine Serum (FBS) (0.5 % v/v, 50 μL in DPBS) was added to make the total volume to 100 μL. Finally, ONPG solution (2 mg mL^{-1}, 100 μL, Sigma Aldrich, Dorset, UK) was transferred to each well. The absorption was measured at 420 nm in an ELx808 microplate reader (Bio-tek instruments, Potton, UK). Values were expressed in mU per well and compared to the data observed with the naked plasmid DNA, polymer by itself, untreated cells and the positive control lipofectamine.

Lipofectamine 2000 (Invitrogen, Paisley, UK)-DNA complexes were prepared with a 1:2.5 ratio of DNA(μg):Lipofectamine(μL) according to the manufacturer´s specifications, and were used as a positive control. Cells were incubated for six hours with lipofectamine-DNA complexes (0.1μg DNA/well) in serum-free medium, and then replenished with complete media and incubated for further 48h.

Transfection with Chloroquine

Chloroquine is a cationic, amphiphilic compound with a hydrophobic aromatic ring and a positively charged side chain. It has two tertiary amines on its side chain behaving as a weak base. In acidic environments, such as inside lysosomes, chloroquine becomes fully protonated due to the low pH in these compartments [199]. Consequently there is a swelling and rupture of the endocytic vesicles allowing the release of the genetic material introduced in the cell to the cytoplasm [180, 200]

Transfection experiments were carried out using chloroquine to investigate the endosomal escape of the polyplexes. All experiments were performed with the same methods as detailed in section 4.2.2, except that the cells were incubated with cell medium containing 100μM chloroquine (Sigma Aldrich, Dorset, UK). The cells were transfected for 4 hours before the medium was changed.

4.3 Results

4.3.1 MTT Assay

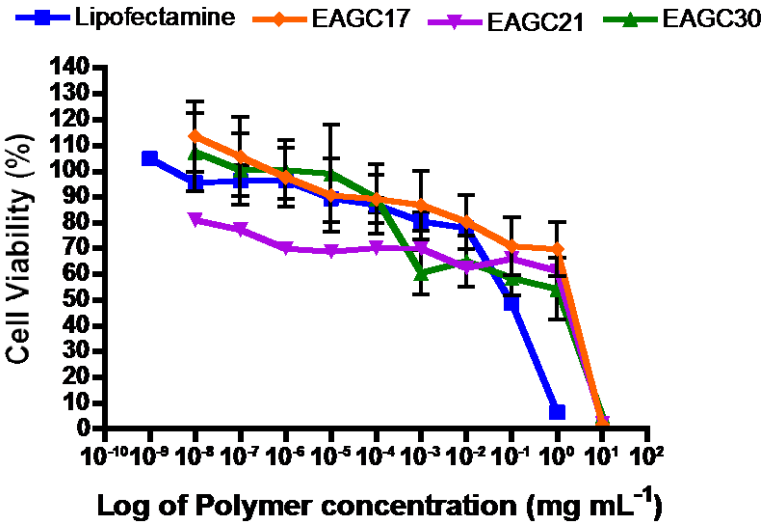

Figure 69 - MTT assay results in A431cells for, EAGC17, EAGC21, EAGC30 and lipofectamine after 6h incubation with treatments. Relative cell viability is presented as relative value (%) to untreated cells. The data was expressed as mean values ± standard error of 3 experiments.

The cytotoxicity of EAGC17, EAGC21, EAGC30 and lipofectamine to A431 cells was investigated by MTT assay, as shown in Figure 69. Lipofectamine was the comparison reagent since it is a well-described *in vitro* transfection agent, and it was used as positive control for the transfection experiments. Relative cell viability for lipofectamine abruptly decreased to 50% at approximately 0.1 mg mL^{-1} and to 5% at 1 mg mL^{-1} (Figure 69). All the EAGC polymers were statistically more biocompatible than lipofectamine (Table 26). EAGC30 (IC50 = 0.522 ± 0.17 mg mL^{-1}) was the polymer with the lowest IC50 (i.e. the highest toxicity); however, it was still more biocompatible than lipofectamine (*$p \leq 0.05$, IC50 = 0.071 ± 0.01 mg mL^{-1}). EAGC17 was the least toxic polymer (IC50 = 1.826 ± 0.09 mg mL^{-1}) followed by EAGC21 (IC50 = 0.863 ± 0.16 mg mL^{-1}); both of the polymers were statistically significantly less toxic than lipofectamine (***$p \leq 0.001$, Table 26). When compared with PEI (25 kDa, IC50 = 0.0019 mg mL^{-1}) the polymers also showed lower toxicity to the A431 cell line [101].

The difference between the three EAGC polymers, with EAGC17 being statistically less toxic than all the other EAGC polymers ($^{###}p \leq 0.001$), was probably due to molecular weight and charge density disparities. There was no statistical difference between the

IC50 of EAGC21 and EAGC30. It has been described that chitosan toxicity is intimately related with its molecular weight and charge density. Chitosans of high molecular weight (>100 kDa) and degree of deacetylation (higher charge density) were more toxic than low molecular weight polymers [95, 103, 104]. The toxicity results of EAGC follow this trend. EAGC17, with the lowest toxicity, also had the lowest charge density and molecular weight of the three polymers. EAGC21 presented the same molecular weight of EAGC17 but higher charge density. The polymer with the highest molecular weight and charge density of the three polymers was EAGC30, which consequently showed the highest toxicity.

Table 26 - IC50 values of EAGC17, EAGC21, EAGC30 and Lipofectamine in A431 cells lines after 6h of incubation with treatments. The data was expressed as mean values ± standard error of 3 experiments. One way ANOVA, Bonferonni post hoc test, EAGC17, EAGC21 and EAGC30 vs Lipofectamine *p≤0.05, **p≤ 0.01, ***p≤0.001 and EAGC17 vs EAGC21 and EAGC30 $^{\#}$p≤0.05, $^{\#\#}$p≤ 0.01, $^{\#\#\#}$p≤0.001.

Reagent	**IC50 (mg mL^{-1})**
EAGC17	1.826 ± 0.09 *** / ###
EAGC21	0.863 ± 0.16 ***
EAGC30	0.522 ± 0.17 *
Lipofectamine	0.071 ± 0.01

4.3.2 Cell Transfection efficiency

The transfection efficiency of EAGC polymers was evaluated *in vitro* by delivery of plasmid DNA into A431 cells. The polyplexes between the three polymers (EAGC17, EAGC21 and EAGC30) and DNA (1 µg per well) were prepared at increasing polymer, DNA mass ratios (1-60). The positive control was lipofectamine, a well-described *in vitro* transfection agent [201]. Lipofectamine transfection was performed with 0.1µg DNA per well due to its toxicity at high plasmid DNA levels. The negative controls were naked plasmid DNA, naked polymer and untransfected cells. The transfection efficiency was determined by measuring the enzyme activity of β-galactosidase (in mU/well) using the ONPG assay.

Different parameters that might influence the transfection efficiency of plasmid DNA were studied in order to optimize the transfection protocol. Preliminary experiments

were made with EAGC21. EAGC21 was chosen due to its characteristics regarding complexation with DNA, stability in biological medium and biocompatibility. EAGC17 produced less stable particles when compared to EAGC21 and EAGC30 was less biocompatible. Once optimum transfection conditions had been achieved these were later applied to the transfection of the three polymers (EAGC17, EAGC21 and EAGC30).

a. Endosomal escape

The main objective of EAGC synthesis was to increase the buffer capacity of chitosan and in this way enhance its transfection ability. The first study performed was transfection of A431 cells in the presence of chloroquine. Chloroquine is a transfection enhancement agent, buffering the endosomes, causing its disruption and therefore increasing the transfection efficiency of polymers without buffer capacity [180].

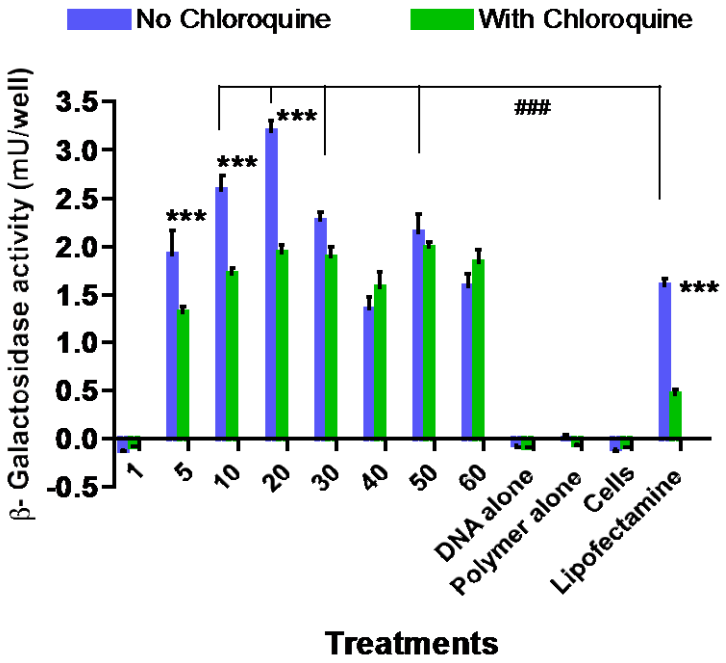

Figure 70 - Effect of the presence of chloroquine on β-Galactosidase gene expression in A431 cell line. The transfection was performed for 4h in MEM without serum. Lipofectamine 0.1µg DNA per well. Polymer treatments 1µg DNA per well. Mean ± SEM (n=5), Two way ANOVA, Bonferonni post hoc test, No Chloroquine vs With Chloroquine *p≤0.05, **p≤ 0.01, ***p≤0.001 and EAGC21, DNA mass ratios (No Chloroquine) vs Lipofectamine (No Chloroquine) $^{\#}$p≤0.05, $^{\#\#}$p≤ 0.01, $^{\#\#\#}$p≤0.001 .

It was reported that chloroquine can support endosomal escape of polyplexes via its own proton sponge effect and thus enhance the transfection efficiency of the polyplex [180]. Exogenous chloroquine did not improve the transfection efficiency for any polymer, DNA mass ratio (Figure 70). EAGC21 showed transfection ability in the absence of chloroquine for all polymer, DNA mass ratios. Furthermore, for polymer, DNA mass ratios 5, 10 and 20 the transfection efficiency of EAGC21 was higher in the absence of chloroquine (***p≤0.001). These results reveal that EAGC21 may have its own ability for endosomal escape, probably due to its buffer capacity, as previously shown in the titration experiments (Section 2.3.3). These results confirm that EAGC was able to deliver plasmid DNA into the cells *in vitro*. The transfection results in the absence of chloroquine were at least as good as lipofectamine, and for polymer, DNA mass ratios 10, 20, 30 and 50 were higher ($^{###}$p≤0.001). No transfection was seen in the negative controls, or EAGC21, DNA mass ratio 1. The positive control, lipofectamine, showed its best results in the absence of chloroquine.

b. Incubation time

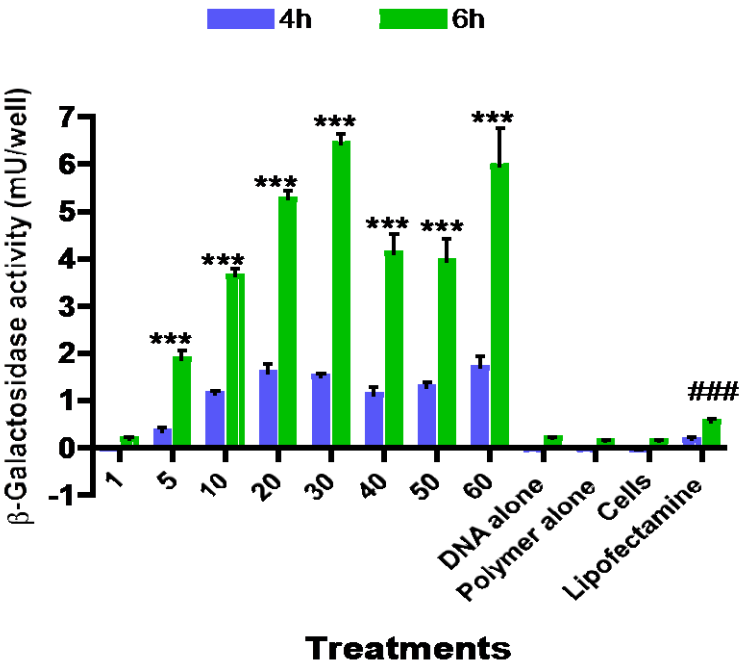

Figure 71 - Effect of the transfection time on β-Galactosidase gene expression in A431 cell line. The transfection was performed with MEM without serum. Lipofectamine 0.1µg DNA per well. Polymer treatments 1µg DNA per well. Mean ± SEM (n=5), Two way ANOVA, Bonferonni post hoc test, 4h vs 6h *p≤0.05, **p≤ 0.01, ***p≤0.001 and EAGC21, DNA mass ratios (6h) vs Lipofectamine (6h) $^{#}$p≤0.05, $^{##}$p≤ 0.01, $^{###}$p≤0.001.

The optimal time of incubation of the complexes with cells should balance detectable expression with limited toxicity [179]. Two lengths of incubation of the complexes with cells were studied: 4 and 6 hours. After each time point, the cell medium was substituted for new medium without complexes. It is possible to observe in Figure 71 that the transfection values, after 6h, were statistically significantly higher ($p \leq 0.001$) for all polymer, DNA mass ratios when compared with 4h incubation (except for polymer, DNA mass ratio 1). No transfection was seen in the negative controls at any time point. Lipofectamine presented very low transfection (less than 1 mU per well) for both time points. The transfection efficiency for all polymer, DNA mass ratios, except 1, was statistically higher ($p \leq 0.001$) when compared with Lipofectamine. The improved transfection results after 6h of incubation were only possible due to the good cytotoxicity profile of EAGC21. The MTT results revealed that after 6h of incubation the EAGC21 IC50 (IC50 = 0.863 ± 0.16 mg mL^{-1}) was higher than the maximum polymer concentration transfected (0.6 mg mL^{-1}), allowing a good cell viability throughout the incubation period. Regarding these results it was decided to perform the following transfection experiments with an incubation time of 6 hours.

c. Presence of proteins

The composition of the cell medium can highly affect the final results of an *in vitro* transfection experiment. As seen in the previous chapters, the presence of proteins can affect the characteristics of the complexes and, consequently, their transfection ability.

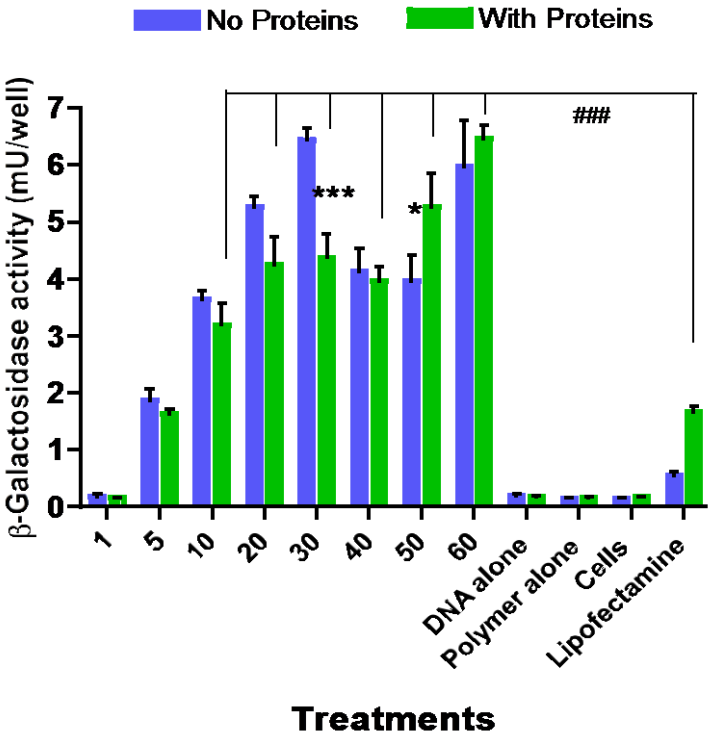

Figure 72 - Effect of the presence of proteins on cell medium on β-Galactosidase gene expression in A431 cell line with an incubation time of 6h. Lipofectamine 0.1µg DNA per well. Polymer treatments 1µg DNA per well. Mean ± SEM (n=5), Two was ANOVA, Bonferonni post hoc test, No proteins vs proteins *p≤0.05, **p≤ 0.01, ***p≤0.001 and EAGC21, DNA mass ratios (with proteins) vs Lipofectamine (with proteins) $^{\#}$p≤0.05, $^{\#\#}$p≤ 0.01, $^{\#\#\#}$p≤0.001.

The impact of the presence of proteins on the transfection efficiency of EAGC21 was studied as shown in Figure 72. The complexes were added to the cell medium with or without FBS. It is possible to observe that the presence of proteins did not impair the transfection of the plasmid DNA by EAGC21. The transfection efficiencies in the presence or absence of proteins were comparable for all EAGC21, DNA mass ratios with the exception of EAGC21, DNA mass ratio 30 and 50. For EAGC, DNA mass ratio 30, the transfection efficiency in the absence of serum was significantly higher (***p≤0.001). EAGC21, DNA mass ratio 1 did not show any transfection with or without proteins in the medium, and the same results were obtained for the negative controls (naked plasmid DNA, naked polymer and not transfected cells). Lipofectamine showed

higher transfection in the presence of serum (not statistically significant) but lower transfected units when compared with all EAGC21, DNA mass ratios greater than 5 ($^{\#\#\#}p \leq 0.001$). The good performance of the EAGC21 in the presence of serum is comparable to the behaviour of chitosan nanoparticles in cell medium with FBS [57, 122]. Despite the probability of aggregation of the chitosan polymers due the ionic interactions with negatively charged proteins, leading to lower transfection results, the presence of serum allows an increased cell viability that in the end led to better transfection efficiency [105].

d. Comparable amount of DNA

The amount of DNA used in cell transfection experiments should be chosen such that expression can be detected while toxicity remains limited. The DNA dose may vary from 0.1 to 1µg DNA per well (on 96 well plates) but higher doses have been used. Higher doses of DNA may result in higher expression levels but with increased toxicity [104, 120].

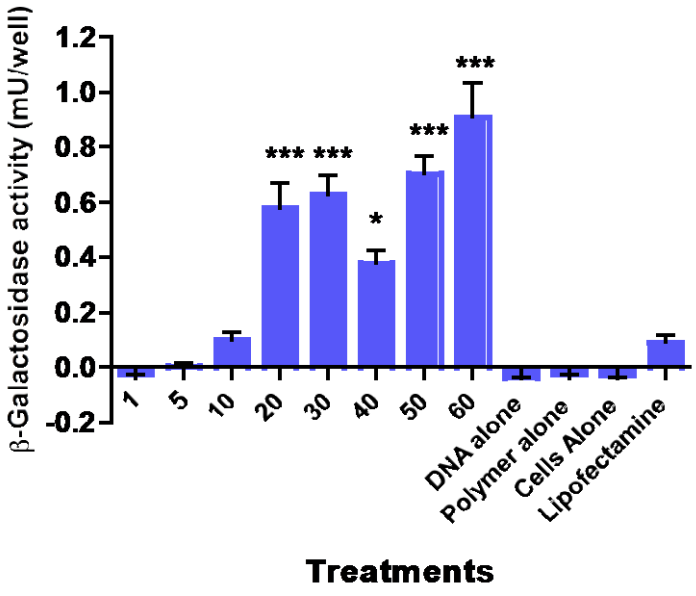

Figure 73 - Comparison on β-Galactosidase gene expression in A431 cell line between different EAGC21, DNA mass ratios and Lipofectamine using the same amount of plasmid DNA (0.1µg per well). The complexes were incubated for 6h in MEM without serum. Mean ± SEM (n=5), One way ANOVA, Bonferonni post hoc test, EAGC21, DNA mass ratios vs Lipofectamine *p≤0.05, **p≤ 0.01, ***p≤0.001.

Lipofectamine is a powerful transfection reagent that is able to achieve high transfection efficiency with low doses of DNA [201]. However, MTT results showed that lipofectamine was statistically more toxic (***$p \leq 0.001$) than EAGC21 in the A431 cell line. This lower toxicity of the polymer enabled a higher concentration of polymer per well and consequently a higher dose of transfected DNA. In previous experiments the dose of DNA per well in the polymer treatments was 0.1 to 1µg of DNA with lipofectamine (following the manufacturer's instructions). The objective of this experiment was to compare the transfection efficiency of the nanoparticles formed with EAGC21 and lipofectamine with the same dose of DNA per well (0.1 µg). In Figure 73 it is possible to observe that the polymer achieved better results for all EAGC21, DNA mass ratios higher than 10 (***$p \leq 0.001$) with the exception of EAGC21, DNA mass ratio 40 (*$p \leq 0.05$).

e. Cell line

Transfection efficiency is highly dependent on the cell line chosen to perform the *in vitro* studies [179]. EAGC21 gene expression was studied in more than one cell line in order to confirm the polymer's transfection capacity. Three human adherent monolayer cell types (A431, MiaPaCa-2 and U87MG) were chosen, considering that the majority of the published transfection studies use cell models with these characteristics. U87MG, a human brain cell line, was specifically chosen considering the final therapeutic target for gene delivery system of this study.

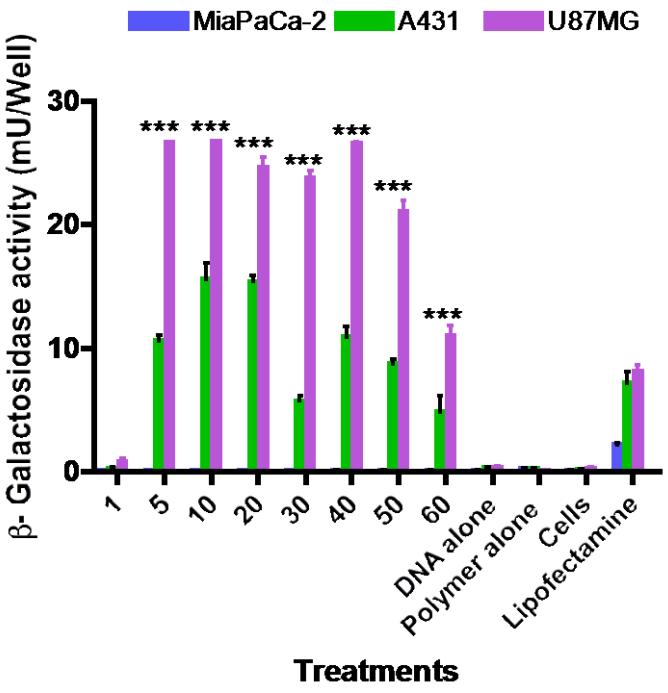

Figure 74 – Comparison between three different cell lines, MiaPaCa-2, A431 and U87MG on β-Galactosidase gene expression with an incubation time of 6h in medium without serum. Lipofectamine 0.1µg DNA per well. Polymer treatments 1µg DNA per well. Mean ± SEM (n=5), Two way ANOVA, Bonferonni post hoc test, U87MGvs A431 and MiaPaCa-2 *p≤0.05, **p≤ 0.01, ***p≤0.001.

There is a clear cell dependence regarding transfection results of plasmid DNA (Figure 74). U87MG showed the highest transfection values, being statistically different (***p≤0.001) from A431 and MiaPaCa-2 cell lines for all EAGC21, DNA mass ratios, except 1. In fact, the MiaPaCa-2 cell line did not show any transfection for any of the EAGC21, DNA formulations. The transfection results for U87MG were comparable between EAGC21, DNA mass ratios 5 to 40 with a decrease on the mU values for the higher EAGC21, DNA mass ratios (50 and 60). This decrease in transfection may be due to polymer toxicity or stability of the nanoparticles.

f. Polymer substitution

The EAGC17, EAGC21 and EAGC30 transfection efficiencies were evaluated in the A431 cell line after 6h of incubation and in the absence of serum. As shown in Figures 75 to 78, the transfection efficiency is dependent on the degree of substitution of the polymers and the mixing ratio of polymer to plasmid DNA.

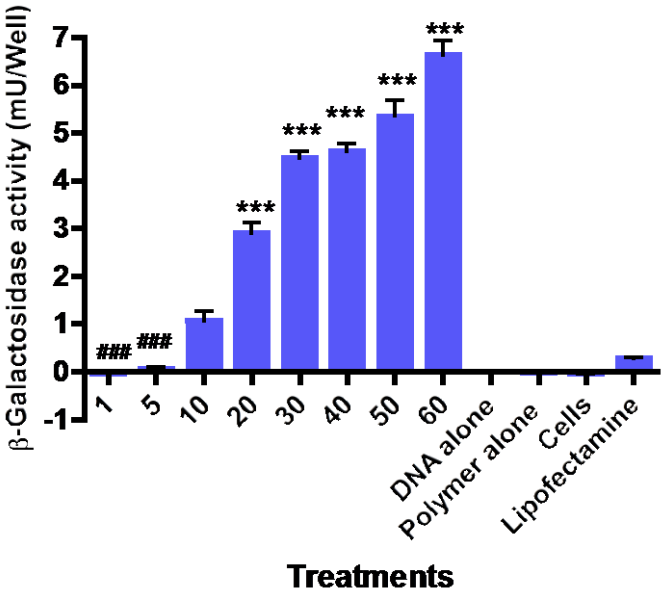

Figure 75 – β-Galactosidase gene delivery by EAGC17 in A431 cell line with an incubation time of 6h in MEM without serum. Lipofectamine 0.1µg DNA per well. Polymer treatments 1µg DNA per well. Mean ± SEM (n=5), One way ANOVA, Bonferonni post hoc test, EAGC17, DNA mass ratios vs Lipofectamine *p≤0.05, **p≤ 0.01, ***p≤0.001 and EAGC17, DNA mass ratios 1 and 5 vs other EAGC17, DNA mass ratios $^{\#}$p≤0.05, $^{\#\#}$p≤ 0.01, $^{\#\#\#}$p≤0.001.

The transfection efficiency of EAGC17 at EAGC17, DNA mass ratios 1 and 5 was very low when compared with all the other EAGC17, DNA mass ratios ($^{\#\#\#}$p≤0.001, Figure 75). In the agarose gel retardation assay (Section 3.3.1) EAGC17 showed no ability to fully retard the plasmid DNA for EAGC17, DNA mass ratio 1 and 5. The agarose gel results explain the lack of transfection for EAGC21, DNA mass ratios 1 and 5 since the polymer did not have ability to condense the DNA to allow gene delivery. The transfection ability of EAGC17 increased with the increase of the EAGC17, DNA mass ratios with the maximum transfection efficiency being achieved at EAGC17, DNA mass ratio 60. Transfection results for EAGC17, DNA mass ratios higher than 5 were statistically higher than lipofectamine (***p≤0.001).

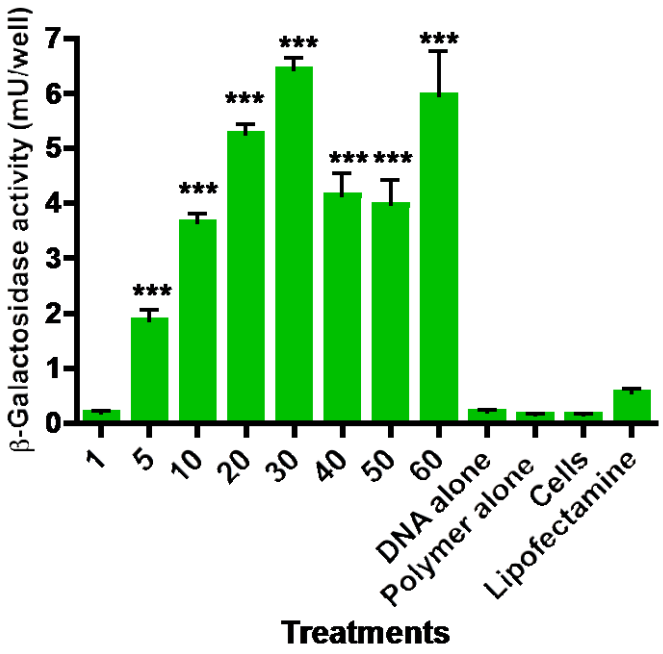

Figure 76 – β-Galactosidase gene delivery by EAGC21 in A431 cell line with an incubation time of 6h in MEM without serum. Lipofectamine 0.1µg DNA per well. Polymer treatments 1µg DNA per well. Mean ± SEM (n=5), One way ANOVA, Bonferonni post hoc test, EAGC21, DNA mass ratios vs Lipofectamine *p≤0.05, **p≤ 0.01, ***p≤0.001.

EAGC21 also did not show any transfection at EAGC21, DNA mass ratio 1. However, EAGC21, DNA mass ratio 5 presented a transfection of 2mU per well (Figure 76). With the increase of the EAGC21, DNA mass ratios, transfection efficiency increased with the exception of EAGC21, DNA mass ratios 40 and 50. Transfection with EAGC21 was superior to lipofectamine for all polymer, DNA mass ratios apart from the EAGC21, DNA mass ratio 1 (***p≤0.001).

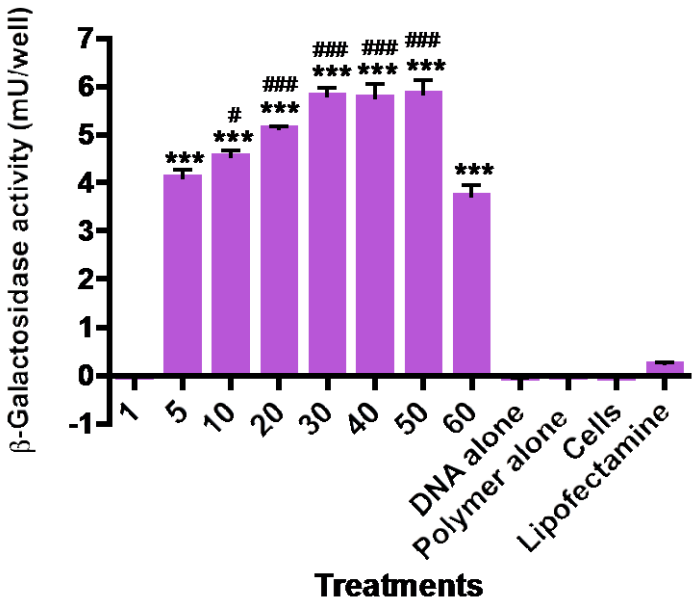

Figure 77 – β-Galactosidase gene delivery by EAGC30 in A431 cell line with an incubation time of 6h in MEM without serum. Lipofectamine 0.1µg DNA per well. Polymer treatments 1µg DNA per well. Mean ± SEM (n=5), One way ANOVA, Bonferonni post hoc test, EAGC30, DNA mass ratios vs Lipofectamine *p≤0.05, **p≤ 0.01, ***p≤0.001. EAGC30, DNA mass ratios 60 vs other EAGC30, DNA mass ratios $^{\#}$p≤0.05, $^{\#\#}$p≤ 0.01, $^{\#\#\#}$p≤0.001.

EAGC30 showed high transfection efficiency even for low EAGC30, DNA mass ratios (Figure 77). EAGC30, DNA mass ratio 5 had a transfection of 4 mU per well, compared with 2mU for EAGC21 and there was no transfection for EAGC17 at an EAGC17, DNA mass ratio of 5. The polymer presented the best results regarding complexation with DNA and the highest stability in biological fluids (Chapter 3). This behaviour was reflected in the transfection efficiency of EAGC30, reaching higher values of transfected units for all EAGC30, DNA mass ratios when compared with lipofectamine (***p≤0.001). The transfection ability of the polymer increased with the increase of the EAGC30, DNA mass ratio until it reached a plateau for EAGC30, DNA mass ratios 30, 40 and 50. The values of transfection decreased for EAGC30, DNA mass ratio 60 ($^{\#\#\#}$p≤0.001 when compared with EAGC30, DNA mass ratios 20, 30, 40 and 50) probably due to polymer toxicity or stability of the nanoparticles. The polymer concentration transfected for EAGC30, DNA mass ratio 60 was 0.6 mg mL^{-1} very close to the IC50 of EAGC30 (0.523 ± 0.17 mg mL^{-1}). The cells' viability might have been compromised at this polymer, DNA mass ratio, and consequently lower transfection results were obtained. Furthermore, the agarose gel assay in the previous chapter showed how stable the nanoparticles were with EAGC30. This stability may have inhibited the release of DNA inside the cell causing the low gene expression observed.

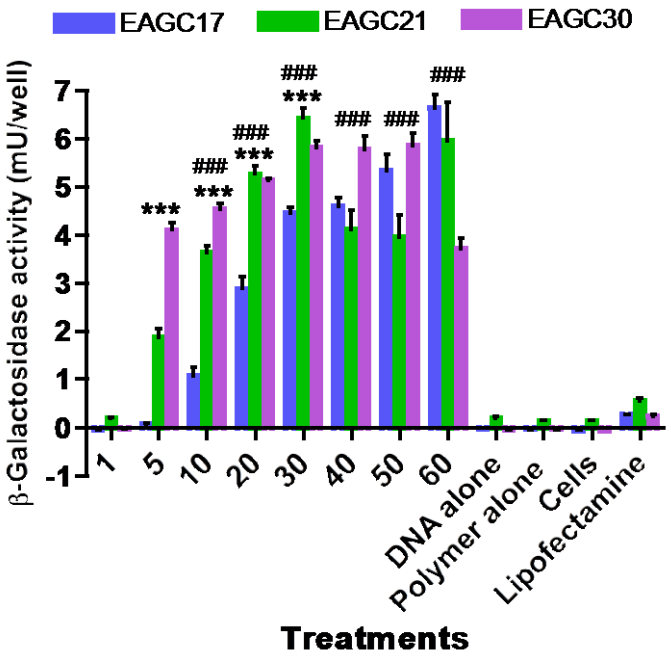

Figure 78 – Comparison between EAGC17, EAGC21 and EAGC30 with respect to β-Galactosidase gene expression in the A431 cell line with an incubation time of 6h in MEM without serum. Lipofectamine 0.1µg DNA per well. Polymer treatments 1µg DNA per well. Mean ± SEM (n=5), Two way ANOVA, Bonferonni post hoc test, EAGC17 vs EAGC21 and EAGC30 *p≤0.05, **p≤ 0.01, ***p≤0.001. EAGC17, EAGC21, EAGC30 vs Lipofectamine $^{\#}$p≤0.05, $^{\#\#}$p≤ 0.01, $^{\#\#\#}$p≤0.001.

When comparing the three polymers (Figure 78) it is possible to observe that EAGC17 (with the lowest charge density due to a lower degree of substitution with ethylamino groups) did not show any transfection for low EAGC17, DNA mass ratios 1 and 5. Furthermore, its transfection results were statistically significantly lower (***p≤0.001) for EAGC17, DNA mass ratios 5, 10, 20 and 30 when compared with EAGC21 and EAGC30. In the previous chapter it was concluded that the increase of the number of amines in the EAGC backbone led to more stable nanoparticles for lower EAGC, DNA mass ratios. This stability led to increased levels of transfection, as it is possible to observe in Figure 78. EAGC17 and EAGC21 showed a maximum transfection efficiency for EAGC, DNA mass ratio 60 while EAGC30 achieved a plateau for EAGC30, DNA mass ratios 30, 40 and 50 and then a decrease in transfection for EAGC30, DNA mass ratio 60. All the polymers produced higher transfection results than lipofectamine for all EAGC, DNA mass ratio higher than 5 (###p≤0.001) confirming the polymers may have its own ability for endosomal escape, probably due to its buffer capacity, leading to a higher gene expression.

4.4 Discussion

Different polymer characteristics can influence the toxicity of gene delivery vectors. Molecular weight as well as charge density of cationic polymers were described as key parameters that can exacerbate cytotoxic effects [71, 180]. Polymers with a high charge density like PEI present higher toxicity when compared with chitosan and chitosan derivatives [72, 86, 92, 102].

It has been described that chitosan cell biocompatibility is intimately related with its molecular weight and charge density. Chitosans of high molecular weight (>100 kDa) and degree of deacetylation were less biocompatible than low molecular weight polymers [95, 103, 105]. Moreover, the number of positive charges has a greater effect on chitosan toxicity than the molecular weight [95, 104]. The same was reported for chitosan derivatives. Trimethyl chitosan is less biocompatible than chitosan and its toxicity was found to be directly related with the degree of trimethylation (charge density) [102]. These findings corroborate the biocompatibility results for EAGC polymers. EAGC17 (IC50 = 1.826 ± 0.09 mg mL^{-1}), with the highest biocompatibility, also had the lowest charge density and molecular weight of the three polymers. EAGC21 (IC50 = 0.863 ± 0.16 mg mL^{-1}) presented the same molecular weight of EAGC17 but higher charge density leading to a lower IC50. The polymer with the highest molecular weight and charge density of the three polymers was EAGC30 that also showed the highest toxicity (IC50 = 0.522 ± 0.17 mg mL^{-1}). Nevertheless, all polymers were less toxic than lipofectamine (IC50 = 0.071 ± 0.01 mg mL^{-1}) and PEI [101].

EAGC is a chitosan derivative that was synthesized with the main objective of increasing chitosan transfection efficiency. An ethylamino group was introduced on to the glycol chitosan backbone in order to enhance the condensation of the polymer with nucleic acids at low polymer, DNA mass ratios and physiological pH as well as to improve the buffer capacity of the synthesized polymer, and allow endosomal escape resulting in improved gene expression.

Different parameters that might influence the transfection efficiency of plasmid DNA were studied in order to optimize the transfection protocol. In the absence of chloroquine, EAGC21 showed increased transfection for low EAGC21, DNA mass ratios. The lower transfection efficiencies in the presence of chloroquine may be due to the displacement of the polymer, by chloroquine, from the plasmid DNA [180, 200]. When compared with the positive control, lipofectamine in the absence of chloroquine,

EAGC21 performed better for EAGC21, DNA mass ratios 10, 20, 30 and 50 ($^{###}p \leq 0.001$). For the other polymer, DNA mass ratios the results were comparable in the presence and absence of chloroquine. In summary, exogenous chloroquine did not improve the transfection efficiency for any polymer, DNA mass ratio. These results revealed that EAGC21 may have its own ability for endosomal escape, probably due to its buffer capacity, previously studied in Chapter 2.

One of the factors that affects transfection is the incubation time of complexes with cells. The optimal time should balance detectable expression with limited toxicity [179]. Previous studies had demonstrated that genetic expression tends to increase sharply with increasing incubation times up to a certain time point (normally around four hours). After four hours expression levels may either reach a plateau, continue to increase less steeply, or decrease [179]. The transfection efficiency of EAGC21 was studied for two time points: 4 and 6 hours. After 6 hours, transfection values were three times higher when compared with 4 hours of incubation for all EAGC21, DNA mass ratios ($^{***}p \leq 0.001$). Also, for 6h of incubation the results of the polymer-DNA treatments were significantly better when compared with lipofectamine ($^{###}p \leq 0.001$). The increased transfection with time confirmed the viability of the cells when in contact with the complexes for 6 hours leading to an increase of the mU. This was only possible due to the good cell biocompatibility of EAGC21.

After *in vivo* administration, release of DNA from the polyplex can occur due to an interaction of the complex with serum proteins. These negatively charged proteins can also led to aggregation and serum clearance of the DNA complexes from the bloodstream [31, 202]. *In vitro,* the presence of proteins can impair the transfection of the plasmid DNA due to non-specific interactions between the nanoparticles and the serum components in the cell medium [120]. In the previous chapter, complexes made with EAGC21 showed good stability in the presence of heparin with the release of plasmid only occurring at high heparin concentration and small polymer, DNA mass ratios. The presence of 10% of FBS in cell medium did not interfere with the transfection ability of the EAGC21 nanoparticles. Similar transfection results were obtained in the presence and absence of proteins. In fact, for EAGC21, DNA mass ratios higher than 5, the transfection results were better when compared with lipofectamine in the presence of proteins ($^{###}p \leq 0.001$). These results confirm that EAGC polymers are able to condense and deliver plasmid DNA in the presence of the biological challenges posed by serum proteins. The good performance of the EAGC21 in the presence of serum is comparable to the behaviour of chitosan nanoparticles in

cell medium with FBS but contrary to PEI behaviour [57, 122]. In the presence of serum PEI transfection efficiency decreased for all the N:P ratios studied [57]. Despite the probability of aggregation of the chitosan polymers due the ionic interactions with negatively charged proteins, leading to lower transfection results, the presence of serum allows an increased cell viability that in the end leads to better transfection efficiency [105].

In summary, preliminary studies with EAGC21 showed that the newly synthesized polymer is capable of gene delivery to A431 and U87MG cells *in vitro.* The polymer showed good transfection efficiency in the absence of chloroquine and in the presence of serum proteins. Furthermore, the low toxicity of the EAGC21 allowed a prolonged incubation time (6h) and a higher dose of DNA transfected per well. When compared with lipofectamine the polymer showed lower toxicity and increased transfection efficiency.

It has previously been demonstrated that the transfection efficiency of chitosan is dependent on the pH of the transfection medium, requiring a slightly acid solution in order to condense DNA and provide an overall positive charge to the particles that allow binding to the cell membrane [95, 110, 114, 117, 118]. The presence of the ethylamino group on EAGC increased the charge density of the polymer at physiological pH. Due to the primary amines of the EAGC (pKa ≈ 9-10), the polymer was soluble at physiological pH and presented a positive charge allowing condensation with plasmid DNA and formation of nanoparticles with a positive surface charge. This characteristic of EAGC allowed transfection at physiological pH without the need to prepare the complexes in acidic buffers.

The transfection results for EAGC17, EAGC21 and EAGC30 showed transfection ability is dependent on the degree of substitution of the polymers (charge density). The transfection ability increased with the number of amines in the polymer backbone (i.e. increased charge density), correlating with results previously described for chitosan in the literature. Kiang *et al.* studied chitosan-DNA nanoparticles with a chitosan with molecular weight of 390 kDa and degrees of deacetylation of 62%, 70% and 90% were tested. The formulations with the lower two degrees of deacetylation resulted in lower gene expression levels, not significantly greater than the background [117]. Huang *et al.* reached the same results for a chitosan with 213 kDa and degrees of deacetylation of 61% and 46% [95, 118]. Koping-Hoggart *et al*. only obtained gene transfection for a chitosan with a minimum degree of deacetylation of 65% [110].

The increase of the transfection efficiency of the EAGC polymers with the increase of the degree of substitution may be due to the increase of the nanoparticles' stability. The agarose gel assay in Chapter 3 showed that there was a higher ability of EAGC21 and EAGC30 to condense with plasmid DNA. Also, the nanoparticles formed with EAGC30 showed higher stability in biological fluids. This has been previously described by Strand *et al*. [55], who found that increasing the N:P ratio resulted in lower gene expression due to complexes high stability that impaired the release of DNA inside the cell.

Furthermore, the buffer capacity of EAGC increased with the degree of substitution (Chapter 2). The buffer capacity of cationic polymers is intimately related with their capacity for gene expression due to the "proton sponge effect" [183, 203]. EAGC30 was the polymer with the highest buffer capacity and this could explain the good results for all EAGC30, DNA mass ratios. Overall, in the assays described in this chapter, EACG polymers were superior transfection agents to the positive control, lipofectamine.

EAGC polymers with a low molecular weight (17 kDa and 27 kDa) showed good transfection capacity even at low polymer, DNA mass ratios such as EAGC30, DNA mass ratio 5, due to the increased charge density introduced by the ethylamino group. The gene expression results for low polymer, DNA mass ratios increased with the increase of the polymer substitution. For the three polymers, an increase of EAGC, DNA mass ratio led to an increased transfection, with EAGC30 reaching a plateau at EAGC30, DNA mass ratio of 30.

These results were also seen in a study by Strand *et al.*, who studied a range of chitosans (5-146 kDa) at N:P ratios 3, 5, 10 and 20. Gene expression was found to be dependent on the N:P ratio, increasing with the increase of the N:P ratios, and achieving a plateau after which transfection efficiency decreased [55].

Furthermore, the polymer, DNA mass ratios required for successful transfection of EACG-DNA complexes were lower than those reported for chitosan alone. Chitosan (<4.7 kDa) transfection efficiency was studied at three N:P ratios: 10, 30 and 60. N:P 60 showed the highest transfection ability, 100-fold higher than transfection results obtained with N:P 10 [126].

In a wide-ranging study, Lavertu *et al.* demonstrated a trend between molecular weight, degree of acetylation and polymer, DNA mass ratios. High transfection efficiency of chitosan required high molecular weight and degree of deacetylation at low polymer,

DNA mass ratios. If low molecular weight and degree of acetylation are chosen then the charge ratio needs to be high to deliver stable complexes [104]. The results presented in this chapter suggest that for EAGC, good transfection can be achieved using a low molecular weight chitosan derivative at low polymer, DNA mass ratios due to the increased charge density introduced by the ethylamino substitutions.

In conclusion, the results presented in this chapter confirmed EAGC as a chitosan derivative with improved characteristics to overcome the low transfection efficiencies described previously for chitosan. EAGC was as biocompatible as chitosan, and showed superior cell biocompatibility when compared with PEI. EAGC polymers with a low molecular weight (17 and 27 kDa) demonstrated transfection ability at physiological pH at small polymer, DNA mass ratios. Furthermore, transfection efficiencies were higher than the positive control lipofectamine, for EAGC17, EAGC21 and EAGC30. The results showed that the polymers may have sufficient buffer capacity to allow the release of the nanoparticles from the endosome, resulting in high gene expression. This expression is dependent on the EAGC, DNA mass ratios and degree of substitution of the polymer.

5. Biological studies with siRNA

5.1 Introduction

In 1998, Mello *et al.* discovered the RNA interference mechanism in the nematode *Caenorhabditis elegans* [18]. Gene expression silencing can be described as follows (Figure 79): after the introduction of a double stranded RNA in the cell this is cleaved by the enzyme Dicer (cytoplasmic ribonuclease III) into small fragments (21-23 nucleotides long) called short interfering RNA. siRNAs are relatively small macromolecules (approximately 13 kDa) comprising two strands: the sense and antisense [20]. When in the cytoplasm, siRNA is integrated into a protein complex called RNA induced silencing complex (RISC). Argonaut 2 (the protein part of the RISC complex) unwinds the double strands of siRNA and these are separated. The activated RISC, containing the antisense strand, pairs with a complementary sequence of messenger RNA and degrades it thereby preventing its translation into a protein (posttranscriptional gene silencing) [204]. This complementarity determines the target selectivity of siRNA. The same activated RISC can cleave further complementary mRNA strands allowing a prolonged therapeutic effect of siRNA for 3-7 days in dividing cells. siRNA can be synthetically produced and directly introduced in the cell at the level of RISC circumventing the Dicer mechanism [19-21]. The RNAi pathway is fundamental in eukaryotic cells for post-transcriptional protein expression regulation [19, 20].

The therapeutic use of siRNA depends on its delivery to the intracellular space. siRNA is an anionic and hydrophilic molecule with enhanced susceptibility to hydrolysis by systemic ribonucleases. It presents a short biological life (rapid elimination from circulation) and fast renal clearance. siRNA lacks cell/tissue targeting, being unlikely to interact with the negatively charged cell membrane, leading to a poor cellular uptake [205, 206]. In the therapeutic use of siRNA, effective design of the sequence can avoid off target effects, and ensure specific regions within the target mRNA are reached [207]. Chemical modifications of siRNA can increase its stability as well as decrease its inherent toxicity. However, for therapeutic applications, a delivery system is required not only to protect the siRNA from enzymatic degradation but also to enhance siRNA delivery to the target organ, cellular uptake and finally to release the siRNA in the cell cytoplasm in order to be incorporated in the RNAi machinery [142].

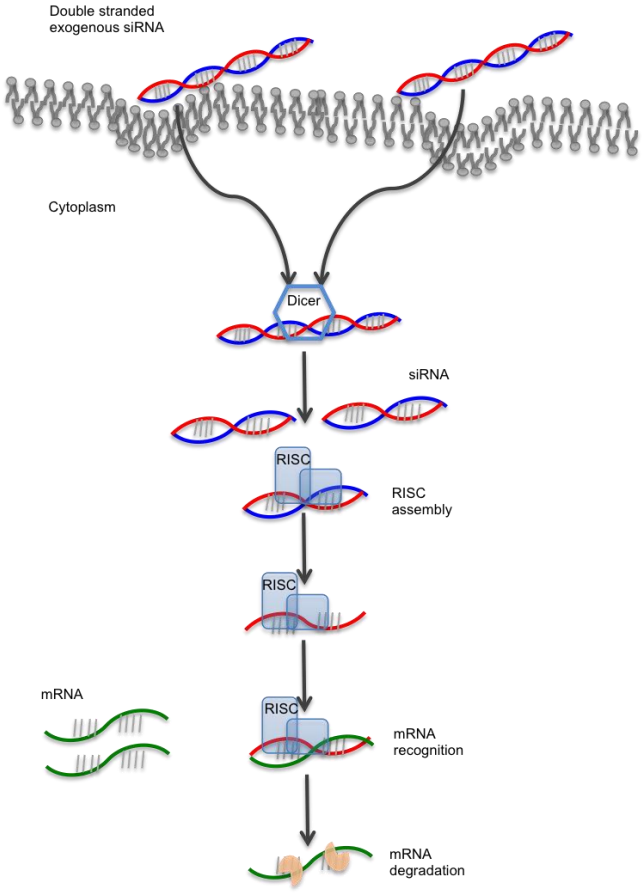

Figure 79 - Schematic representation of RNAi mechanism. Adapted from Guzman-Villanueva *et al.* [208].

Cationic polymers are good candidates to improve the pharmacokinetics, pharmacodynamics, biodistribution and toxicology of siRNA [19]. These are efficient transfection agents due to their ability to bind and condense the nucleic acids into stabilized nanoparticles [19]. They have also demonstrated cellular uptake through nonspecific endocytosis and endosomal escape [19]. Due to the similar physicochemical properties of DNA and siRNA, cationic systems developed for the delivery of plasmid DNA have also been applied to siRNA. Nevertheless, it should be stated that siRNA is a much smaller molecule than plasmid DNA, resulting in a higher compaction of the nucleic acid and therefore smaller polyplexes [157]. Also, siRNA molecules need only to reach the cytosol (the site of RNAi mechanism), while plasmid DNA needs to be transported to the nucleus [157]. The electrostatic stabilization of siRNA polyplexes is weaker when compared with plasmid DNA, and this results in poor stability of the siRNA complexes when in the presence of biological challenges [190]. In fact, results presented in Chapter 3 concur with the previous. In the presence of

heparin, siRNA polyplexes showed release of siRNA for smaller EAGC30, siRNA mass ratios when compared with EAGC30-DNA complexes.

Different cationic polymers like PEI and chitosan have been studied to improve the intracellular delivery of siRNA [209]. The cationic charge of these polymers interacts with the anionic phosphates in the siRNA backbone, allowing complexation and the formation of positively-charged nanoparticles (when the polymer is in excess). This facilitates interaction with the negatively-charged cell membrane and internalization of the complexes [210]. PEI has shown high transfection efficiency of siRNA in *in vitro* conditions [211]. However, the polymer's toxicity remains a major hurdle in its further progress to the clinic. Therefore, research is now focused on PEI derivatives with low molecular weight [211].

Chitosan has also been used for siRNA delivery. Chitosan presents a cationic structure at acidic pH (due to the protonation of the amines, pKa = 6.5) that enables complexation with the anionic phosphates in the siRNA backbone. It is also biodegradable and biocompatible, desirable characteristics in an ideal vector for siRNA delivery [142, 159]. Previous studies revealed that siRNA transfection with chitosan is dependent on the molecular weight, degree of deacetylation and the N:P ratios.

Chitosans with molecular weights lower than 20 kDa showed poor results [125, 212], as did chitosans with very high molecular weight (>200 kDa) [129] indicating that there is an optimum range for chitosan molecular weight in order to achieve complete gene silencing (20-200 kDa).

Howard *et al.* showed siRNA delivery with chitosan (114 kDa, 84% degree of deacetylation) *in vitro* and *in vivo*. Western blotting results demonstrated approximately 90% knockdown of BCR/ABL-1 protein in K562 cells at an N:P ratio of 57. Significant knockdown of EGFP was reported in human lung carcinoma cells 48h post-transfection. The transfection levels achieved (77.9%) were comparable to the positive control (78%, TransIT-TKO) [20].

Jogersen *et al* evaluated two chitosans, with molecular weights of 75.7 and 150 kDa, as siRNA carriers targeting the gene S100A4. A silencing effect of 60% was obtained with 75.5 kDa chitosan, the better of the two polymers in RMS melanoma cell line and SKBR3 breast cancer cell line. A higher knockdown effect was obtained in OHS cell line (95%) [128].

Techaarpornkul *et al.* concluded that both the molecular weight of chitosan and the chitosan, siRNA mass ratios of the nanoparticles influence the final gene knockdown results more than the nature of the salt forms. EGFP silencing (around 50%) was achieved with chitosan molecular weight of 20 kDa at a chitosan, siRNA mass ratio of 32, while gene knockdown of chitosans with molecular weights of 200 and 460 kDa was rather poor (below 20%).

Regarding the degree of deacetylation, it is the consensus that more deacetylated chitosan performs better at siRNA delivery, since these chitosans have a higher charge density. Deacetylated chitosan was more efficient in EGFP downregulation than N-acetylated chitosan in a study by Malmo *et al.* [212].

The N:P ratios used in the different studies vary, but it was possible to observe that low molecular weight chitosans need higher N:P ratios (N:P 30-60) to obtain gene silencing as shown by Techaarpornkul *et al*.. Gene silencing results were lower for low polymer, siRNA mass ratios (mass ratio 4 had a gene silencing of 20%) when compared with higher polymer, siRNA mass ratios of 16 and 32 for a chitosan with 20 kDa [129]. Lower N:P ratios (N:P 2-20) have been used with chitosans of higher molecular weight [213]. Malmo *et al.* concluded that the uptake of siRNA increased with the increase of the N:P ratios from 10 to 60 for chitosans with a molecular weight of 16, 35, 55 and 75 kDa. For chitosans with molecular weights of between 50 and 140 kDa the gene knockdown happened at N:P ratios of 10, 30 and 60, while for chitosans with a lower molecular weight, an N:P of 60 was required to obtain comparable results [212].

Different derivatives of chitosan have been synthesized to address some of the issues that impair the transfection efficiency of chitosan, such as buffer capacity and poor solubility at physiological pH.

Tripathi *et al.* showed improved transfection efficiency of a chitosan-PEI derivative when compared with chitosan. Chitosan-PEI-siRNA nanoparticles resulted in a 77% gene knockdown when compared with only 49% of the positive control (lipofectamine) [138]. Also, chitosan-PEI resulted in a 55% EGFP silencing in A549 cells, whereas PEI 25 kDa was only capable of 19% silencing [139].

Trimethyl chitosans are another group of chitosan derivatives that have been studied for siRNA delivery. Different chitosans and trimethyl chitosans were tested for their ability to downregulate EGFP. Formulations with trimethyl chitosan performed better when compared with chitosan. EGFP expression decreased between 3.9 and 12.3% for chitosan polyplexes and 24.3-37.1% with trimethyl chitosans. The gene expression

decrease obtained by trimethyl chitosan with a molecular weight of 50 kDa and 27% quaternization was significantly ($p < 0.05$) higher when compared to all of the chitosans used in the study [214].

Although chitosan-siRNA polyplexes have demonstrated good transfection efficiencies *in vitro*, use of chitosan *in vivo* is restricted by the same issues previously discussed: poor solubility at physiological pH, poor buffer capacity, and instability in the presence of endogenous blood components [143].

In vivo administration of most compounds – including nucleic acids – to the central nervous system is prevented by the blood brain barrier (BBB). Only small (molecular weight < 500 Da), lipophilic molecules are able to cross the BBB via transcellular passive diffusion, with a small number of other compounds able to cross using selective receptors [146, 147].

siRNA is a hydrophilic molecule with a molecular weight of 13 kDa that does not cross the BBB passively. Intranasal administration is a non-invasive method of bypassing the BBB. This route is the most direct, non-invasive entry into the brain, avoiding the adverse effects of systemic delivery. Nose to brain delivery is mainly mediated by the olfactory and trigeminal nerve pathways that connect the brain with the nasal cavity [146-148]. However, this kind of delivery presents some limitations such as a restricted compound molecular weight, variability in the concentration achieved in different regions of the brain and rapid elimination of the substances from the nasal cavity due to mucocilliary clearance [149, 150].

The delivery of siRNA to the brain through the nasal cavity has been tried by different groups [151, 152]. Different delivery systems have been tested to protect the siRNA from enzymatic degradation and to enhance its delivery, cellular uptake and release in the cell cytoplasm in order to be incorporated in the RNAi machinery [153-155].

Kim *et al.* examined the efficiency of intranasal delivery of naked siRNA to normal rat brains. *In vivo* target gene knockdown by the intranasal delivery of αB-crystallin siRNA was examined in the olfactory bulb, amygdala and hypothalamus. After 3 hours of delivery there was no change in αB-crystallin immunoreactivity in any of the brain areas studied. However, after 12 hours of siRNA delivery, αB-crystallin levels were significantly reduced in all three regions. These results indicated that the intranasal siRNA delivery enhanced the access to the central nervous system by the olfactory nerve pathway, allowing gene silencing in specific regions of the brain [151].

The work of Renner *et al.* confirmed the role of the olfactory nerve pathway in the delivery of siRNA to the central nervous system. Thirty minutes after administration of fluorescently-labelled naked siRNA, it was possible to observe siRNA in the olfactory epithelia, olfactory bulbs and along the length of the olfactory nerve pathway. Furthermore, intact siRNA was extracted from the olfactory bulbs of the mice [152].

Intranasal delivery of fluorescently-labelled siRNA with a biodegradable PAMAM dendrimer was reported [153]. The efficiency of intranasal siRNA delivery was studied in normal rat brains by FITC-labelled control siRNA, cell-type specific immunostaining, and DAPI staining. One hour after intranasal delivery, fluorescently-labelled cells were observed in the frontal cortex, olfactory bulb, amygdala and hypothalamus. The same was observed after 3 and 12 hours. Expression levels of HMGB1 were studied after delivery of HMGB1 siRNA or nonspecific siRNA with a PAMAM dendrimer. The immunoreactivity of HMGB1 decreased in the olfactory bulb, amygdala and hypothalamus after 3 hours of siRNA intranasal delivery. In contrast, no decrease of HMGB1 expression was found for nonspecific siRNA. These results indicated that access to the central nervous system through the olfactory pathway was possible after intranasal administration [153].

Intranasal delivery of siRNA with micellar copolymers prepared from methoxy poly(ethylene glycol) (MPEG) and polycaprolactone (PCL), conjugated with a cell-penetrating peptide, Tat (MPEG**-**PCL**-**Tat). The brain distribution of fluorescently-labelled siRNA was significantly higher after intranasal administration when compared with intravenous administration. Levels in the olfactory bulb after intranasal delivery of siRNA with MPEG**-**PCL**-**Tat were higher when compared with naked siRNA, suggesting the delivery of siRNA to the brain is through the olfactory bulb pathway. Similar results were obtained in the trigeminal nerve, suggesting that it is also a possible way to reach the brain [154].

The intranasal delivery of siRNA with the previous micellar system was studied in an intracranial C6 glioma model, evaluating the association of siRNA with an anti-cancer drug (CPT). Untreated rats had a mean survival period of 16.6 days, compared with 18.4 days for rats treated with naked siRNA solution. Significant differences were observed when the previous results were compared with the mean survival period of rats treated with MPEG-PCL-Tat/siRaf-1 (20.4 days), CPT-loaded MPEG-PCL-Tat/siRNA Control (20.6 days), and CPT-loaded MPEG-PCL-Tat/siRaf-1 (28.4 days) [155].

Until now, chitosan has only been used for siRNA delivery from nose to the brain as an adjuvant in a dendrimer-siRNA formulation. [^{32}P]-siRNA, complexed with PAMAM G7 dendrimers, was administered intranasally within an *in situ*-forming mucoadhesive gel. Brain radioactivity was higher after intranasal delivery of dendriplexes both in the gel and in the buffer when compared with the intravenous route. After two doses of siRNA gel delivery the brain radioactivity increased by two-fold when compared with siRNA buffer delivery, and by eight-fold when compared with naked siRNA. Radioactivity was higher in the olfactory bulb and hypothalamus after siRNA intranasal gel administration than after intravenous or intranasal in buffer administration [156].

The previous data of this study has suggested the striking ability of the Ethylamino Glycol Chitosan polymer to perform as a plasmid DNA carrier. Therefore, the use of Ethylamino Glycol Chitosan as a siRNA carrier was analyzed. This chapter presents the results for *in vitro* and *in vivo* biological studies with siRNA and EAGC30 as delivery system. The polymer delivery efficiency, *in vitro,* was studied by Western Blotting. A small *in vivo* pilot study was performed to demonstrate the capacity of the polymer to deliver siRNA to the brain after intranasal administration.

5.2 Methods

5.2.1 *In vitro* transfection

Briefly, 6-well plates were seeded with 500000 cells (A431) per well and incubated overnight. The complexes were prepared to a final ITCH siRNA/scrambled siRNA (Eurofins mwg/operon, London, UK) concentration of 533nM. Polymer stock solution (EAGC30) was prepared in sterile dextrose (5% (w/v) filtered with a 0.22 μm Millex filter) to which was added equal volumes of the ITCH siRNA/scrambled siRNA stock solution (insiMAX universal buffer) to give EAGC30, siRNA mass ratios of 1 to 60. The complexes were allowed to incubate at room temperature for 1 hour, after which the EAGC30-ITCH siRNA/-scrambled siRNA complexes were added to the cells (750μL, 533nM ITCH siRNA/scrambled siRNA per well) and incubated for 6h in medium (MEM, Life Technologies, Paisley, UK) serum free. The complexes were replaced with fresh MEM and the cells were then incubated for a further 48 hours. The transfection efficiency was determined by Western blotting.

Lipofectamine 2000 (Invitrogen, Paisley, UK)-siRNA complexes were prepared according to the manufacturer's specifications and were used as a positive control. Cells were incubated for six hours with lipofectamine-siRNA complexes (66.7nM siRNA/well), in serum-free medium and then replenished with complete media.

5.2.2 Western Blotting

Western blotting is a protein analysis technique that identifies with specific antibodies proteins that are on the surface of a membrane. Firstly, the proteins are separated according with their size by gel electrophoresis. These are then transferred to a membrane that is blocked to prevent non-specific binding of the antibodies. The proteins in the membrane are detected by specific antibodies and are revealed through different detection methods, such as chemiluminescence. Western blotting is a qualitative and semiquantitative method where the intensity of the signal should correlate with the abundance of protein in the membrane [215, 216].

Forty-eight hours after siRNA delivery, protein extracts were obtained from A431 cells using lysis buffer containing protease inhibitors (Radio-Immunoprecipitation Assay (RIPA) buffer Sigma Aldrich, Dorset, UK). Protein content was determined with the Bicinchoninic Acid (BCA) Assay using Bovine Serum Albumin standards. 20 μg of total

protein was resuspended in NuPAGE® lithium dodecyl sulfate sample buffer (Life Technologies, Paisley, UK) and dithiothreitol sample buffer (Life Technologies, Paisley, UK), incubated for 15 min at 95ºC, and loaded onto a 4-12% polyacrylamide gel. After electrophoresis the proteins were blotted onto a nitrocellulose membrane. After blocking in 5% non-fat milk, overnight at 4 degrees, the membrane was incubated with an anti-ITCH (1:500) (BD Bioscience, San Jose, USA) and anti-actin antibody (1:2500) (Abcam, Cambridge, UK) for 2h at room temperature, and with horseradish peroxidase (HRP) secondary antibody (1:1000) (Invitrogen, Paisley, UK) for 1h at room temperature. Between the incubation periods the blots were washed several times with 10% PBS and 1% Tween 20 in PBS. The membrane was incubated with SuperSignal West Pico Chemiluminescent Substrate (Thermo Scientific, Waltham, USA) for 5 min at room temperature and then submitted to detection with ChemiDoc™ XRS+ System (Bio Rad, Hemel, UK). For each membrane, the analysis of band intensity was performed using the Image Lab software (BioRad, Hemel, UK).

5.2.3 *In vivo* administration

Animals

Sprague Dawley rats (200-250 g) were housed four per cage in an air conditioned unit maintained at 20-22°C and 50-60 % humidity, and were allowed free access to standard rodent chow and water. Lighting was controlled on a twelve-hour cycle, lights on at 07.00 hr. Animals were habituated for 7 days prior to experimentation and acclimatised to the procedure room for 1h prior to testing at 8.00 hr. All protocols were conducted under a UK Home office licence and approved by a local ethical committee.

Formulations

Rats (2 for each study group) were intranasally administered with siRNA alone (15 µg, 80 µL, BLOCK-iT™ Alexa Fluor® Red Fluorescent Control, Life Technologies, Paisley, UK) and EAGC30-siRNA polyplex formulation at a EAGC30, siRNA mass ratio of 60 (80µL. 15 µg of siRNA, BLOCK-iT™ Alexa Fluor® Red Fluorescent Control). Animals were briefly anesthetised with isoflurane and intranasally administered the formulation using an insulin syringe attached to PE10 tubing (15 mm). The tubing was inserted into one of the nares [217]. The brains were harvested after 5min. These brains were fixed in formalin and 0.5mm thick coronal sections were prepared for microscopy.

5.2.4 CARS Microscopy

Coherent anti-stokes Raman scattering (CARS) is a four-wave mixing process in which a pump beam at frequency ω_p and a Stokes beam at frequency ω_s interact within a sample. When the beam frequency (ω_p - ω_s) matches the frequency of a Raman active vibrational mode, molecules are coherently driven with the excitation fields, generating a strong anti-stokes signal ($\omega_{as} = 2\omega_p - \omega_s$) [218, 219]. CARS microscopy has allowed visualization of DNA (phosphate stretch vibration), protein (amide I vibration) and lipids (CH group of stretching vibrations). CARS microscopy presents several advantages over conventional imaging: up to several hundred micron depth penetration into biological tissue, intrinsic optical sectioning and high spatial resolution, and label-free chemical-specific contrast [220, 221].

Two Photon Fluorescence (TPF) microscopy is used in thick specimens allowing imaging depths of ≈ 500mm and reduced phototoxicity. Two low energy photons cause a higher energy electronic transition in a fluorescent molecule. Local heating generated by the optical absorption is detected [222].

CARS and TPF images were detected using a photomultiplier tube (R3896, Hamamatsu) in the epi-direction using a 750 nm long pass dichroic (750dcxr 229 Chroma) and two filters centred at 660 nm (Ealing Inc.) to separate the signal from the laser fundamental, using a 60× 1.0NA water immersion objective lens (LUMFI, 210 Olympus) to direct the laser light to the sample from the olfactory bulb region of sample (5 minutes after nasal dosing).

Red contrast comes from the CARS signal, with the pump and Stokes beams tuned to excite the CH_2 stretch at 2845 cm^{-1} (characteristic of lipid-rich structures such as myelin sheaths and lipid droplets etc.)

The green contrast is derived from epi-detected two-photon fluorescence, excited by a single picosecond 1064 nm beam (532 nm absorption). The naturally occurring background fluorescence from the brain was separated from the particle fluorescence by adjusting the brightness and contrast of the images: the 16-bit data sets (i.e. a possible pixel intensity range of 0 – 65536) exhibited a maximum intensity value of 270 for the control samples, and 4079 for the samples exposed to the particles. The combined laser power was kept below 40 mW at the sample. This power was sufficiently low enough to prevent photodamage from occurring.

This experiment was performed by Dr. Natalie Garrett at the University of Exeter.

5.3 Results

5.3.1 *In vitro* results – Western Blotting

The transfection efficiency of siRNA by EAGC30 was evaluated *in vitro* by the delivery of anti-ITCH siRNA into A431 cells. ITCH is an ubiquitin ligase that is involved in controlling cell growth, differentiation and apoptotic process. Its targets are transcription factors and growth factor receptors that act as gene expression regulators [223]. The polyplexes were prepared at increasing polymer, siRNA mass ratios (1 - 60). The positive control was lipofectamine with anti-ITCH siRNA, a well-described *in vitro* transfection agent, and the negative controls were naked anti-ITCH siRNA, polymer alone, non-transfected cells and scrambled siRNA. Scrambled siRNA presents a sequence that does not target any particular gene. It was used as a negative control to distinguish non-specific effects from specific gene knockdown effect [224]. β-Actin is a housekeeping gene that was chosen as the "internal" control. Housekeeping genes encode proteins that are essential for maintenance of cell function. β-Actin allowed the control of cell toxicity and death, and was also used for normalization of the final results [225]. The transfection efficiency was determined by Western blotting analysis.

Different parameters that might influence the transfection efficiency of siRNA were studied in order to optimize the transfection protocol. Variables such as siRNA dose, volume of transfected solutions and EAGC30, siRNA mass ratios were analyzed.

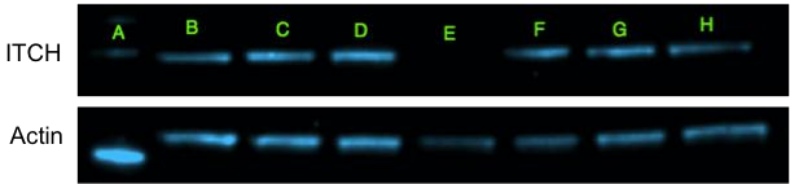

Figure 80 - Western blotting analysis of ITCH knockdown in A431 cells. Study of different EAGC, siRNA mass ratios with 133nM of siRNA after 6 hours incubation with the polyplexes. β - Actin was used as internal control. 5 mL of cell medium without serum to 50 µL complexes solution. A – Molecular weight marker, B – Untreated Cells, C – Polymer alone, D – Naked ITCH siRNA E – Lipofectamine + ITCH siRNA (133 nM siRNA), F – EAGC30, Scrambled siRNA (10:1), G – EAGC30, ITCH siRNA (10:1), H – EAGC30, ITCH siRNA (30:1).

Two different EAGC30, siRNA mass ratios were investigated: 10 and 30. It is possible to observe in Figure 80 that there was no ITCH silencing for either of the EAGC30, siRNA mass ratios used. This may have happened due to the concentration of siRNA. The dose of siRNA used in *in vitro* studies for gene down regulation is not standard in

the literature. Howard *et al.* registered no difference in the gene silencing levels when increasing the siRNA dose from 100 and 200nM [20]. However, concentrations as low as 15nM have been used with the maximum gene knockdown achieved at 45nM [212]. Other studies have used concentrations between 100 and 200nM [127, 226]. The siRNA dose used in this experiment was 133 nM, the same as that of the positive control – lipofectamine. Alternatively, the EAGC30, siRNA mass ratios studied may not be stable enough in presence of cell medium to transfect effectively. Agarose gels (Chapter 3) showed that in presence of 150mM of NaCl there was dissociation of the complexes between EAGC30 and siRNA at EAGC30, siRNA mass ratio 10. Scrambled siRNA did not show any down-regulation. The positive control, lipofectamine, completely silenced ITCH while all the negative controls showed no gene silencing. The internal control in the treatments, β-Actin, did not show any decrease when compared with untreated cells, indicating cell viability.

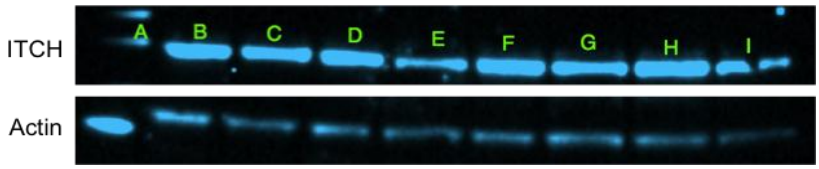

Figure 81 - Western Blotting analysis of ITCH knockdown in A431 cells. Study of different EAGC, siRNA mass ratios with 267nM and 533nM of siRNA after 6 hours incubation with polyplexes. β - Actin was used as internal control. 5 mL cell medium without serum to 100 or 200 µL complexes solution. A – Molecular weight marker, B – Untreated Cells, C – Polymer alone, D – Naked ITCH siRNA E – Lipofectamine + ITCH siRNA (133 nM siRNA), F – EAGC30, Scrambled siRNA (30:1, 267nM siRNA), G – EAGC30, ITCH siRNA (60:1, 267nM siRNA), H – EAGC30, ITCH siRNA (30:1, 533nM siRNA), I – EAGC30, ITCH siRNA (60:1, 533nM siRNA).

In a subsequent experiment, the dose of siRNA transfected was increased. Figure 81 shows the results for 267nM (lanes F and G) and 533nM (lanes H and I) of siRNA. Two EAGC30, siRNA mass ratios were chosen: 30 and 60. The EAGC30, siRNA mass ratio 30 allowed direct comparison with the results in Figure 80 while EAGC, siRNA mass ratio 60 enables us to understand if higher EAGC30, siRNA mass ratios increase gene silencing.

There was no reduction of protein expression with any of the polymer treatments, meaning that increasing the amount of siRNA or the EAGC, siRNA mass ratios had no influence in decreasing the final protein expression. Negative controls showed similar results. The lipofectamine was the only formulation that showed gene silencing. The change of the dose of siRNA and the EAGC30, siRNA mass ratios did not improve the

silencing results. Other factors that might influence the transfection efficiency of EAGC30 were therefore analyzed.

Previously, it was observed that large polyplexes have a faster sedimentation leading to increased transfection results due to easier contact with the cells surface. In this way, small complexes benefited from a reduction of the transfection volume in order to facilitate contact with the cells and enhance transfection of nucleic acids [179]. In this study (Chapter 3), TEM and size results showed that complexes formed between EAGC30 and siRNA presented a small size, between 50 and 200nm (for all EAGC30, siRNA mass ratios higher than 1). The previous transfection experiments were performed with 5 mL of cell medium to a maximum volume of complex solution of 200µL. To analyze the effect of the transfection volume on protein expression, different volumes of cell medium and complex solutions were used. Figure 82 presents the results for two different doses of siRNA (267 and 533nM) and two different EAGC30, siRNA mass ratios, 60 and 80. The cell medium volume was reduced from 5 mL to 2 mL and 100 and 200µL of complex solution was used.

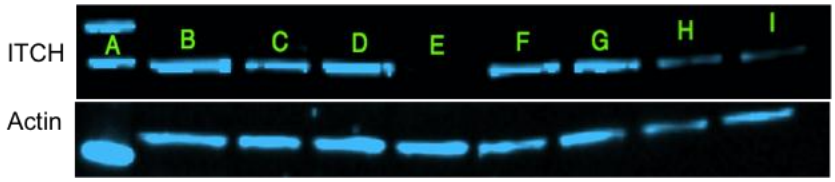

Figure 82 - Western Blotting analysis of ITCH knockdown in A431 cells. Study of different EAGC, siRNA mass ratios with 267 and 533 nM of siRNA after 6 hours incubation with polyplexes. β - Actin was used as internal control. 2 mL cell medium without serum to 100 or 200 µL complexes solution. A – Molecular weight marker, B – Untreated Cells, C – Polymer alone, D – Naked ITCH siRNA E – Lipofectamine + ITCH siRNA (133nM siRNA), F – EAGC30, ITCH siRNA (60:1, 267nM siRNA), G – EAGC30, ITCH siRNA (80:1, 267nM siRNA), H – EAGC30, ITCH siRNA (60:1, 533nM siRNA), I – EAGC30, ITCH siRNA (80:1, 533nM siRNA).

It was possible to observe a slight decrease in protein expression for EAGC30, siRNA mass ratios 60 and 80 with 533nM (lane H and I) of siRNA when compared with EAGC30, siRNA mass ratios 60 and 80 with 267nM (lane F and G). This indicates that a higher dose of siRNA was necessary for down-regulation of ITCH gene. The comparison between lane H of Figure 82 with lane I of Figure 81 (EAGC30, siRNA mass ratio 60, 533 nM of siRNA) allowed to conclude that the transfection volume is an important factor, affecting the final protein expression.

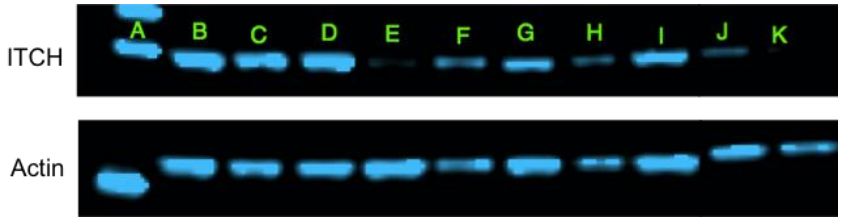

Figure 83 - Western Blotting analysis of ITCH knockdown in A431 cells. Study of different EAGC, siRNA mass ratios with 533nM of siRNA after 6 hours incubation with polyplexes. β - Actin was used as internal control. 750μL cell medium without serum to 750μL complexes solution. A – Molecular weight marker, B – Untreated Cells, C – Polymer alone, D – Naked ITCH siRNA E – Lipofectamine + ITCH siRNA (133nM siRNA), F – EAGC30, ITCH siRNA (10:1), G – EAGC30, Scrambled siRNA (10:1), H – EAGC30, ITCH siRNA (30:1), I – EAGC30, Scrambled siRNA (30:1), J – EAGC30, Scrambled siRNA (60:1), K – EAGC30, ITCH siRNA (60:1).

Figure 83 shows the results for gene silencing after transfecting the cells with 750 μL of complexes in dextrose (5%) with 750 μL of cell medium per well. The most pronounced downregulation was achieved after delivery of anti-ITCH siRNA by EAGC30 prepared at EAGC30, siRNA mass ratio 60 (lane K). The cellular levels of ITCH protein were also reduced for EAGC30, siRNA mass ratio 30 (lane H). To confirm the sequence specificity of siRNA anti-ITCH and the absence of off-target effects, the cells were also incubated with scrambled siRNA. Gene silencing was found to be specific, since no ITCH knockdown was observed with scrambled siRNA (lanes G, I and J). The levels of β-actin were constant for all tested formulations, and showed no cell toxicity. The increase of the transfection volume increased the delivery of siRNA resulting in high levels of gene silencing.

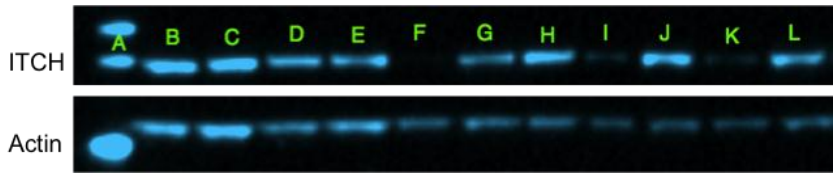

Figure 84 - Western Blotting analysis of ITCH knockdown in A431 cells. Study of different EAGC, siRNA mass ratios with 533nM of siRNA after 6 hours incubation with polyplexes. β - Actin was used as internal control. 750μL cell medium without serum to 750μL complexes solution. A – Molecular weight marker, B – Untreated Cells, C – Polymer alone, D – Naked ITCH siRNA E – Naked Scrambled siRNA F – Lipofectamine + ITCH siRNA (133nM siRNA), G – EAGC30, ITCH siRNA (1:10), H – EAGC30, Scrambled siRNA (10:1), I – EAGC30, ITCH siRNA (30:1), J – EAGC30, Scrambled siRNA (30:1), K – EAGC30, ITCH siRNA (60:1), L – EAGC30:Scrambled siRNA (60:1).

Figure 84 shows a repetition of the transfection with increasing EAGC30, siRNA mass ratios. In this experiment a new negative control was included, naked scrambled siRNA (lane E), that did not show any knock-down effect on the target proteins. Likewise, none of the other negative controls produced any down-regulation effect. The results were comparable with Figure 83, indicating reproducibility of gene silencing with EAGC30, siRNA mass ratio 30 and 60.

Table 27 summarises the different features that were studied to optimize the transfection protocol and obtain gene silencing with EAGC30. EAGC30, siRNA complexes were able to achieve down-regulation with a small dose of siRNA at an EAGC30, siRNA mass ratio of 30. From this study it is also possible to conclude that the transfection volume is an important factor with impact in the final results.

Table 27 - Summary of transfection conditions for siRNA.

Figure	Dose of siRNA (nM)	EAGC30, siRNA mass ratios	Volume of complexes transfected (µL)	Volume of cell medium in the wells (µL)	Specific down-regulation
80	133	10 and 30	50	5000	X
81	267 and 533	30 and 60	100 or 200	5000	X
82	267 and 533	30 and 60	100 or 200	2000	X
83	533	30 and 60	750	750	√
84	533	30 and 60	750	750	√

5.3.2 *In vivo* results – CARS Microscopy

To understand the behaviour of the EAGC30, siRNA nanoparticles *in vivo*, a small pilot study was designed. The main objectives were the evaluation of nasal delivery to the brain with EAGC30 nanoparticles, and the polymer's capacity to protect siRNA from degradation *in vivo*. Therefore, three animals groups were studied: untreated, treated with naked siRNA (Alexa Fluor® Fluorescent) and treated with EAGC30, siRNA nanoparticles at an EAGC30, siRNA mass ratio of 60. The brain tissue was harvested 5 min after nasal administration of the treatments. CARS images of the olfactory bulb were taken to evaluate the delivery of fluorescently labelled siRNA. Figure 85 shows the results for the untreated samples. The red contrast comes from CARS signal, with the beams tuned to excite the CH_2 stretch characteristic of lipid-rich structures such as myelin sheaths.

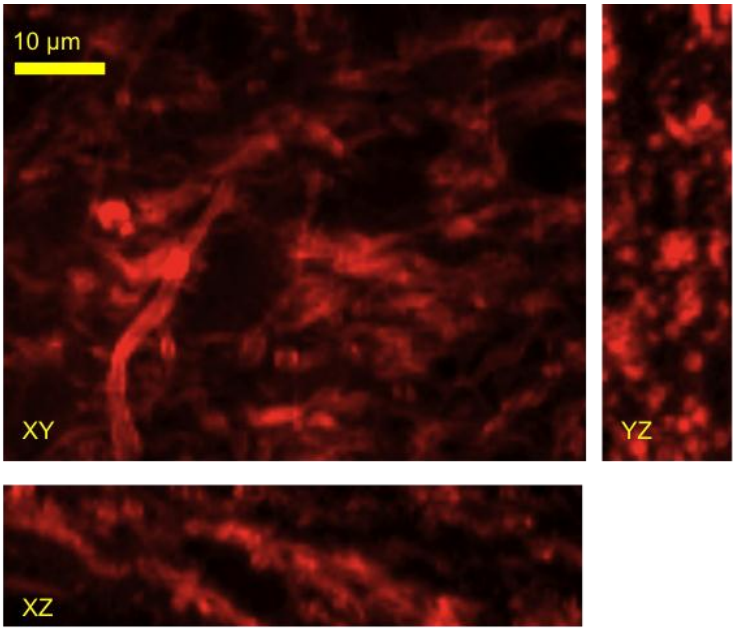

Figure 85 - Orthogonal view reconstructions of depth-stack images of an olfactory bulb sample (untreated group) using CARS with the pump and Stokes beams tuned to excite the CH_2 stretch at 2845 cm^{-1} (red – brain tissue).

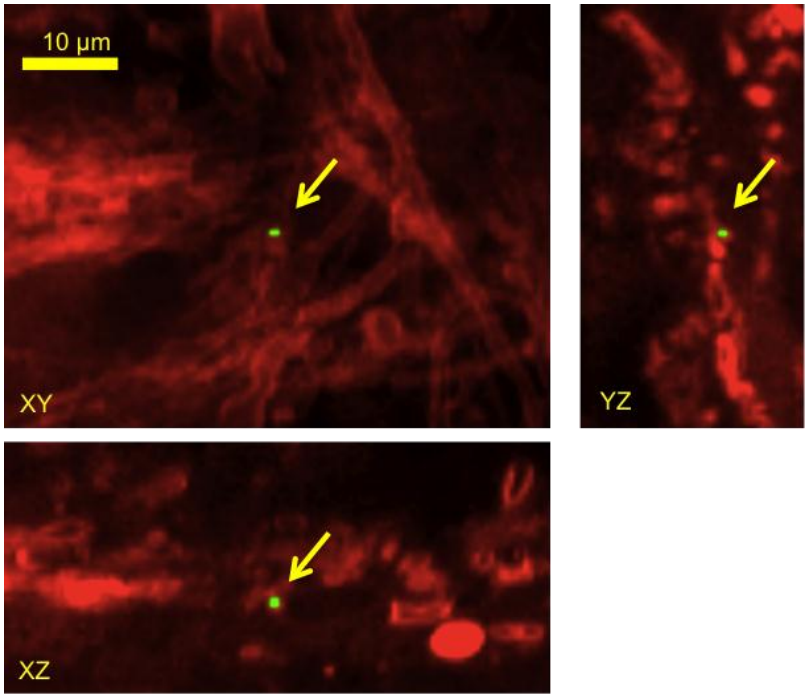

Figure 86 - Orthogonal view reconstructions of depth-stack images of an olfactory bulb sample, harvested 5 min after nasal administration of EAGC30, siRNA nanoparticles with an EAGC30, siRNA mass ratio of 60 using contrast from TPF (green – siRNA Alexa Fluor® Fluorescent) and CARS with the pump and Stokes beams tuned to excite the CH_2 stretch at 2845 cm^{-1} (red – brain tissue).

Figure 86 shows the results for the group treated with EAGC30, siRNA nanoparticles at an EAGC30, siRNA mass ratio of 60. It is possible to observe the red contrast from CARS signal of the brain tissues and the presence of the green fluorescence signal from the EAGC30, siRNA nanoparticles. These images demonstrate that nasal delivery to the brain (olfactory bulb) was possible with EAGC30 nanoparticles. The results from the analysis of the samples treated with naked siRNA have not yet been obtained. These results will allow the study of the polymer's ability to protect the siRNA from degradation in the *in vivo* environment.

5.4 Discussion

A literature review regarding siRNA *in vitro* delivery with chitosan showed good gene silencing results [20, 125, 212]. However, chitosan's low solubility at physiological pH and poor buffer capacity are still a major drawback for its use *in vivo,* resulting in instability and insufficient intracellular siRNA release [142]. The previous data in this thesis has suggested the striking ability of the Ethylamino Glycol Chitosan polymer to perform as a plasmid DNA carrier. It is able to condense the gene, offers it protection from nuclease digestion and enables intracellular delivery. Therefore, the use of Ethylamino Glycol Chitosan as a siRNA carrier was studied.

The transfection efficiency of EAGC30 *in vitro* was analysed by Western blotting. Western blotting is a qualitative and semiquantitative method that allows identification of specific proteins and evaluation of their abundance in the cells [216]. Different parameters that might influence the transfection efficiency of siRNA were studied, such as siRNA dose, volume of transfected solutions and EAGC30, siRNA mass ratios.

Three different doses of siRNA were studied: 133, 267 and 533 nM (Table 27). The highest dose was revealed to be necessary for ITCH down-regulation. Different doses of siRNA had been reported in the literature. Howard *et al.* registered no difference in the gene silencing levels when increasing the siRNA dose from 100 and 200nM [20]. In another study, concentrations as low as 15nM were used, with the maximum gene knockdown achieved at 45nM [212]. Other studies have used concentrations between 100 and 200nM [127, 226]. When comparing the different doses of siRNA between studies it is important to consider the number of cells transfected with each dose, otherwise direct comparison is not possible. Considering the concentration of siRNA per 1000 cells seeded, the values range from 0.5nM per 1000 cells in Howard *et al.* study [20] up to 25nM per 1000 cells [226]. The dose used in this study, which delivered the best results, was 1nM per 1000 cells. This falls in the lower range of the doses in the published literature. This direct comparison confirms the good transfection capacity of EAGC30 and its potential as delivery system, since the dose used to produce complete gene silencing is low compared with other studies.

Increasing EAGC30, siRNA mass ratios (1-60) were tested for gene silencing. EAGC30, siRNA mass ratios 30 and 60 achieved down-regulation of ITCH *in vitro*. Lower EAGC30, siRNA mass ratios were not capable of gene silencing since they were quite unstable in the presence of biological challenges such as heparin and salt (Chapter 3). These results are in line with the literature, where it has been reported

that low molecular weight polymers need higher polymer, siRNA mass ratios to cause gene down regulation.

For a 20 kDa chitosan the optimal gene silencing was obtained at a polymer, siRNA mass ratio of 32, with lower gene silencing reported for polymer, siRNA mass ratios of 4 and 8 [129]. Malmo *et al.* have found that fully deacetylated chitosans of low molecular weights (10 kDa) required N:P ratios up to 60 for efficient silencing while at higher molecular weights, all 3 tested ratios (10, 30, 60) performed equally with about an 80% silencing achieved at pH 7.2 [212]. This need for high N:P ratios is partially explained by the ionic interactions between siRNA and chitosan. Previous studies showed that the binding capacity of siRNA to chitosan is weaker when compared with the binding capacity of plasmid DNA with chitosan [127].

Finally, the volume of transfected complexes was also studied (Table 27). It was observed that large polyplexes have a fast sedimentation, which increased transfection results due to facilitated contact with the cell surface. In this way, small complexes benefited from a reduction of the transfection volume in order to facilitate contact with the cells and enhance transfection of nucleic acids [179]. Different cell medium-complex solution volume ratios were analyzed. Throughout the study, the cell medium volume was decreased and the complex medium volume was increased until a final ratio of 1:1 was achieved. This was found to be the optimal ratio to deliver the best gene silencing results.

In summary, *in vitro* siRNA delivery with EAGC30 was achieved with high levels of gene silencing. The polymer showed similar results to previous studies with chitosan, where low molecular weight chitosans performed better at higher N:P ratios. However, the dose of siRNA necessary to achieve complete down-regulation of proteins was low, confirming the high transfection capacity of EAGC30. Furthermore, the polymer is soluble at physiological pH, and does not need to be applied in a low pH buffer; this overcomes one of the principal disadvantages of the use of chitosan *in vivo*.

In vivo administration of nucleic acids to the central nervous system is restrained by the blood brain barrier. The intranasal route of administration is a non-invasive method of bypassing it. The delivery of siRNA to the brain through the nasal cavity has been tried by different groups. Different delivery systems have been tested to protect the siRNA from enzymatic degradation and to enhance its *in vivo* delivery [151, 152, 155, 156].

Encouraging results were obtained in the small pilot *in vivo* study performed of siRNA delivery with EAGC30 to the brain. The olfactory bulb tissue was analyzed for the

presence of fluorescent siRNA after nasal administration of EAGC-siRNA fluorescent nanoparticles at an EAGC30, siRNA mass ratio of 60. The results showed that EAGC30-siRNA nanoparticles were able to reach the brain when compared to a non-treated sample. Despite the good initial results obtained further experiments are needed, including treatment of the brain with naked siRNA, in order to confirm the polymer's capacity to protect siRNA from enzymatic degradation *in vivo*.

Furthermore, the nanoparticles distribution through the different tissues of the brain as well as the system's capacity for specific protein down-regulation *in vivo* should be evaluated. However, the preliminary results of this study introduce EAGC30 as a good candidate for *in vivo* siRNA delivery to the brain.

6. Conclusion and Future Work

Despite the efforts to develop chitosan-based vectors, the therapeutic effectiveness of chitosan-based gene therapy still needs to be improved in order to achieve clinical significance. To date there are no reports of clinical trials for the delivery of DNA or siRNA using chitosan as the delivery system [54]. This work introduces a new chitosan based polymer: N-(2-ethylamino)-6-O-glycol chitosan (Ethylamino Glycol Chitosan, EAGC). EAGC was synthesized with four important considerations in mind: (i) the resulting polymer should be soluble at physiological pH; (ii) it should efficiently complex with the nucleic acids to provide stable polyplexes; (iii) it should have improved buffering capacity to be able to release the nucleic acids inside the cell; and (iv) it should retain the biocompatibility and low cell toxicity of chitosan.

During the synthesis of EAGC, two main characteristics of the polymer were considered: molecular weight and charge density. An appropriate polymer molecular weight was needed to confer enough stability to the complexes for nucleic acid protection, without inhibiting intracellular release of DNA or siRNA [159]. Nucleic acid release is required to obtain high levels of transfection. The molecular weight of the three different polymers was confirmed by GPC. Two molecular weight (17 and 27 kDa) variants of EAGC were chosen. Low molecular weight polymers were preferred to avoid the previously discussed drawbacks presented by high molecular weight polymers, such as low solubility and low biocompatibility. The initial glycol chitosan was substituted with ethylamino groups in order to increase the charge density of the polymer. Furthermore, the ethylamino group introduced in glycol chitosan had the additional objectives of increasing the solubility of the polymer at physiological pH and increasing the buffer capacity of the polymer.

The chemical structure and degree of substitution of EAGC were confirmed by NMR. The ^{1}H-NMR spectra of EAGC17, EAGC20 and EAGC30 revealed that increasing the molar ratio of GC:$BrCH_2CH_2NH_2$ increased the overall substitution of the polymers. The substitution of the primary amines of chitosan with one or two ethylamino groups provided the new polymers with primary, secondary and tertiary amines that are required for good buffering, proper binding and release of nucleic acids [138, 178].

The buffer capacity of EAGC polymers was determined from acid–base titration curves. All the EAGC polymers showed an increased buffer capacity compared with GC. Also, it was possible to observe that the buffer capacity of EAGC increased with the

increasing degree of substitution. It has been previously described that tertiary amines, with a pKa similar to the pH of the endosome, contribute to the increase of the buffer capacity of cationic polymers [138, 178]. The calculation of the percentage of the different amino groups in each synthesized EAGC polymer revealed that the most substituted polymer presented the highest percentage of tertiary amines. This is likely to have been responsible for the trend in increasing buffer capacity across the EAGC polymers with increasing degrees of substitution.

The final degree of substitution of the different batches of EAGC was controlled by the molar ratio of GC:$BrCH_2CH_2NHBoc$. However, it was not possible to control the number of double or single substitutions during synthesis. Further work is necessary to completely understand the mechanism of the reaction and enable full control of the number of primary, secondary and tertiary amines present in the final polymer.

The capacity of cationic polymers, like EAGC, to compact the structure of nucleic acids relies on electrostatic interactions between the positively charged polymer and negatively charged DNA or siRNA. The agarose gel retardation assay revealed that GC28 and GC17 were not able to completely condense with DNA at any polymer, DNA mass ratio. EAGC14, with the lowest amount of amines introduced on the GC backbone, revealed condensation results as poor as GC17. However, when the number of amines was increased, through the introduction of the ethylamino double substitution, EAGC13 and EAGC17 showed improved retention capacity of the DNA after 1h of incubation. EAGC30 presented the strongest DNA binding ability, as the DNA mobility was fully retarded at polymer, DNA mass ratios as low as 5 after 30min of incubation.

All EAGC polymers contain primary amines displaying high pKa values, between 9 and 10. This makes them fully protonated at physiological pH, and the resulting positive charge readily enables condensation with the negatively charged nucleic acids. This is in particular contrast to chitosan, where the pKa of the amine groups, as previously discussed, does not allow them to be protonated at physiological pH [114].

EAGC30 was the polymer chosen to condense siRNA due to the particular characteristics of the nucleic acid. Previously, some authors had demonstrated that to achieve stable nanoparticles, siRNA requires polymers with higher molecular weight, charge density and N:P ratio [125, 190]. Agarose gel results for EAGC30 with siRNA showed that this polymer was able to retain the nucleic acid for EAGC30, siRNA mass

ratios as low as 5, and after just 30 minutes of incubation, despite its relatively low molecular weight (molecular weight of 27 kDa).

Morphological characterization of the polyplexes formed between EAGC and DNA/siRNA was made by TEM. The complexes were spherical or toroid for all EAGC-DNA and EAGC30-siRNA nanoparticles. Particle size was determined by nanoparticle tracking analysis for the three polymers EAGC17, EAGC21 and EAGC30 complexed with plasmid DNA. EAGC nanoparticles with plasmid DNA showed a maximum diameter of 450 nm for all three polymers studied. The particles formed between EAGC30 and siRNA between 150 and 500nm in size. The polyplexes formed between EAGC17, EAGC21 and EAGC30 and DNA presented a positive charge of around +40mV for all EACG, DNA mass ratios above 5. Similar results were obtained for siRNA nanoparticles with EAGC30. These results confirmed the high protonation of EAGC polymers, even at physiological pH.

The extra- and intracellular environment has a strong impact on the stability of nanoparticles formed with cationic polymers. Anionic proteins, salt and nucleases are among the major hurdles that polyplexes need to overcome even before reaching the cell surface [179]. Increasing the substitution of the polymer, leading to higher charge density, improved the capacity of the polymers to retain the DNA in the presence of heparin, with EAGC30 retaining the DNA for a polymer, DNA mass ratio as low as 10. For siRNA nanoparticles, EAGC30 was only able to completely retain the siRNA for an EAGC30, siRNA mass ratio of 30. EAGC complexes showed good stability in the presence of NaCl (150nM). EAGC17 presented the most unstable particles, while EAGC30 did not release the plasmid DNA at any polymer, DNA mass ratios. EAGC30-siRNA particles were unstable in the presence of NaCl for small EAGC30, siRNA mass ratios, 5 and 10. Finally, the complexes were tested against the presence of nucleases. All polymers were able to protect the DNA from degradation at all polymer, DNA mass ratios, and EAGC30 also was able to protect siRNA for all EAGC30, siRNA mass ratios. It was clear that an increase in molecular weight and charge density of EAGC resulted in a greater stability to biological challenges.

In summary, EAGC30, siRNA nanoparticles were less stable in the presence of the different biological challenges when compared with DNA, EAGC30 nanoparticles. This increased instability has been described before and it is attributed to the smaller size of siRNA and its lower charge density compared with DNA [125, 190].

The toxicity of chitosan is intimately related with its molecular weight and charge density. Chitosans of high molecular weight (>100 kDa) and degree of deacetylation [95] were less biocompatible than low molecular weight polymers (10 kDa) [105]. The toxicity of EAGC polymers increased with the charge density. EAGC17 presented the lowest toxicity (IC50 = 1.826 ± 0.09 mg mL^{-1}), since it had the lowest molecular weight and charge density of the three polymers. EAGC30 was the least biocompatible polymer (IC50 = 0.522 ± 0.17 mg mL^{-1}). All EAGC polymers were more biocompatible than PEI [101] and the introduction of the extra positive charge did not decrease the polymer's biocompatibility when compared with chitosan [86].

Different parameters that might influence the transfection efficiency of plasmid DNA, such as incubation time of the complexes with cells, were studied in order to optimize the transfection protocol. The optimal time should balance detectable expression with limited toxicity. After 6 hours the transfection values were three times higher when compared with 4 hours of incubation. Also, for 6h of incubation, the results of the polymer-DNA treatments were significantly better when compared with lipofectamine ($^{###}p \leq 0.001$). The presence of proteins can impair the transfection of the plasmid DNA due to non-specific interactions between the nanoparticles and the serum components [120]. The presence of 10% of FBS in cell medium did not interfere with the transfection ability of the EAGC21 nanoparticles. Similar transfection results were obtained in the presence or absence of proteins.

The results for EAGC17, EAGC21 and EAGC30 showed that transfection ability is dependent on the degree of substitution of the polymers and EAGC, DNA mass ratios. The transfection ability increased with the number of amines in the polymer backbone. The increased number of primary amines, with pKa of 9-10, allowed EAGC to be protonated at physiological pH. Thus, transfection was achieved without the use of acidic buffers. The additional secondary and tertiary amines introduced by the ethylamino substitution increased the buffer capacity; buffer capacity was higher for polymers with a higher degrees of substitution. This may have enhanced the ability of the EAGC-DNA complexes to cause endosomal rupture. All polymers studied in this project were superior transfection agents than the positive control, lipofectamine, especially at high polymer, DNA mass ratios.

For the three polymers, an increase of polymer, DNA mass ratio led to an increase in transfection, with EAGC30 reaching a plateau at EAGC30, DNA mass ratio of 30. The increased charge density at low molecular weights displayed by EAGC also allowed good transfection even at polymer, DNA mass ratios as low as 5.

The *in vitro* transfection efficiency of siRNA by EAGC30 was analysed by Western blotting. Different parameters that might influence the transfection efficiency of siRNA were studied, including siRNA dose, volume of transfected solutions and EAGC30, siRNA mass ratios. Three different doses of siRNA were studied: 133, 267 and 533 nM. The highest dose was revealed to be necessary for ITCH down-regulation. This falls in the lower range of the doses in the published literature [127, 212, 226] confirming the high transfection capacity of the new polymer, EAGC30, and its potential as a gene delivery system.

Increasing EAGC30, siRNA mass ratios (1-60) were tested for gene silencing. EAGC30, siRNA mass ratios 30 and 60 achieved high levels of down-regulation of ITCH *in vitro*. These results are in line with the literature, where it has been reported that low molecular weight polymers need higher polymer, siRNA mass ratios to obtain down-regulation [129, 212]. Also, the EAGC30-siRNA nanoparticles had shown higher stability in the presence of heparin and salt for EAGC30, siRNA mass ratios 30 and 60 than at lower EAGC30, siRNA mass ratios. This need for high N:P ratios is partially explained by the weak ionic interactions between siRNA and chitosan [127]. Finally, the volume of transfected complexes was also studied. Different cell medium, complex solution volume ratios were analyzed until an optimal ratio of 1:1 was reached; this delivered the best gene silencing results.

In vivo administration of nucleic acids to the central nervous system is restrained by the blood brain barrier. The intranasal route of administration is a non-invasive method of bypassing it. Different delivery systems have previously been tested to protect the siRNA from enzymatic degradation and to enhance its *in vivo* delivery [151, 152, 155, 156]. Encouraging results were obtained in the small pilot *in vivo* study of siRNA delivery to the brain using EAGC30. The olfactory bulb tissue was analyzed for the presence of fluorescent siRNA after nasal administration of siRNA fluorescent nanoparticles at EAGC30, siRNA mass ratio 60. The results showed that EAGC30-siRNA nanoparticles were able to reach the brain, and could be visualized by CARS microscopy. Despite the good results obtained further experiments are needed, including treatment of the brain with naked siRNA, in order to confirm the polymer's ability to protect the siRNA from enzymatic degradation *in vivo*. Furthermore, the nanoparticles distribution through the different tissues of the brain, as well as the system's capacity for specific protein down-regulation *in vivo*, should be fully evaluated.

In conclusion, a new chitosan-based polymer for gene delivery, Ethylamino Glycol Chitosan, was synthesized and characterized. Three different polymers (EAGC17,

EAGC21 and EAGC30), with increased degree of ethylamine substitution, were studied. The nanoparticles obtained between the different polymers and DNA/siRNA were characterized regarding size, zeta potential, morphology, and behaviour when in the presence of biological challenges. Ethylamino Glycol Chitosan demonstrated good biocompatibility when compared with PEI and chitosan. *In vitro* transfection efficiency with DNA was carried out in A431 cells, and all three polymers were shown to be better transfection agents than lipofectamine, particularly at high polymer, DNA mass ratios. EAGC30 was capable of *in vitro* gene silencing, and the preliminary *in vivo* results of this study introduced EAGC30 as a good candidate for *in vivo* siRNA delivery to the brain.

Bibliography

1. Pushpendra, S., Arvind, P., and Anil, B., *Nucleic Acids as Therapeutics*, in *From Nucleic Acids Sequences to Molecular Medicine*, V.A. Erdmann and J. Barciszewski, Editors. 2012, Springer-Verlag: Berlin. p. 19-45.
2. Mulligan, R.C., Howard, B.H., and Berg, P., Synthesis of rabbit beta-globin in cultured monkey kidney cells following infection with a SV40 beta-globin recombinant genome. *Nature*. 1979; 277: 108-114.
3. Fraley, R., Subramani, S., Berg, P., and Papahadjopoulos, D., Introduction of Liposome-encapsulated SV40 DNA into Cells*. The Journal of Biological Chemistry*. 1980; 255: 10431-10435.
4. Wu, G.Y. and Wu, C.H., Receptor-mediated *in Vitro* Gene Transformation by a Soluble DNA Carrier System*. The Journal of Biological Chemistry*. 1987; 262: 4429-4432.
5. Boussif, O., Lezoualc, F., Zanta, M.A., Mergny, M.D., Sherman, D., Demeneix, B., and Behr, J.-P., A versatile vector for gene and oligonucleotide transfer into cells in culture and *in vivo:* Polyethylenimine*. Proc. Natl. Acad. Sci. USA*. 1995; 92: 7297-7301.
6. Murphy, S.L. and High, K.A., Gene therapy for haemophilia*. Br J Haematol*. 2008; 140: 479-87.
7. van Deutekom, J.C. and van Ommen, G.J., Advances in Duchenne muscular dystrophy gene therapy*. Nat Rev Genet*. 2003; 4: 774-83.
8. Ferrari, S., Geddes, D.M., and Alton, E.W.F.W., Barriers to and new approaches for gene therapy and gene delivery in cystic fibrosis*. Advanced Drug Delivery Reviews*. 2002; 54: 1373-1393.
9. Kaiser, P.K., Symons, R.C., Shah, S.M., Quinlan, E.J., Tabandeh, H., Do, D.V., Reisen, G., Lockridge, J.A., Short, B., Guerciolini, R., and Nguyen, Q.D., RNAi-based treatment for neovascular age-related macular degeneration by Sirna*. Am J Ophthalmol*. 2010; 150: 33-39 e2.
10. Brewster, L.P., Brey, E.M., and Greisler, H.P., Cardiovascular gene delivery: The good road is awaiting*. Adv Drug Deliv Rev*. 2006; 58: 604-29.
11. Nanou, A. and Azzouz, M., Gene therapy for neurodegenerative diseases based on lentiviral vectors*. Progress in Brain Research*. 2009; 175: 187-200.
12. Johnson, L.A., Morgan, R.A., Dudley, M.E., Cassard, L., Yang, J.C., Hughes, M.S., Kammula, U.S., Royal, R.E., Sherry, R.M., Wunderlich, J.R., Lee, C.C., Restifo, N.P., Schwarz, S.L., Cogdill, A.P., Bishop, R.J., Kim, H., Brewer, C.C., Rudy, S.F., VanWaes, C., Davis, J.L., Mathur, A., Ripley, R.T., Nathan, D.A., Laurencot, C.M., and Rosenberg, S.A., Gene therapy with human and mouse T-cell receptors mediates cancer regression and targets normal tissues expressing cognate antigen*. Blood*. 2009; 114: 535-46.
13. Pathak, A., Patnaik, S., and Gupta, K.C., Recent trends in non-viral vector-mediated gene delivery*. Journal Biotechnology*. 2009; 4: 1559-1572.
14. Raemdonck, K., Martens, T.F., Braeckmans, K., Demeester, J., and Smedt, S.C.D., Polysaccharide-based nucleic acid nanoformulations*. Advanced Drug Delivery Reviews*. 2013; 65: 1123-1147.

15. Liang, W. and Lam, J.K.W., *Endosomal Escape Pathways for Non-Viral Nucleic Acid Delivery Systems* in *Molecular Regulation of Endocytosis*, B. Ceresa, Editor 2012.

16. Edinger, D. and Wagner, E., Bioresponsive polymers for the delivery of therapeutic nucleic acids*. Wiley Interdiscip Rev Nanomed Nanobiotechnol*. 2011; 3: 33-46.

17. Scholz, C. and Wagner, E., Therapeutic plasmid DNA versus siRNA delivery: common and different tasks for synthetic carriers*. J Control Release*. 2012; 161: 554-65.

18. Fire, A., Xu, S., Montgomery, M.K., Kostas, S.A., Driver, S.E., and Mello, C.C., Potent and specific genetic interference by double-stranded RNA in *Caenorhabditis elegans. Nature*. 1998; 391: 806-811.

19. Whitehead, K.A., Langer, R., and Anderson, D.G., Knocking down barriers: advances in siRNA delivery*. Nat Rev Drug Discov*. 2009; 8: 129-38.

20. Howard A. Kenneth, R.L.U., Liu Xiudong, Damgaard K. Christian, Glud Zoffmann Sys, Andersen Morten, Hovgaard B. Mads, Schmitz Alexander, Nyengaard R. Jens, Besenbacher Flemming, Kjems Jorgen, RNA Interference *in Vitro* and *in Vivo* Using a Chitosan/siRNA Nanoparticle System*. Molecular Therapy*. 2006; 14: 476-484.

21. Leung, R.K. and Whittaker, P.A., RNA interference: from gene silencing to gene-specific therapeutics*. Pharmacol Ther*. 2005; 107: 222-39.

22. Ginn, S.L., Alexander, I.E., Edelstein, M.L., Abedi, M.R., and Wixon, J., Gene therapy clinical trials worldwide to 2012 - an update*. J Gene Med*. 2013; 15: 65-77.

23. Cavazzana-Calvo, M., Gene Therapy of Human Severe Combined Immunodeficiency (SCID)-X1 Disease*. Science*. 2000; 288: 669-672.

24. Gaspar, H.B., Cooray, S., Gilmour, K.C., Parsley, K.L., Adams, S., Howe, S.J., Al Ghonaium, A., Bayford, J., Brown, L., Davies, E.G., Kinnon, C., and Thrasher, A.J., Long-term persistence of a polyclonal T cell repertoire after gene therapy for X-linked severe combined immunodeficiency*. Sci Transl Med*. 2011; 3: 97-79.

25. Wirth, T., Parker, N., and Yla-Herttuala, S., History of gene therapy*. Gene*. 2013; 525: 162-9.

26. Kim, S., Peng, Z., and Kaneda, Y., Current status of gene therapy in Asia*. Mol Ther*. 2008; 16: 237-43.

27. Yao, J., Fan, Y., Li, Y., and Huang, L., Strategies on the nuclear-targeted delivery of genes*. J Drug Target*. 2013; 21: 926-39.

28. Khalil, I.A., Kogure, K., Akita, H., and Harashime, H., Uptake Pathways and Subsequent Intracellular Trafficking in Nonviral Gene Delivery*. Pharmacol Rev*. 2006; 58: 32-45.

29. Lechardeur, D., Verkman, A.S., and Lukacs, G.L., Intracellular routing of plasmid DNA during non-viral gene transfer*. Adv Drug Deliv Rev*. 2005; 57: 755-67.

30. Varkouhi, A.K., Scholte, M., Storm, G., and Haisma, H.J., Endosomal escape pathways for delivery of biologicals*. Journal of Controlled Release*. 2011; 151: 220-228.

31. Aied, A., Greiser, U., Pandit, A., and Wang, W., Polymer gene delivery: overcoming the obstacles*. Drug Discov Today*. 2013; 18: 1090-8.

32. Ibraheem, D., Elaissari, A., and Fessi, H., Gene therapy and DNA delivery systems*. Int J Pharm*. 2014; 459: 70-83.

33. Choi, Y.S., Lee, M.Y., David, A.E., and Park, Y.S., Nanoparticles for gene delivery: therapeutic and toxic effects*. Molecular & Cellular Toxicology*. 2014; 10: 1-8.

34. Al-Dosari, M.S. and Gao, X., Nonviral Gene Delivery: Principle, Limitations and Recent Progress*. American Association of Pharmaceutical Scientists Journal*. 2009; 11: 671-681.

35. Zhang, G., Gao, X., Song, Y.K., Vollmer, R., Stolz, D.B., Gasiorowski, J.Z., Dean, D.A., and Liu, D., Hydroporation as the mechanism of hydrodynamic delivery*. Gene Ther*. 2004; 11: 675-82.

36. Andre, F. and Mir, L.M., DNA electrotransfer: its principles and an updated review of its therapeutic applications*. Gene Ther*. 2004; 11 Suppl 1: S33-42.

37. Nguyen-Hoai, T., Kobelt, D., Hohn, O., Vu, M.D., Schlag, P.M., Dorken, B., Norley, S., Lipp, M., Walther, W., Pezzutto, A., and Westermann, J., HER2/neu DNA vaccination by intradermal gene delivery in a mouse tumor model: Gene gun is superior to jet injector in inducing CTL responses and protective immunity*. Oncoimmunology*. 2012; 1: 1537-1545.

38. Jin, L., Zeng, X., Liu, M., Deng, Y., and He, N., Current progress in gene delivery technology based on chemical methods and nano-carriers*. Theranostics*. 2014; 4: 240-55.

39. Verma, I.M. and Weitzman, M.D., Gene Therapy: Twenty-First Century Medicine*. Annual Reviews Biochemistry*. 2005; 74: 711-738.

40. de Ilarduya, C.T., Sun, Y., and Duzgunes, N., Gene delivery by lipoplexes and polyplexes*. European Journal of Pharmaceutical Sciences*. 2010; 40: 159-170.

41. Wasungu, L. and Hoekstra, D., Cationic lipids, lipoplexes and intracellular delivery of genes*. J Control Release*. 2006; 116: 255-64.

42. Ozpolat, B., Sood, A.K., and Lopez-Berestein, G., Liposomal siRNA nanocarriers for cancer therapy*. Adv Drug Deliv Rev*. 2014; 66: 110-6.

43. Felgner, P.L., Gadex, T.R., Holm, M., Roman, R., Chan, H.W., Wenz, M., Northrop, J.P., Ringold, G.M., and Danielsen, M., Lipofection: A highly efficient, lipid-mediated DNA-transfection procedure*. Proc. Natl. Acad. Sci. USA*. 1987; 84: 7413-7417.

44. Charoensit, P., Kawakami, S., Higuchi, Y., Yamashita, F., and Hashida, M., Enhanced growth inhibition of metastatic lung tumors by intravenous injection of ATRA-cationic liposome/IL-12 pDNA complexes in mice*. Cancer Gene Ther*. 2010; 17: 512-22.

45. Buyens, K., De Smedt, S.C., Braeckmans, K., Demeester, J., Peeters, L., van Grunsven, L.A., de Mollerat du Jeu, X., Sawant, R., Torchilin, V., Farkasova, K., Ogris, M., and Sanders, N.N., Liposome based systems for systemic siRNA delivery: stability in blood sets the requirements for optimal carrier design*. J Control Release*. 2012; 158: 362-70.

46. Tagami, T., Suzuki, T., Matsunaga, M., Nakamura, K., Moriyoshi, N., Ishida, T., and Kiwada, H., Anti-angiogenic therapy via cationic liposome-mediated systemic siRNA delivery*. Int J Pharm*. 2012; 422: 280-9.

47. Zauner, W., Ogris, M., and Wagner, E., Polylysine-based transfection systems utilizing receptor-mediated delivery*. Advanced Drug Delivery Reviews*. 1998; 30: 97-113.

48. Wang, Y.Q., Su, J., Wu, F., Lu, P., Yuan, L.F., Yuan, W.E., Sheng, J., and Jin, T., Biscarbamate cross-linked polyethylenimine derivative with low molecular weight, low cytotoxicity, and high efficiency for gene delivery*. Int J Nanomedicine*. 2012; 7: 693-704.

49. Sun, C., Tang, T., Uludag, H., and Cuervo, J.E., Molecular dynamics simulations of DNA/PEI complexes: effect of PEI branching and protonation state*. Biophys J*. 2011; 100: 2754-63.

50. Buyens, K., Meyer, M., Wagner, E., Demeester, J., De Smedt, S.C., and Sanders, N.N., Monitoring the disassembly of siRNA polyplexes in serum is crucial for predicting their biological efficacy*. J Control Release*. 2010; 141: 38-41.

51. Maeda, H., Wu, J., Sawa, T., Matsumura, Y., and Hori, K., Tumor vascular permeability and the EPR effect in macromolecular therapeutics: a review*. Journal of Controlled Release*. 2000; 65: 271-284.

52. Iyer, A.K., Khaled, G., Fang, J., and Maeda, H., Exploiting the enhanced permeability and retention effect for tumor targeting*. Drug Discov Today*. 2006; 11: 812-8.

53. Lee, H., Lytton-Jean, A.K.R., Chen, Y., Love, K.T., Park, A.I., Karagiannis, E.D., Sehgal, A., Querbes, W., Zurenko, C.S., Jayaraman, M., Peng, C.G., Charisse, K., Borodovsky, A., Manoharan, M., Donahoe, J.S., Truelove, J., Nahrendorf, M., Langer, R., and Anderson, D.G., Molecularly self-assembled nucleic acid nanoparticles for targeted in vivo siRNA delivery*. Nature - Nanotechnology*. 2012; 7: 389-393.

54. Buschmann, M.D., Merzouki, A., Lavertu, M., Thibault, M., Jean, M., and Darras, V., Chitosan for delivery of nucleic acids*. Advanced Drug Delivery Reviews*. 2013; 65: 1234-1270.

55. Strand, S.P., Lelu, S., Reitan, N.K., de Lange Davies, C., Artursson, P., and Varum, K.M., Molecular design of chitosan gene delivery systems with an optimized balance between polyplex stability and polyplex unpacking*. Biomaterials*. 2010; 31: 975-987.

56. Godbey, W.T., Wu, K.K., and Mikos, A.G., Poly(ethylenimine)-mediated gene delivery affects endothelial cell function and viability*. Biomaterials*. 2001; 22: 471-480.

57. Erbacher, P., Zou, S., Bettinger, T., Steffan, A.-M., and Remy, J.-S., Chitosan-Based Vector/DNA Complexes for Gene Delivery: Biophysical Characteristics and Transfection Ability*. Pharmaceutical Research*. 1998; 15: 1332-1339.

58. Wolfert, M.A., Dash, P.R., Nazarova, O., Oupicky, D., Seymour, L.W., Smart, S., Strohalm, J., and Ulbrich, K., Polyelectrolyte Vectors for Gene Delivery: Influence of Cationic Polymer on Biophysical Properties of Complexes formed with DNA*. Bioconjugate Chem.* 1999; 10: 993-1004.

59. Mintzer, M.A. and Simanek, E.E., Nonviral Vectors for Gene Delivery*. Chem Rev*. 2009; 109: 259-302.

60. Kim, J.-M., Shin, E., Ryou, S.-M., Yeom, J.-H., and Lee, K., Gene delivery platforms*. Biotechnology and Bioprocess Engineering*. 2013; 18: 637-647.

61. Putnam, D., Gentry, C.A., Pack, D.W., and Langer, R., Polymer-based gene delivery with low cytotoxicity by a unique balance of side-chain termini. *Proc Natl Acad Sci U S A*. 2001; 98: 1200-5.

62. Parhiz, H., Shier, W.T., and Ramezani, M., From rationally designed polymeric and peptidic systems to sophisticated gene delivery nano-vectors. *Int J Pharm*. 2013; 457: 237-59.

63. Shen, J., Zhao, D.J., Li, W., Hu, Q.L., Wang, Q.W., Xu, F.J., and Tang, G.P., A polyethylenimine-mimetic biodegradable polycation gene vector and the effect of amine composition in transfection efficiency. *Biomaterials*. 2013; 34: 4520-31.

64. Suh, J., Paik, H.-J., and Hwang, B.K., Ionization of Poly(ethylenimine) and Poly(allylamine) at various pH's. *Bioorganic Chemistry*. 1994; 22: 318-327.

65. Berh, J.-P., The Proton Sponge: a Trick to Enter Cells the Viruses Did Not Exploit. *Chimia*. 1997; 51: 34-36.

66. Neu, M., Fischer, D., and Kissel, T., Recent advances in rational gene transfer vector design based on poly(ethylene imine) and its derivatives. *J Gene Med*. 2005; 7: 992-1009.

67. Tang, M. and Szoka, F., The influence of polymer structure on the interactions of cationic polymers with DNA and morphology of the resulting complexes. *Gene Therapy*. 1997; 4: 823-832.

68. Reschel, T., Konak, C., Oupicky, D., Seymour, L.W., and Ulbrich, K., Physical properties and in vitro transfection efficiency of gene delivery vectors based on complexes of DNA with synthetic polycations. *Journal of Controlled Release* 2002; 81: 201-217.

69. Wightman, L., Kircheis, R., Rossler, V., Carotta, S., Ruzicka, R., Kursa, M., and Wagner, E., Different behavior of branched and linear polyethylenimine for gene delivery in vitro and in vivo. *J Gene Med*. 2001; 3: 362-72.

70. Kwok, A. and Hart, S.L., Comparative structural and functional studies of nanoparticle formulations for DNA and siRNA delivery. *Nanomedicine*. 2011; 7: 210-9.

71. Fisher, D., Li, Y., Ahlemeyer, B., Krieglstein, J., and Kissel, T., In vitro cytotoxicity testing of polycations: influence of polymer structure on cell viability and hemolysis. *Biomaterials*. 2003; 24: 1121-1131.

72. Fischer, D., Bieber, T., Li, Y., Elsasser, H.-P., and Kissel, T., A Novel Non-Viral Vector for DNA delivey Based on Low Molecular Weight, branched Polyethylenimine: Effect of Molecular Weight on Transfection Efficiency and Cytotoxicity. *Pharmaceutical Research*. 1999; 16: 1273-1279.

73. Moghimi, S.M., Symonds, P., Murray, J.C., Hunter, A.C., Debska, G., and Szewczyk, A., A two-stage poly(ethylenimine)-mediated cytotoxicity: implications for gene transfer/therapy. *Mol Ther*. 2005; 11: 990-5.

74. Patnaik, S. and Gupta, K.C., Novel polyethylenimine-derived nanoparticles for *in vivo* gene delivery. *Expert Opinion Drug Delivery*. 2013; 10: 215-228.

75. Breunig, M., Lungwitz, U., Liebl, R., and Goepferich, A., Breaking up the correlation between efficacy and toxicity for nonviral gene delivery. *Proc Natl Acad Sci U S A*. 2007; 104: 14454-9.

76. Kim, Y.H., Park, J.H., Lee, M., Kim, Y.H., Park, T.G., and Kim, S.W., Polyethylenimine with acid-labile linkages as a biodegradable gene carrier. *J Control Release*. 2005; 103: 209-19.

77. Lungwitz, U., Breunig, M., Blunk, T., and Gopferich, A., Polyethylenimine-based non-viral gene delivery systems. *Eur J Pharm Biopharm*. 2005; 60: 247-66.

78. Wang, D., Narang, A.S., Kotb, M., Gaber, O., Miller, D.D., Kim, S.W., and Mahato, R.I., Novel Branched Poly(Ethylenimine)-Cholesterol Water-Soluble Lipopolymers for Gene Delivery. *Biomacromolecules.* 2002; 3: 1197-1207.

79. Lu, Z.X., Liu, L.T., and Qi, X.R., Development of small interfering RNA delivery system using PEI-PEG-APRPG polymer for antiangiogenic vascular endothelial growth factor tumor-targeted therapy. *Int J Nanomedicine*. 2011; 6: 1661-73.

80. Chaplot, S.P. and Rupenthal, I.D., Dendrimers for gene delivery--a potential approach for ocular therapy? *J Pharm Pharmacol*. 2014; 66: 542-56.

81. Dufes, C., Uchegbu, I.F., and Schatzlein, A.G., Dendrimers in gene delivery. *Adv Drug Deliv Rev*. 2005; 57: 2177-202.

82. Peng, S.F., Su, C.J., Wei, M.C., Chen, C.Y., Liao, Z.X., Lee, P.W., Chen, H.L., and Sung, H.W., Effects of the nanostructure of dendrimer/DNA complexes on their endocytosis and gene expression. *Biomaterials*. 2010; 31: 5660-70.

83. Alves, N.M. and Mano, J.F., Chitosan derivatives obtained by chemical modifications for biomedical and environmental applications. *International Journal of Biological Macromolecules*. 2008; 43: 401-414.

84. Sorlier, P., Denuziere, A., Viton, C., and Domard, A., Relation between the Degree of Acetylation and the Electrostatic Properties of Chitin and Chitosan. *Biomacromolecules.* 2001; 2: 765-772.

85. Pillai, C.K.S., Paul, W., and P.Sharma, C., Chitin and chitosan polymers: Chemistry, solubility and fiber formation. *Progress in Polymer Science*. 2009; 34: 641-678.

86. Kean, T. and Thanou, M., Biodegradation, biodistribution and toxicity of chitosan. *Adv Drug Deliv Rev*. 2010; 62: 3-11.

87. Pan, Y., Li, Y.-j., Zhao, H.-y., Zheng, J.-m., Xu, H., Wei, G., Hao, J.-s., and Cui, F.-d., Bioadhesive polysacharide in protein delivery system: chitosan nanoparticles improve the intestinal absorption of insulin in vivo. *International Journal of Pharmaceutics*. 2002; 249: 139-147.

88. Crini, G., Recent developments in polysaccharide-based materials used as adsorbents in wastewater treatment. *Progress in Polymer Science*. 2005; 30: 38-70.

89. Ham-Pichavant, F., Sèbe, G., Pardon, P., and Coma, V., Fat resistance properties of chitosan-based paper packaging for food applications. *Carbohydrate Polymers*. 2005; 61: 259-265.

90. Sun, L., Du, Y., Yang, J., Shi, X., Li, J., Wang, X., and Kennedy, J.F., Conversion of crystal structure of the chitin to facilitate preparation of a 6-carboxychitin with moisture absorption–retention abilities. *Carbohydrate Polymers*. 2006; 66: 168-175.

91. Chung, Y., Effect of abiotic factors on the antibacterial activity of chitosan against waterborne pathogens. *Bioresource Technology*. 2003; 88: 179-184.

92. Lv, H., Zhang, S., Wang, B., Cui, S., and Yan, J., Toxicity of cationic lipids and cationic polymers in gene delivery. *J Control Release*. 2006; 114: 100-9.

93. Choksakulnimitr, S., Masuda, S., Tokuda, H., Takakura, Y., and Hashida, M., In vitro cytotoxicity of macromolecules in different cell culture systems. *Journal of Controlled Release*. 1995; 34: 233-241.

94. Lee, M., Nah, J.-W., Kwon, Y., Koh, J.J., Ko, K.S., and Kin, S.W., Water-Soluble and Low Molecular Weight Chitosan-Based Plasmid DNA Delivery. *Pharmaceutical Research*. 2001; 18: 427-431.

95. Huang, M., Khor, E., and Lim, L.-Y., Uptake and Cytotoxicity of Chitosan Molecules and Nanoparticles: Effects of Molecular Weight and Degree of Deacetylation. *Pharmaceutical Research*. 2004; 21: 344-353.

96. Malmo, J., Varum, K.M., and Strand, S.P., Effect of chitosan chain architecture on gene delivery: comparison of self-branched and linear chitosans. *Biomacromolecules*. 2011; 12: 721-9.

97. Dekie, L., Toncheva, V., Dubruel, P., Schacht, E.H., Barrett, L., and Seymour, L.W., Poly-L-glutamic acid derivatives as vectors for gene therapy. *Journal of Controlled Release*. 2000; 65: 187-202.

98. Jevprasesphant, R., Penny, J., Jalal, R., Attwood, D., McKeown, N.B., and D'Emanuele, A., The influence of surface modification on the cytotoxicity of PAMAM dendrimers. *International Journal of Pharmaceutics*. 2003; 252: 263-266.

99. Hunter, A.C., Molecular hurdles in polyfectin design and mechanistic background to polycation induced cytotoxicity. *Adv Drug Deliv Rev*. 2006; 58: 1523-31.

100. Hunter, A.C. and Moghimi, S.M., Cationic carriers of genetic material and cell death: a mitochondrial tale. *Biochim Biophys Acta*. 2010; 1797: 1203-9.

101. Brownlie, A., Uchegbu, I.F., and Schatzlein, A.G., PEI-based vesicle-polymer hybrid gene delivery system with improved biocompatibility. *Int J Pharm*. 2004; 274: 41-52.

102. Kean, T., Roth, S., and Thanou, M., Trimethylated chitosans as non-viral gene delivery vectors:Cytotoxicity and transfection efficiency. *Journal of Controlled Release*. 2005; 103: 643-653.

103. Richardson, S.C.W., Kolbe, H.V.J., and Duncan, R., Potential of low molecular mass chitosan as a DNA delivery system: biocompatibility, body distribution and ability to complex and protect DNA. *International Journal of Pharmaceutics*. 1999; 178: 231-243.

104. Lavertu, M., Méthot, S., Tran-Khanh, N., and Buschmann, M.D., High efficiency gene transfer using chitosan/DNA nanoparticles with specific combinations of molecular weight and degree of deacetylation. *Biomaterials*. 2006; 27: 4815-4824.

105. Nimesh, S., Thibault, M.M., Lavertu, M., and Buschmann, M.D., Enhanced gene delivery mediated by low molecular weight chitosan/DNA complexes: effect of pH and serum. *Mol Biotechnol*. 2010; 46: 182-96.

106. Schipper, N.G.M., Varum, K.M., and Artursson, P., Chitosans as Absorption Enhancers for Poorly Absorbable Drugs. 1: Influence of Molecular Weight and Degree of Acetylation on Drug Transport Across Human Intestinal Epithelial(Caco-2) Cells. *Pharmaceutical Research*. 1996; 13: 1686-1692.

107. Schipper, N.G.M., Varum, K.M., Stenberg, P., Ockling, G., Lennernas, H., and Artursson, P., Chitosans as absorption enhancers of poorly absorbable drugs 3: Influence of mucus on absorption enhancement. *European Journal of Pharmaceutical Sciences*. 1999; 8: 335-343.

108. Carreño-Gomez, B. and Duncan, R., Evaluation of the biological properties of soluble chitosan and chitosan microspheres*. International Journal of Pharmaceutics*. 1997; 148: 231-240.

109. Saranya, N., Moorthi, A., Saravanan, S., Devi, M.P., and Selvamurugan, N., Chitosan and its derivatives for gene delivey*. International Journal of Biological Macromolecules*. 2011; 48: 234-238.

110. Hoggard-Koping, M., Tubulekas, I., Guan, H., Edwards, K., Nilsson, M., Varum, K., and Artursson, P., Chitosan as a nonviral gene delivery system. Structure-property relationships and characteristics compared with polyethylenimine *in vitro* and after lung administration *in vivo. Gene Therapy*. 2001; 8: 1108-1121.

111. Moreira, C., Oliveira, H., Pires, L.R., Simoes, S., Barbosa, M.A., and Pego, A.P., Improving chitosan-mediated gene transfer by the introduction of intracellular buffering moieties into the chitosan backbone*. Acta Biomater*. 2009; 5: 2995-3006.

112. MacLaughlin, F.C., Mumper, R.J., Wang, J., Tagliaferri, J.M., Gill, I., Hinchcliffe, M., and Rollanda, A.P., Chitosan and depolymerized chitosan oligomers as condensing carriers for in vivo plasmid delivery*. Journal of Controlled Release*. 1998; 56: 259-272.

113. Leong, K.W., Mao, H.Q., Truong-Le, V.L., K.Roy, Walsh, S.M., and August, J.T., DNA-polycation nanospheres as non-viral gene delivery vehicles*. Journal of Controlled Release* 1998; 53: 183-193.

114. Filion, D., Lavertu, M., and Buschmann, M.D., Ionization and Solubility of Chitosan Solutions Related to Thermosensitive Chitosan/Glycerol-Phosphate Systems*. Biomacromolecules*. 2007; 8: 3224-3234.

115. Sato, T., Ishii, T., and Okahata, Y., In vitro gene delivey mediated by chitosan. Effect of pH, serum and molecular mass of chitosan on the transfection efficiency*. Biomaterials*. 2001; 22: 2075-2080.

116. Zhao, X., Yu, S.B., Wu, F.L., Mao, Z.B., and Yu, C.L., Transfection of primary chondrocytes using chitosan-pEGFP nanoparticles*. J Control Release*. 2006; 112: 223-8.

117. Kiang, T., Wen, J., Lim, H.W., and Leong, K.W., The effect of the degree of chitosan deacetylation on the efficiency of gene transfection*. Biomaterials*. 2004; 25: 5293-5301.

118. Huang, M., Fong, C.-W., Khor, E., and Lim, L.-Y., Transfection efficiency of chitosan vectors: Effect of polymer molecular weight and degree of deacetylation*. Journal of Controlled Release*. 2005; 106: 391-406.

119. Koping-Hoggard, M., Mel'nikova, Y.S., Varum, K.M., Lindman, B., and Artursson, P., Relationship between the physical shape and the efficiency of oligomeric chitosan as a gene delivery system *in vitro* and *in vivo. The Journal of Gene Medicine*. 2003; 5: 130-141.

120. Ishii, T., Okahata, Y., and Sato, T., Mechanism of cell transfection with plasmid/chitosan complexes*. Biochimica et Biophysica Acta*. 2001; 1514: 51-64.

121. Delgado, D., del Pozo-Rodríguez, A., Solinís, M.A., Bartkowiak, A., and Rodríguez-Gascón, A., New gene delivery system based on oligochitosan and solid lipid nanoparticles: 'in vitro' and 'in vivo' evaluation*. Eur J Pharm Sci*. 2013; 50: 484-91.

122. Mao, H.-Q., Roy, K., Troung-Le, V.L., Janes, K.A., Lin, K.Y., Wang, Y., August, J.T., and Leong, K.W., Chitosan-DNA nanoparticles as gene carriers: synthesis,

characterization and transfection efficiency*. Journal of Controlled Release*. 2001; 70: 399-421.

123. Katas, H. and Alpar, H.O., Development and characterisation of chitosan nanoparticles for siRNA delivery*. Journal of Controlled Release*. 2006; 115: 216-225.

124. Ji, A.M., Su, D., Che, O., Li, W.S., Sun, L., Zhang, Z.Y., Yang, B., and Xu, F., Functional gene silencing mediated by chitosan/siRNA nanocomplexes*. Nanotechnology*. 2009; 20: 405103.

125. Liu, X., Howard, K.A., Dong, M., Andersen, M.O., Rahbek, U.L., Johnsen, M.G., Hansen, O.C., Besenbacher, F., and Kjems, J., The influence of polymeric properties on chitosan/siRNA nanoparticle formulation and gene silencing*. Biomaterials*. 2007; 28: 1280-8.

126. Koping-Hoggard, M., Varum, K., Issa, M., Danielsen, S., Christensen, B., Stokke, B., and Artursson, P., Improved chitosan-mediated gene delivery based on easily dissociated chitosan polyplexes of highly defined chitosan oligomers*. Gene Therapy*. 2004; 11: 1441-1452.

127. Holzerny, P., Ajdini, B., Heusermann, W., Bruno, K., Schuleit, M., Meinel, L., and Keller, M., Biophysical properties of chitosan/siRNA polyplexes: profiling the polymer/siRNA interactions and bioactivity*. J Control Release*. 2012; 157: 297-304.

128. Jorgensen, J.A., Hovig, E., and Boe, S.L., Potent gene silencing in vitro at physiological pH using chitosan polymers*. Nucleic Acid Ther*. 2012; 22: 96-102.

129. Techaarpornkul, S., Wongkupasert, S., Opanasopit, P., Apirakaramwong, A., Nunthanid, J., and Ruktanonchai, U., Chitosan-mediated siRNA delivery in vitro: effect of polymer molecular weight, concentration and salt forms*. AAPS PharmSciTech*. 2010; 11: 64-72.

130. Romøren, K., Pedersen, S., Smistad, G., Evensen, Ø., and Thu, B.J., The influence of formulation variables on in vitro transfection efficiency and physicochemical properties of chitosan-based polyplexes*. International Journal of Pharmaceutics*. 2003; 261: 115-127.

131. Mao, S., Shuai, X., Unger, F., Wittmar, M., Xie, X., and Kissel, T., Synthesis, characterization and cytotoxicity of poly(ethylene glycol)-graft-trimethyl chitosan block copolymers*. Biomaterials*. 2005; 26: 6343-6356.

132. Issa, M.M., Koping-Hoggard, M., Tommeraas, K., Varum, K.M., Christensen, B.E., Strand, S.P., and Artursson, P., Targeted gene delivery with trisaccharide-substituted chitosan oligomers in vitro and after lung administration in vivo*. J Control Release*. 2006; 115: 103-12.

133. Morris, V.B. and Sharma, C.P., Folate mediated in vitro targeting of depolymerised trimethylated chitosan having arginine functionality*. J Colloid Interface Sci*. 2010; 348: 360-8.

134. Xu, Z., Wan, X., Zhang, W., Wang, Z., Peng, R., Tao, F., Cai, L., Li, Y., Jiang, Q., and Gao, R., Synthesis of biodegradable polycationic methoxy poly(ethylene glycol)–polyethylenimine–chitosan and its potential as gene carrier*. Carbohydrate Polymers*. 2009; 78: 46-53.

135. Thanou, M., Florea, B.I., Geldof, M., Junginger, H.E., and Borchard, G., Quaternized chitosan oligomers as novel gene delivery vectors in epithelial cell lines*. Biomaterials*. 2002; 23: 153-159.

136. Kim, T.H., Ihm, J.E., Choi, Y.J., Nah, J.W., and Cho, C.S., Efficient gene delivery by urocanic acid-modified chitosan*. Journal of Controlled Release*. 2003; 93: 389-402.

137. Wong, K., Sun, G., Zhang, X., Dai, H., Liu, Y., He, C., and Leong, K.W., Pei-g-chitosan, a Novel Gene Delivery System with Transfection Efficiency Comparable to Polyethylenimine in Vitro and after Liver Administration in Vivo*. Bioconjugate Chem.* 2006; 17: 152-158.

138. Tripathi, S.K., Goyal, R., Kumar, P., and Gupta, K.C., Linear polyethylenimine-graft-chitosan copolymers as efficient DNA/siRNA delivery vectors in vitro and in vivo*. Nanomedicine: nanotechnology, Biology, and Medicine*. 2012; 8: 337-345.

139. Jere, D., Jiang, H.-L., Kim, Y.-K., Arote, R., Choi, Y.-J., Yun, C.-H., Cho, M.-H., and Cho, C.-S., Chitosan-graft-polyethylenimine for Akt1 siRNA delivery to lung cancer cells*. International Journal of Pharmaceutics*. 2009; 378: 194-200.

140. Germershaus, O., Mao, S., Sitterberg, J., Bakowsky, U., and Kissel, T., Gene delivery using chitosan, trimethyl chitosan or polyethylenglycol-graft-trimethyl chitosan block copolymers: Establishment of structure-activity relationships in vitro*. Journal of Controlled Release*. 2008; 125: 145-154.

141. Verheul, R.J., Wal, S.v.d., and Hennink, W.E., Tailorable Thiolated Trimethyl Chitosan for Covalently Stabilized Nanoparticles*. Biomacromolecules.* 2010; 11: 1965-1971.

142. Ragelle, H., Vandermeulen, G., and Preat, V., Chitosan-based siRNA delivery systems*. J Control Release*. 2013; 172: 207-18.

143. Castanotto, D. and Rossi, J.J., The promises and pitfalls of RNA-interference-based therapeutics*. Nature*. 2009; 457: 426-33.

144. DeVincenzo, J., Cehelsky, J.E., Alvarez, R., Elbashir, S., Harborth, J., Toudjarska, I., Nechev, L., Murugaiah, V., Van Vliet, A., Vaishnaw, A.K., and Meyers, R., Evaluation of the safety, tolerability and pharmacokinetics of ALN-RSV01, a novel RNAi antiviral therapeutic directed against respiratory syncytial virus (RSV)*. Antiviral Res*. 2008; 77: 225-31.

145. Leachman, S.A., Hickerson, R.P., Schwartz, M.E., Bullough, E.E., Hutcherson, S.L., Boucher, K.M., Hansen, C.D., Eliason, M.J., Srivatsa, G.S., Kornbrust, D.J., Smith, F.J., McLean, W.I., Milstone, L.M., and Kaspar, R.L., First-in-human mutation-targeted siRNA phase Ib trial of an inherited skin disorder*. Mol Ther*. 2010; 18: 442-6.

146. Lochhead, J.J. and Thorne, R.G., Intranasal delivery of biologics to the central nervous system*. Adv Drug Deliv Rev*. 2012; 64: 614-28.

147. Nishina, K., Mizusawa, H., and Yokota, T., Short interfering RNA and the central nervous system: development of nonviral delivery systems. *Drug Delivery*. 2013; 10: 289-292.

148. Talegaonkar, S. and Mishra, P.R., Intranasal delivery: An approach to bypass the blood brain barrier *Indian J Pharmacol* 2004; 36: 140-147.

149. Pardeshi, C.V. and Belgamwar, V.S., Direct nose to brain drug delivery via integrated nerve pathways bypassing the blood/brain barrier: an excellent platform for brain targeting*. Expert Opinion Drug Delivery*. 2013; 10: 957-972.

150. Jadhav, K.R., Gambhire, M.N., Shaikh, I.M., Kadam, V.J., and Pisal, S.S., Nasal Drug Delivery System-Factors Affecting and Applications*. Current Drug Therapy*. 2007; 2: 27-38.

151. Kim, I.-D., Kim, S.-W., and Lee, J.-K., Gene Knockdown in Olfactory Bulb, Amygdala, and Hypothalamus by Intranasal siRNA Administration*. The Korean J. Anat*. 2009; 42: 285-292.

152. Renner, D.B., II, W.H.F., and Hanson, L.R., Intranasal delivery of siRNA to the olfactory bulbs of mice via the olfactory nerve pathway*. Neurosci Lett*. 2012; 513: 193-7.

153. Kim, I.D., Shin, J.H., Kim, S.W., Choi, S., Ahn, J., Han, P.L., Park, J.S., and Lee, J.K., Intranasal delivery of HMGB1 siRNA confers target gene knockdown and robust neuroprotection in the postischemic brain*. Mol Ther*. 2012; 20: 829-39.

154. Kanazawa, T., Akiyama, F., Kakizaki, S., Takashima, Y., and Seta, Y., Delivery of siRNA to the brain using a combination of nose-to-brain delivery and cell-penetrating peptide-modified nano-micelles*. Biomaterials*. 2013; 34: 9220-6.

155. Kanazawa, T., Morisaki, K., Suzuki, S., and Takashima, Y., Prolongation of life in rats with malignant glioma by intranasal siRNA/drug codelivery to the brain with cell-penetrating peptide-modified micelles*. Mol Pharm*. 2014; 11: 1471-8.

156. Perez, A.P., Mundina-Weilenmann, C., Romero, E.L., and Morilla, M.J., Increased brain radioactivity by intranasal P-labeled siRNA dendriplexes within in situ-forming mucoadhesive gels*. Int J Nanomedicine*. 2012; 7: 1373-85.

157. Bruno, K., Using drug-excipient interactions for siRNA delivery*. Advanced Drug Delivery Reviews*. 2011; 63: 1210-1226.

158. Bernkop-Schnurch, A. and Dunnhaupt, S., Chitosan-based drug delivery systems*. Eur J Pharm Biopharm*. 2012; 81: 463-9.

159. Mao, S., Sun, W., and Kissel, T., Chitosan-based formulations for delivery of DNA and siRNA*. Advanced Drug Delivery Reviews*. 2010; 62: 12-27.

160. Mansouri, S., Lavigne, P., Corsi, K., Benderdour, M., Beaumont, E., and Fernandes, J.C., Chitosan-DNA nanoparticles as non-viral vectors in gene therapy: startegies to improve transfection efficay. *European Journal of Pharmaceutical and Biopharmaceutics*. 2004; 57: 1-8.

161. Lai, W.-F. and Lin, M.C.-M., Nucleic acid delivery with chitosan and its derivatives*. Journal of Controlled Release*. 2009; 134: 158-168.

162. Kim, T.-H., Jiang, H.-L., Jere, D., Park, I.-K., Cho, M.-H., Nah, J.-W., Choi, Y.-J., Akaike, T., and Cho, C.-S., Chemical modification of chitosan as a gene carrier *in vitro* and *in vivo. Progress in Polymer Science*. 2007; 32: 726-753.

163. Wang, W., McConaghy, Marie;, A., Tetley, L., and Uchegbu, I.F., Controls on Polymer Molecula Weight May Be Used To Control the Size of Palmitoyl Glycol Chitosan Polymeric Vesicles*. Langmuir*. 2001; 17: 631-636.

164. Uchegbu, I.F. and Schatzlein, A.G., *Polymers in Drug Delivery*2006: Taylor & Francis.

165. Solomons, T.W.G. and Fryhle, C.B., *Organic Chemistry* 2011: John Wiley & Sons, Inc.

166. Williams, D. and Fleming, I., *Spectroscopic Methods in Organic Chemistry* 2008: Mc Graw-Hill.

167. Skoog, D.A., West, D.M., Holler, F.J., and Crouch, S.R., *Fundamentals of Analytical Chemistry*. 9th ed. 2004: Brooks/Cole.

168. Lin, C., Blaauboer, C.-J., Timoneda, M.M., Martin C, L., Steenbergen, M.v., Hennink, W.E., Zhong, Z., Feijen, J., and Engbersen, J.F.J., Bioreducible

poly(amido amine)s with oligoamin side chains: Synthesis, characterization, and structural effects on gene delivery. *Journal of Controlled Release*. 2008; 126: 166-174.

169. Clayden, J., Greeves, N., Warren, S., and Wothers, P., *Organic Chemistry* 2001: Oxford.

170. Makuska, R. and Gorochovceva, N., Regioselective grafting of poly(ethyene glycol) onto chitosan through C-6 position of glucosamine units. *Carbohydrate polymers.* 2006; 64: 319-327.

171. Tharanathan, R.N. and Kittur, F.S., Chitin-the undisputed biomolecule of great potential. *Crit Rev Food Sci Nutr*. 2003; 43: 61-87.

172. Gorochovceva, N. and Makuska, R., Syntheis and study of water soluble chitosan-O-poly(ethylene glycol) graft copolymers. *European Polymer Journal*. 2004; 40: 685-691.

173. Godbey, W.T., Wub, K.K., and Mikos, A.G., Poly(ethylenimine) and its role in gene delivery. *Journal of Controlled Release*. 1999; 60: 149-160.

174. Kanayama, N., Fukushima, S., Nishiyama, N., Itaka, K., Jang, W.-D., Miyata, K., Yamasaki, Y., Chung, U.-i., and Kataoka, K., A PEG-Based Biocompatible Block Catiomer with High Buffering Capacity for the Construction of Polyplex Micelles Showing Efficient Gene Transfer toward Primary Cells. *ChemMedChem*. 2006; 1: 439-444.

175. Piest, M. and Engbersen, J.F.J., Effects of charge density and hydrophobity of poly(amido amine)s for non-viral gene delivery. *Journal of Controlled Release*. 2010; 148: 83-90.

176. Wong, S.Y., Pelet, J.M., and Putman, D., Polymer systems for gene delivery - Past, present, and future. *Prog. Polym. Sci.* 2007; 32: 799-837.

177. Lu, H., Dai, Y., Lv, L., and Zhao, H., Chitosan-graft-polyethylenimine/DNA nanoparticles as novel non-viral gene delivery vectors targeting osteoarthritis. *PLoS One*. 2014; 9: e84703.

178. Morille, M., Passirani, C., Vonarbourg, A., Clavreul, A., and Benoit, J.-P., Progress in developing cationic vectors for non-viral systemic gene therapy against cancer. *Biomaterials*. 2008; 29: 3477-3496.

179. Gaal, E.V.B.v., Eijk, R.v., Ossting, R.S., Kok, R.J., Hennink, W.E., Crommelin, D.J.A., and Mastrobattista, E., How to screen non-viral gene delivery systems in vitro? *Journal of Controlled Release*. 2011; 154: 218-232.

180. Kim, T.-i., Rothmund, T., Kissel, T., and Kim, S.W., Bioreducible polymers with cell penetrating and endosome buffering functionality for gene delivery systems. *Journal of Controlled Release*. 2011; 152: 110-119.

181. Pack, D.W., Hoffman, A.S., Pun, S., and Stayton, P.S., Design and development of polymers for gene delivery. *Nat Rev Drug Discov*. 2005; 4: 581-93.

182. Lai, E. and Zanten, H.H.v., Monitoring DNA/Poly-l-Lysine Polyplex Formation with Time-Resolved Multiangle Laser Light Scattering. *Biophysical Journal*. 2001; 80: 864-873.

183. Khalil, I.A., Kogure, K., Akita, H., and Harashima, H., Uptake pathways and subsequent intracellular trafficking in nonviral gene delivery. *Pharmacol Rev*. 2006; 58: 32-45.

184. Mislick, K.A. and Baldeschwieler, J.D., Evidence for the role of proteoglycans in cation-mediated gene transfer*. Proc. Natl. Acad. Sci. USA*. 1996; 93: 12349-12354.

185. Wiethoff, C.M. and Middaugh, C.R., Barriers to Nonviral Gene Delivery*. Journal of Oharmaceutical Sciences*. 2002; 92: 203-217.

186. Perumal, O.P., Inapagolla, R., Kannan, S., and Kannan, R.M., The effect of surface functionality on cellular trafficking of dendrimers*. Biomaterials*. 2008; 29: 3469-76.

187. Abdelhady, H.G., Allen, S., Davies, M.c., Roberts, C.J., tendler, S.J.B., and Williams, P.M., Direct real-time molecular scale visualisation of the degradation of condensed DNA complexes exposed to DNase I*. Nucleic Acids Research*. 2003; 31: 4001-4005.

188. Reimer, L. and Kohl, H., *Transmission Electron Microscopy*. 5th ed. 2008: Springer Verlag.

189. Carr, B. and Wright, M., *Nanoparticle Tracking Analysis*, N. Ltd, Editor 2013.

190. Wagner, E., Polymers for siRNA Delivery: Inspired by Viruses to be targeted, Dynamic, and Precise. *Accounts of Chemical research*. 2011; 45: 1005-1013.

191. Hsu, C.Y. and Uludag, H., Effects of size and topology of DNA molecules on intracellular delivery with non-viral gene carriers*. BMC Biotechnol*. 2008; 8: 23.

192. Alameh, M., Dejesus, D., Jean, M., Darras, V., Thibault, M., Lavertu, M., Buschmann, M.D., and Merzouki, A., Low molecular weight chitosan nanoparticulate system at low N:P ratio for nontoxic polynucleotide delivery*. Int J Nanomedicine*. 2012; 7: 1399-414.

193. Lu, B., Wang, C.-F., Wu, D.-Q., Li, C., Zhang, X.-Z., and Zhuo, R.-X., Chitosan based oligoamine polymers: Synthesis, characterization and gene delivery*. Journal of Controlled Release*. 2009; 137: 54-62.

194. Rungsardthong, U., Ehtezazi, T., Bailey, L., Armes, S.P., Garnett, M.C., and Stolnik, S., Effect of Polymer Ionization on the Interaction with DNA in Nonviral Gene Delivery Systems*. Biomacromolecules.* 2003; 4: 683-690.

195. Ou, M., Wang, X.-L., Xu, R., Chang, C.-W., Bull, D.A., and Kim, S.W., Novel Biodegradable Poly(disulfide amine)s for Gene Delivery with High Efficiency and Low Cytotoxicity*. Bioconjugate Chemistry*. 2008; 19: 626-633.

196. Pezzoli, D. and Candiani, G., Non-viral gene delivery strategies for gene therapy: a “ménage à trois” among nucleic acids, materials, and the biological environment*. Journal of Nanoparticle Research*. 2013; 15.

197. Nishikawa, M. and Huang, L., Nonviral Vectors in the New Millennium: Delivery Barriers in Gene Transfer*. Human Gene Therapy*. 2001; 12: 861-870.

198. Mosmann, T., Rapid Colorimetric Assay for Cellular Growth and Survivor: Application to Proliferation and Cytotoxicity Assays*. Journal of Immunological Methods*. 1983; 65: 55-63.

199. Tietz, P.S., Yamazaki, K., and LaRusso, N.F., Time-dependent effects of chloroquine on pH of hepatocyte lysosomes. *Biochemical Pharmacology*. 1990; 40: 1419-1421.

200. Cheng, J., Zeidan, R., Mishra, S., Liu, A., Pun, S.H., Kulkarni, R.P., Jensen, G.S., Bellocq, N.C., and Davis, M.E., Structure-Function Correlation of Chloroquine and Analogues as Transgene Expression Enhancers in Nonviral Gene Delivery*. J. Med. Chem*. 2006; 49: 6522-6531.

201. Maurisse, R., Semir, D.D., Emamekhoo, H., Bedayat, B., Abdolmohammadi, A., Parsi, H., and Gruenert, D.C., Comparative transfection of DNA into primary and transformed mammalian cells form different lineages*. BMC Biotechnology*. 2010; 10:9.

202. Dash, P., Read, M., Barret, L., Wolfert, M., and Seymour, L., Factors affecting blood clearance and in vivo distribution of polyelectrolyte complexes for gene delivery*. Gene Therapy*. 1999; 6: 643-650.

203. Varkouhi, A.K., Lammers, T., Schiffelers, R.M., Steenbergen, M.J.v., Hennink, W.E., and Storm, G., Gene silencing activity of siRNA polyplexesbased on biodegradable polymers*. European Journal of Pharmaceutics and Biopharmaceutics*. 2011; 77: 450-457.

204. Rao, D.D., Vorhies, J.S., Senzer, N., and Nemunaitis, J., siRNA vs. shRNA: Similarities and differences*. Advanced Drug Delivery Reviews*. 2009; 61: 746-759.

205. Gallas, A., Alexander, C., Davies, M.C., Puri, S., and Allen, S., Chemistry and formulations for siRNA therapeutics*. Chem Soc Rev*. 2013; 42: 7983-97.

206. Ballarin-Gonzalez, B. and Howard, K.A., Polycation-based nanoparticle delivery of RNAi therapeutics: adverse effects and solutions*. Adv Drug Deliv Rev*. 2012; 64: 1717-29.

207. Shim, M.S. and Kwon, Y.J., Efficient and targeted delivery of siRNA *in vivo. FEBS Journal*. 2010; 277: 4814-4827.

208. Guzman-Villanueva, D., El-Sherbiny, I.M., Herrera-Ruiz, D., Vlassov, A.V., and Smyth, H.D., Formulation approaches to short interfering RNA and MicroRNA: challenges and implications*. J Pharm Sci*. 2012; 101: 4046-66.

209. Wang, J., Lu, Z., Wientjes, M.G., and Au, J.L.-S., Delivery of siRNA Therapeutics: Barriers and Carriers*. American Association of Pharmaceutical Scientists Journal*. 2010; 12: 492-503.

210. Molinaro, R., Wolfram, J., Federico, C., Cilurzo, F., Marzio, L.D., Ventura, C.A., Carafa, M., Celia, C., and Fresta, M., Polyethylenimine and chitosan carriers for the delivery of RNA interference effectors*. Expert Opinion Drug Delivery*. 2013; 10: 1653-1668.

211. Meng, Q., Yin, Q., and Li, Y., Nanocarriers for siRNA delivery to overcome cancer multidrug resistance*. Chinese Science Bulletin*. 2013; 58: 4021-4030.

212. Malmo, J., Sorgard, H., Varum, K.M., and Strand, S.P., siRNA delivery with chitosan nanoparticles: Molecular properties favoring efficient gene silencing*. J Control Release*. 2012; 158: 261-8.

213. Yang, A., Walker, N., Bronson, R., Kaghad, M., Oosterwegel, M., Bonnin, J., Vagner, C., Bonnet, H., Dikkesk, P., Sharpe, A., McKeon, F., and Caput, D., p73-deficient mice have neurological, pheromonal and inflammatory defects but lack spontaneous tumours*. Nature*. 2000; 404: 99-103.

214. Dehousse, V., Garbacki, N., Jaspart, S., Castagne, D., Piel, G., Colige, A., and Evrard, B., Comparison of chitosan/siRNA and trimethylchitosan/siRNA complexes behaviour in vitro*. Int J Biol Macromol*. 2010; 46: 342-9.

215. Abcam, *Western Blotting - A Begginer's Guide*.

216. Thermo Scientific, Western Blotting Handbook and Troubleshooting Tools*.*

217. Charlton, S.T., Davis, S.S., and Illum, L., Nasal administration of an angiotensin antagonist in the rat model: effect of bioadhesive formulations on the

distribution of drugs to the systemic and central nervous systems. *Int J Pharm*. 2007; 338: 94-103.

218. Downes, A., Mouras, R., and Elfick, A., A versatile CARS microscope for biological imaging. *Journal of Raman Spectroscopy*. 2009; 40: 757-762.

219. Evans, C.L. and Xie, X.S., Coherent anti-stokes Raman scattering microscopy: chemical imaging for biology and medicine. *Annu Rev Anal Chem* 2008; 1: 883-909.

220. Garrett, N.L., Lalatsa, A., Begley, D., Mihoreanu, L., Uchegbu, I.F., Schätzlein, A.G., and Moger, J., Label-free imaging of polymeric nanomedicines using coherent anti-stokes Raman scattering microscopy. *Journal of Raman Spectroscopy*. 2012; 43: 681-688.

221. Moger, J., Garrett, N.L., Begley, D., Mihoreanu, L., Lalatsa, A., Lozano, M.V., Mazza, M., Schatzlein, A., and Uchegbu, I., Imaging cortical vasculature with stimulated Raman scattering and two-photon photothermal lensing microscopy. *Journal of Raman Spectroscopy*. 2012; 43: 668-674.

222. Svoboda, K. and Yasuda, R., Principles of two-photon excitation microscopy and its applications to neuroscience. *Neuron*. 2006; 50: 823-39.

223. Melino, G., Gallagher, E., Aqeilan, R.I., Knight, R., Peschiaroli, A., Rossi, M., Scialpi, F., Malatesta, M., Zocchi, L., Browne, G., Ciechanover, A., and Bernassola, F., Itch: a HECT-type E3 ligase regulating immunity, skin and cancer. *Cell Death Differ*. 2008; 15: 1103-12.

224. Invitrogen, RNAi and epigenetics source book life tehcnologies 2012.

225. Roche, Roche Applied Science Technical Note No. LC 15/2002. 2002.

226. Ragelle, H., Riva, R., Vandermeulen, G., Naeye, B., Pourcelle, V., Le Duff, C.S., D'Haese, C., Nysten, B., Braeckmans, K., De Smedt, S.C., Jerome, C., and Preat, V., Chitosan nanoparticles for siRNA delivery: optimizing formulation to increase stability and efficiency. *J Control Release*. 2014; 176: 54-63.

Appendix

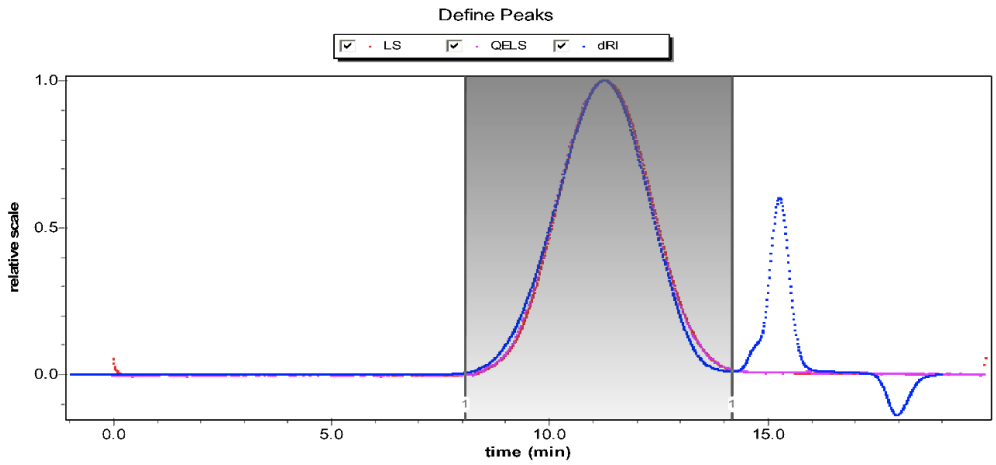

Figure A.1 - GPC-MALLS Chromatogram of degraded GC (4h) (5mg mL^{-1}).

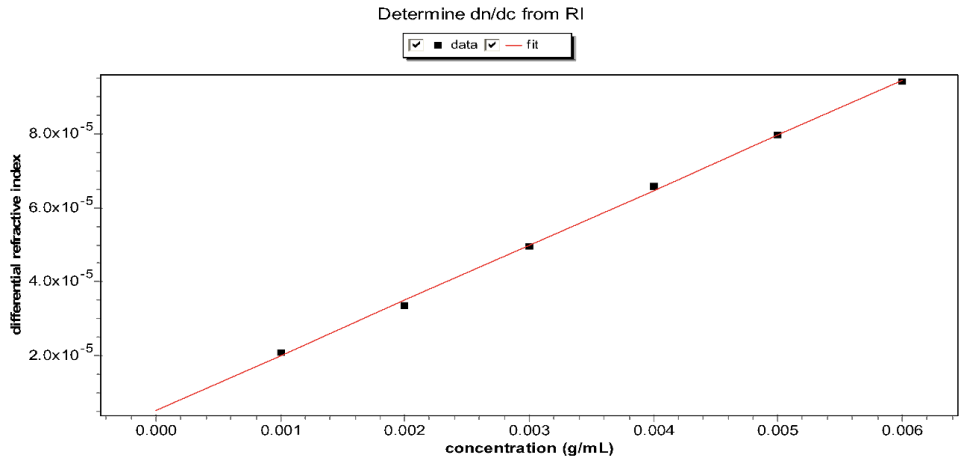

Figure A.2 - dn/dc curve of Glycol Chitosan (4h).

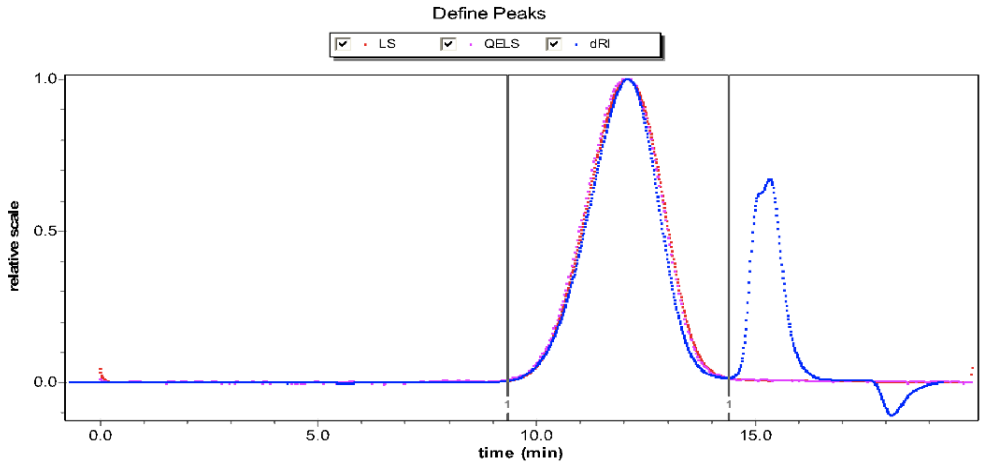

Figure A.3 - GPC-MALLS Chromatogram of EAGC17 (5mg mL^{-1}).

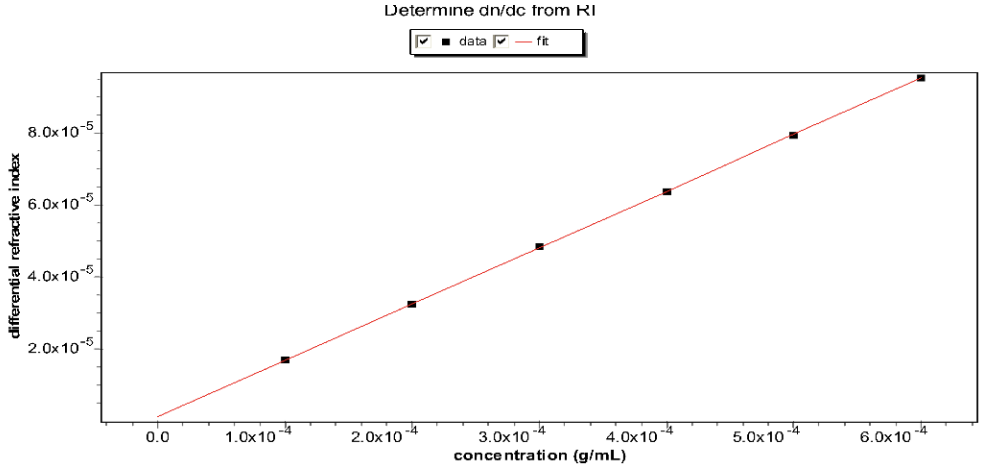

Figure A.4 - dn/dc curve of Ethylamino Glycol Chitosan (EAGC17).

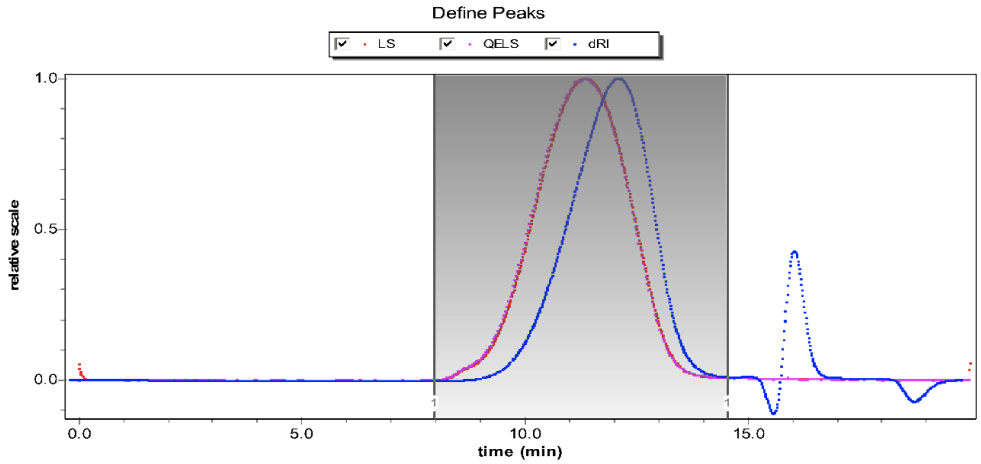

Figure A.5 - GPC-MALLS Chromatogram of EAGC30 (5mg mL^{-1}).

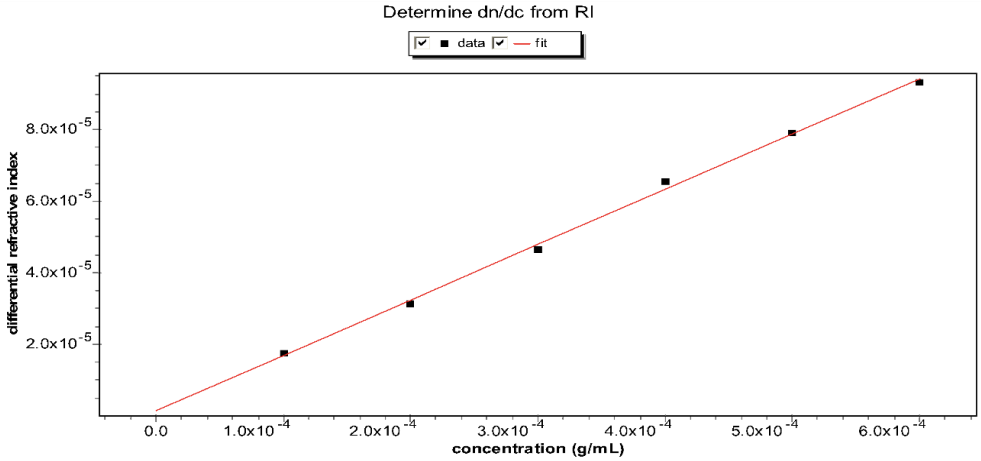

Figure A.6 - dn/dc curve of Ethylamino Glycol Chitosan (EAGC30).

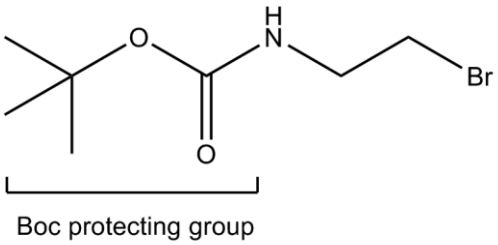

Figure A.7 - Chemical structure of 2-(Boc-amino) ethyl bromide.

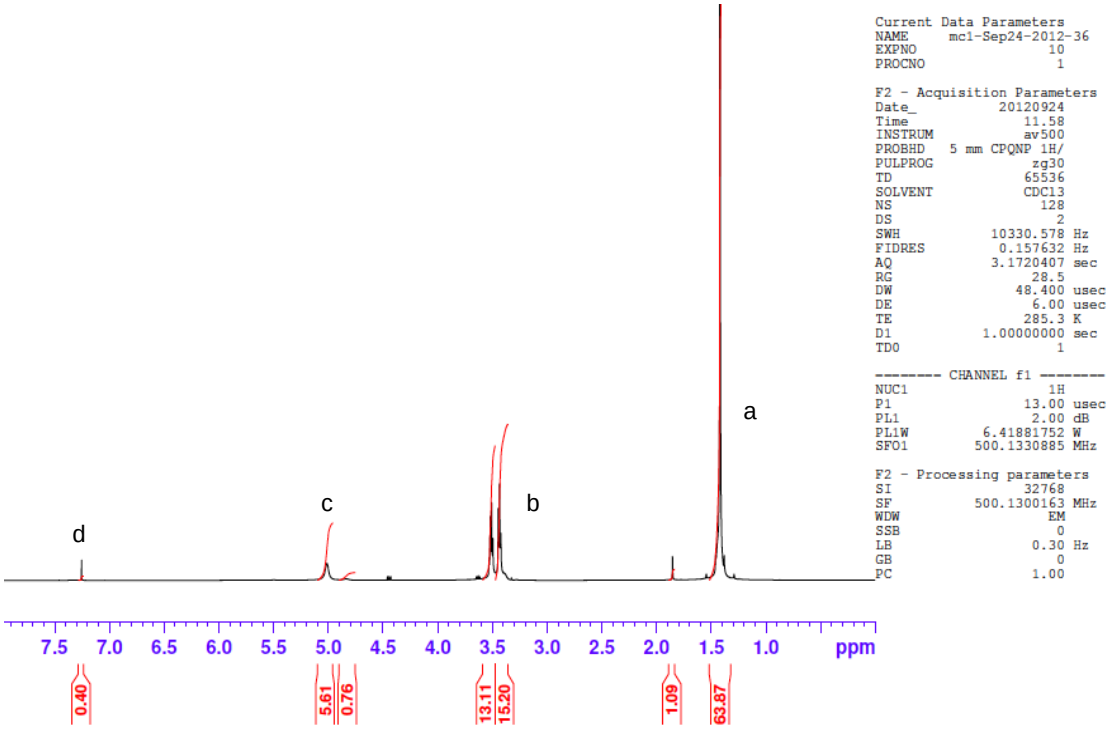

Figure A.8 - ^{1}H NMR of 2-(Boc-amino) ethyl bromide.

Table A.1 - Protons assignments and chemical shifts for 2-(Boc-amino) ethyl bromide.

Position on the H-NMR spectra	**NMR Chemical Shift**	**Corresponding proton on the structure**
a	1.5 ppm	$(CH3)_3$ (Boc Group)
b	3.5ppm	CH_2 (ethyl amino group)
c	5ppm	NH
d	7.3 ppm	CDC13

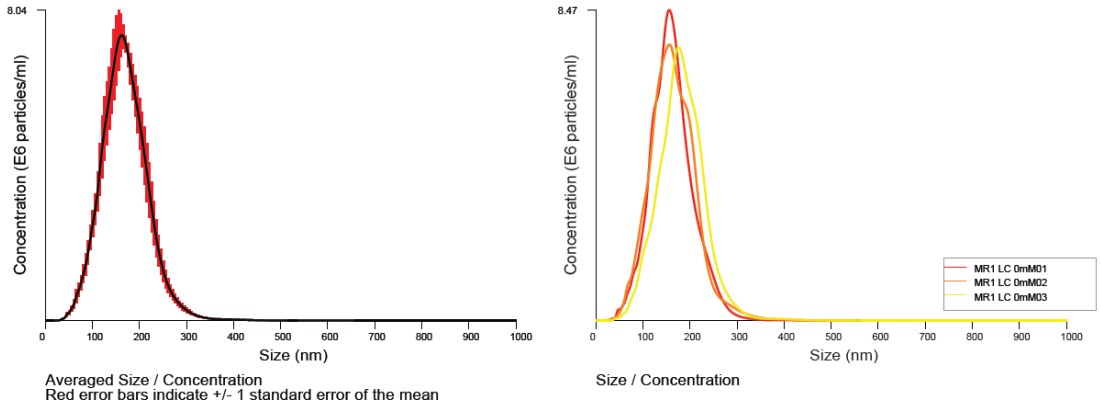

Figure A.9 – Nanosight particle tracking analysis results for the particle size distribution of EAGC30-DNA particles at polymer, DNA mass ratio 1. EAGC30 was incubated with DNA in dextrose 5% for 1h. DNA concentration 0.1 mg mL^{-1}. The data was expressed as mean values (± standard error) of three experiments.

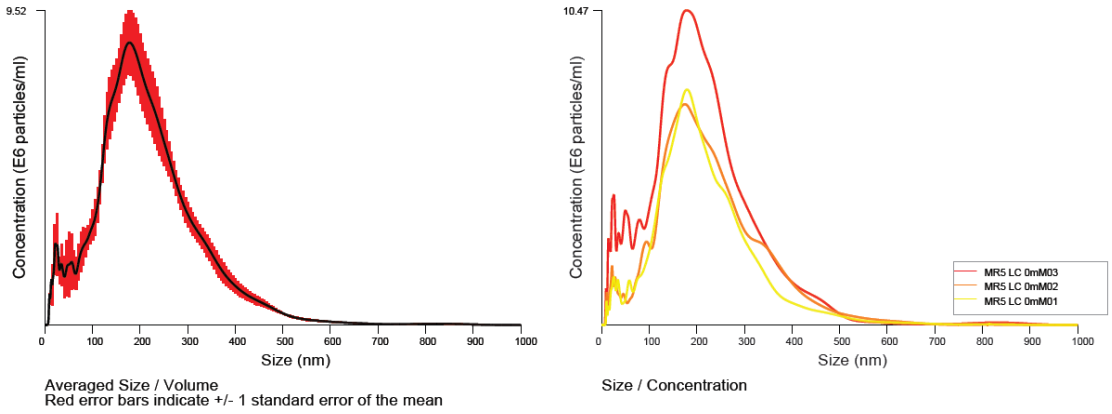

Figure A.10 – Nanosight particle tracking analysis results for the particle size distribution of EAGC17-DNA particles at polymer, DNA mass ratio 5. EAGC17 was incubated with DNA in dextrose 5% for 1h. DNA concentration 0.1 mg mL^{-1}. The data was expressed as mean values (± standard error) of three experiments.